NTNU – Trondheim
Norwegian University of
Science and Technology

Production and Characterization of a Zr-based Bulk Metallic Glass

The possibility of a future biomaterial

Marius Hansen

Chemical Engineering and Biotechnology
Submission date: June 2013
Supervisor: Ragnhild Aune, IMTE
Co-supervisor: Nuria Espallargas, IPM

Norwegian University of Science and Technology
Department of Materials Science and Engineering

Jeg erklærer herved at arbeidet har blitt utført selvstendig og i samsvar med Reglement for Sivilarkitekt- og Sivilingeniøreksamen ved NTNU.

I hereby declare that this work has been carried out independently and in compliance with the examination regulations of the Norwegian University of Science and Technology, NTNU.

X

Marius Hansen
Trondheim, 24.06.2013

Abstract

Materials put under strain while exposed to the harsh environment of the human body, must not only be chemically stable, but also have good tribocorrosion properties, i.e. a combination of good corrosion and wear properties.

In the present work the tribocorrosion properties of a new zirconium-based Bulk Metallic Glass (BMG) with low copper content ($Zr_{65}Cu_{18}Ni_7Al_{10}$), has been investigated, and the results compared to conventional biomaterials used in load-bearing implants, i.e. hip and knee implants. The aim of the study was to evaluate if an amorphous BMG would be better suited for prolonged clinical use, than the materials presently in use today, i.e. stainless steel, Cobalt-Chromium-Molybdenum (CoCrMo) alloy and Titanium.

An experimental program was designed to compare the tribocorrosion properties of the amorphous BMG with the properties of medical grade CoCrMo alloy, as well as with pure medical grade Titanium (Ti 99.6 %). The materials were exposed to two different Phosphate Buffered Solutions (PBS) with an addition sodium chloride, to simulate the salinity of the body. One of the solutions had the original buffer pH of 7.4, and the other 5.2, which was obtained by the addition of hydrochloric acid (HCl), to simulate a body with an inflammatory response. Both solutions were made in two batches; one with and one without additions of albumin protein. Electrochemical measurements were performed at normal body temperature (37 °C), and Linear Polarization (LP) curves were obtained for all materials in all solutions. Dry tribological and tribocorrosive tests were also performed on all materials, and in all solutions. A Confocal Microscope (CM) and a Scanning Electron Microscope (SEM), was used for analyzing the results and thereby trying to assess the wear mechanisms.

Based on the obtained results, it was established that the CoCrMo alloy was the most wear resistant of the materials, under the conditions chosen, followed by the BMG and lastly the Titanium. It is believed that by altering the chemical composition of the amorphous BMG alloy, the tribocorrosion properties could be improved. This must, however, be investigated in a further study.

Sammendrag

Materialer som blir utsatt for slitasje i kroppens ugjestmilde miljø må, i tillegg til å være kjemisk stabile, ha gode tribokorrosenjonsegenskaper, dvs. kombinasjon av gode korrosive og mekaniske egenskaper.

Arbeidet som presenteres her har hatt som formål å utforske de tribokorrosive egenskapene til et nytt zirkonium-basert Bulk-Metallisk Glass (BMG) med lavt kobberinnhold ($Zr_{65}Cu_{18}Ni_7Al_{10}$). Resultatene ble sammenliknet med konvensjonelle biomaterialer som benyttes i bærende implantater, dvs. kne- og hofteleddsproteser. Målet ved studien var å evaluere hvorvidt en amorf BMG er bedre skikket til vedvarende klinisk bruk enn materialer som brukes i dag, dvs. kirurgisk rustfritt stål, en Kobolt-Krom-Molybden legering (CoCrMo) og titan.

Et eksperimentelt program ble utformet for å sammenlikne tribokorrosjonsegenskapene til en amorf BMG, med egenskapene til medisinsk CoCrMo, og ren kirurgisk Titan (Ti 99,6 %). Materialene ble utsatt for to ulike fosfat-bufrede løsninger med en tilsats av natriumklorid for å simulere saltinnholdet i kroppen. Én av løsningene hadde den originale pH-en på 7,4, og den andre 5,2, som ble oppnådd ved å tilsette saltsyre, for å simulere en situasjon med inflammatorisk respons. Begge løsningene ble tillaget i to partier, én med og én uten tilsats av proteinet albumin. Elektrokjemiske målinger ble utført ved normal kroppstemperatur (37 °C), og lineære polarisasjonskurver ble målt på alle materialer i alle elektrolytter. Tribologiske tester og tribokorrosjonstester ble også utført på alle materialer i alle løsninger. Et konfokalt mikroskop, så vel som et elektronmikroskop, ble benyttet for å analysere resultatene og således forsøke å avgjøre slitasjemekanismene. Basert på resultatene ble det avgjort at CoCrMo-legeringen var det mest standhaftige materialet av dem alle, under de valgte forholdene, etterfulgt av BMG-en og deretter titanet. Det formodes at ved å endre den kjemiske sammensetningen til den amorfe BMG-en, så kan de tribokorrosive egenskapene forbedres. Dette må imidlertid undersøkes i et fremtidig studium.

Preface

The work described in this thesis was carried out at the Department of Materials Science and Engineering at the Norwegian University of Science and Technology during the summer of 2013.

Firstly I would like to thank my supervisor Ragnhild Elizabeth Aune for her guidance and support. Her eager and willingness to allow me to study the field of biomaterials and organize related subjects has been very important to me.

Secondly I would also thank my co-supervisor Nuria Espallargas, whom has organized the use of the equipment I have utilized for this thesis for me, and helped me interpret the results.

Finally I would also like to thank the PhD. candidates that have done previous research into this field, and especially Cristian Torres whom has instructed me in the use of the equipment, helped me whenever it started to act up, and shared his experience on this subject with me.

Marius Hansen

Contents

List of abbreviations

BMG – Bulk Metallic Glass

CoCrMo – Cobalt-Chrome-Molybdenum alloy F75, surgical grade

COF – Coefficient Of Friction

DLC – Diamond-Like Carbon

E_{corr} – Corrosion potential

GPa – Giga Pascal

HCl – Hydrochloric acid

HR – Hip Resurfacing

ICP-MS – Inductively Coupled Mass Spectrometry

LP – Linear Polarization

mM – millimoles per liter

MPa – Mega Pascal

OCP – Open Circuit Potential

PBS – Phosphate Buffered Solution

RSP – Rapid Solidification Processing

SEM – Scanning Electron Microscopy

THA – Total Hip Arthroplasty

THR – Total Hip Replacement

UHMWPE – Ultra-High Molecular Weight Polyethylene

WAC – Wear Accelerated Corrosion

XRD – X-Ray Diffraction

1. Introduction

In Norway in 2011 it was performed in total 8380 hip arthroplastic surgeries [1].These types of operations are very common, and the success rate for the operation in itself is very high. In Sweden in 2010 the number of conducted operations was approx. 16 000, of which approximately 10 % of them were revisions [2]. The main cause for a primary Total Hip Replacement (THR) (also known as a Total Hip Arthroplasty (THA)) or Hip Resurfacing (HR) is because of wear and osteoarthritis. Revisions are mainly done because of worn out prosthesis parts, but also due to other complications. The most common complications are loosening, luxation and infection [1] [2].

However, another problem that has existed as long as the surgical method itself, and is closely related to the number of revisions, is the problem of the longevity of the implant. Today the lifetime of an implant is assumed to be on average 10-15 years. It is self-explanatory that today, where the average Norwegian lives to be more than 79 years for men and 83,5 for women [3], this means that a patient whom is operated within the largest age group (60-79 years [1] [2]) will, most likely, have to perform at least one revision during the course of his/her life.

The materials that have been used so far include Ultra-High Molecular Weight Poly Ethylene (UHMWPE), Stainless Steel AISI 316L, Cobalt-Chrome-Molybdenum (CoCrMo) alloys, Titanium alloys and ceramics [4]. All of these have proven themselves to have their own strengths and weaknesses, pros and cons. What they all have in common, on the other hand, is that they are all biocompatible. Issues that have been fairly common for all the different configurations these materials can be found in are wear particles and their effects. All of the materials will eventually degrade and release particles that do both physical and physiological damage. The degradation is caused by the extreme environment that actually exists in our body.

In an effort to prolong the longevity and durability of the implants, new materials, coatings and alloys are constantly being evaluated. Coatings that are worth mentioning on basis of good results are Diamond-Like Carbon (DLC) and nitridation [5] [6]. A material that has gotten more focus over the past few years is Bulk Metallic Glasses (BMG). The main reason

for this is that they exhibit both very good tribological and corrosion resistant properties, and at the same time are biocompatible and retain most of the mechanical properties of their crystalline counterparts [7]. So far there has been done research on copper and zirconium based BMGs, but titanium based has, to the present knowledge of the author, not been extensively explored.

1.1. Aim of the thesis

The aim of the present work is to investigate the corrosive, tribological and tribocorrosive properties of a new zirconium based BMG with low copper content. It will be compared to well known, commercially available, biocompatible materials, to assess the possibility of future use as a biomaterial.

Therefore, aspects such as dry tribological wear; polarization behavior and tribocorrosive stability will be tested, to see how it reacts to different degradation mechanisms and environments. Polarization curves will be measured by the use of a potensiostat/galvanostat to establish the general corrosion behavior of the materials. A custom built tribocorrosimeter will be used to obtain data on the tribological and tribocorrosive properties of the materials.

Finally, the samples will be studied with different microscopy techniques to assess the wear of the materials. Confocal microscopy will be used to investigate the wear volume and roughness profile, while scanning electron microscopy will be used to assess the wear mechanisms that act on the materials.

2. Theory

2.1. Applications of materials in medicine

The human body is a rather astonishing piece of biological engineering: It has a long lifetime, great regeneration and incredible cognitive and physical capabilities. Some of its solutions are incredible, and technology constantly strives to create analogues with similar capabilities in many fields. But, it is in many viewpoints frail and inadequate. With this many bits and pieces that have to function optimally, it is no surprise that even the tiniest malfunction may have great consequences. Some parts of the body may fail long before the rest perishes, and this often causes a great deal of pain and suffering. In an effort to relieve patients of their pain, and to restore the body to full operating capability, persons with medical insight have for thousands of years used different techniques to solve different problems. Today, with the latest technologies and materials it is possible to replace or repair many of the body parts that most commonly fail, such as heart valves, dental parts, and bones. But none of these substitutes come even near the body analogue in terms of longevity and biocompatibility. Therefore it is literally vital that research into these fields is conducted.

2.1.1. Degradation of materials in the biological environment

The body is, from a material science standpoint, a rather hostile environment. Not only is there many different chemical compounds, such as proteins and free radicals, in different states that can and will react with metals, ceramics and plastics, but the environment is completely individual meaning that there is no one ideal solution. Even in a single person the internal environment can change drastically depending on the physical and physiological state of the person [5]. With regards to implants these reactions lead to corrosion and degradation of the materials, and ultimately failure. Another aspect of the degradation is the mechanical wear; in joint prosthesis there is a wear factor increases the degradation of the parts in contact. When coupled with a corrosive environment this leads to the synergetic effect of tribocorrosion, which is even more severe than the two components, corrosion and wear, put together [8]. This aspect of degradation is under increasing study, and is of

key importance to improve the longevity of prosthetics [8]. Examples of worn out prosthesis' can be seen in Figure 2-1.

Figure 2-1: (a) A worn Charnley total hip prosthesis, (b) an aged UHMWPE acetabular cup showing cracking and delamination, and (c) an example of wear debris on an UHMWPE knee joint.

2.1.2. Influence of environmental and material conditions

As mentioned, the environment in the body is rather hostile; the pH is usually around 7, but it can drop to about 5 if the body has some immunological response. This is mostly accredited to the species released as a response to viruses and infections; they often contain acidic functional groups. The temperature of the body is fairly constant around 37 °C, but even this low temperature has impact on the reactivity of the surface of some materials, and on the species in the body. In addition to acidic species, the bio fluids often contain ions, dissolved gasses and free radicals that have great impact on the material [9]. Also, the body has some fierce reactions towards foreign bodies that have huge impact on the devices [10]. All of these factors ultimately lead to corrosion, ion release and particle release, which in turn lead to failure (cracking, fatigue), aseptic loosening, metal sensitizing or metal poisoning.

2.1.2.1. Influence of protein

The synovial fluid is primarily built up of a mixture of proteins, and there is no doubt that they play an important role in the tribological aspects of a THR, and the degradation of the materials, although this is not yet fully understood [11].

Almost immediately after an implant has been introduced to the body, proteins will adsorb on the surface. What type of proteins that adsorb, and how they react with the cells is dependent on the surface properties. This in turn will dictate how the body reacts towards the foreign body, and how the environment

will change [10]. Proteins contain many functional groups, and most noticeable are the acidic groups. These can contribute to the lowering of the pH at the surface of the material, and thus increased corrosive wear [11].

The effect of proteins is not just detrimental; denatured proteins may adhere to the surface and affect the tribological contact in the form of a solid lubricant. The proteins may actually denature during the sliding motion, and therefore this mechanism is in a sense self-lubricating [12].

For the sake of body simulation, bovine albumin protein is often chosen to supply an insight into how proteins will affect the metal surface [12] [13] [14]. It is known that since proteins are amphoteric, the charge of the molecule is affected by the pH in the surrounding environment. When the molecule carries no net charge, it is said to be at its isoelectric point, or pI. When the pH is higher than the pI, the molecule will be negative since the concentration of protons is too low to dominate the hydroxide groups. It follows that when the pH is lower than the pI, the proton concentration is high, and the molecule becomes positively charged.

2.1.3. Orthopedic applications

The field of orthopedic biomaterials is wide; it ranges from the smallest staples and screws (fixation devices, to the largest hip implants (joint replacement devices). What they have in common is their ability to survive for a great time in the human body without loss of functionality, and to withstand cyclic load-bearing applications. The materials used are often metals, ceramics or polymers, with metals being the most popular and well researched of them all [15].

2.1.3.1. Anatomy of the human hip joint

The human hip joint, or acetabulofemoral joint, is a synovial ball joint consisting of the acetabulum (the cup), the femoral head (the ball) and the femoral stem. Figure 2-2 shows a general synovial joint, while Figure 2-3 shows a cross section of a hip joint. The acetabulum covers almost half of the femoral head, and the grip is enhanced by the acetabular labrum which is a ring-shaped fibrocartilaginous lip [16].

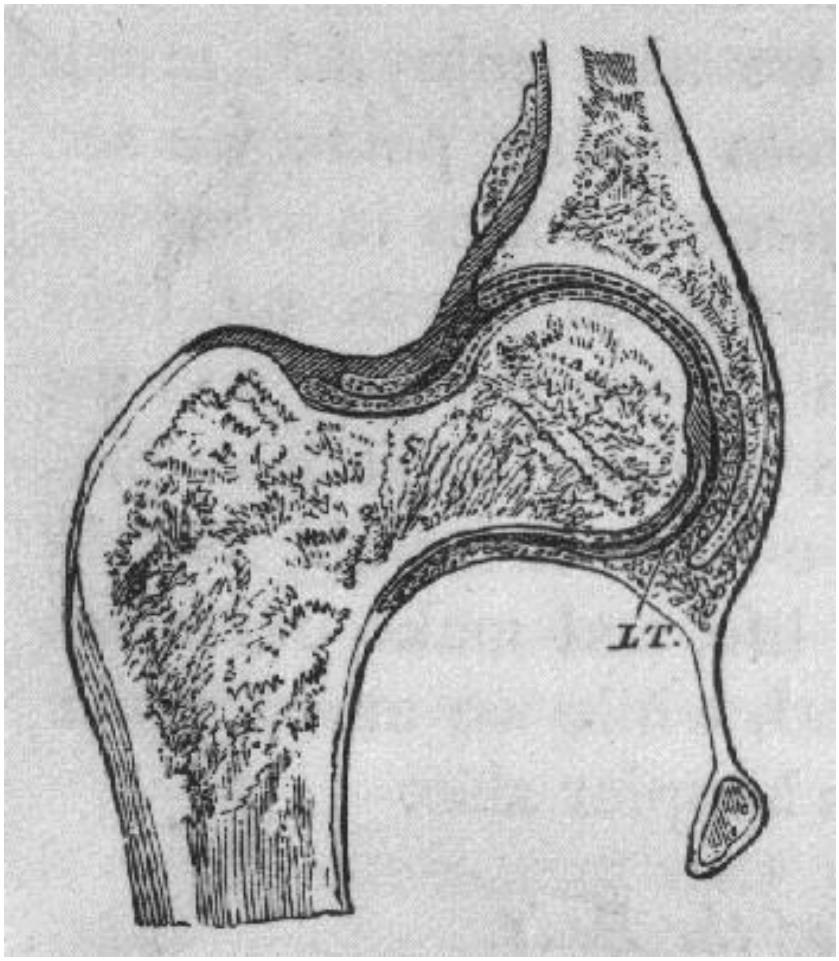

Figure 2-2: Cross section of a human hip joint [17]

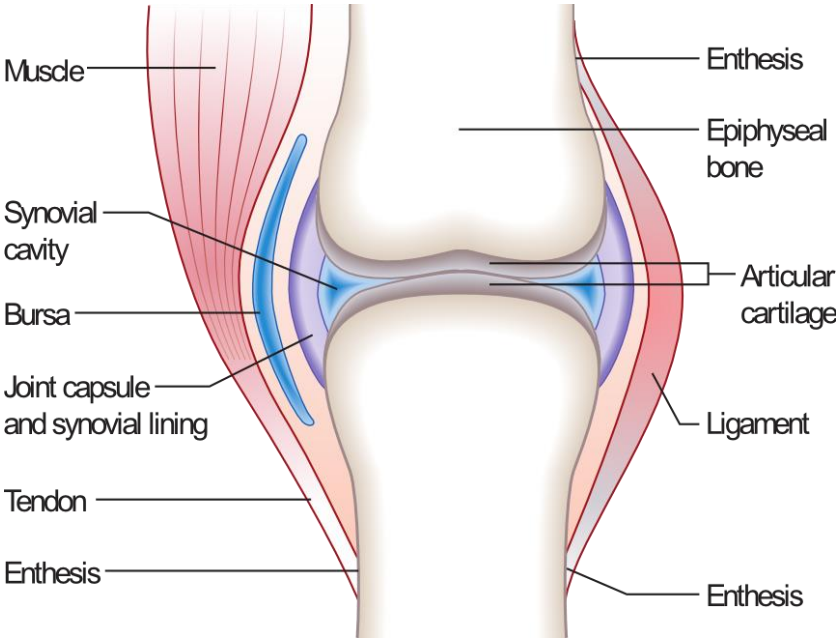

Figure 2-3: General depiction of a synovial joint [18]

2.1.3.2. General description of a THA

The total hip replacement is a surgical procedure where the whole hip joint is replaced by a prosthetic implant. A simple presentation of the procedure is shown in Figure 2-4.

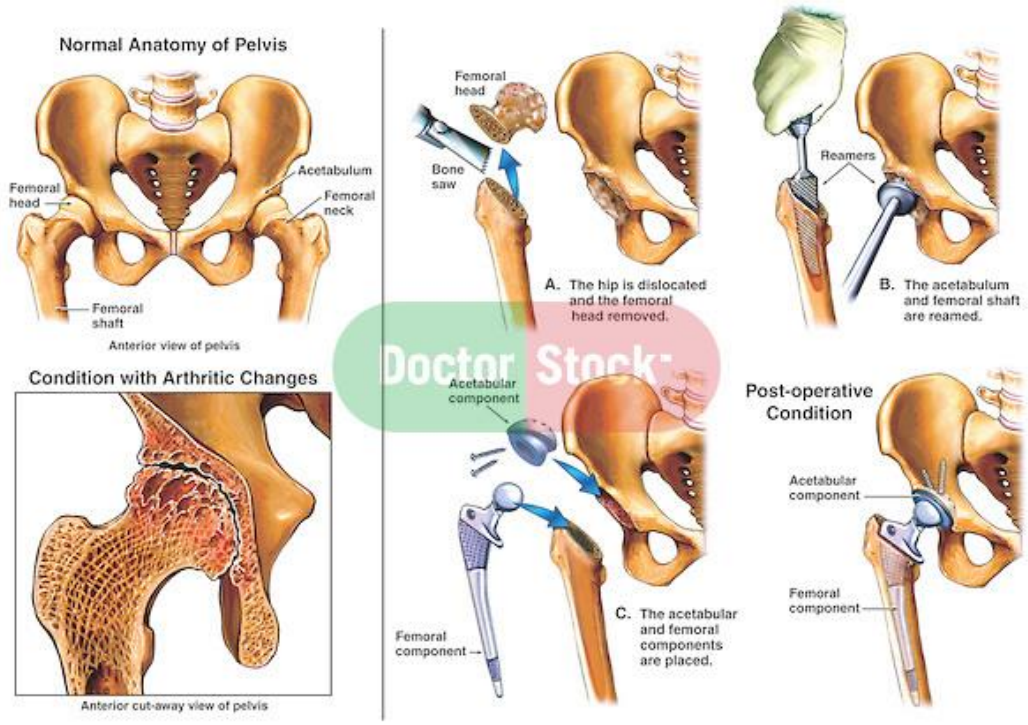

Figure 2-4: Illustration of hip replacement [19]

2.1.3.3. Materials and designs in hip replacements

Hip implants consist of two components; the femur (stem) and the acetabulum (cup). Some configurations are made to be one system, such as the Charnley prosthesis, but often the hip implant consists of two separately produced components of two separate designs. There are many designs, and the evolution towards a better and more applicable design is constant. In Norway it is used over 40 different designs, but some are more used than others [1]. The most popular and most researched is the Charnley total hip replacement prosthesis, which was introduced in 1962 and has since then been redesigned and improved [20].

2.1.3.3.1. Configurations

There are four common material configurations (stem/cup): Metal/Plastic, Metal/Metal (MoM), Ceramic/Ceramic and Ceramic/Plastic. The by far most used combination is the Metal/Plastic, because of availability, cost and the relative ease of which it can be produced [4]. However they all have their own strengths and weaknesses, and none of them are in the real sense ideal. Table 2-1 gives a listing of the most pronounced advantages and disadvantages of these combinations.

Table 2-1: Comparison of different bearing surface combinations, [4]

Bearing surface combination	Advantages	Disadvantages
Metal-on-polyethylene	• Most forgiving combination in terms of component alignment • Least expensive • Used for elderly patients with low functional demands	• Highest wear of all three combinations • Smaller femoral heads with relative decrease in stability and range of motion compared to metal-on-metal • Boundary lubrication mechanism which increases wear with bigger femoral head • Backside wear
Ceramic-on-polyethylene	• Increased hardness, scratch resistance and burst strength • Increased wettability for improved lubrication • Lower wear rates compared with metal-on-polyethylene • Excellent clinical results	• Risk of fracture of the ceramic • Higher wear rates than ceramic-on-ceramic
Metal-on-metal	• Larger femoral heads available with increased stability, jump distance and range of motion • Mixed fluid film lubrication mechanism which decreases wear with bigger femoral heads • Self-polishing capacity • Better wear resistance than metal-on-polyethylene (low volumetric loss) • Used in young patients with high functional demands	• Highest biological reactivity and cytotoxicity with highest number of wear particles • Highest levels of metal ions in blood, urine and remote organs • Not used in females in their reproductive years or patients with renal failure • Metal sensitivity (delayed type hyper sensitivity) • Possible carcinogenesis and genetic damage • Perfect component positioning is essential to prevent failure
Ceramic-on-ceramic	• Lowest biological reactivity • Low friction and wettability • Low surface roughness • Highest wear resistance • Reserved for young, high functional demand with metal sensitivity	• Brittleness and possible component failure • Small femoral heads with decreased range of motion • Stripe wear with possible squeaking • Less forgiving combination • Most expensive

2.1.3.3.2. Materials

Of these different configurations the most common materials are UHMWPE, CoCrMo, Titanium (pure and alloyed), AISI 316L, NiTiNOL, Zirconium, Alumina and Hydroxyapatite. The only materials used for any wear surfaces are the ceramics, UHMWPE and CoCrMo alloy [5] [21] [22].

2.1.3.3.3. Designs

There are many existing designs on the market, and the biomedical manufacturers are constantly trying to find the best design solution and combination of materials that give the correct load transfer and integration. The most commonly used designs and combinations in Norway are [1]:

- Cemented (stem/cup): Charnley/Charnley, Exeter/Exeter, Spectron-EF/Reflection All Poly, Titan/Titan, Exeter/Contemporary and SP II/IP.
- Un-cemented: Corail/Tropic, Filler/Igloo, Corail/Trilogy, Corail/Aroll, Corail/Reflection, Corail/Duraloc, Zweimüller/Bicon-Plus, SCP/Unique/Trilogy,
- Hybrid: Titan/Tropic, MS-30/Morscher, Charnley/Trilogy, Exeter/Trilogy, Titan/Endler.

However, there has been a dispute in the medical community whether or not this diversity of models is at the expense of patients' health and wellbeing. This is based on the time it takes to establish if the prosthesis is up to standards or not, which may take a decade to ascertain [23].

2.1.3.4. Causes of device failure

The main causes for a reoperations following a device failure is, in most cases, not caused by an actual failure of the material in the device, but in the interaction with the body. Most reoperations are done based on aseptic loosening of either acetabulum or femur component. Other common causes are luxation (dislocation) and infection [1] [2] [24].

Aseptic loosening is caused by many different things; mechanical or biological. Osteolysis (bone resorption) as a reaction towards wear debris in the tissue

around the implant is one important factor [25]. Osteolysis caused by mechanical factors is also a contributor. Because of the higher stiffness and difference in load distribution after implantation, the femoral bone will enter a state of atrophy as a reaction to less stress and strain [26]. Luxation is often caused by misalignment in the two components of the prosthesis, because of wrong ball joint diameter or severe wear of the ball or cup component [27] [28]. Infection is caused by transfer of bacteria from skin surface to the deep tissue during surgery, by contamination of implant or through other aspects of the surgical procedure [29] [30].

2.1.3.5. Economic impact

With this many THAs and revisions conducted worldwide every year, there is little doubt that this has an economic impact on the different governments, health programs and private persons. In Norway alone this amounts to a staggering 700 million NOK (EUR 88.9 million) of which 18 % stems from revisions. [31]. In the USA it is done approx. 285 000 THRs a year, and this is expected to double by 2030. By 2015 it is expected that the cost of these will reach up to $65.2 billion [32]. With this in mind, there exist some rather great incentives for increasing the longevity of hip implants, and thereby decreasing the need for revisions and reoperations.

2.1.3.6. Wear and wear debris

As mentioned, the implants are subjected to both mechanical and chemical wear in what is known as a tribocorrosion system. This leads to a much more severe degradation than can be anticipated by any modeling, and the interaction causes corrosion products and the removal of surface particulates. These particles are then released into the nearby environment, or contribute to an increased wear of the surfaces by different wear mechanisms. Both ceramic and polymers will give wear debris exclusively in particulate form. These particulates will cause the body to react in several different ways depending on the particulates size and nature. Any implant in the body will cause foreign-body reaction, the particles will also cause activation of macrophages, with following release of inflammatory

mediators leading to inflammation, phagocytosis, and ultimately osteolysis [25] [33] [34].

2.1.3.7. Ion release and toxicity

Where metals are used as articulating surfaces, metallic wear particles will also be present. Usually they will take other forms as corrosion debris such as colloidal organometallic complexes; free metallic ions; inorganic salts/oxides; or isolated in organic storages [35]. Many metal ions are known for their human toxicity and/or allergenic properties, and a few of them are used as alloying metals in some devices such as Copper, Cobalt, Chromium and Nickel. However there is still some debate to which extent the toxic ions released from implants will have an effect in the body, since they usually are released as compounds, although great caution is being taken to prevent this [11]. Some of the concerns with metal ion release are revolving around the spread of said ions throughout the body. Most of the ions seem to stay in the vicinity of the implant, but studies have shown that they can be transported through the bloodstream and lymphatic system to remote organs, and that they then may exert toxic properties [36]. The effect of these particulates in remote organs have as of yet not been studied to any great extent. In addition to the toxicological effects, metal particulates will also cause some of the same immunological reactions as UHMWPE and ceramics; inflammatory, foreign-body granulation tissue that can invade the interface between the bone and the implant, and thus causing progressive, periprosthetic bone loss. The reactions are however somewhat individual [37], but there is no doubt that a prosthetic device will cause chronic elevation of metal content in serum and urine. A further concern is if the implants are carcinogenic, and some evidence suggests that there is a heightened possibility of developing periprosthetic tumors, although the numbers of cases are too few to draw any conclusions [35].

2.1.4. Biomedical Potential of Bulk Amorphous Alloys as Load Bearing Implants

Pure metals and alloys, as most of us know them, exist in their crystalline solid state. However, like most materials that have a crystalline state, they also have an

amorphous one. This state is characterized by its absence of grain boundaries, dislocations and associated slip planes. This gives a material with utterly unusual properties. BMGs bring to the table strengths and elasticity's that surpass their crystalline counterparts, and thus also the materials currently used for biomedical applications. The amorphous structures also promote good corrosion and wear resistance, which is yet another bonus, and the sum of all this makes BMGs rather promising with regards to biomedical applications [38]. But, as with most things, there is a duality to consider; BMGs have this far been difficult to produce in large scale, and in larger bulk pieces, and with the purity that is necessary. This is however a field with great development and much of the early thresholds have long since been crossed [39].

2.1.4.1. Formation and crystallization

When creating super-alloys, medical metals or BMGs, the purity needed and the complexity of the system calls for a special melting process. The arc melting process is capable of producing materials with high purity and high homogeneity. It does so by re-melting consumable electrodes with an electrical arc in vacuum. High voltage DC current causes an arc between the two electrodes, and the resulting high temperature melts the electrodes into a water-cooled high purity copper mold. The primary advantages of this method is that the vacuum removes dissolved gasses, reduces the amount of trace elements with high vapor pressure, and gives less oxide formation [40].

To produce an amorphous alloy usually means to cool down a metallic melt fast enough to hinder that it crystallizes, this is known as undercooling. This requires a cooling rate of at least 10^4 K/s (normal water quenching gives about 10^2-10^3 K/s), which is a rather daunting task to achieve in any practical size, or by removal of heterogeneous nucleation sites. The method that was first introduced, and has since been used with great success is the Rapid Solidification Processing (RSP). The RSP method uses droplet, jet or surface melting technologies to produce a thin film, ribbon, wire or powder (20-50µm) of amorphous material. It commonly involves ejecting metal melt at a heat sink or

conducting surface which induces rapid cooling of the metal puddle and possibly expelling into fibers and sheets by melt spinning [41].

Understandably RSP is rather impractical if you try to make bulk materials which have radii of several millimeters. Luckily, newer research and methods have made it possible to form BMGs with significantly lower cooling rates, and thus made it extremely more available. The low critical cooling rates of BMG alloys make it possible to use a simple method like water quenching. Here the specimen is melted, fluxed and placed in a quartz crucible/tube. It is then reheated to liquidus temperature and quenched in water. Other methods are High-pressure Die Casting, Copper Mold Casting, Cap-Cast Technique, Suction Casting Method, Squeeze Casting Method, Arc Melting Method, Unidirectional Zone Melting Method, and Electromagnetic Vibration Process. [41]

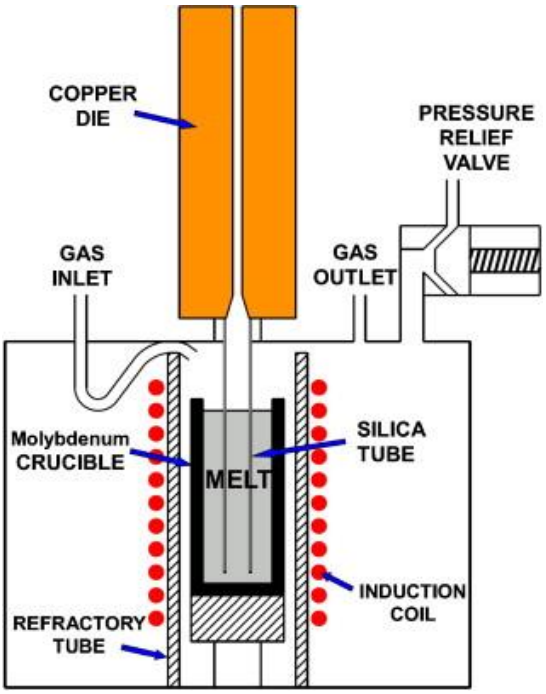

Figure 2-5: Illustration of High Pressure Die Casting method [42]

Apart from the physical methods of production, the chemistry is also rather important. There are three key factors to creating a BMG: Significantly different atomic size among the constituents, a large and negative enthalpy of mixing, and a high crystallization barrier. The last factor means that it becomes rather difficult for heterogeneous crystallization to take place, since the components

cannot move readily. This is caused by several elements, such as increased viscosity (lower diffusion) and simply by the number of components. By increasing the number of components, it becomes increasingly difficult to satisfy the different criterions of the different crystal phases; the crystallization becomes “frustrated”. In addition, by creating the correct mixture of alloying metals, the phase diagram will give a deep eutectic point, in which it is possible to cool down without precipitation of crystalline phases. It will also cause the cooling rate to be low enough to make it feasible, and increase the reduced glass transition temperature (the ratio between glass transition temperature and melting temperature) impairing homogeneous nucleation. All of these factors will increase the glass forming ability and the thickness obtainable from the material [43].

Understandably; crystallization is unwanted with regards to produce a pure and flawless BMG. The material often loses its beneficial properties, such as corrosion resistance, and the magnetic properties change. Great steps are taken to find the perfect solution to give low cooling rates and pure BMG, but crystals in the glass matrix is not always detrimental to the material properties: Composites of metal crystals in glass matrix has shown some interesting mechanical properties like increased strength, large amounts of induced ductility, and in some cases actually increased corrosion resistance. With the better understanding of crystallization in BMGs it has been possible to tailor these materials, with regards to properties, to a great extent [41].

2.1.4.2. Material Properties for Bulk Amorphous Alloys

2.1.4.2.1. Mechanical performance

There have been few reviews of the mechanical behavior of the BMGs [41]. What little has been reported have, as mentioned, observed that the BMGs exhibit far better mechanical properties than their crystalline counterparts, and they even come close to theoretical values. They have for instance high hardness, toughness, and superior wear properties [44] [45], and with strengths exceeding 1GPa in most cases [41]. Some of these properties are

owed to the fact that it can undergo shear flow without cavitation, which dissipates energy and hinders fracture, and when a shear band propagates, the surrounding material will recover elastically and arrest the propagation. This gives values for fracture energy and –toughness comparable to those of the toughest engineering metals known [46].

A mechanical aspect in which the BMGs come short is the yield strength. At room temperature the BMGs have very low ductility, and will fail shortly after yielding without any significant plastic deformation. This type of behavior at room temperature is described as inhomogeneous, deformation is concentrated to a few shear bands, and this results in a mechanically unstable material at high stresses.

In contrast to crystalline materials, which undergo strain hardening, the BMGs have been observed to exhibit strain softening; an increase in strain makes the material softer and makes it possible to deform it at lower stresses and higher rates. A direct consequence of this is the appearance of shear bands, which again is attributed to local decrease in viscosity.

The BMGs are, as other glasses, brittle, and have little ductility. They are however malleable and can be bent plastically.

Even though they have very high tensile strengths and the fatigue crack propagation is similar to crystalline metal, the BMGs are somehow susceptible to crack initiation [41].

A set of informative tables of mechanical properties of some metallic glasses can be found in [41], and should be compared to the material properties of more common biomaterials listed in [22] and [47], to give a good picture of the superiority of the BMGs. Some common values are also listed in Table 2-2.

2.2. Tribology

2.2.1. Theory

Tribology is defined as the science and technology of interacting surfaces in relative motion, including related subjects and practices [48]. Furthermore the tribological system is defined as a body whose functional behavior is connected with interacting surfaces in relative motion [49]. The parameters that influence the tribological system are presented in Figure 2-6.

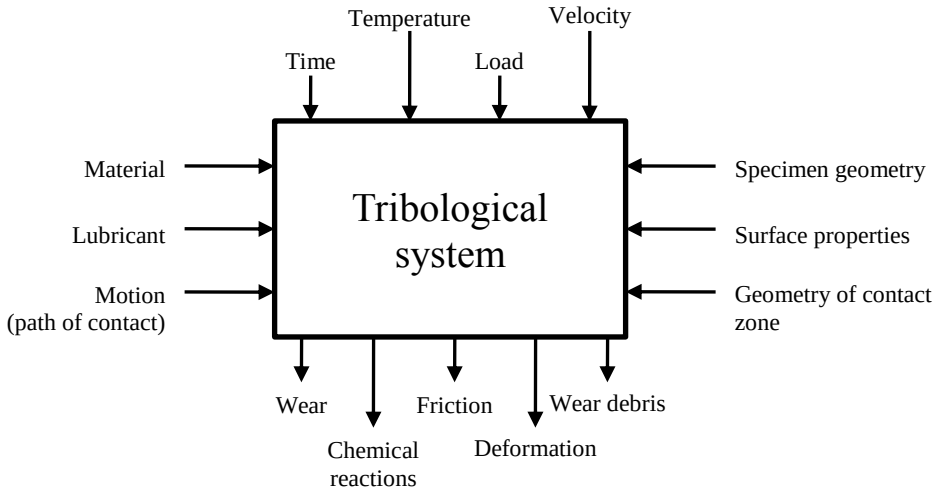

Figure 2-6: Parameters that influence a tribological system [50]

Due to microscopic roughness the real surface contact area is much smaller than the nominal surface area, and under static conditions with moderate loads this area is proportional to the contact force. Logically the contact area increases proportionally as the load increases until it becomes as large as the nominal area. On the other hand softer materials will deform and smear out over a harder counter surface, causing the real contact area to be equal to the nominal area. This effect can be seen in Figure 2-7.

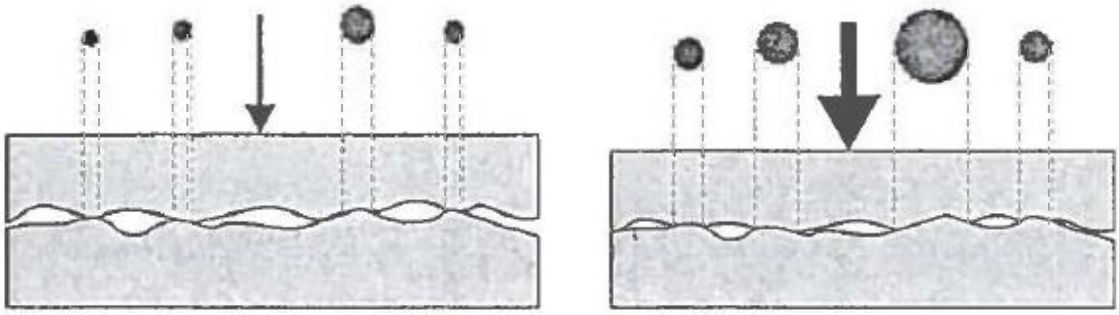

Figure 2-7: Growth of contact area by increased load [50]

In a tribological contact wear will ultimately ensue. This means loss of material from a contacting surface, but not necessarily from the system. Particles can often be trapped between the surfaces or embed themselves into the other surface. Wear is governed by many different mechanisms, of which four are most commonly used to explain wear:

Adhesive: Here the two contacting surfaces will cold weld together due to high contact pressure in small asperities. When movement follows, material will transfer from one surface to the other.

Abrasive: Caused by particles, grit or asperities harder than the contacting surface. These are often oxides that are trapped between the surfaces and they cause either two-body or three-body wear as seen in Figure 2-8. Other mechanisms are plowing, fracturing, fatigue and grain pull-out, as shown in Figure 2-9.

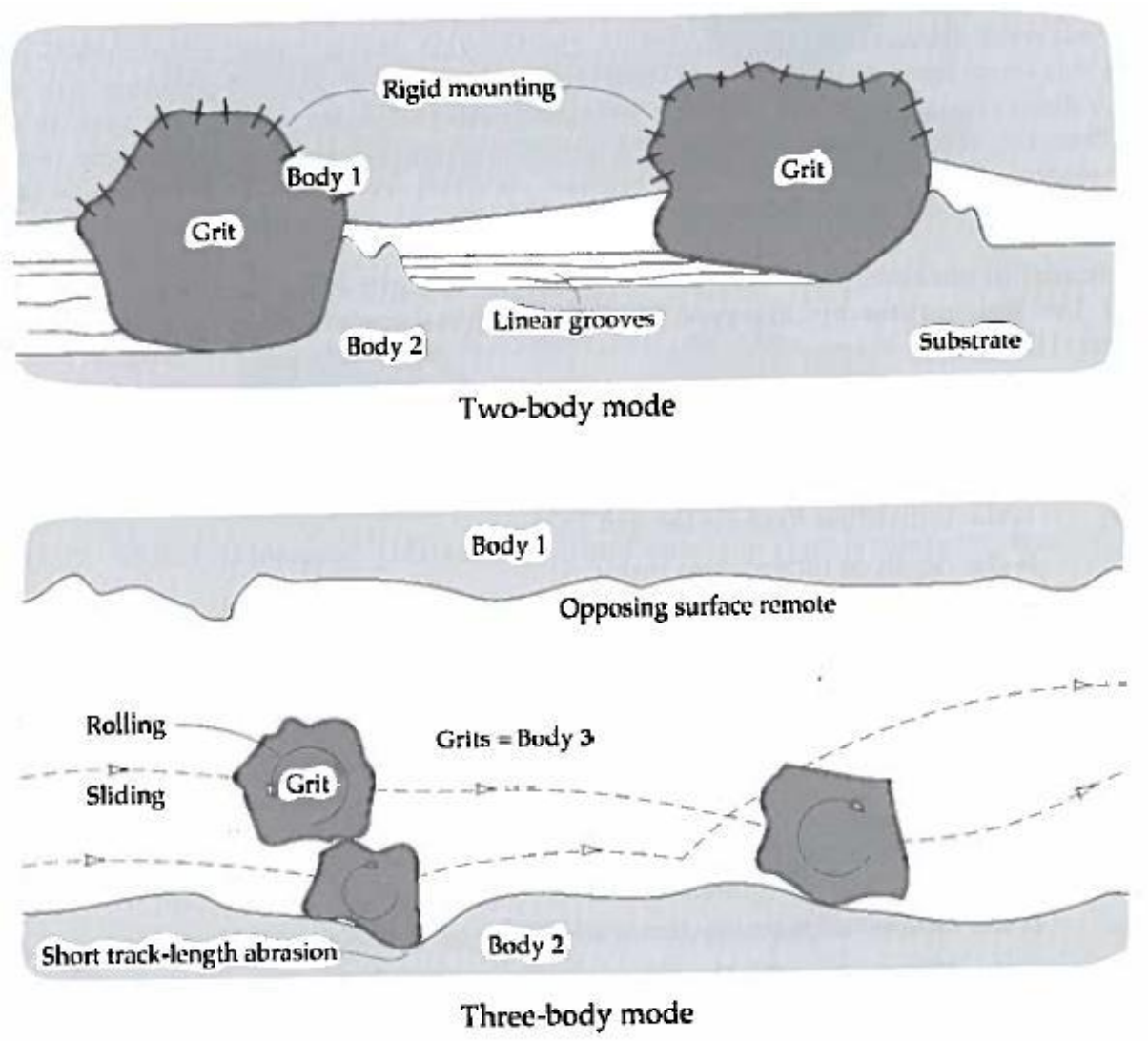

Figure 2-8: Two-body and three-body abrasion mechanisms [51]

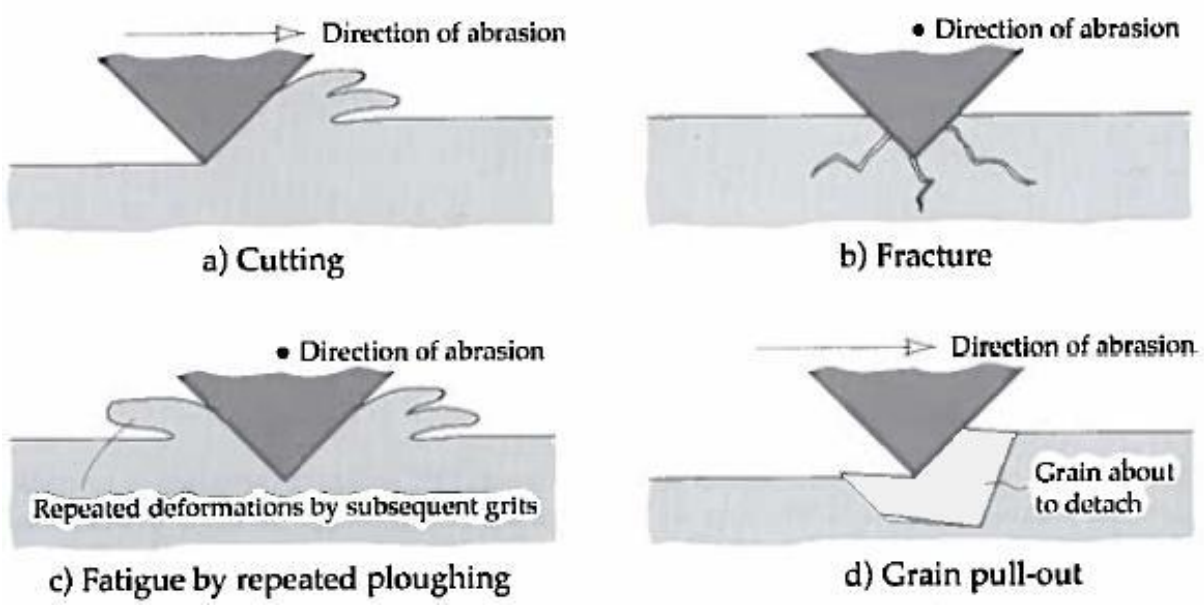

Figure 2-9: Abrasive wear mechanisms [51]

Fatigue: This mechanism is caused by repeated motion and changing load, such as repeated sliding motion on an area where the load is continuously changing within the same region. Figure 2-10 shows the repeating movement of a pin-on-plate tribological system, and Figure 2-11 shows the development of a fatigue crack.

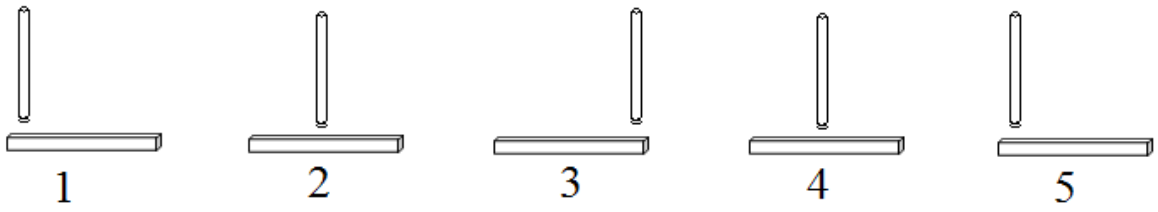

Figure 2-10: Reciprocal movement of pin-on-plate system [52]

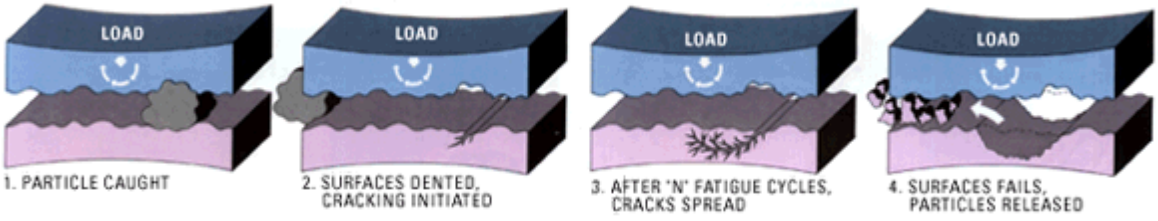

Figure 2-11: Fatigue wear mechanism [51]

The fourth mechanism is tribocorrosion, and, as this is more important with regards to the experiments, it will be given a more thorough explanation later.

2.2.2. Tribology of a hip joint

The hip joint has a cyclic load motion which lasts for about 1.2 seconds during normal walking. The sliding velocity during this motion ranges from zero to 100 mm/s, adding to this the loads on the surfaces vary dramatically during the cycle. It can actually reach as high as four times the body weight, as seen in Figure 2-12. The peak loads correspond to the points with lowest sliding velocity, and conversely the lowest loads are during the highest velocities. Thus the highest loads are only generated for a brief moment of time, while the low loads occur in periods up to half a second CITE RAGNHILD.

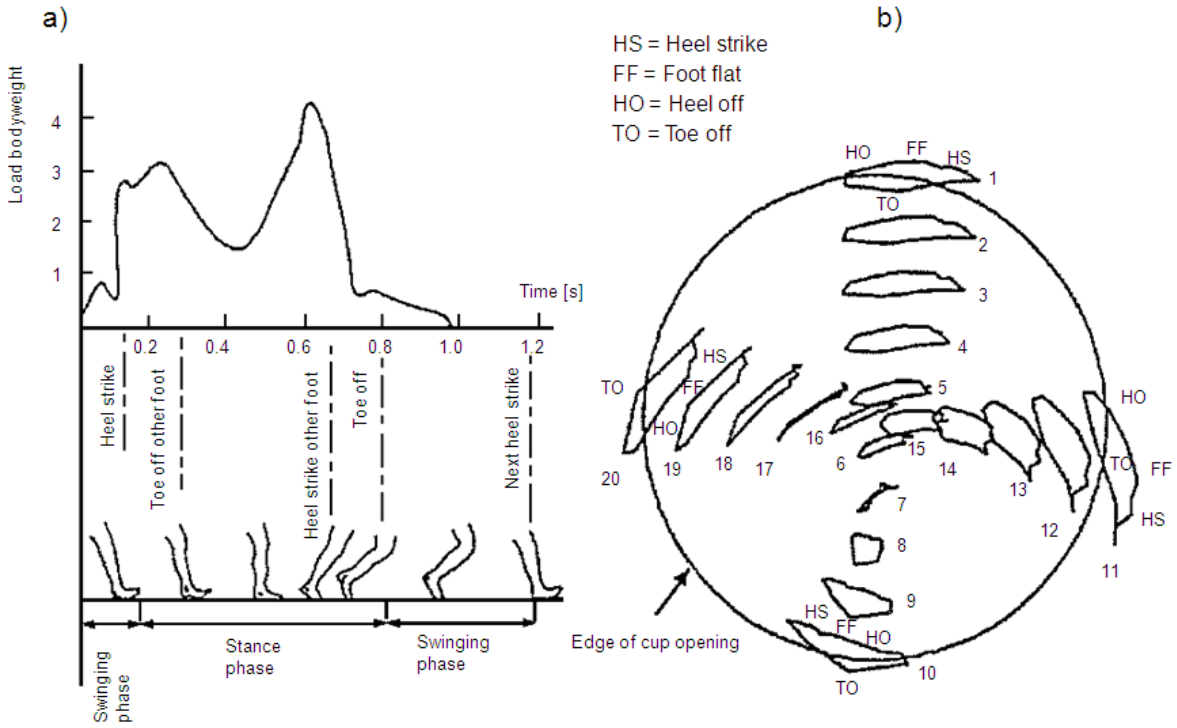

Figure 2-12: (a) Hip joint forces [53]. b) Patterns traced by 20 points on the femoral head against polyethylene during one cycle of gait. Physiological clinical gait pathways are used [54].

2.2.3. Electrochemistry and tribocorrosion

While both the effects of electrochemical and mechanical degradation of materials and devices are well known, and their fields thoroughly and extensively researched, the combination of these two fields has only relatively recently gained attention. The field of tribocorrosion is constantly growing, and researchers are getting more and more aware of its use and importance. Though not all of the mechanisms and effects are fully understood, there is no doubt that these effects are present and must be

taken into consideration when designing and developing, for instance, medical devices.

When a surface is introduced to an electrolyte, passivizing layers of oxides tend to form on the surface, causing the material to stabilize and become electrochemically inert. The stability of this passive layer determines the materials resistivity to further electrochemical reactions. For instance, iron has the tendency to form iron(II)oxide and iron(III)oxide on the surface. These are not very strong and stable layers and tend to flake off due to the flow of the electrolyte or some mechanical contact. This causes the surface to become active once more, and the whole process “eats away” the metal in a third-body type of wear mechanism. Aluminum on the other hand forms a very stable and tough surface layer of alumina, and makes it very corrosion resistant.

As mentioned mechanical breakdown will remove the passivizing surface layer, thus exposing the underlying surface for more electrochemical breakdown. And this is where the field of tribocorrosion comes into play. The combination of both electrochemical wear and mechanical wear has proven to give a synergetic effect causing a wear much more severe than the pure summation of the separate effects. If one is to measure the volume loss from electrochemical and mechanical wear separately and sum this up, it would not be comparable to the volume loss of a tribocorrosion contact. The wear debris caused by wearing down the oxide layer is much harder and more abrasive than the metallic wear debris. This will cause a larger mechanical wear and in turn make a surface more susceptible to electrochemical wear and ion release, as seen in Figure 2-13 [55] [56] [57].

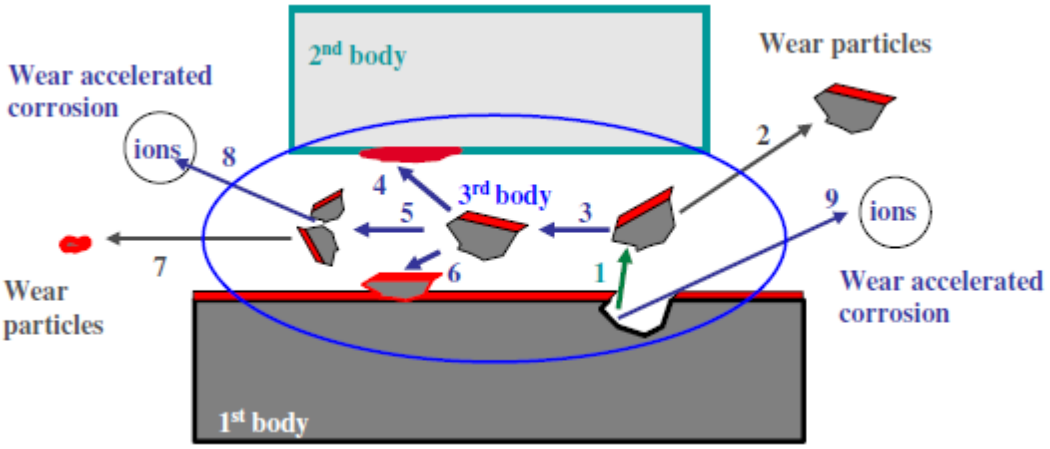

Figure 2-13: Third body tribocorrosion mechanism [58]

To create an environment with stable and selectable pH a buffer is used as electrolyte, with the addition of Sodium Chloride (NaCl) to simulate the salinity of the body fluid. While the pH of a human body is very individual, and subject to much fluctuation, the normal convention is a pH of 7.4 for a healthy human being, which is achieved with a Phosphate Buffered Solution (PBS) [59]. Inflammation or immunological reactions will cause the pH to lower, and a pH of 5.2 is seen as a good simulated value [14].

Table 2-2: Data for Standard Bulk Metallic Glasses, source unknown

Series	Alloy composition (features)	Critical Diameter (mm)	Standard Diameter (mm)	T_g (K)	T_x (K)	T_l (K)	E (GPa)	ε_y (%)	σ_y (MPa)	CUE (kJ/m^2)
Z Alloy	Z1 Zr50Cu40Al10 (Ternary Eutectic)	14	10	706	792	1092	88*	2.1*	1860*	104
	Z2 Zr55Cu30Ni5Al10 (High Glass-Forming Ability)	30	10	683	767	1163	90*	2.0*	1830*	125
	Z3 Zr60Cu20Ni10Al10 (High Proof against Structural Relaxation Embrittlement)	20	10	662	754	1164	80	2.2	1750	87
	Z4 Zr65Cu17.5Ni10Al7.5 (High Stability of Supercooled Liquid)	16	10	625	750	1164	82	1.9	1528	85
C Alloy	C1 Cu36Zr48Al8Ag8 (High Glass-Forming Ability)	25	10	683	792	1142	102	1.8	1850	-
	C2 Cu42Zr42Al8Ag8 (High Strength)	14	10	705	780	1213	108	1.8	1986	-
T Alloy	TN Ti50Cu25Ni15Zr5Sn5 (High Corrosion Resistance)	5	3	706	765	1245	105	1.9	2070	-
	TP Ti-Based BMG (Biomaterial)	10	5	689	739	1126	118	1.7	2000	-

***: tensile test data. The others for E (Young's modulus), εy (Yield Strain), σ_y (Yield Stress) are data under compression.**

The abbreviation CUE stands for U-notched Charpy Energy, and T_g, T_x, T_l are symbols for glass transition temperature, crystallization temperature and liquidus surface temperature, respectively.

2.2.3.1.1. Biocompatibility

That a material is biocompatible means that it does not induce reactions with cells, or the environment in the body, that will degrade the material in any way. A good definition that really gives an understanding of biocompatibility is as follows:

> *"Biocompatibility is the ability of a material to perform with an appropriate host response in a specific application"* [60]

How well a material behaves in the human body depends on its bulk properties as well as its surface properties, both on the nanometer and micrometer scale. This means that different alloys can behave quite differently under the same conditions. It has been shown that some BMGs have a strong adhesion of proteins and cells, similar to crystalline metals. Fibroblasts have displayed monolayer formation and good attachment on BMGs, while crystalline metal gave poor attachment. BMGs have also shown clustering of foreign body giant cells, which is a normal implant response, and an overall normal foreign body response. Studies have concluded that BMGs are generally non-toxic towards cells, compatible with cell growth and tissue function, and generally useful for implant purposes [38].

The elasticity of the BMGs makes them unique in the way that they can flex with the bending of the bones and thus distribute the stresses more uniformly, resulting in faster healing rates and lessened or no osteolysis. Some BMGs may even also surpass the crystalline counterparts with regards to MRIs, and they all seem to be at least comparable to current implant materials with regards to biocompatibility [61].

To increase the biocompatibility it is also important to consider the alloying elements and whether or not they can be replaced to give a BMG with better biocompatibility, and even better mechanical properties. Elements that are cytotoxic include copper, nickel and aluminum. Some BMGs show better wear resistance than commonly used metals and with similar or better cytotoxicity and cell viability [62] [63] [64].

2.2.3.1.2. Corrosion behavior

Apart from the excellent mechanical properties that several amorphous alloys have shown, they are also turning out to have rather astonishing corrosion properties compared to crystalline metals. The reason for this is mainly that they are chemically and structurally homogeneous. This results in the lack of local electrochemically active sites, which promote corrosion. The fact that they can be tailored to consist of almost any metal combination also make them extra resistant towards corrosion if one chooses to use strongly passivizing elements [65]. However, some BMGs are prone to pitting corrosion. This is believed to be caused by microcrystalline inclusions in the amorphous matrix, but it is possible to reduce by increasing the glass forming ability [66].

This corrosion behavior can be explained from the fact that the BMGs are formed at relatively low cooling rates, therefore they often end up with a more heterogeneous chemical structure. This leads to the formation of secondary crystalline phases, oxide particles which act as chemically active sites susceptible to corrosion. Apart from this generalization, the diversity of BMGs makes it a bit difficult to comment in general on the corrosion properties of BMGs. It is therefore advisable to seek out information and research done on similar BMGs if one is to explore the properties and uses of a particular material [41].

3. Experimental

3.1. Materials

Two different materials were chosen to compare with the performance of the BMG. These materials are the most frequently used metal materials for hip-implants.

3.1.1. Ti 99.6 %

Pure Ti 99.6 % (ASTM F67) has been a regular choice for implant material, because of its inherent biocompatibility and strength vs. weight ratio. Because of its commonality and biocompatibility it has been chosen to be a reference to the BMG [22]. The composition is given in Table 3-1. It should be noted, however, that this is not a material used for wear surfaces.

3.1.2. Surgical Grade CoCrMo-alloy

This highly alloyed material is often used because of its great corrosion resistance, and good mechanical properties. It is as of this date the only metal used for articulating surfaces in hip implants [31] [14] [67] [13]. It is, however, alloyed with materials that have proven to be cytotoxic [11] [68]. The material used in this study was the Bioline ASTM F75 produced by Sandvik Materials Technology. Composition is given in Table 3-1.

3.1.3. Zirconium based BMG $Zr_{65}Cu_{18}Ni_7Al_{10}$

This low copper, low nickel BMG is a brand new alloy from Tohoku University in Sendai, Japan. It has never been tested before, but its low content of aluminum, copper and nickel gives promise of a good biocompatibility. Other zirconium-based BMGs have been tested in earlier experiments and their biocompatibility and mechanical properties have already been established [52] [61] [67]. However, a few micro hardness tests were perform to establish within what range the hardness of the material was. The material contains several elements that are regarded as cytotoxic, but this aspect has been discussed elsewhere [52] [69].

Table 3-1: Chemical Compositions of Metals Used for Implants, [70] [71] [72]

Material	ASTM	Composition (wt. %)	Vickers Hardness (HV)
CoCrMo	F75	58.9–69.5 Co	310
		27.0–30.0 Cr	
		2 5.0–7.0 Mo	
		max 1.0 Mn	
		max 1.0 Si	
		max 2.5 Ni	
		max 0.75	
		max 0.35 C	
Ti 99.6 %	F67	Balance Ti	200
		max 0.10 C	
		max 0.5 Fe	
		max 0.0125–0.015 H	
		max 0.05 N	
		max 0.40 O	
BMG		65 Zr*	440**
		18 Cu*	
		7 Ni*	
		10 Al*	

***Atomic percentage**

****Based on two micro hardness tests**

3.2. Polarization tests

Polarization tests were performed on all materials to determine the corrosion potential (E_{corr}), and open circuit potential (OCP), used in the tribocorrosion tests. A set-up was done using the Autolab PG-STAT 302 and NOVA software with a silver – silver chloride (Ag/AgCl) reference electrode. The set-up is described in Figure 3-1 and Figure 3-2, and in Table 3-2. The experimental parameters for the experiments are given in

Table 3-3, and were chosen according to [52].

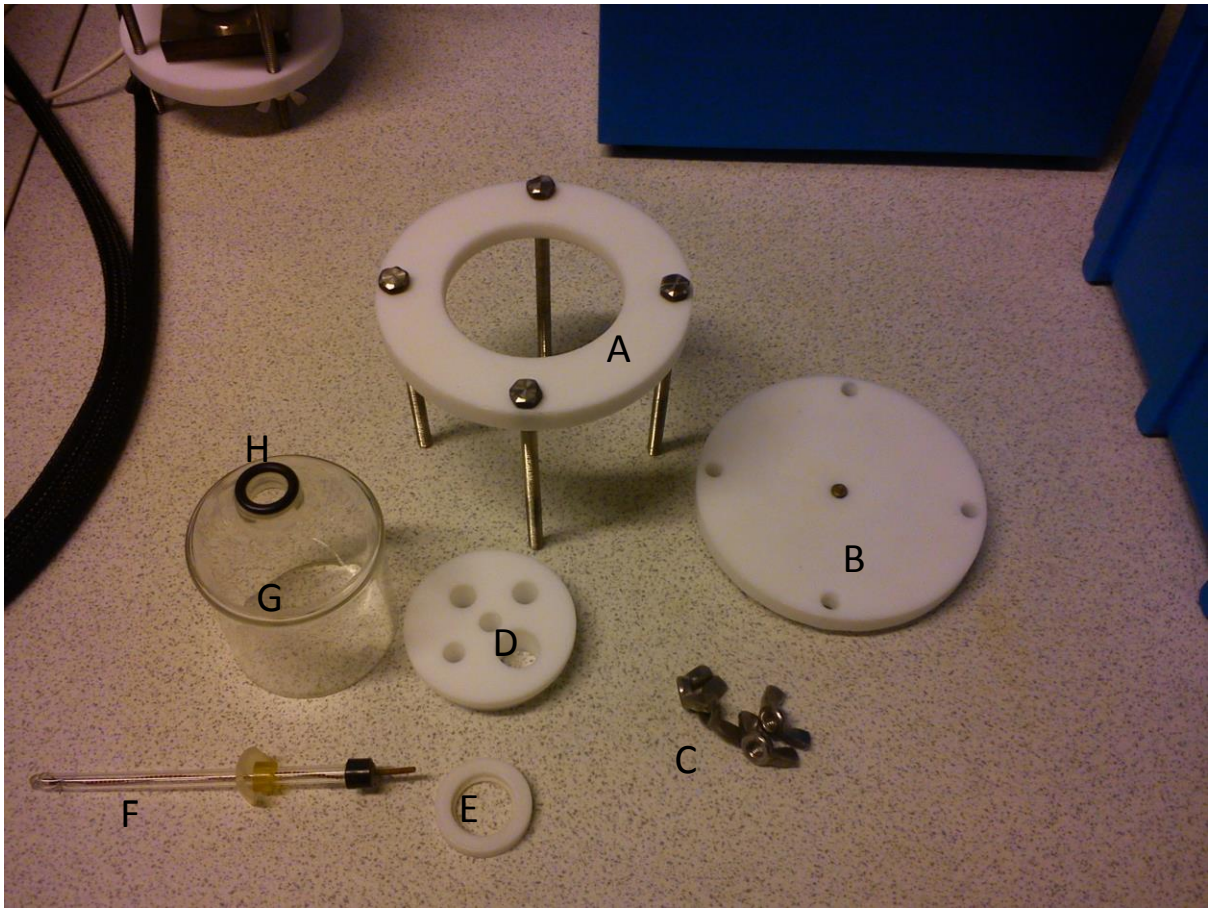

Figure 3-1: Electrochemical cell before assembly

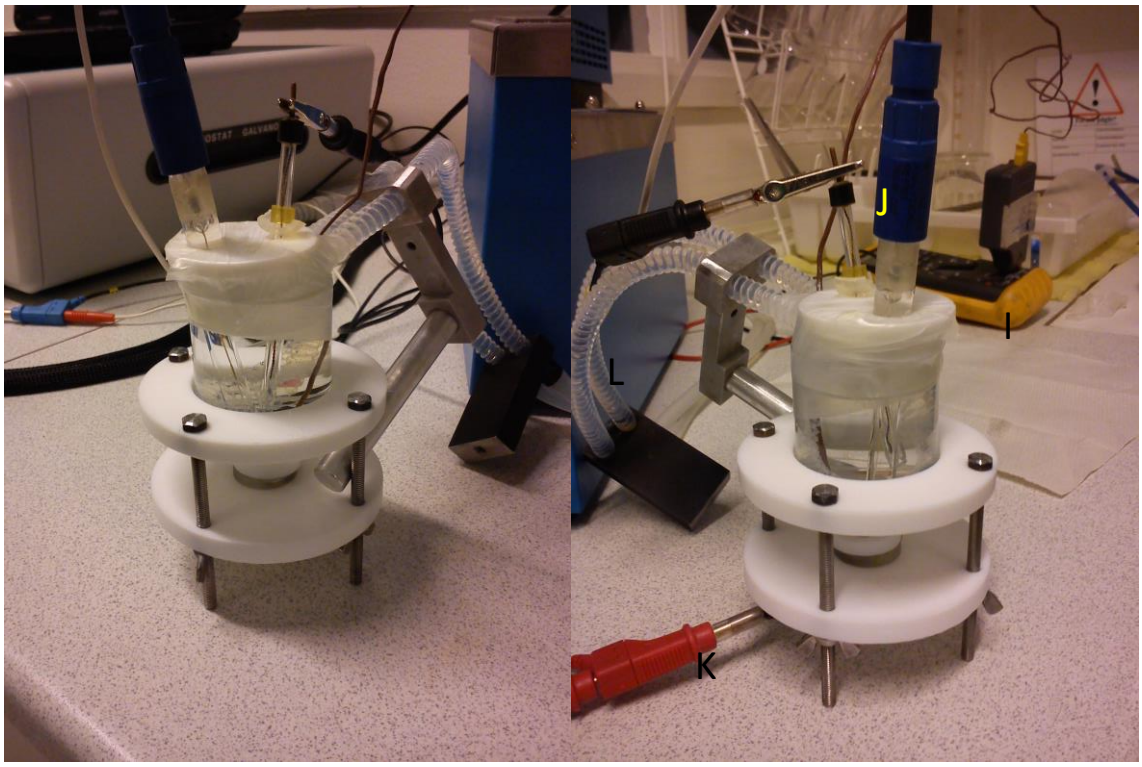

Figure 3-2: Electrochemical cell after assembly, with sample, connected electrodes, thermometer and heating

The set-up was covered with a plastic film to hinder evaporation of the electrolyte.

Table 3-2: Electro chemical set-up

Name	Part
A	Clamp
B	Bottom plate with WE connection
C	Wing nuts
D	Lid
E	Seal holder
F	Counter Electrode
G	Electrolyte cell
H	O-ring seal
I	Multimeter with thermometer add-on
J	Ag/AgCl Reference Electrode
K	Work Electrode connection
L	Heater

Table 3-3: Electro chemical parameters

Parameter	Value
OCP determination [s]	600
Potential range [mV]	- 700 to + 700
Sweep [mV/min]	5

3.3. Dry tribological testing

Dry tribological testing was performed on all materials to assess the friction force without liquid and protein as possible lubricants. The set-up is similar to that of the tribocorrosion test, but without the electrodes and electrolyte as seen in Figure 3-3 and Figure 3-4.

3.4. Tribocorrosion testing

All samples were subject to a tribological wear tests, using PBS and PBS with added HCl, to lower the pH, as electrolytes. Protein was also added to each electrolyte to test the effect it has on the tribocorrosion regime. The set-up is described in Figure 3-3 and Figure 3-4, and the parameters of the tribocorrosion tests are according to [52], and are given in Table 3-4.

Table 3-4: Tribocorrosion parameters

Parameter	Value
Normal force [N]	2
Frequency [Hz]	1
Cycles	3600
Track length [mm]	5
Velocity [mm/s]	10
Dwell time [s]	0.001

Before the tests were started, the samples would be immersed in the electrolyte for 10 minutes while data was gathered, to establish an OCP value. After 10 minutes the rubbing motion was started.

3.4.1. Sample preparations

All samples were grinded (Struers Knuth-Rotor) with #500P, #1200P and #2400P SiC paper for at least two minutes or until the grind marks from the preceding treatment had disappeared.

The samples were then polished using Struers DPU-3 at 150 RPM with successively 6µm MD-Mol, 3µm MD-Mol and 1 µm MD-Nap cloths accompanied by DP-Spray M with corresponding grain size.

An exception had to be made for the Ti 99.6 % because this material is extremely ductile and prone to mechanical deformation. Therefore a solution of silica and hydrogen peroxide was used to fine polish the surface. Grinding with SiC paper was also avoided, instead a diamond suspension was used. The method used is as recommended and described by Struers [73].

3.4.2. Electrolyte

To simulate the pH and salinity of the body, while keeping the system as simple as possible with a minimum of variables a Phosphate Buffered Solution with 0.9 % NaCl was chosen. The PBS was prepared as described elsewhere [14] [13]. A solution with pH 5.2 was chosen to simulate a body suffering from an inflammation or immunological reaction. The solution to this was to add HCl to the regular buffer to lower the pH as done earlier [14]. This is, from a chemistry point of view, deemed to be a wrongful use of a buffer; adding acid in such amounts to a buffer not only weakens the buffer capacity, but may all together destroy the very functionality and purpose of the buffer. The buffer capacity is the ability of the buffer to neutralize any added protons or hydroxyl groups while still maintaining a constant pH, and is measured in millimoles (mM). The addition of HCl to the PBS to lower the pH is therefore not a good solution, since the sole purpose of a buffer is to keep a stable pH. The pH of 5.2 is well outside the buffer capacity of the PBS buffer, and thus makes for a more unstable pH, which needs to be controlled often. The reason for doing this, however, is that a more suitable buffer such as sodium acetate, which has the pH of 5.2, has not been frequently used in earlier works [8] [11] [52] [55] [14] [68]. Thus the effects of it and the behavior of the metals in contact with it is, as of

yet, not well known. The unpredictable behavior of the materials in this electrolyte may be caused by an unstable buffer, or unknown reactions with metal ions as acetate ions are fairly reactive towards metal cations. Therefore a modified PBS was seen as the best solution.

The protein added was bovine albumin protein, with a concentration of 2 g/L. The isoelectric point of albumin has been reported to be 4.7 [74], which is lower than the pH used in the two solutions. This means that the proteins will be negatively charged in both solutions, and thus attracted to the surface when it is positively charged.

The surface is positively charged depending on the oxides forming on the surface. Titania has an isoelectric point between 3.9 and 8.2 [75] which means that in both electrolytes it has zero charge on the surface.

Zirconia is reported to have a pI of 4-11 [75], and will remain neutral in both pH solutions.

Chromia has a pI between 6.2 and 8.1 [75] meaning that for the low pH electrolyte the surface will be positive, while it will remain neutral in the high pH solution. Furthermore Molybdenum has a pI of 2.5, rendering it negatively charged in both electrolytes [76].

This adsorption behavior can be observed in the OCP measurements of the materials in electrolytes with protein. During the sweep, the proteins would then adsorb to the surface due to the opposing charges of the oxide and the protein, and cause changes and disturbances in the data acquired.

3.4.3. Measurement

A custom built corrosimeter was used to measure the tribocorrosive properties of the materials. The experimental set-up is described in Figure 3-3 and Figure 3-4 and explained in Table 3-5.

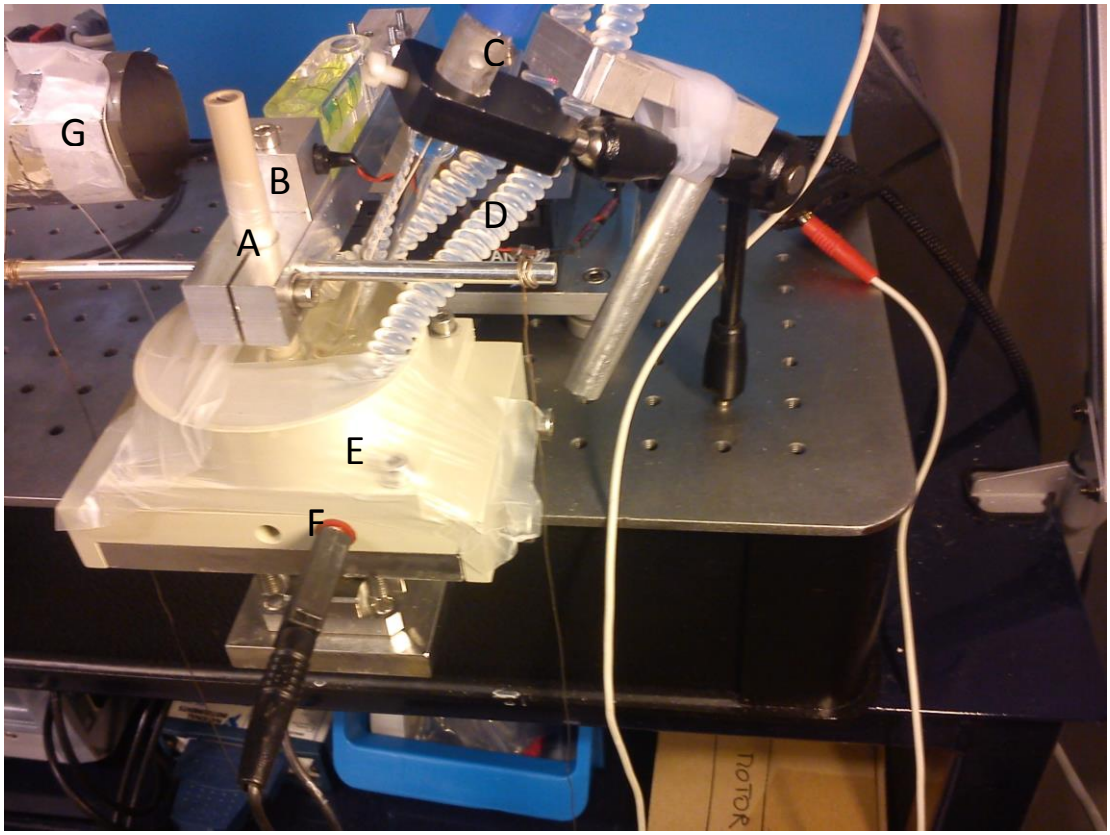

Figure 3-3: Tribocorrosion set-up

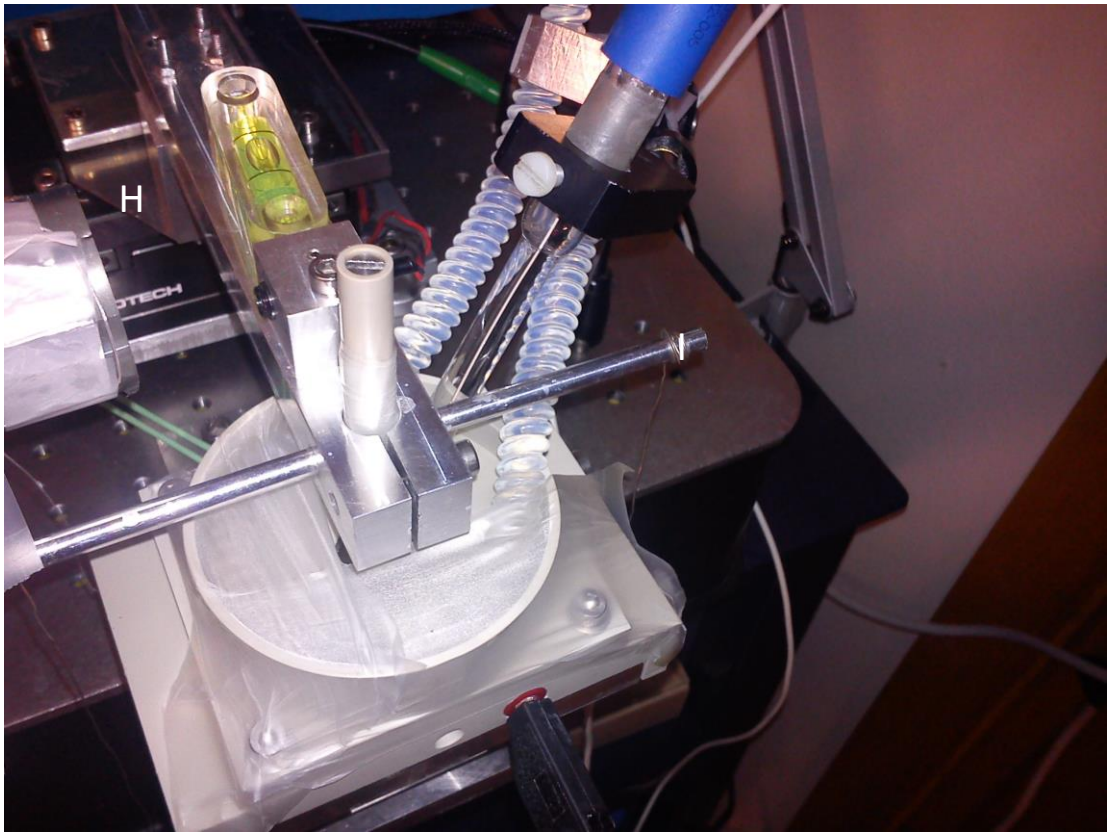

Figure 3-4: Tribocorrosion set-up

Table 3-5: Description of Tribocorrosion set-up

Part	Description
A	Pin with alumina ball
B	Trigger LASER
C	Reference Electrode (Ag/AgCl)
D	Heating
E	Electrolyte cell
F	Work Electrode
G	Trigger tube
H	Motor
I	Load arm

The set-up is a reciprocating pin on plate configuration consisting of a 6 mm Ø alumina-ball placed in a moving arm connected to a load cell and an interchangeable load. For the tribocorrosive test the electrolyte is filled in the cup in which the sample sits at the bottom of. A reference electrode is placed in the electrolyte and is, along with the sample, coupled to a potentiometer. The heating system was placed in the cup and set to reach 37 °C, and a thermometer was used to control the electrolyte temperature. A trigger system is used to control the data acquisition and reduce noise, and a plastic film covered the cup to hinder evaporation.

3.5. Confocal Microscopy

To further assess the influence of tribocorrosion on the surface, confocal microscopy is used to model and analyze the surface in 3D, to obtain data on surface profile and wear volume. Simply explained the confocal microscope is a scanning fluorescence microscope that utilizes a conventional light (or LASER light), scanning mirrors and a pinhole aperture to create several images with a small depth of field as seen in Figure 3-5. A computer then collects these and builds them together into a clean, three-dimensional image [77].

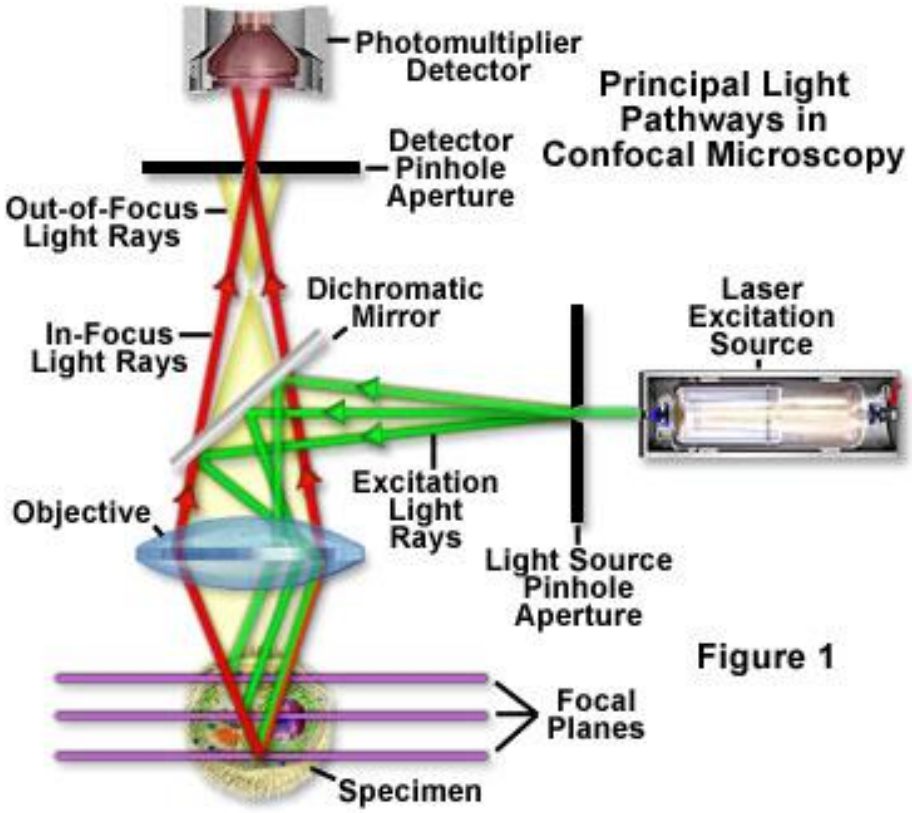

Figure 3-5: Structure and pathways of a confocal microscope [78]

4. Results and discussion

4.1. Polarization tests

The pH in the PBS was determined to be 7.4 with some variance; the variance in the pH is most probably caused by inaccuracy in measuring the different ingredients of the electrolyte solution. The pH of the low pH solution was measured to be 5.2, which was the expected value. The low pH solution was measured several times during the course of its use to confirm that the pH was stable. Also the low pH protein solution was only added the HCl directly before use, to diminish the degradation factor of the proteins by the low pH.

The temperature was measured several times during the experiments and was found not to reach 37 °C in the whole electrolyte. The temperature was in fact consistently around 34 °C at the sample surface. The deviance in temperature between the bulk of the electrolyte and at the sample surface may call for a stirring effect in the electrolyte, but since this is OCP measurements, stirring is not an alternative. Another option is to increase the bulk temperature to ensure a higher temperature at the surface. This is, however, not suitable with the combination of proteins used in the solutions, since they would denaturize if the temperature in the bulk has to be relatively high to reach body temperature at the sample surface. Some increase in temperature is possible, however, and further experimentation on this may be needed to find best practice.

The polishing left all the samples with a mirror finish indicating a surface with roughness of only a few hundred nm.

The deviances in the results between the samples of the same material can be explained by the simple fact that they all have minute differences in surface conditions due to material properties and surface preparation. Some of the differences in OCP values are unavoidable, but they are mostly small enough to be negligible. In the cases where the deviation was deemed too large, the experiments were done several times to find results consistent enough.

A summary of the OCP values can be found in Table 4-1.

Table 4-1: Results of LP-tests

Solution/Material	Ti 99.6 %	CoCrMo	BMG
PBS	-0.27	-0.22	-0.13
PBS w/protein	-0.32*	-0.2*	-0.16
PBS pH 5.2	-0.2	-0.12*	-0.21
PBS 5.2 w/protein	N/A*	-0.04*	-0.19

*OCP value based on only one data set

4.1.1. Ti 99.6 %

4.1.1.1. PBS 7.4

E_{corr} was found to be -0.27 V on average for Ti 99.6 %in PBS, as shown in Figure 4-1. For Ti 99.6 % in PBS with protein it was found to be approx. -0.32 V.

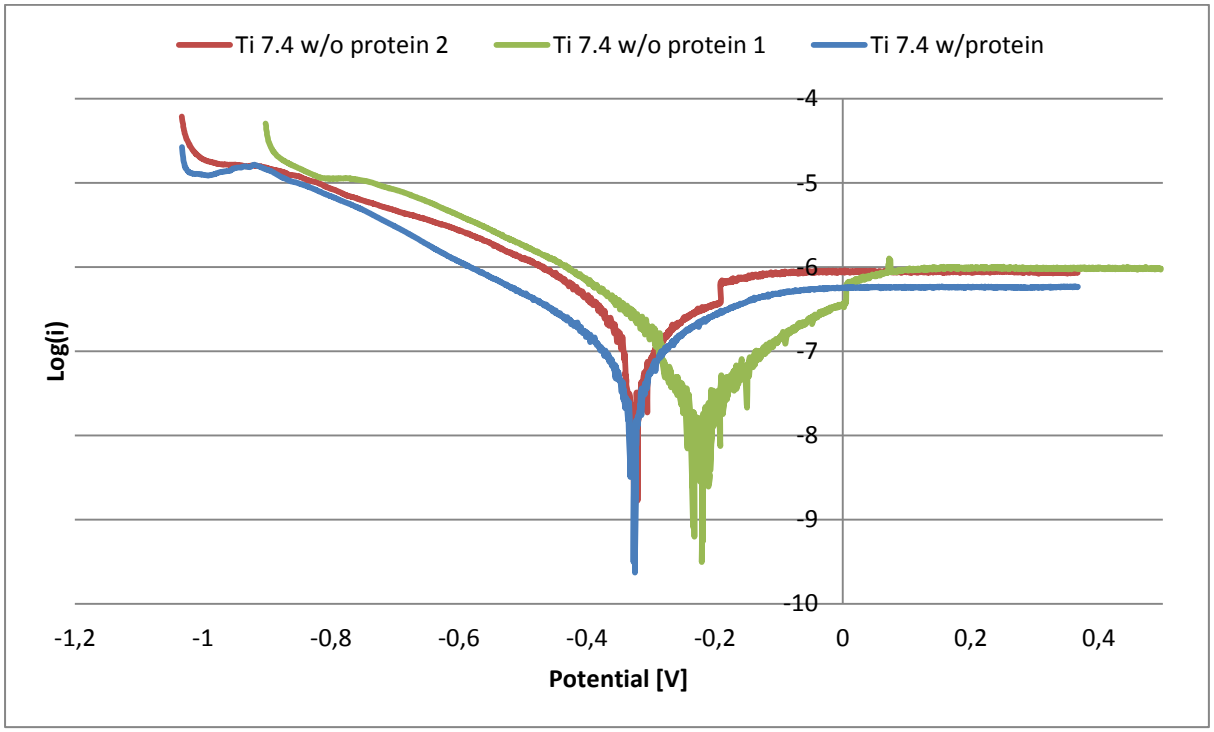

Figure 4-1: E-Log(i) for Ti 99.6 % in PBS

The polarization curves for pure Ti 99.6 % in PBS (Figure 4-1), show a lot of sudden drops in the current around the corrosion potential. These drops in the curve and width of the OCP-drop around -0.2 V is most likely caused by hydrogen bubbles forming at low potential and releasing during the experiment causing

disruption in the measurement. All tests show that the material is passive in every solution. Figure 4-1 shows that the current is lower for the protein solution; this is due to proteins in the solution adsorbing on the surface, and is as expected. The differences in the two curves done without proteins can be caused by differences in surface conditions. This shows, however, that the repeatability might be low, and that more tests should be conducted to fully establish the OCP. Only one test was done with proteins due to time constraints, but the seemingly more cathodic OCP might indicate a lower corrosion resistance.

4.1.1.2. PBS 5.2

E_{corr} was found to be -0.2 V for Ti 99.6 % in PBS with added HCl, for the protein solution it was indeterminable as shown in Figure 4-2.

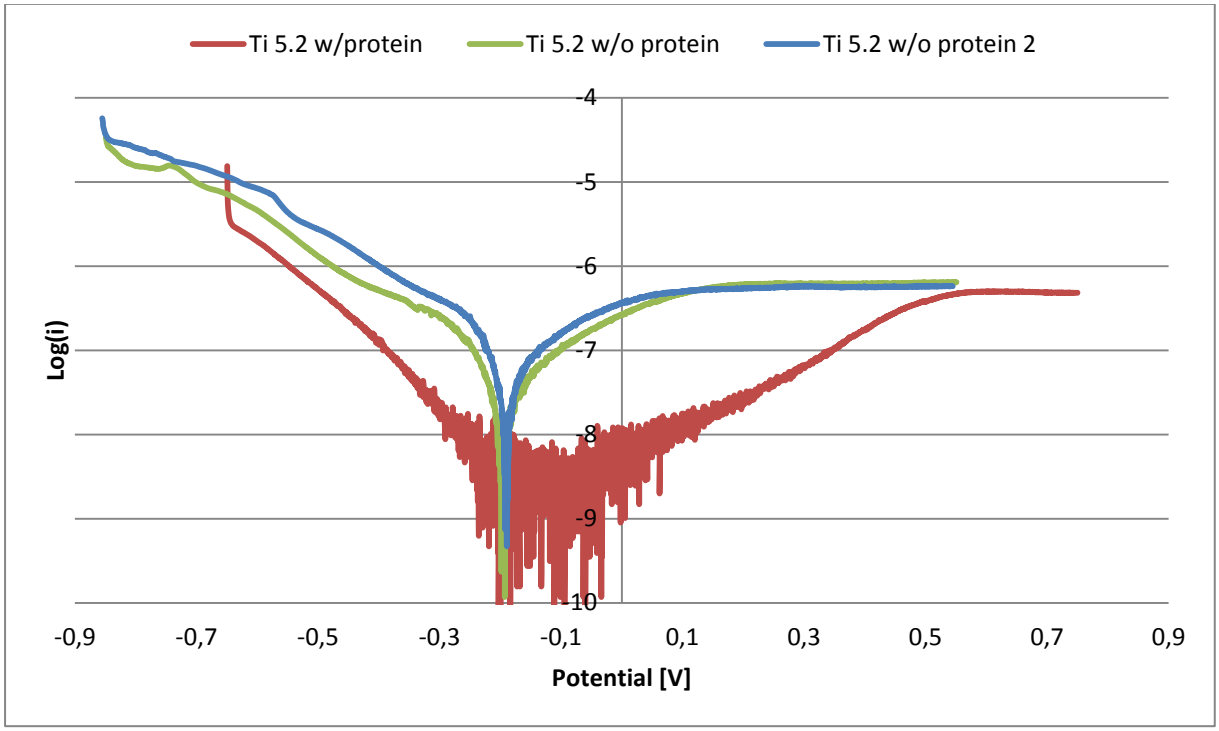

Figure 4-2: E-Log(i) for Ti 99.6 % in PBS with pH 5.2

Ti 99.6 % in PBS with HCl has OCP values very close to -0.2, and has a stable passive region.as seen in Figure 4-2. This can be explained by the fact that Ti 99.6 % forms a quite stable oxide layer. Evidence of this is found when comparing the pourbaix diagram for Ti Figure 0-4 and the LP results (Table 4-1). Here Ti will form TiO_2 for all pH values larger than 0 for the OCPs found in these experiments. The

protein solution has clearly a lowered current and adsorption causing the instability of the readings in the region around OCP. This makes OCP more or less impossible to determine, and is possibly caused by adsorption of proteins on the surface. This is however a bit unclear, as the pI of TiO_2 is, as mentioned earlier, between 3.9 and 8.2, which is a very large region. According to this the titania should remain neutrally charged and not cause any adsorption, this does therefore not explain the behavior seen in the graph. The graph clearly shows some form of surface interaction, so it is possible that titania has a very unstable pI and that it may vary in different solutions thus causing it to be higher than 5.2 in this case, and thus render it positively charged. Furthermore it seems that the OCP might be more anodic, and that Ti 99.6 % is less prone to corrosion with proteins at this pH.

4.1.2. CoCrMo

4.1.2.1. PBS 7.4

E_{corr} was found to be on average -0.22 V for CoCrMo in PBS, and -0.2 for the protein solution. The results are shown in Figure 4-3.

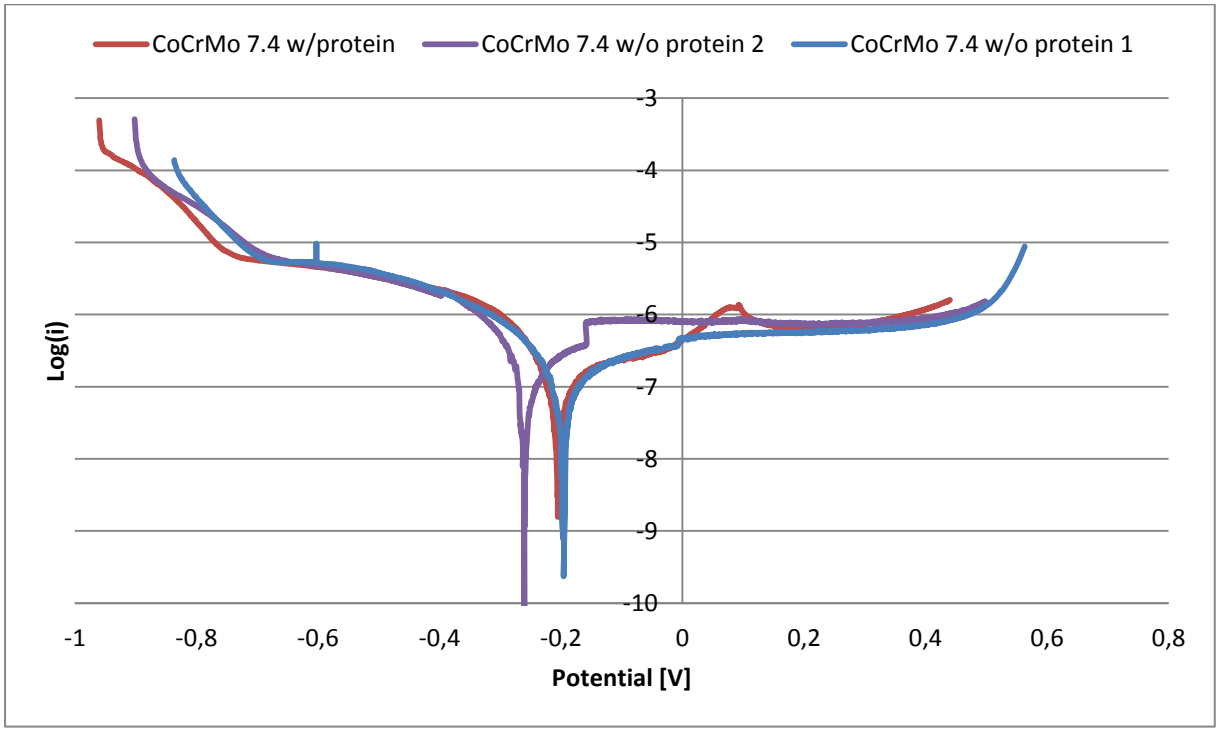

Figure 4-3: E-Log(i) diagram for CoCrMo in PBS

Earlier reports of tests done with CoCrMo in PBS with and without albumin protein have concluded that the addition of protein affect the potentiodynamic curves. In the cathodic domain, the protein diminishes the current slightly, while it shifts the corrosion potentials towards more cathodic potentials in the transition region. The phosphate ions have the opposite effect, except in the presence of albumin, and the albumin therefore determines the electrochemical behavior of the alloy in the transition domain. Furthermore the phosphate ions decrease the passive current, while the protein increases it [79]. Due to the low repeatability of the electrochemical experiments, it is difficult to see if this is truly the case in these results, but several similarities in the curves represented in Figure 4-3, such as the passive region and the shoulder also in the passive region, indicate that these results are comparable. The shoulder indicates a possible formation of ion phosphate complexes, which may activate transpassive dissolution [79]. Apart from this the material shows good passive behavior in the electrolytes. However, in these experiments it seems that proteins shift the curves towards more anodic values. This creates a system with less corrosion, and is not in accordance with [79]. With regards to isoelectric points Chromia has pI between 6.2 and 8.1 meaning that for the PBS the surface will be neutral, while in the low pH electrolyte the surface will be positive. This makes it possible for a good adsorption of proteins on the material surface at this pH. As mentioned, the repeatability of these experiments is low as well, and therefore it is necessary to do more experimentation to establish an exact OCP. The higher OCP for the protein experiment might imply a higher resistance to corrosion, which is in accordance with earlier findings [79].

4.1.2.2. PBS 5.2

E_{corr} was found to be -0.12 V for CoCrMo in PBS with HCl, with protein added it was found to be around -0.04 V. The results are shown in Figure 4-4.

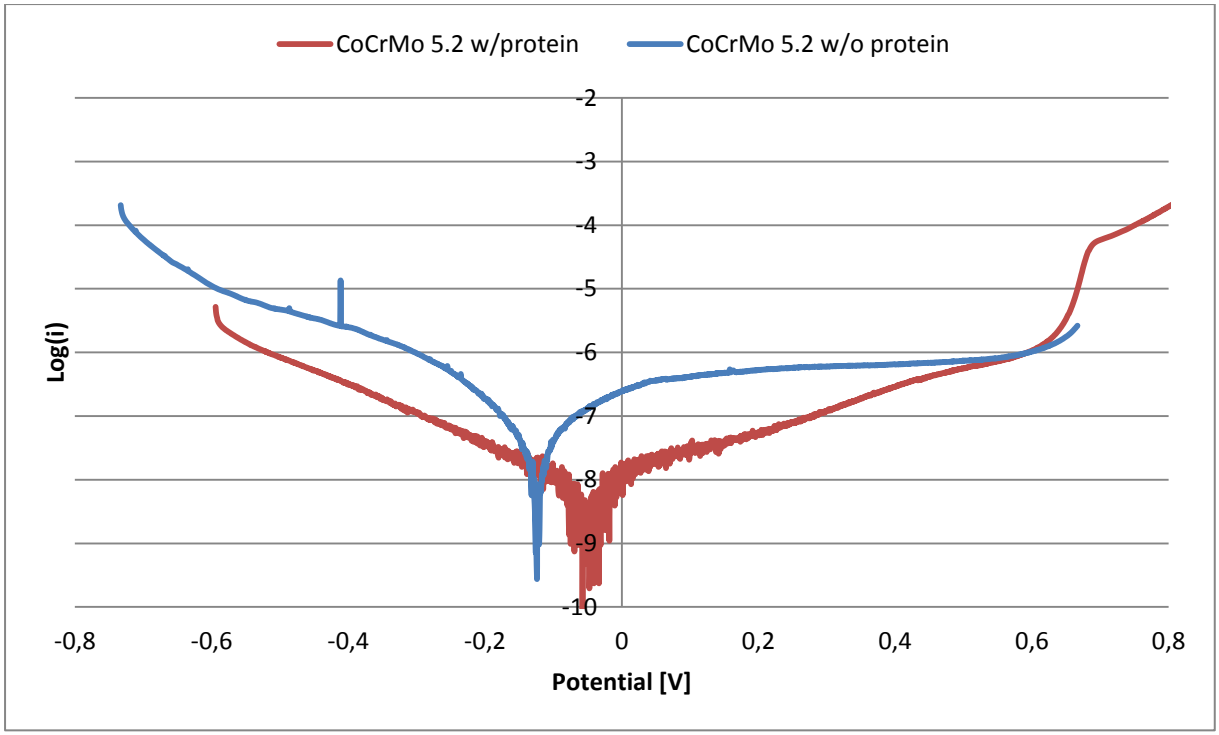

Figure 4-4: E-Log(i) diagram for CoCrMo in PBS with pH 5.2

The CoCrMo alloy shows passive behavior for both electrolytes, which is evident when the OCP results in Figure 4-3 and Figure 4-4 are compared to the pourbaix diagram for both chromium (Figure 0-1) and cobalt (Figure 0-2) in Appendix A. Again the protein causes problems around the OCP due to adsorption, as suspected from the pI of chromia. Chromia will be positive, while the protein still has pI lower than pH and will be negative, and thus attracted to the surface. The OCP is clearly more positive in this pH, indicating that the material is less prone to corrosion in the solution with, and even more so with proteins. Here as well the material shows passive behavior in both electrolytes.

4.1.3. BMG

4.1.3.1. PBS 7.4

E_{corr} was found to be on average -0.13 V for BMG in PBS, and -0.16 for the protein solution. They are shown in Figure 4-5.

Figure 4-5 clearly shows the passivizing behavior of the BMG in the solution where proteins are present. There are, however, some differences in the tests with no protein, where the material shows both active and passive behavior. This

may be caused by unknown differences in structure and composition, and is evident in the fact that three different tests were done to confirm the OCP. Although the OCPs are the same for the two tests without protein presented here, their electrochemical behavior still differs; one shows active behavior, the other passive. While XRD tests were performed to confirm that the prepared samples used were amorphous, some crystalline inclusions were found in other parts of the BMG rod supplied. It is possible to assume that further crystalline inclusions exist through the bulk of the material, but they may be so small that the XRD used was unable to detect them and differentiate them from the background noise.

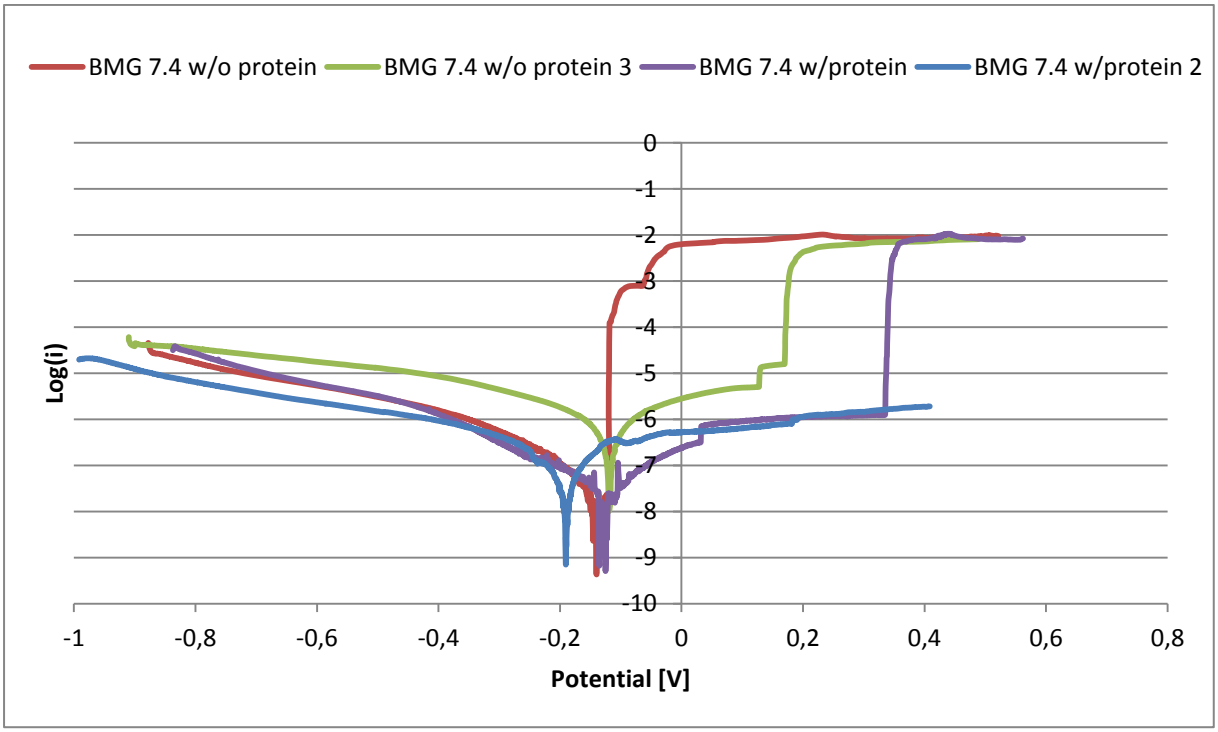

Figure 4-5: E-log(i) diagram for BMG in PBS

According to the Pourbaix diagram for zirconia (Figure 0-3 Appendix A), the material should be passive in this electrolyte and at this OCP, however earlier reports have shown that this active behavior is closer related to the copper alloying element [52]. When protein is introduced, the currents are lowered both in anodic and cathodic region, and an overall a more stable material behavior is observed. These results are not in accordance with earlier findings on higher alloyed Zr-based BMGs, and may call for further investigation to see of this is due

to the difference in composition [13]. Some protein adsorption might be detected in one of the tests, but the results are very unclear on this point, and further tests may give clearer answers. This does go against the information on the pI of zirconia, but the alloying elements may affect this behavior. Another more observable effect of the protein is the large impact on the current, where it shifts the curves at least one decade lower. The test showing active corrosion is at the same current density level, but this only shows that the surface conditions are so variable and that the adsorbance of proteins different form sample to sample. This calls for several more tests to be conducted, in order to establish electrochemical behavior more exact. One problem with this is that the OCP measurements often cause a lot of corrosion, and is very destructive towards the material. This becomes a problem since the supply of this specialized material is low, and production time is long.

4.1.3.2. PBS 5.2

E_{corr} was found to be -0.21 V for BMG in PBS with HCl, and -0.19 for the protein solution. The results are shown in Figure 4-6.

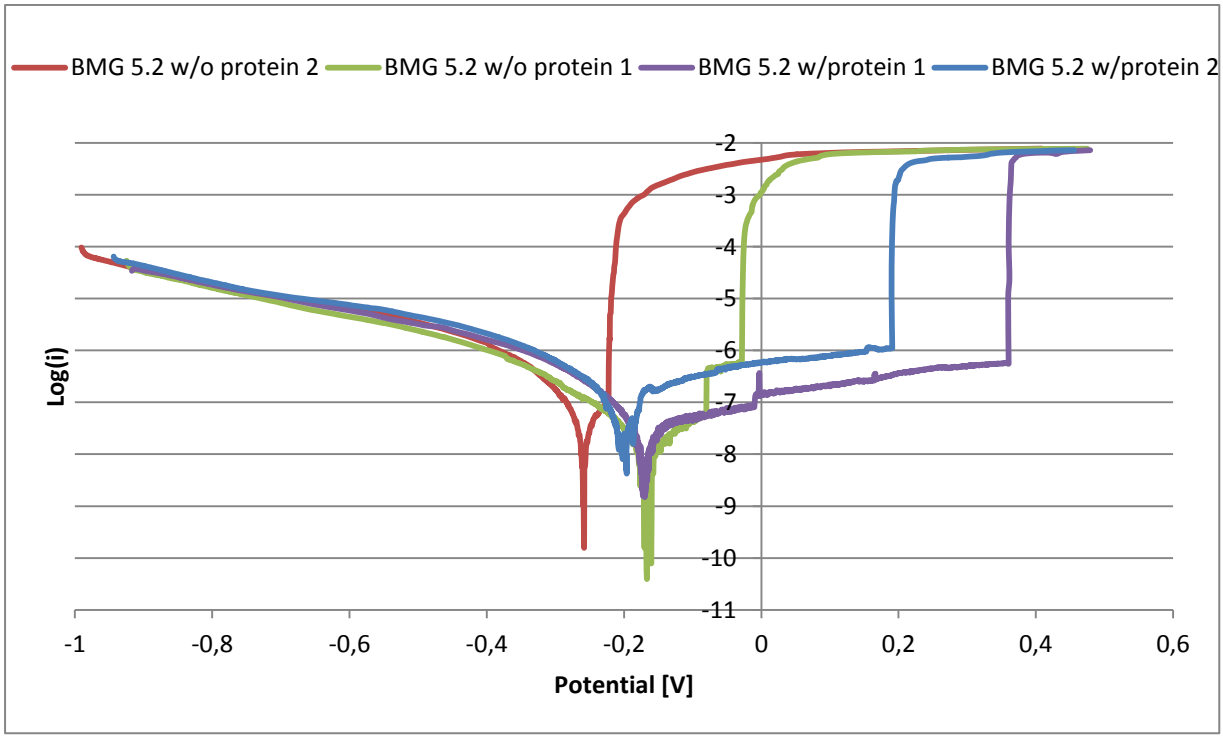

Figure 4-6: E-Log(i) diagram for BMG in PBS with pH 5.2

In the low pH range the BMG shows highly active behavior, and that this material is prone to corrosion. When proteins are introduced, however, it passivizes and becomes much more electrochemically stable. Regarding shifts in current density, there are no practical differences between the solution with or without proteins. Again this is explained by the differing surface conditions. Very little adsorption disturbances are observable from these tests. However, one test without protein shows some passivation and deviance in OCP. Further experiments are therefore recommended. The results in Figure 4-5 and Figure 4-6 shows that without proteins present the electrochemical behavior of the BMG is very unstable, and the results are very variable.

The OCP data presented in Table 4-1 are mostly averages of two data sets. While this is no statistically significant foundation, the small variance between the tests and the need for one single OCP value to refer to made the calculation necessary. It is of course important for future reference to establish the OCPs after making several more tests, creating a statistically significant data basis. This would further aid the research in this field. If the results in Table 4-1 is compared to the data from the Pourbaix diagrams (appendix A), it is evident that the electrochemical behavior of the materials in the different electrolytes is in accordance with this data. The only deviance is that of the BMG, which shows a tendency to active corrosion in situations where it should be passive. This behavior is explained earlier in this chapter, and may be linked to the alloying elements in the BMG. The only material that may exhibit active behavior is CoCrMo. One aspect that should be noted is that the Pourbaix diagrams are based on thermodynamic data, while the results presented here are kinetic. This would then cause some deviation between the behavior observed in the LP tests, and that presented in the diagrams.

4.2. Friction tests

From the friction tests it is seen that CoCrMo is the material with the lowest coefficient of friction (COF) (Figure 4-8) followed by the Ti 99.6 % (Figure 4-7) and BMG (Figure 4-9), which is a bit unexpected when their hardness is considered (Table 3-1). Ti 99.6 % has in fact an equal average COF as the BMG, and both are very unstable and ranges from 0.4

to almost 1.0. With this in mind it can be seen from the photographs of the surfaces used in the experiments, presented in Appendix B that both the BMG and the Ti 99.6 % have a much deeper and wider wear scar than the CoCrMo.

For Ti 99.6 % the friction coefficient was found to be on average 0.68. The results are shown in Figure 4-7. The friction coefficient was found to be on average 0.39 for CoCrMo. The results are shown in Figure 4-8. The friction coefficient for the BMG was found to be on average 0.68, and these results are shown in Figure 4-9. The average COF from all the tests are summarized in Table 4-1.

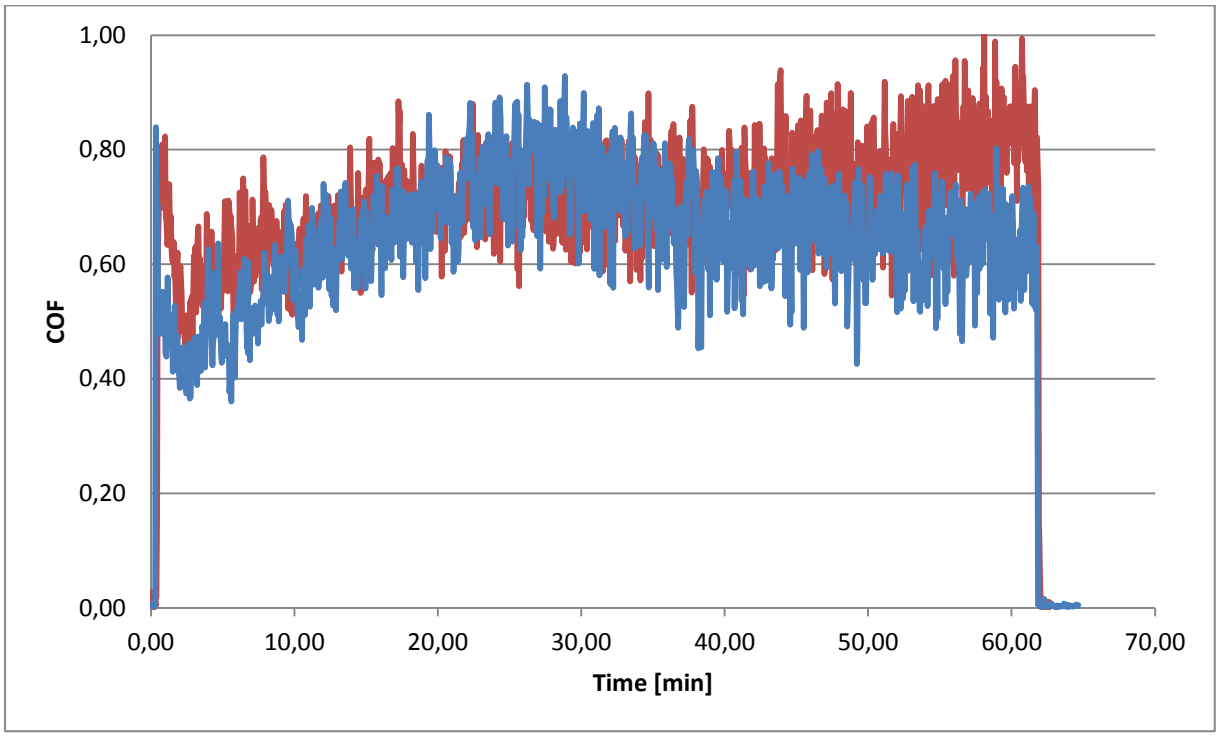

Figure 4-7: Coefficient Of Friction diagram for Ti 99.6 %

On a general note the results of the COFs alone do not give any indication on the magnitude of the wear on the materials, and the reason for doing dry tests is to determine a baseline comparison of the COF. This way it is possible to see of the friction increases or decreases in the different environments. In itself the COF is only an arbitrary number without denomination, and highly material dependent. Therefore it is no use in comparing the COF between different materials.

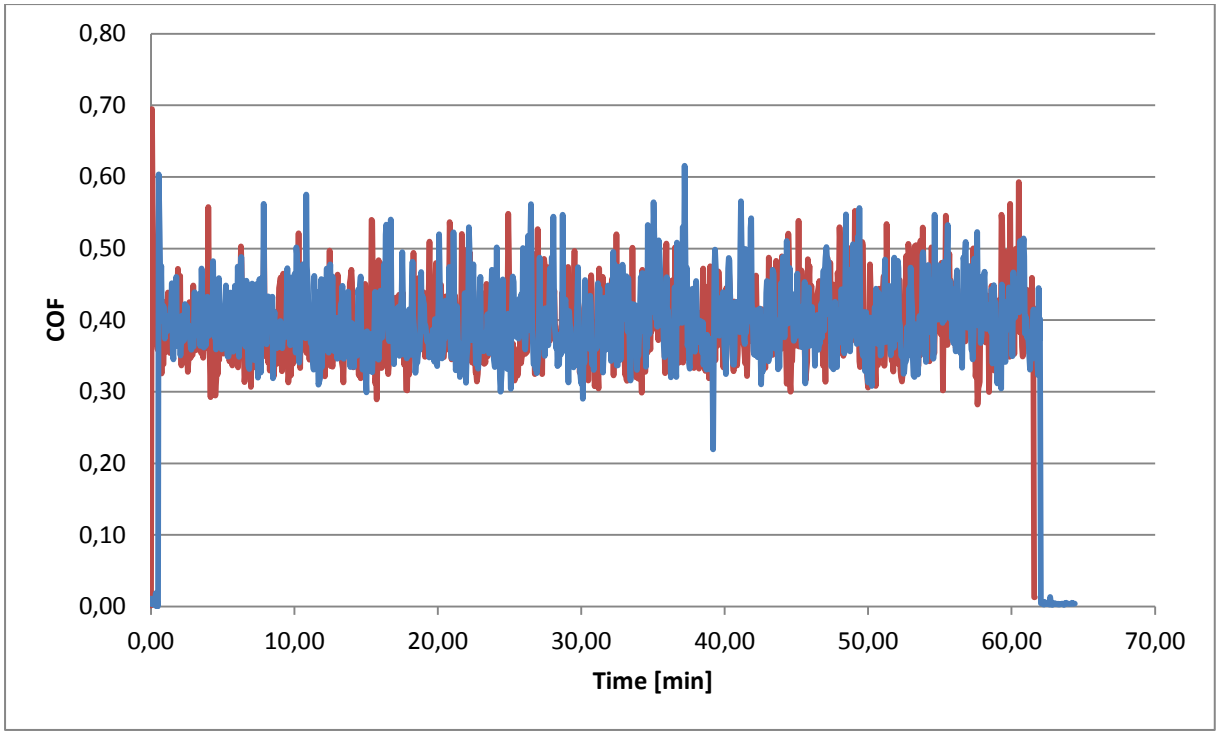

Figure 4-8: Coefficient Of Friction diagram for CoCrMo

To further establish a baseline comparison of the different materials, more experiments are beneficial. This will help mapping the material behavior and create a statistically significant data basis.

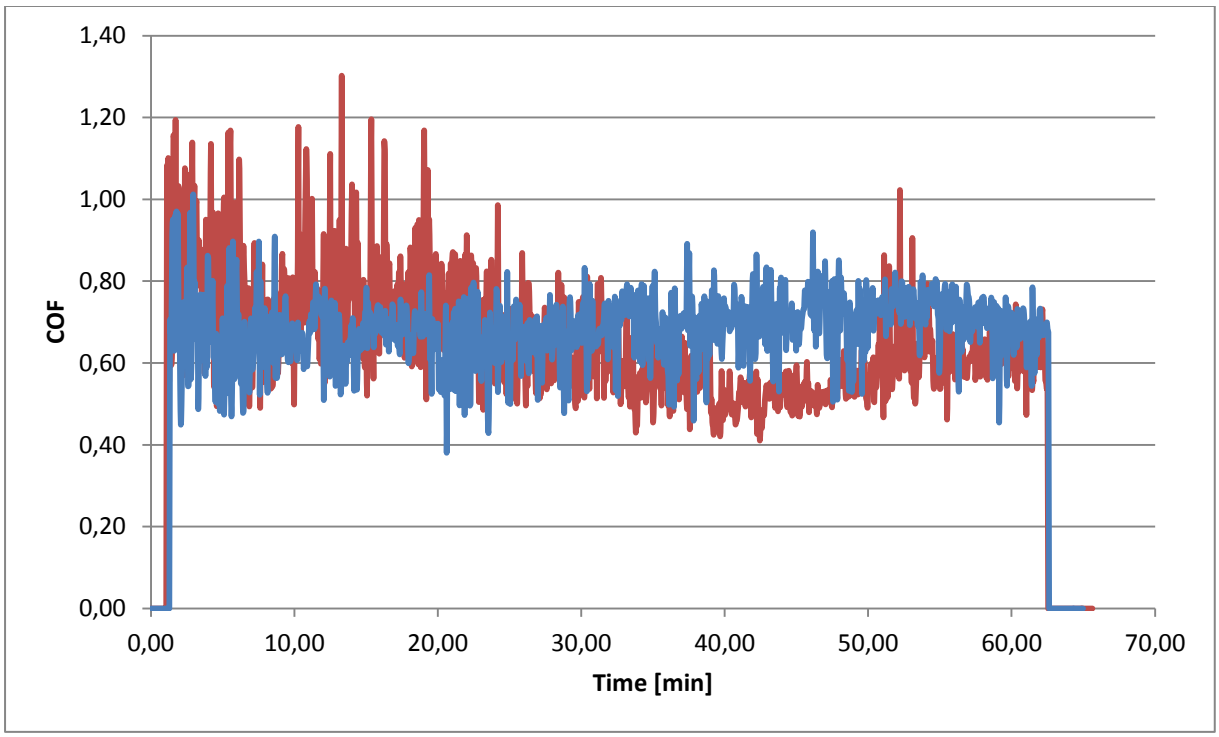

Figure 4-9: Coefficient Of Friction diagram for BMG

Table 4-2: Results of dry tribological testing

Material	Ti 99.6%	CoCrMo	BMG
Average COF	0.68	0.39	0.68

The photographs of the alumina balls from the dry tests, presented in Appendix B, also show much metal deposition on the balls for Ti 99.6 % and the BMG. This deposition of debris is evidence of the softness of the Ti 99.6 % material and the wear mechanism of the BMG, and indicates that a lot of debris and particles have added to an increased wear. In comparison one can look at the photographs of the CoCrMo surface and the accompanying alumina ball that the wear is very small. CoCrMo has left almost no visible mark (for the naked eye) on the ball, in accordance with the lack of debris and the hardness of possible particles. Based on this it is safe to assume that both the BMG and Ti 99.6 % will have the largest and most severe mechanical wear of the three in a pure dry tribological contact. This also gives an indication as to why CoCrMo is the only one of these materials in current use for articulating surfaces. Regarding the equality of the COF for BMG and Ti 99.6 %, it is most likely caused by the fact that the BMG is harder than the Ti 99.6 % and two-body abrasive wear is the dominating wear mechanism. In addition this may be explained by the fact that it is amorphous, and therefore wholly different mechanisms govern the wear of the material. This causes the debris produced to exert great friction and a high COF, while the wear volume is smaller than for Ti. The soft Ti 99.6 % has a large wear volume and creates a lot of particles, but the COF is also not as high exactly because of the softness of the material.

4.3. Tribocorrosion tests

The tribocorrosion tests in themselves will give a good indication on how the surfaces react to tribocorrosive wear, but no definite answer. From the graphs it will be possible to interpret whether or not the material surface passivizes during the tests, based on how the potential curve develops during the test. It will also be possible to see if it suffers from wear accelerated corrosion (WAC) from how big the potential drop is. The potential drop is the difference between the OCP measured at the beginning of the test, and the potential shortly after the rubbing has been engaged. Based on the results of previous experiments on similar BMG alloys, the polarization curves, and the dry

tribological testing presented in the previous chapters, the BMG under investigation may not hold up as well as desired [31] [52] [14] [67] [13].

The temperature was measured to be on average closer to 37 °C than for the LP. This is thought to be caused by the smaller volume of the electrolyte, and combined with some motion causing fluctuations in the liquid.

Most of the samples showed measurements of OCP consistent to those which were conducted in the polarization tests, the deviations that occurred will be explained later. The small potential drop between the OCP of the surfaces and the potential during wear can be explained with the fact that this wear was done with a normal force of only 2N, resulting in a rather mild wear compared to tests with 20N [67]. This would then cause a smaller electrochemical degradation than one might suspect. The mild wear is also evident in that the surfaces re-passivize in a manner close to their initial state, and are close to reaching initial values of OCP after wear. This means that the surfaces have undergone little change from their initial state.

There were some deviances with regards to OCP and mechanical wear between the samples of the same material in these experiments as well. This, however, can also be explained by the surface conditions. Not only were the surfaces by default different, microstructure etc., but since they were prepared by hand this may have led to further differences. The handling of the samples also led to changes in the surface conditions. Exposure to water, ethanol and unintended scratching would cause differences that are near unavoidable. Still, the deviances between the OCP established in the polarization experiments and the OCP recorded in the tribocorrosion experiments differed little, only a few hundreds of a volt, so this is mostly negligible. The differences in COFs on the same material in the same environment are somewhat bigger, but this is a product of many different variables making the differences both expected and negligible. This means that stability and mean COF are the best pointers as to how the electrolyte affects the friction and wear of the material.

It is somewhat expected that the wet samples would have a higher COF than the dry tests, due to the corrosion which would cause increased wear and particle formation. To which extent the COF would be affected is dependent on the stability of the material in

the electrolyte. The water in the electrolyte would not function as a lubricant, as it is a very poor lubricating fluid.

In the experiments presented in this thesis it was chosen to use an alumina ball as counter body. The reason for this is based on earlier studies that have shown that using a ball of UHMWPE, which is the most common material used for the cup-component, is too soft to give any good measurements [14]. Also the use of a counter body of the same material as the sample disc would in many cases, such as CoCrMo, cause extreme wear [67]. Therefore it was chosen to use a ball of alumina to give good, consistent and comparable measurements. The results are thus only material dependent. However, further tests with actual load bearing materials should be tested to even better simulate the real life conditions.

The pH in the PBS was found to vary between 7.4 and 7.7, which is a little higher than earlier reports, but not high enough to cause any significant changes to the behavior of the different materials (see the Pourbaix diagrams in Appendix A; Figure 0-1, Figure 0-2, Figure 0-3, and Figure 0-4). The reason for this pH difference can be explained by some incorrect measuring and mixing of the compounds. The pH of the PBS with HCl was measured to be 5.2, with only slight deviations. The reason for this can be related to the fact that the HCl is so concentrated that highly accurate pipettes are needed for a more accurate pH value.

4.3.1. Ti 99.6 %

While Ti 99.6 % has shown great biocompatible properties, it is evident in this study that it does not hold up as a material in use for articulating surfaces. It does, however, stay in the passive region in both of these electrolytes, and is thus fairly electrochemically stable. The mechanical breakdown of the passivizing surface, on the other hand, causes it to become very unstable, with a lot of wear. This is evident from the pictures presented in the appendices, but also from the graphs presented in this chapter.

4.3.1.1. PBS 7.4

The formation and effectiveness of a galvanic couple is highly dependent on the thickness and regeneration of the passivizing surface film. A more stable

potential curve is evidence of a harder and more stable surface film at this pH, which can be seen for Ti 99.6 % in regular PBS (Figure 4-10). The OCP found here is much lower than the OCP measured during the polarization tests, but the potential seems to be fairly stable through the test as well, indicating that the material has a stable electrochemical situation in these conditions. The reason for the deviation in the OCPs in Figure 4-10 and Figure 0-1 is the fact that during the cathodic sweep of the polarization test any surface film is removed. This surface film, mainly oxide, takes time to rebuild and therefore deviances will occur. In other words: The value presented in the LP tests are based on a more or less fully metallic surface, while the tribocorrosion tests are closer related to real life conditions where a surface film will develop just through atmosphere exposure. In Figure 4-10 and the following tribocorrosion figures, the blue line represents the COF, and the red line represents the potential.

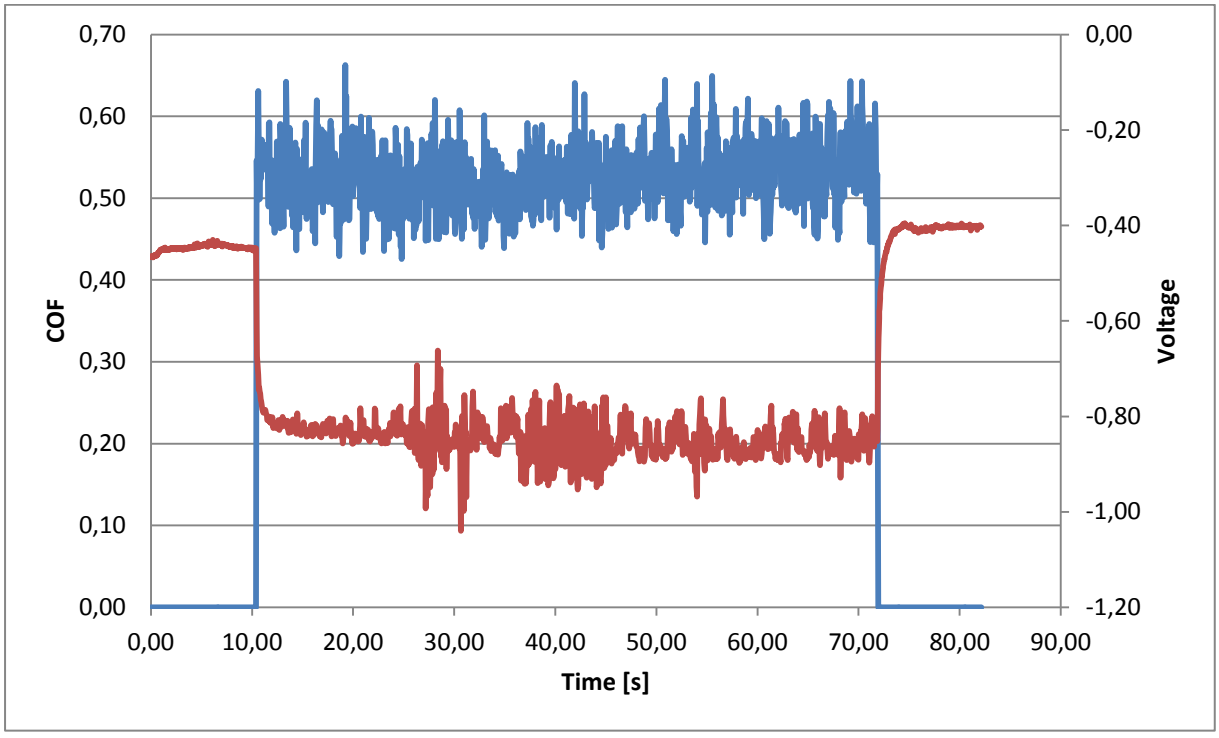

Figure 4-10: Tribocorrosion diagram for Ti 99.6 % in PBS 7.4

The potential drop for the other high pH test (Figure 4-10, Appendix C) presented in Table 4-3 may be somewhat larger than reality, since the material did not stabilize fully at a constant OCP before the rubbing was started. However, the potential drops in both tests indicate a lot of oxide formation and high WAC.

Figure 4-10 shows that the potential curve stabilizes to one level, once the rubbing has started. This behavior tells us that the material quickly reaches a stable wear track area and equilibrium of activation and passivation. This shift between activation and passivation causes a lot of oxide debris to form, and the result is that the potential curve gets disturbances indicating debris in the wear track after a little while. These particles will of course cause a higher wear of the material due to WAC. Although the test presented in Figure 4-10, Appendix C, seems to have a slight increase in the potential during the test, it seems to be over all stable and confirm what the test presented above shows.

4.3.1.2. PBS 7.4 with protein

The potential drops presented in Figure 4-11 and Figure 0-2 were smaller than in the pure PBS, and in addition the OCP was closer to zero compared to the results in Table 4-1. The COF was fairly stable and so were the potential measurements.

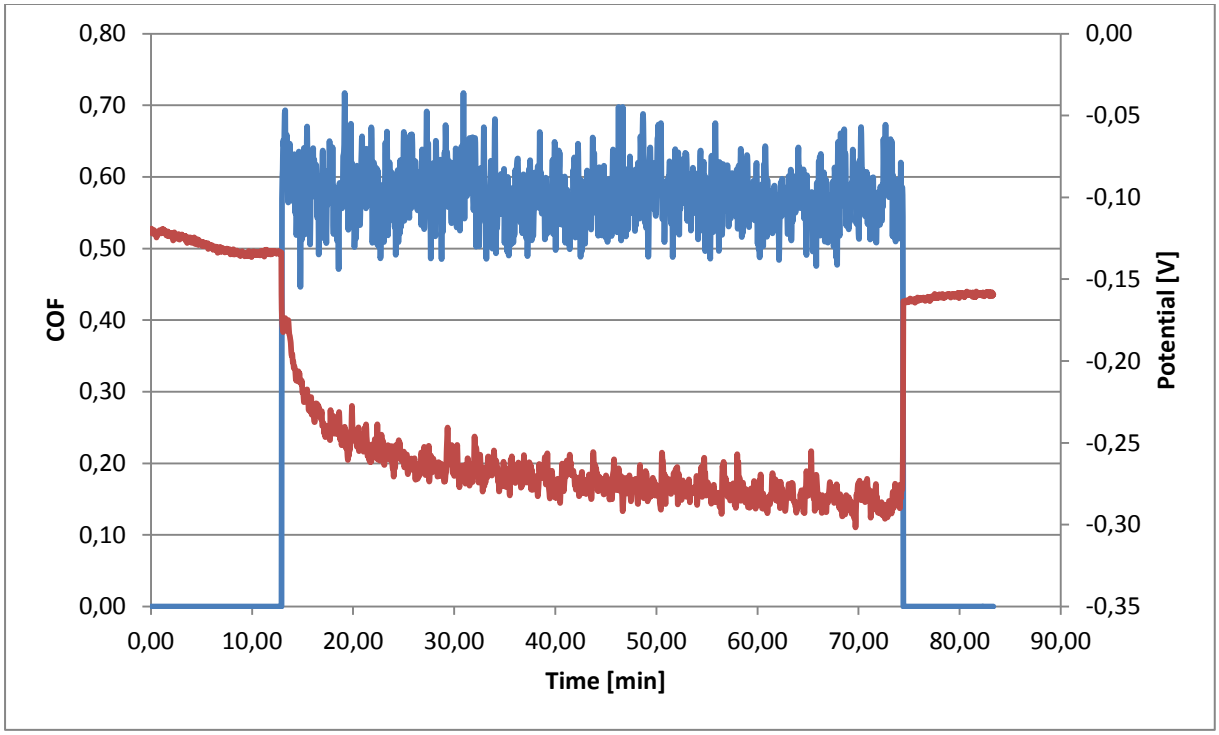

Figure 4-11: Tribocorrosion diagram for Ti 99.6 % in PBS 7.4 with protein

The OCP seems to be shifted towards higher values with the introduction of proteins, which is a positive effect towards the stability of the surface and may decrease oxide formation and wear. In addition some slight deterioration of the potential measurements during the tests can be seen, and this is most likely

caused by the removal of the adsorbed protein film. This causes slower wear and a wear track that increases in area over time. What is important to take note of here is that these test showed the smallest potential drops of all the Ti-tests. This means that the material had relatively little WAC, and that they would suffer relatively little wear. Although the potential drop is even smaller in the other test, presented in Figure 0-2, Appendix C, this test confirms what has been found from the test presented above.

4.3.1.3. PBS 5.2

In low pH Ti 99.6 % has very unstable COF, and relatively large potential drops as seen in Table 4-3 and Figure 4-12 and Figure 0-3. By referring to the pourbaix diagram and OCP (Table 4-3 and Figure 0-4) an explanation for its behavior in low pH (Figure 4-12) is evident; it forms oxide very easily. This would cause the material to be susceptible to WAC, and may explain the results in this low pH electrolyte. It should be noted that the Pourbaix diagrams are thermodynamic, while these tests are kinetic, and thus some differences may occur.

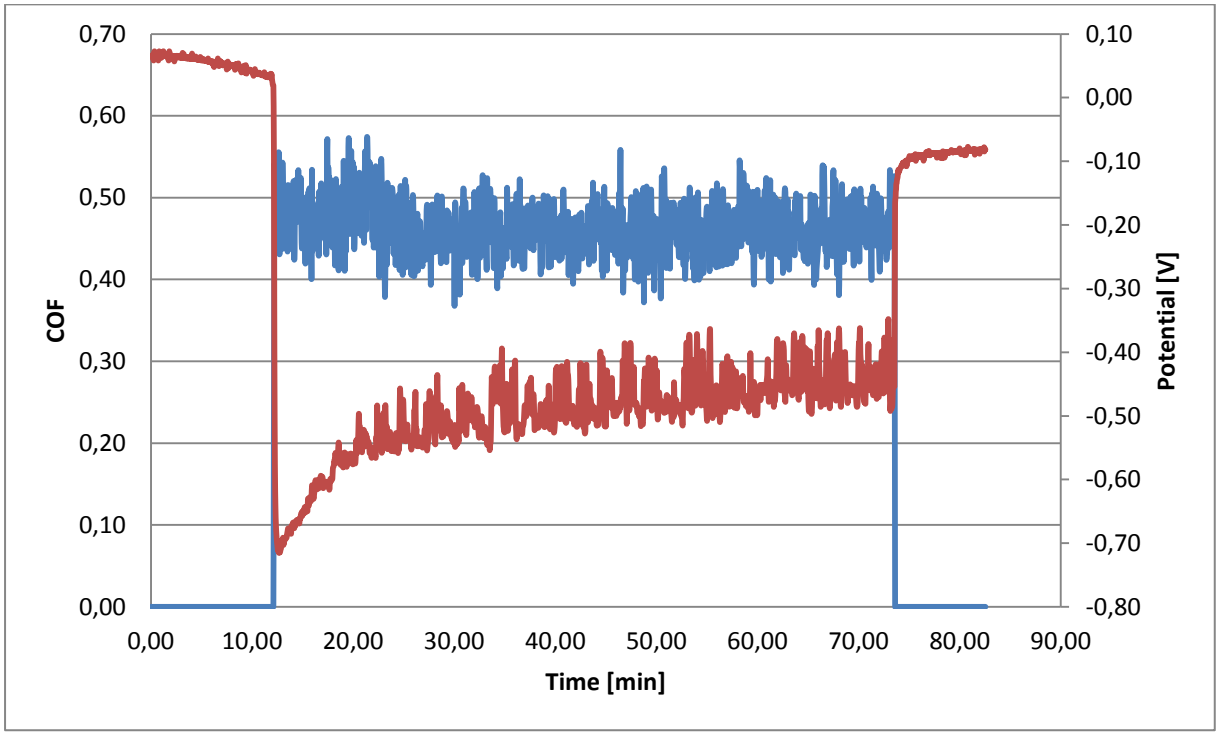

Figure 4-12: Tribocorrosion diagram for Ti 99.6 % in PBS 5.2

The potential curve shows a lot of disturbance and this is again caused by the release of oxide particles by mechanical wear, causing the accelerated wear. With regards to the potential a higher value than the ones obtained in the OCP measurements can be observed, and this behavior is explained earlier in the text. Also the material seems to be activating more towards the end of the test, causing the potential drop to become even smaller. This is a positive development, since this would decrease the WAC. The results for the test presented in Figure 0-4, Appendix C, confirms this behavior.

4.3.1.4. PBS 5.2 with protein

The addition of protein to the high pH solution seemed to increase the potential, and thus stabilizing the surface more. However it seems to lower the potential across the surface of the material in the low pH, as seen in Figure 4-13 and Table 4-3, but it has little or no effect on the COF.

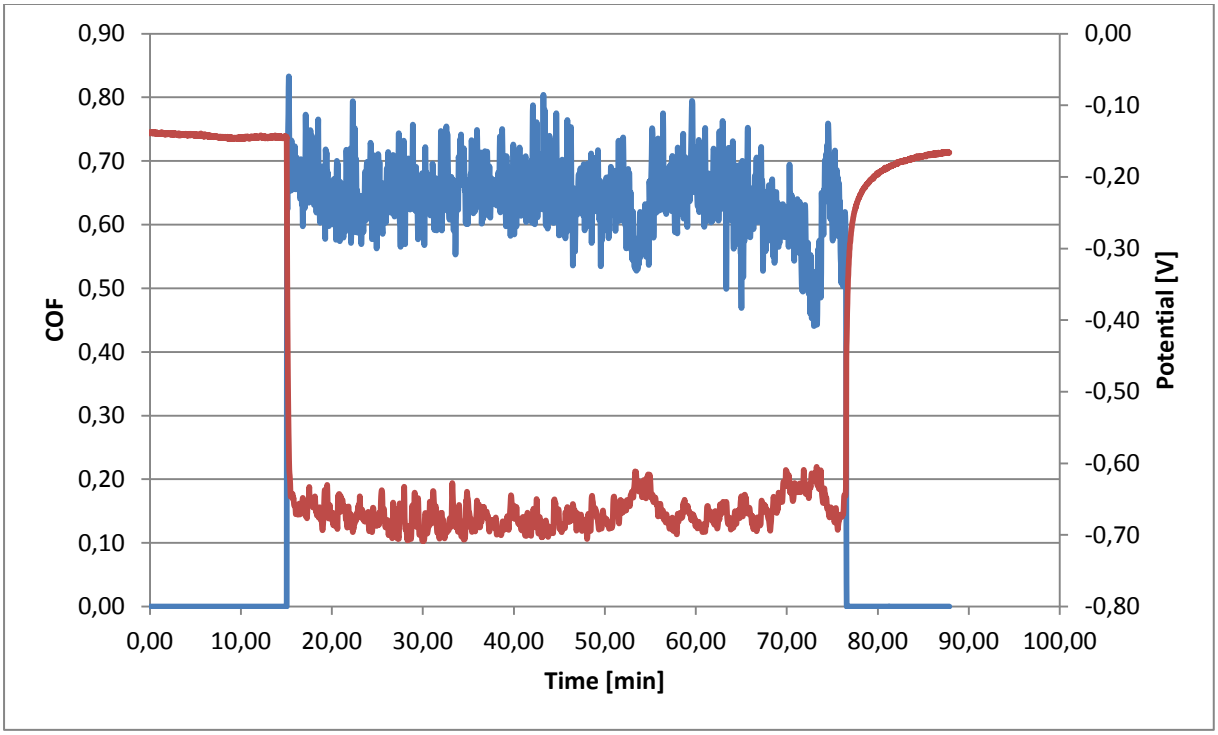

Figure 4-13: Tribocorrosion diagram for Ti 99.6 % in PBS 5.2 with protein

The potential curve in these tests seems to stabilize quickly, although some protein film removal may be observed. Again this gives evidence of a quickly forming wear track and a passivation/activation behavior. This will, as mentioned, cause a high WAC and this is observable from the potential drops as

well. If Figure 4-13 is compared to the results from the test presented in Figure 0-4 a totally different behavior can be seen. Here the material seems to be active and has a much smaller potential drop. This deviance can be connected to the extensive adsorption of proteins on the surface, as seen in Figure 4-2, making this test difficult to repeat with similar results.

Compared to the polarization tests the tribocorrosion results indicate that the OCPs are mostly within the same range, though with some deviation. The potential drop once the test is engaged is very high for all the conditions. This gives reason to believe that Ti 99.6 % is in no respects useable for a tribocorrosion point of view.

4.3.2. CoCrMo

CoCrMo does not have great biocompatible properties; but what it lacks in this consideration it seemingly makes up for with regards as a material in use for articulating surfaces. It does, however, suffer some corrosion in the electrolytes, but it is fairly electrochemically stable and passivizes in all solutions. The mechanical breakdown of the passivizing surface does cause it to suffer some wear, but nothing like the Ti 99.6 %. This is evident from the pictures, but also from the graphs presented in this thesis. The figures and photographs presented in this thesis will show that it is evident that CoCrMo is by far the most stable material with the least wear.

4.3.2.1. PBS 7.4

The COF in one of the PBS tests (Figure 0-5, appendix C) was very noisy, most likely caused by particles, which is not unusual. The average COF is on the other hand was very close to the more stable PBS test presented in Figure 4-14. Also note that the COF is almost double of that recorded in the dry test, meaning that the increased friction is a result of the corrosion and particles formed, which is expected. The potential drop in pH 7.4 is a little higher than in pH 5.2, as seen in Figure 4-14, and is thought to be caused by its increased instability in PBS. This may then be an effect of the reactions with the phosphate ions that are present in the electrolyte. The CoCrMo alloy was designed to be hard and withstand

tribological wear; this is evident in these tests. The behavior of the metal in PBS is as expected [11] [55] [14] [71].

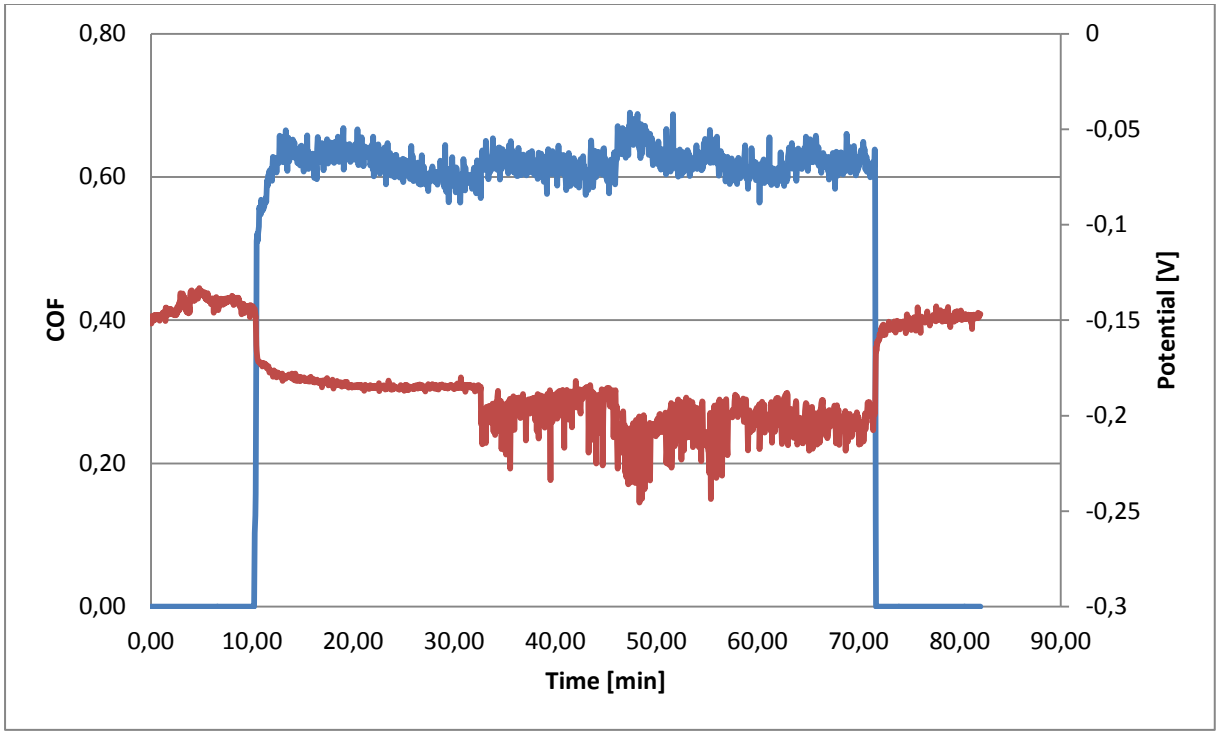

Figure 4-14: Tribocorrosion diagram for CoCrMo in PBS 7.4

The increased instability in the PBS seen in the potential drop and towards the end of the potential measurements gives an indication of WAC, and it is therefore not unlikely that these tests will give some of the most worn samples. The potential measurements show a fairly stable behavior through the test, indicating that it quickly reaches a stable wear track area. It does get somewhat unstable towards the end, and this is caused by particles disturbing the measurements. The OCP is slightly higher but still in accordance with the polarization tests, and the potential drop is very small. This gives good indications of a material with little electrochemical deterioration in these conditions, relative to the other materials. The results of the test presented in Figure 0-5, appendix C confirms this behavior. However, if the material is compared only to itself, these tests will most probably have the most wear of the CoCrMo tests.

4.3.2.2. PBS 7.4 with protein

When proteins are introduced, Figure 4-15 indicates a lowering of the COF indicating that the wear is not as severe, and that particles are not as easily formed. The system seems to undergo less deterioration, and while it is a varying COF to begin with, it stabilizes towards the end of the test.

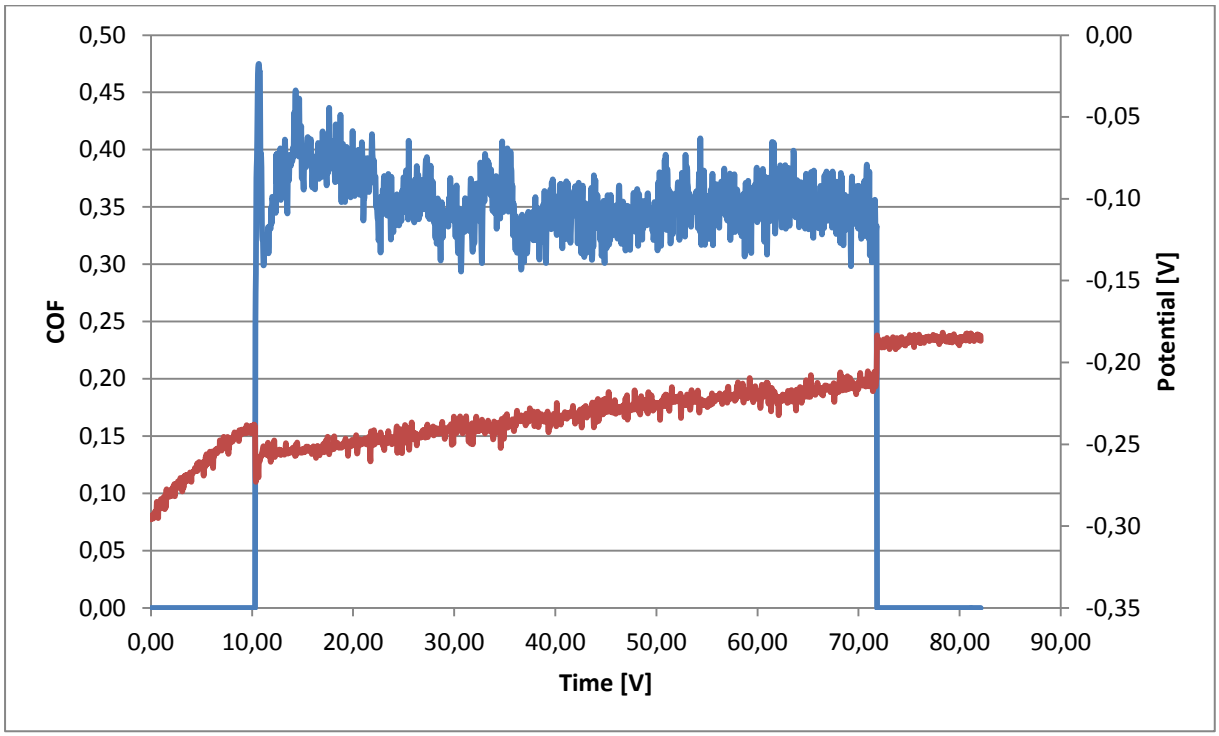

Figure 4-15: Tribocorrosion diagram for CoCrMo in PBS 7.4 with protein

The potential drop is incredibly small compared to the other tests and the slowly increasing potential curve gives a sign of a material that is actually being active under these conditions. Therefore very little electrochemical degradation is taking place, and seemingly little debris is formed causing changes in the COF or the potential measurements. This is a very good behavior as far as WAC is concerned, but with regards to toxic ion release this is not ideal. The other test presented in Figure 0-6 in Appendix C confirms this behavior. This may not only be caused by the surface being active, but may also be caused by proteins acting as a lubricant.

4.3.2.3. PBS 5.2

In low pH (Figure 4-16) the COF is lower than in high pH, but still higher than the tests with proteins. The variation and increase towards the end of the test

indicate a development of wear particles causing increased friction and wear. The potential drop is on the other hand comparable to that of the high pH tests (Table 4-3), and indicate the potential of higher WAC. In accordance with the Pourbaix diagram for cobalt (Figure 0-2 Appendix A) it is clear that in this pH range it is on or beyond the border of being active, although chromium offers some protection if ions are not present in the solution. If chromium ions leak into the electrolyte, it too will become active as seen in the Pourbaix diagram (Figure 0-1 Appendix A). Thus fewer hard oxide particles would form while the reactivity is higher. The material is therefore border lining between good active surface, and high WAC.

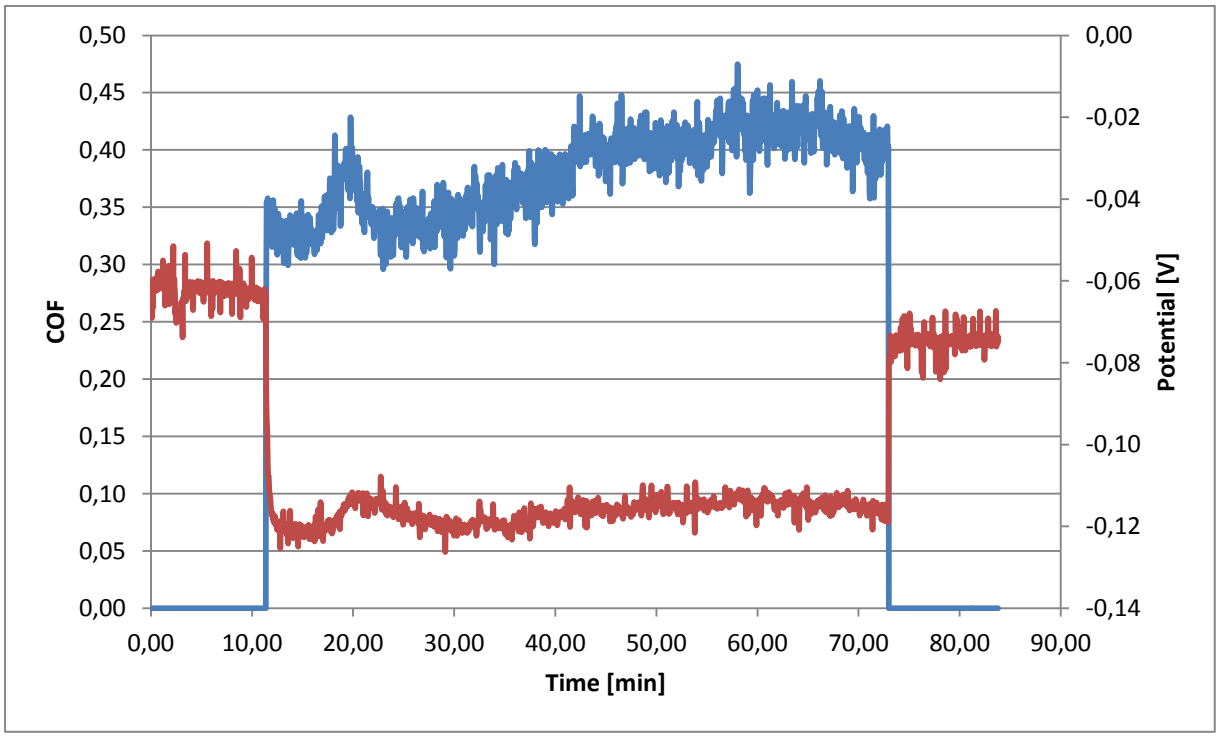

Figure 4-16: Tribocorrosion diagram for CoCrMo in PBS 5.2

Comparing the results to the other materials, evidence is given for that CoCrMo has a very stable potential behavior in low pH, and also potentials fairly close to zero, indicating that this material has good passivizing qualities in this pH, and a constant passivation/activation shift causing the WAC is observable. Figure 4-16 shows a “run-in” period potential-wise: After some time the potential stabilizes and very little chance is seen afterwards. This is a behavior that indicates that the material will reach and stabilize the wear scar area quickly. What needs to be

taken notice of is the very differing behavior of the other test, presented in Figure 0-7 in Appendix C. The behavior seen here is something that would be expected of the tests run in high pH with the addition of proteins. The reason for this deviation may be explained by the fact that the pin-holder in the test rig slipped, and did not move completely in a straight line. These results may be regarded as false and omitted from the evaluation. This calls for more experiments to be conducted to further establish the behavior.

4.3.2.4. PBS 5.2 with protein

The addition of protein also shows a beneficial activation of the material across the surface in the low pH solutions, and the COF is also noticeably lower in these solutions as seen in Figure 4-17.

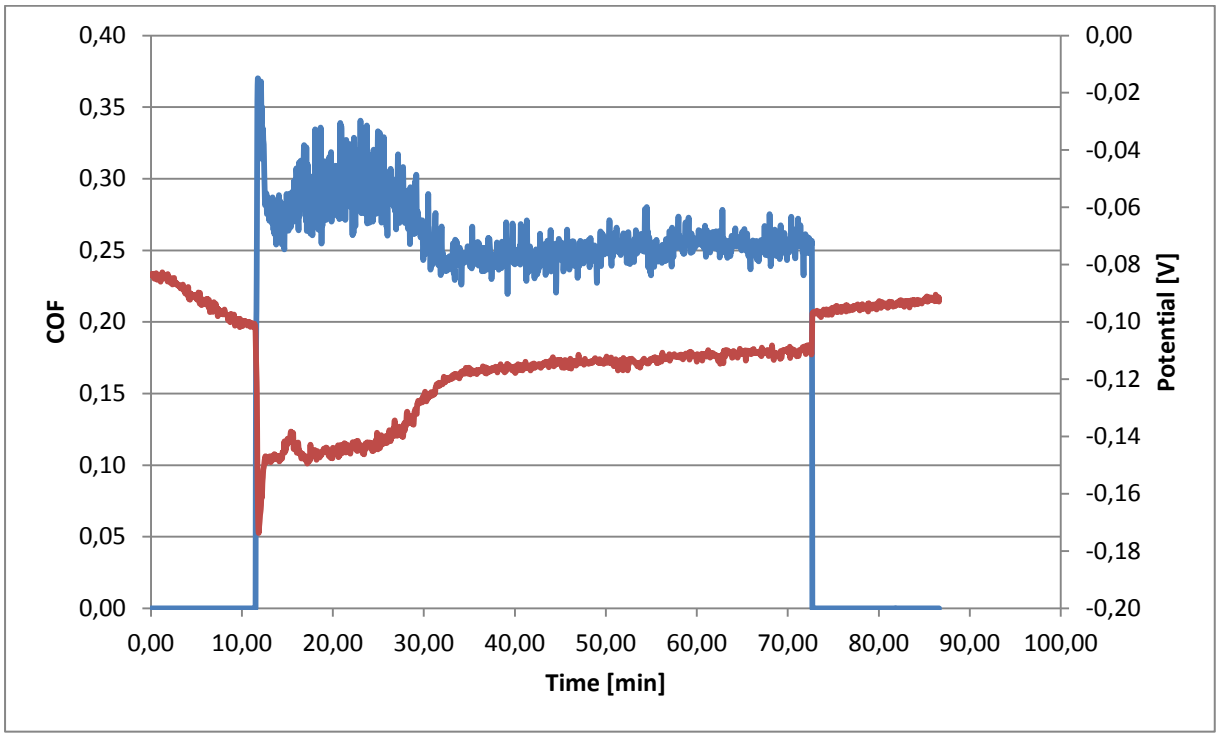

Figure 4-17: Tribocorrosion diagram for CoCrMo in PBS 5.2 with protein

It is possible to assume that the proteins have a beneficial effect on the material. The figure shows that the COF lowers and stabilizes after a short while; this may be caused by the removal of the protein film. The potential drops observed in these tests were comparable to the high pH protein tests, and very promising. Some effect of a "run-in" period on the potential in this test is also observable, and this is again thought to be caused by the removal of the protein that has

adsorbed to the surface. When the proteins are removed it stabilizes and the surface seems to be activated. This is, as mentioned before, beneficial as it greatly reduces the WAC, this is observable in that the disturbances in the potential measurements are minute, indicating that the test had very little debris formed, and a highly stable surface with regards to wear. Furthermore it is shown in Figure 4-17 that the OCP measurement is in accordance with the polarization tests yet again. However, the second results presented in Figure 0-8 Appendix C shows a large deviation in OCP. This is again caused by the fact that the tribocorrosion samples have a surface film when OCP is measured. Other than that, this test shows the same trend and material properties as the one presented above.

4.3.3. BMG

4.3.3.1. PBS 7.4

The results of the tribocorrosion tests for the BMG are not very positive. The COF for all the tests is higher than for both CoCrMo and Ti 99.6 %, but within the expected range for this type of material [52].

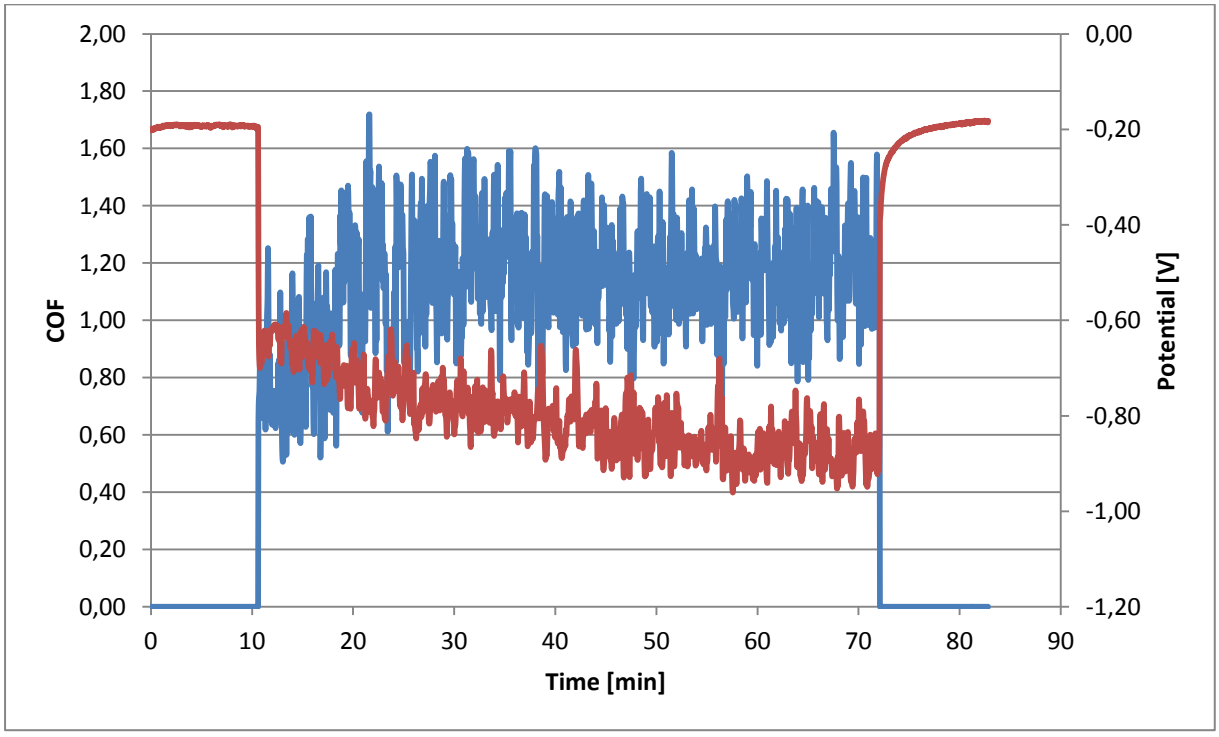

Figure 4-18: Tribocorrosion diagram for BMG in PBS 7.4

This is caused by the fact that the material is amorphous, and that the wear mechanisms that act on this material are different, and not fully understood yet as the use of this type of material is very new. The OCPs are, however, within the range of what has been measured in the polarization tests. In normal PBS, as presented in Figure 4-18, higher potential drops are seen than even for Ti 99.6 % (see Table 4-3). This causes a lot of debris and WAC, therefore the potential is also very unstable. Furthermore the behavior of the material is very dependent on surface conditions; in Figure 4-18 it shows a deteriorating potential, while in Figure 0-9 the potential seems to be increasing in an activating manner. However, Figure 0-9 shows a lot of disturbances due to particles and wear, therefore this increase may to some extent be related to this. In addition the potential drop is much larger, and WAC may be one explanation for the deviances. Furthermore these big differences may be caused by the materials properties and shows the difficulty in repeatability.

4.3.3.2. PBS 7.4 with protein

Again the COF is within the expected range, but there is no sign of any benefits towards friction with regards to the proteins acting as lubrication. What is observed when protein is introduced; however, is a noticeable change for the worse with regards to the potential in Figure 4-19. It is much more stable indicating a constant shift between active and passive surface, and much more negative OCP than the two other materials, and thus more prone to corrosion in this case as well. One of the tests, presented in Figure 0-10 in Appendix C, is showing a diminishing COF caused by slipping of the pin-holder, and is thus regarded as false results.

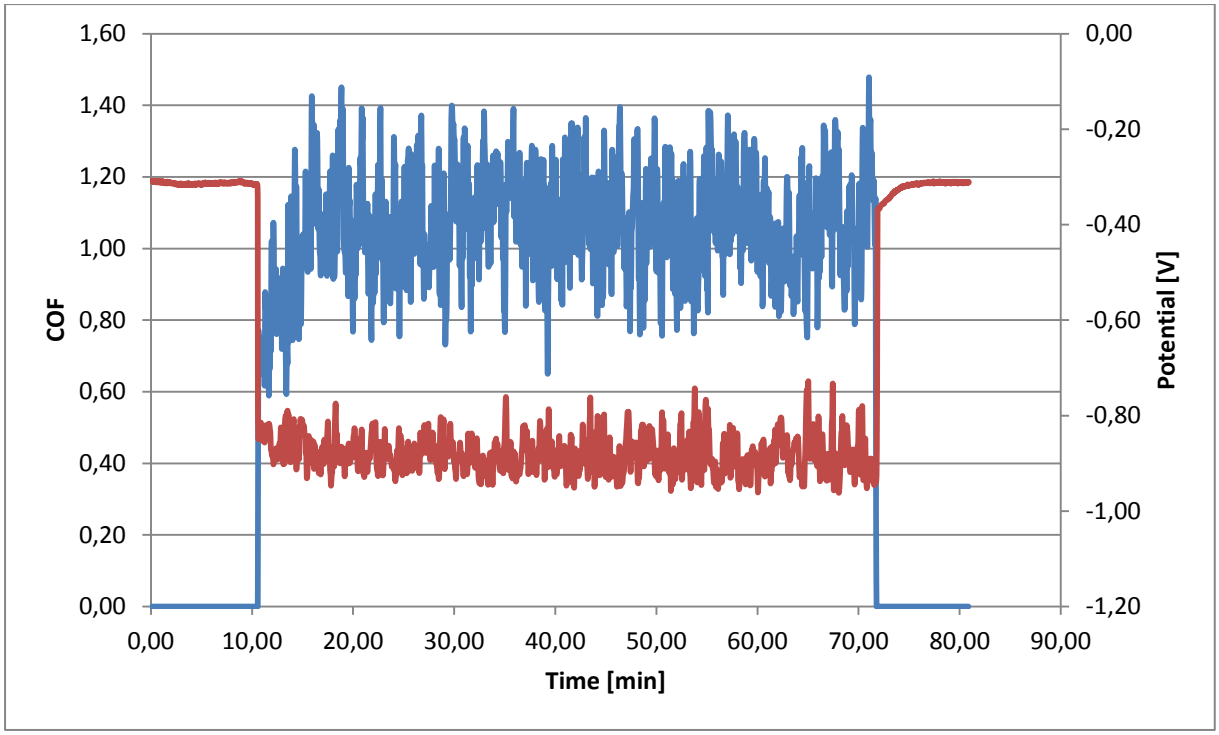

Figure 4-19: Tribocorrosion diagram for BMG in PBS 7.4 with protein

The potential measurements show that the OCP value is in accordance with the polarization test in Table 4-1, although somewhat lower. The potential drop is very large, however, and shows that the metal becomes more susceptible to WAC during rubbing than without proteins. This may be a negative effect of the proteins on the material at this pH. Another observation is that the potential is stable all the way through the test, with no run-in period, indicating little or no protein adsorption and a constant wear area. So, although it is very susceptible to corrosion, the wear is at a stabile level.

4.3.3.3. PBS 5.2

When the behavior in low pH is evaluated, as presented in Figure 4-20 a lower COF is observed, although a bit more unstable at first due to oxides causing debris. The potential is also more unstable, but higher than for the higher pH solutions. This unstable behavior can be explained by the formation of oxides causing disturbances due to wear (see Figure 0-3). The COF also shows to diminish towards the end, and may be a sign of less production of oxides, and an activating surface. The OCP measured here is also in accordance with the

polarization results, and the potential drop is smaller than for the high pH tests, showing a more stable electrochemical situation.

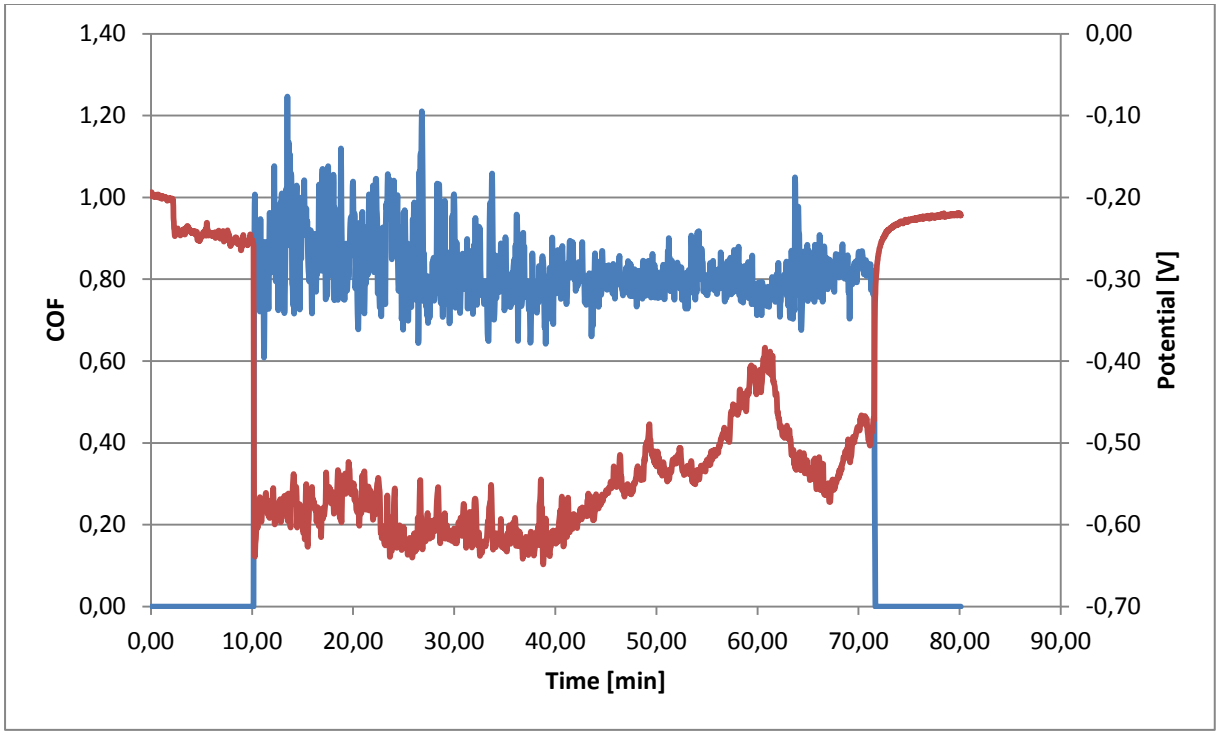

Figure 4-20: Tribocorrosion diagram for BMG in PBS 5.2

The breakdown of the oxide layer causes a large disturbance in the electrochemical reading, which can explain the instability of the curves, but it is possible that there is also a slight increase in the potential towards the end. This might indicate an activating surface, and is a positive development over time. When compared to the other test in Figure 0-11 in Appendix C and the COF, this is most likely the case, but this test suffers from a great deal of corrosion particle disturbances and WAC. This makes it difficult to make any definitive conclusions, but it seems to be shifting between active and passive states at a high rate, so an active surface condition in this environment seems possible.

4.3.3.4. PBS 5.2 with protein

With the protein solution it is more or less no difference in the friction behavior, although it is a bit noisier. This may be caused by proteins on the surface creating friction. The potential is also slowly decreasing during the test as seen in Figure

4-21. This is an indication that the material is not as stable as CoCrMo and Ti 99.6 %, and even not as stable as the BMG in other solutions.

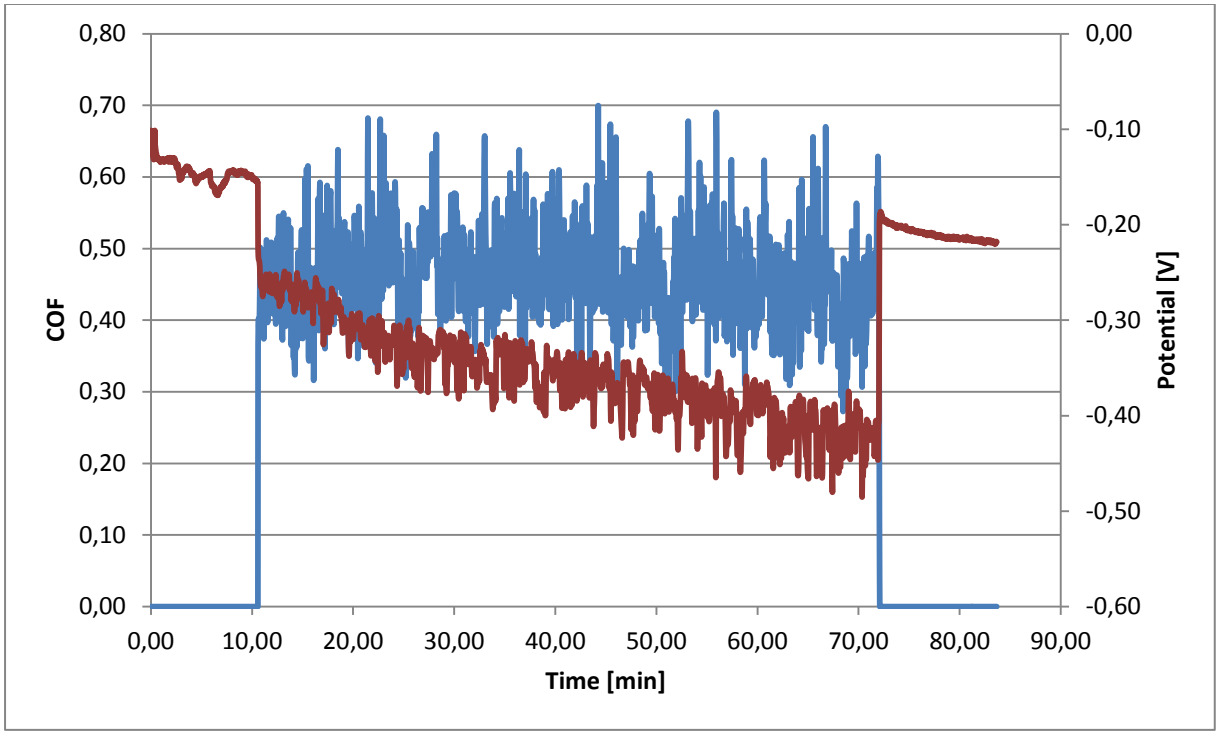

Figure 4-21: Tribocorrosion diagram for BMG in PBS 5.2 with proteins

The potential drop is within the same range as for the low pH tests without proteins, which shows that the stability is coupled to the pH and not to the protein addition in this case. The potential is diminishing throughout the test, however, and it seems that the material takes a long time to stabilize under these conditions. This may explain the deteriorating potential during the test as well, but it is not an indication of a good electrochemical behavior. It may seem that the proteins cause a greater instability of the BMG, with regards to tribocorrosion.

4.3.4. Summary of findings from the tribocorrosion tests

The average values from the tribocorrosion tests are summarized in Table 4-3. And these results sum up the key information from the tribocorrosion tests. Here it is possible to see if the different electrolytes have any influence on the average COF, but it is difficult to see any clear trend and make any definitive conclusions. The variance between two samples of the same material in the same electrolyte is often too big to use draw any conclusions from. And the fact that only two samples are

used as data foundation definitely calls for further experiments to develop a statistically significant amount of data. The table also presents the OCP value gathered at the beginning of the experiments, here denoted as E_{max}. From what can be seen in the tribocorrosion graphs, it can be concluded with that for some tests this value is subject to some uncertainty. Not all tests showed a fully stabilized potential value before the rubbing was started, such as Figure 0-8, however the differences between the highest and the lowest value within this time period is often so small that it is negligible. Of course several more experiments would again help to establish a more definitive value and a better foundation for further work. A similar question can be raised about the minimum potential value, because some tests show an immediate recuperation of the potential after the initial drop, such as Figure 4-17, but again this difference is mostly negligible. As explained earlier, the potential drops give many tell-tale signs of how severe the wear will be for the material in the given electrolyte. It is of course somewhat relative with regards to material, but on a general note the smaller the potential drop is, the less the WAC will be.

Table 4-3: Results of tribocorrosion tests

Material	Electrolyte	Sample	Average COF	E_{max} [V]	E_{min} [V]	ΔE [V]
Ti 99.6 %	PBS 7.4	1	0.67	-0.417	-0.673	0.256
		2	0.53	-0.430	-0.857	0.427
	PBS 7.4 protein	1	0.69	-0.127	-0.174	0.048
		2	0.58	-0.119	-0.302	0.183
	PBS 5.2	1	0.62	-0.004	-0.726	0.722
		2	0.46	0.073	-0.715	0.788
	PBS 5.2 protein	1	0.60	-0.040	-0.842	0.802
		2	0.64	-0.137	-0.709	0.572
CoCrMo	PBS 7.4	1	0.64	-0.086	-0.226	0.140
		2	0.62	-0.133	-0.245	0.112
	PBS 7.4 protein	1	0.36	-0.205	-0.282	0.077
		2	0.38	-0.160	-0.223	0.063
	PBS 5.2	1	0.41	-0.059	-0.209	0.150
		2*	0.38	-0.051	-0.126	0.075
	PBS 5.2 protein	1	0.32	-0.268	-0.332	0.064
		2	0.26	-0.083	-0.174	0.091
BMG	PBS 7.4	1	0.74	-0.141	-0.629	0.488
		2	1.13	-0.189	-0.961	0.772
	PBS 7.4 protein	1	1.06	-0.308	-0.962	0.654
		2*	0.62	-0.273	-0.978	0.705
	PBS 5.2	1	0.45	-0.277	-0.589	0.312
		2	0.82	-0.194	-0.648	0.454
	PBS 5.2 protein	1	0.46	-0.101	-0.485	0.384
		2***	-***	-	-	-

Test results not viable due to mechanical failure

****Test not performed due to time constraints**

4.4. Confocal Microscope Analysis

The pictures presented here have a topography that is enhanced 10 times, to articulate the profile more. However the scale bar of the topographic images is in actual scale. Some of the pictures contain blank areas or faults due to problems with contrast and reflection caused by the highly reflective surfaces of the samples. The roughness profiles are an average of the whole wear scar calculated by the software.

In Table 4-4 the results of the wear volume measurements are represented. These results are by far the most telling with regards to material performance. While the electrochemical results may give an indication as to how stable a material will be, electrochemically, in any given solution, the wear volume give solid proof of how they fare. Many factors will contribute to differences in electrochemical measurements, and the sensitivity of the equipment is large, so consistency is difficult to observe. The results from the wear volume measurements are an average over two samples.

4.4.1. Ti 99.6 %

From the image presented here in Figure 4-22 and in Appendix C, it is easy to conclude that Ti 99.6 % is without a doubt unusable as an articulating material. If any differences in the solutions are to be noted, it is that a high pH solution with proteins seems to have a beneficial influence, and that proteins in general seem to decrease the wear. This is deduced from the wear volume measurements presented in Table 4-4. The 3d images presented here and in Appendix C show that the wear tracks are up to 50-60 µm deep, and that some ductile deformation exists on the edges of the track. This deformation seems to be around 5 µm high.

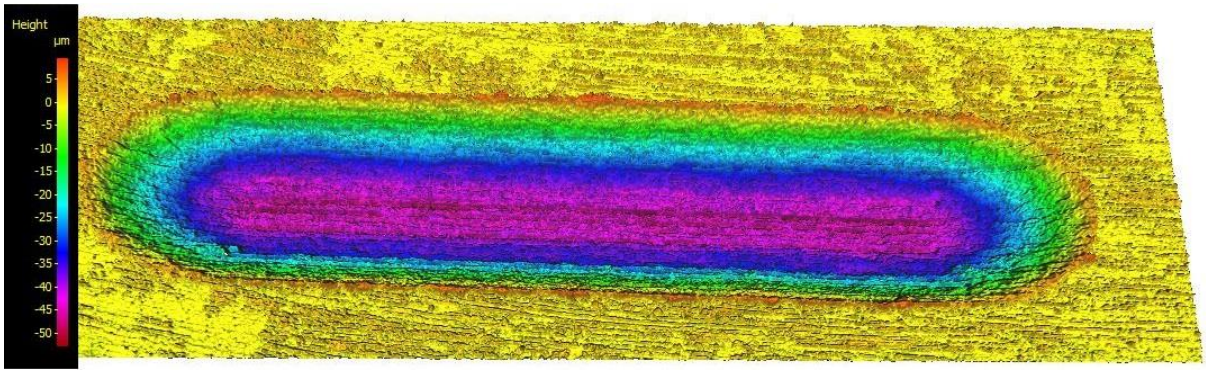

Figure 4-22: Confocal 3d image of Ti 99.6 % PBS 7.4 test 1

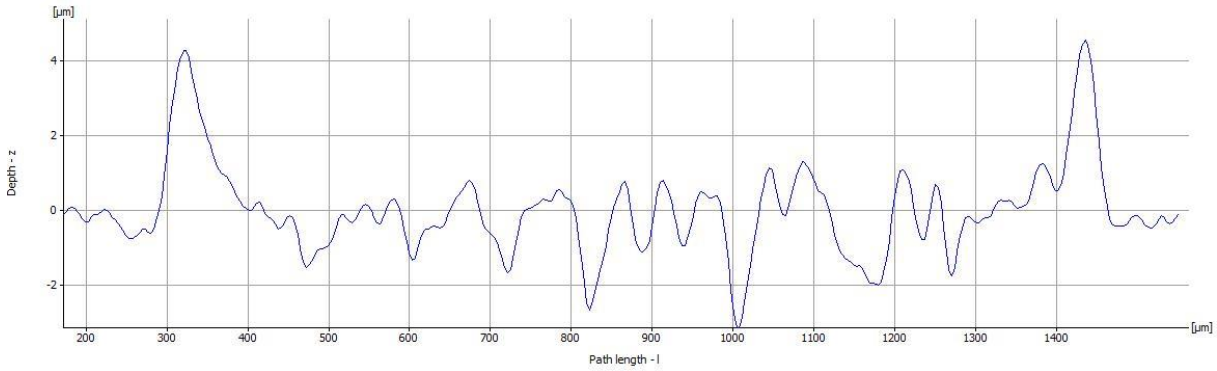

Figure 4-23: Surface cross section profile of Ti 99.6 % PBS 7.4 test 1

From the profile presented in Figure 4-23 it is seen that the roughness in the wear scar is very large, with peaks up to 4 µm, and that the grooves range mostly from 2 to 4 µm. The high edges on the sides of the wear scars are not real, as can be seen when the profile is compared to the images. These "mountains" are caused by the fact that this is a roughness profile, not measuring actual height difference. If one should compare this to the 3d image it is more likely that the top of these mountains are the edges of the wear track, and that the outside surface should be close to this level, and not at the zero level as indicated in the profile image. There is some ductile deformation at the edges, as seen in Figure 4-22, and this may explain the larger mountainous edges.

If the profile graphs of the tests done in PBS without protein are compared with the graphs of the protein tests, both presented in Appendix C, a smoother wear surface can be observed, and also a shallower wear track. This confirms what was interpreted from the tribocorrosion test results, and furthermore in the comparison between the high pH and the low pH it is seen that this also holds up with the findings in the tribocorrosion tests. At low pH increased wear is observed, a rougher wear track comparable to the high pH without protein can be seen, and also little or no effect of proteins at low pH. Due to the large wear volume of these tests, it is more difficult to assess the critical influence of WAC. However, there is a difference to be detected, and this further confirms the indications from the tribocorrosion results.

4.4.2. CoCrMo

From the images in Appendix C it is easy to see that the CoCrMo is the best material by far: In high pH solution, protein addition seems to decrease the wear, and the same effect on the wear can be seen in low pH solution. The wear is more severe in low pH solution not containing proteins, and is somewhat expected with the increased corrosion wear. Most of the surfaces had so little wear that it was nearly impossible to get any good images from the confocal microscope. This is a very good indication of how the material holds up in all the different environments. The CoCrMo PBS 5.2 with protein tests had so little wear that it was impossible for the microscopes software to determine the surface topography and details.

Figure 4-24 and Figure 4-25 shows exactly how small the wear is for the material, and the height differences between the surface and the deepest scars are no more than around 3-5 µm. Compared to the results found in the tribocorrosion tests, it is possible to confirm that WAC is in effect, and that this affects the surface and the wear.

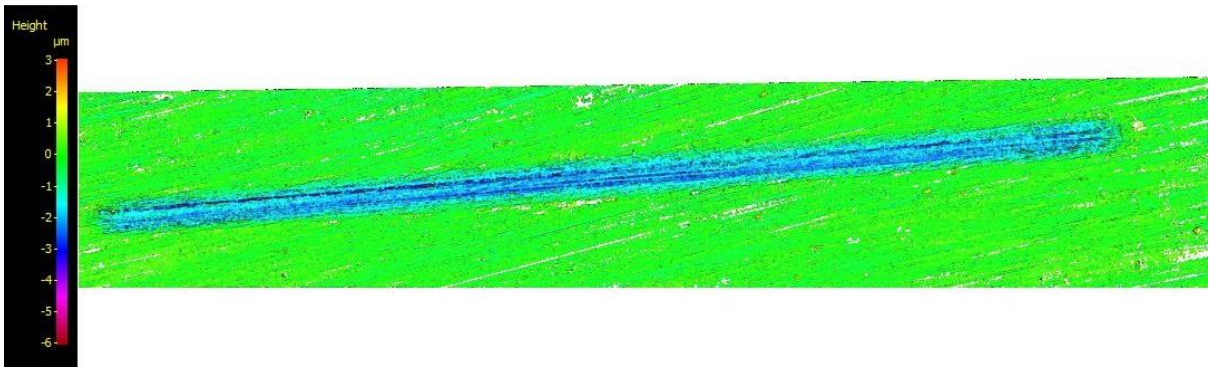

Figure 4-24: Confocal 3d image of CoCrMo PBS 7.4 with protein test 1

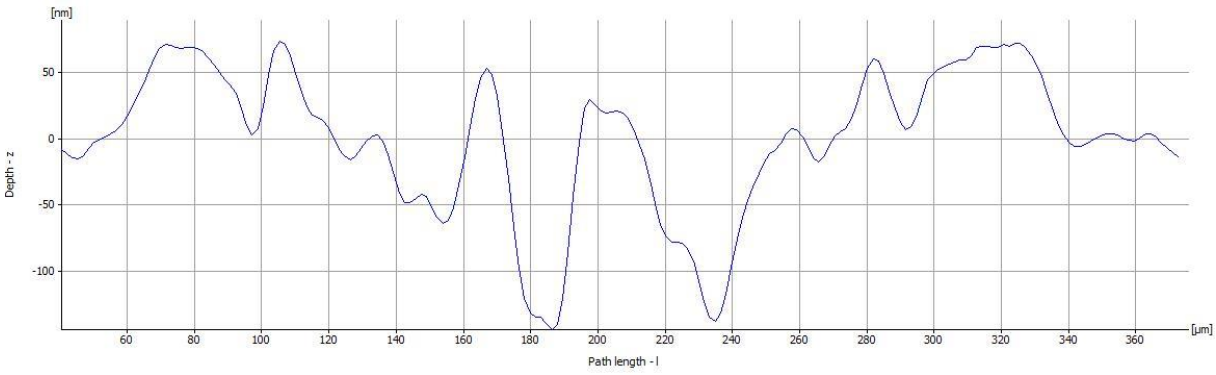

Figure 4-25: Confocal cross section profile of CoCrMo PBS 7.4 with protein test 1

The roughness profiles show very small peaks and grooves, only in the nanometer range. They are often very rounded and sometimes indistinguishable from the roughness outside of the wear track. Comparing the high pH tests with and without proteins (Appendix C) show some differences that indicate a beneficial effect of proteins. Here it is mostly visible in the profile, where the peaks and valleys are fewer and shallower. This is even more pronounced in the low pH tests where there was so little wear on the surface of the protein tests that the microscope was unable to generate any image fit for analysis. In accordance with the tribocorrosion tests, these results show that the wear is higher for the low pH tests without protein, and that proteins do have a beneficial effect. Overall the tribocorrosion results and the confocal microscope results accompany each other very well.

4.4.3. BMG

Figure 4-26 shows that the BMG in no way holds up to the performance of the CoCrMo. Most of the samples have wear scars that are between 20 and 40 µm deep. It has wear mechanisms that are very severe, and therefore has a very large wear volume. From the wear volume measurements it seems that proteins actually have a detrimental influence on the wear volume, and the material also seems to be more prone to wear in high pH environment. This is almost in accordance with the OCP measurements; the only thing that is contradictory to these results is the fact that the OCP for the BMG in low pH with proteins actually shows a more electrochemically stable situation. The reason for this deviation is simply that the material is amorphous. As mentioned earlier with regards to the OCP tests it is very difficult to control the structure and composition of the material. This means that the wear mechanisms and wear development will be totally different from any crystalline material, and this is something that as of yet has been done very little research on. The knowledge of wear on this type of material is therefore very limited, and not fully understood. However, the OCP measurements have shown that the addition of protein seems to stabilize and passivize the surface; this causes oxide formation and in turn increases the WAC. This may then explain some of the increased wear observed.

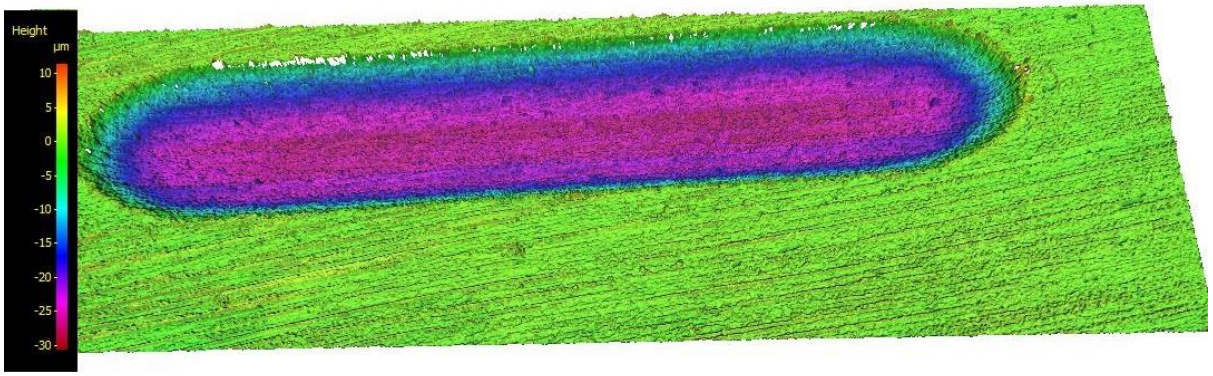

Figure 4-26: Confocal 3d image of BMG PBS 7.4 test 2

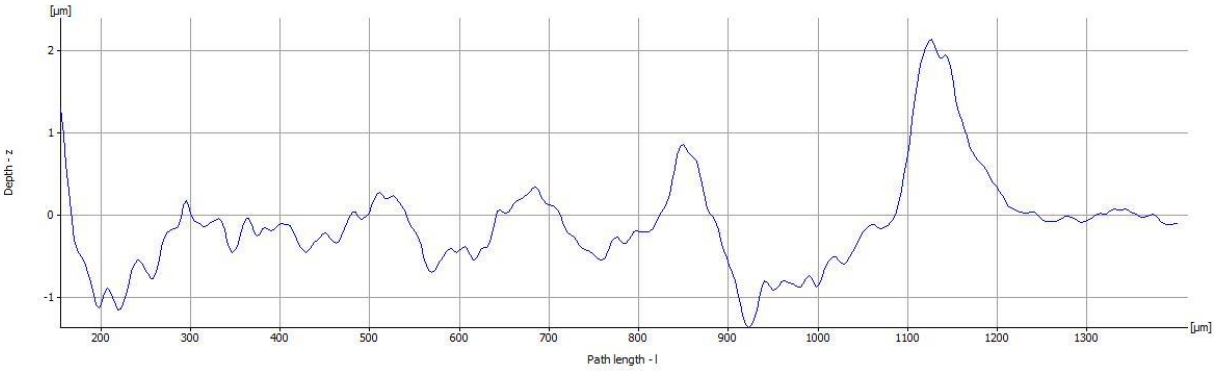

Figure 4-27: Confocal cross section profile of BMG PBS 7.4 test 2

Looking at the wear volume results, it is observable on an overall scale that the wear of the BMG is large. In comparison with itself the wear of the BMG at high pH without protein is moderate with a small amount of peaks and valleys, only 1-2 µm in height as seen in Figure 4-27. This is in accordance with what was found in the tribocorrosion tests. As expected from the tribocorrosion results the wear increases with proteins and a lot of high sharp peaks and valleys in the range of 3 to 4 µm are observed. In the low pH test of the BMG, Figure 4-20, what might have been a slight increase in the potential was seen, indicating activation of the surface, and less wear caused by WAC. When compared to the results in Table 4-4, this seems very likely to be the case. Figure 0-52 to Figure 0-55 also show little wear, small peaks and valleys in the range of 1-3 µm, and Figure 0-53 had very few but larger sized valleys and peaks. When proteins are introduced, the results deviate between the tribocorrosion potential measurements, and the wear volume results. Here large peaks and valleys of 4-6 µm in height difference is seen, albeit fewer than in the other BMG tests (see Figure 0-56 and Figure 0-57). This just goes to show the instability of the material,

and how difficult it is to reproduce results. It should be noted that only one test was performed in low pH with proteins due to time constraints. These results show that the BMG does perform better than Ti 99.6 %, but nowhere near that of the CoCrMo.

4.4.4. Summary of findings from confocal microscopy analysis

The results presented in Table 4-4 and Figure 4-28 are based on an average of two tests, which is not a very broad data foundation. The trend that these results show, however, is that CoCrMo has very little wear in any given situation. It seems to be more stable in high pH than in low, and the addition of proteins seems beneficial in both of the solutions. Again, the results for CoCrMo in PBS 5.2 with protein were unobtainable due to the lack of surface contrast and topography. It can therefore be assumed that the wear was extremely small. The variance of the wear volume in the high pH test without protein was very high and may call for further tests to establish a better average number.

Table 4-4: Wear volume of tribocorrosion tests

Sample	Wear Volume [mm^3]
CoCrMo dry conditions	0.0013
CoCrMo PBS 7.4	0.0011
CoCrMo PBS 7.4 protein	0.0009
CoCrMo PBS 5.2	0.0041*
CoCrMo PBS 5.2 protein	-**
Ti 99.6 % dry conditions	0.0647
Ti 99.6 % PBS 7.4	0.1638
Ti 99.6 % PBS 7.4 protein	0.1268
Ti 99.6 % PBS 5.2	0.1687
Ti 99.6 % PBS 5.2 protein	0.1664
BMG dry conditions	0.0350
BMG PBS 7.4	0.0591
BMG PBS 7.4 protein	0.0762
BMG PBS 5.2	0.0298
BMG PBS 5.2 protein	0.0661*

***Based on one single data set**

****No data available**

In comparison to the dry test, it can be observed that in general the corrosion has some effect on the wear, at least for low pH. However, the wear track seems to be more uneven and rougher in the dry tests, most likely caused by the lack of abrasive oxide particles. It is no surprise that low pH has increased wear due to the formation of oxide particles. That there was little or no difference between the CoCrMo dry test and high pH test can be explained by assuming that the oxide layer remained more or less intact and actually protected the surface.

If the wear volume results are coupled with the data obtained from the polarization tests (Table 4-1) and the Pourbaix diagrams (Appendix A) the results for CoCrMo are very much in accordance with each other. Furthermore the tests with protein have less wear, and it therefore seems that proteins have a beneficial effect.

The biggest problem with Ti 99.6 % is its softness, making CoCrMo a more resistant material albeit not more electrochemically stable. This is a common approach to materials in tribological contacts, but in cases like this, with corrosion as well, other solutions and combinations of more wear resistant materials should be researched. However, some consideration has to be made as to how hard a material should be, because the much harder BMG suffered a greater deal of wear than the CoCrMo. This may be accredited to the amorphous structure of the BMG, making wear predictions difficult. Furthermore the electrochemical stability of a material is not always beneficial with regards to corrosion and wear. As observed; corrosion resistance causes hard oxide film formation and this in turn causes a high WAC. Therefore an active material may be preferable, but there is also the case of cytotoxicity which should be taken into account, making CoCrMo a less favorable material with this in mind.

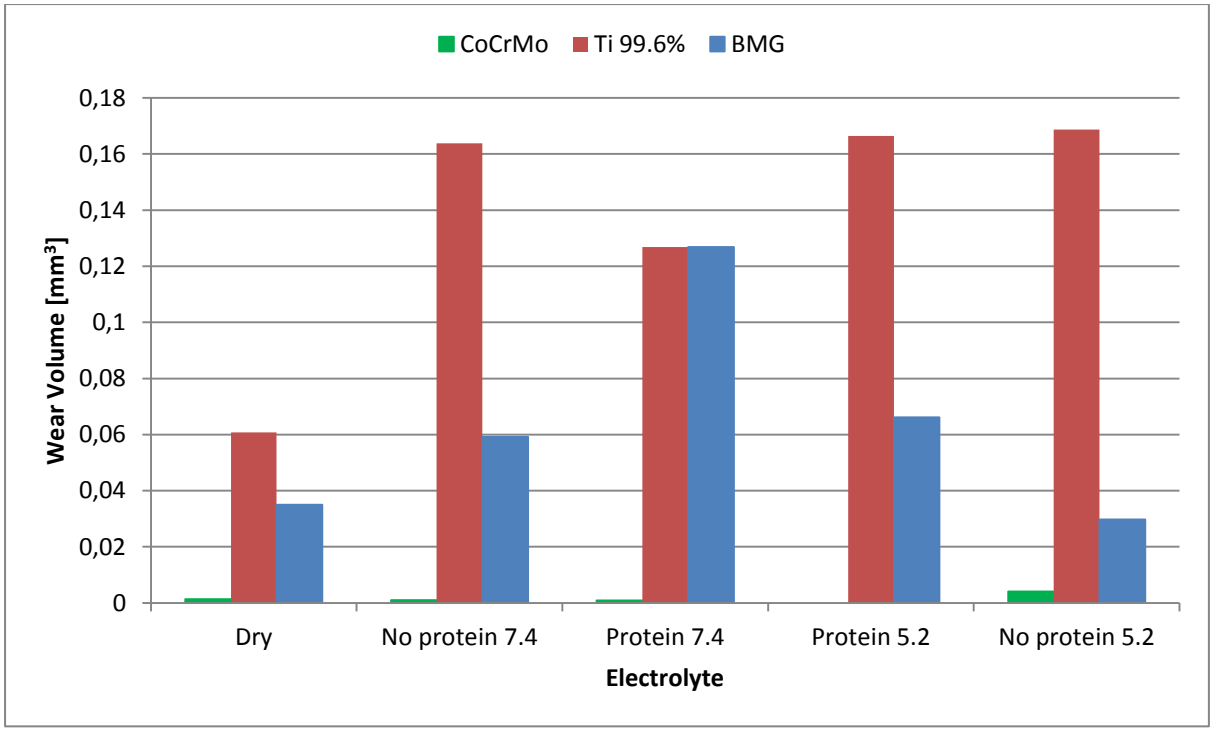

Figure 4-28: Graphical representation of wear volume measurements

In the case of Ti 99.6 % evidence is given for that the wear is highly increased in all the wet tests compared to the dry test. This can be explained by Ti 99.6 %'s affinity to form a stable and hard oxide in almost any environment containing oxide. Furthermore little difference in low and high pH is observable, though it is slightly more wear in the low pH solution. Adding proteins to the solutions seems to have a positive effect by decreasing the wear. For the high pH solution, this is very clear, but it is detectable as well for the low pH. This may be because the protein film shields the material from wear in the initial wear period, and this is consistent with what is seen in the tribocorrosion test results.

CoCrMo has, compared to the other materials, extremely little wear. What can be observed in Figure 4-28, however, is that proteins seem to have the same effect here as on the Ti 99.6 % tests. Also, the material seems to undergo less wear in the wet tests, as compared to the dry. With regards to pH it seems that wear increases when the pH is low, but this effect is negated by the proteins. In fact, the wear seems to be almost non-existent in low pH solution with protein. This decrease in wear may be caused by some lubricating effect of the proteins, which is in accordance with what the tribocorrosion tests showed.

The BMG exhibits almost opposite behavior of the other two materials; lower pH seems to lower the wear of the material, while protein seems to increase it. In fact the wear of the material in high pH with protein is almost equal to that of Ti 99.6 %. With regards to dry versus wet tests, the BMG exhibits the same behavior as the other materials, with one exception: In low pH the wear is actually even less than that observed in the dry tests. This differing behavior of the BMG is raising many questions, which can only be answered through more experiments in order to see any clear trend.

4.5. SEM Analysis

In preparing the samples for imaging in the SEM, the samples were cleaned. The particles that had been produced in the tribocorrosion tests were sampled along with the electrolyte for future ICP-MS testing. No pictures were taken before this was done, and therefore the relative amount of wear particles is not possible to prove. However, the images presented in this chapter do give a very good indication as to which wear mechanisms that were in effect.

4.5.1. Ti 99.6 %

4.5.1.1. Dry Test

Ti 99.6 % suffers under a large development of wear debris in the track, causing third body wear as seen in Figure 4-29. Other mechanisms that are apparent are fatigue wear and ductile deformation. Compared to the other materials this shows no clear sign of adhesive wear.

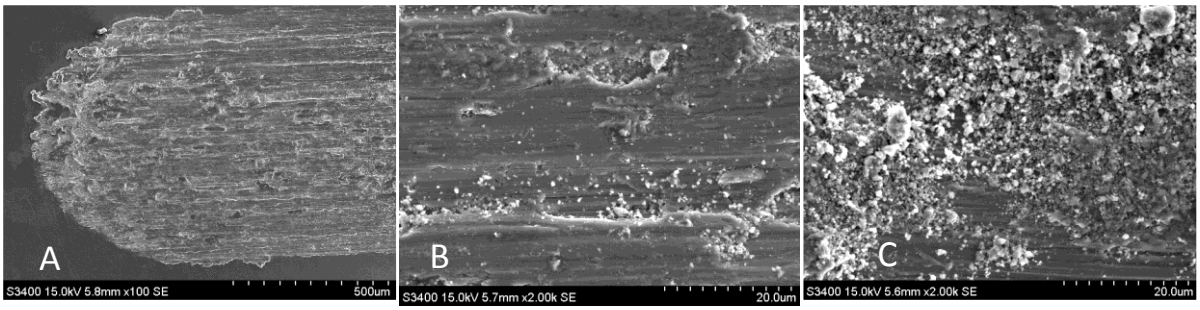

Figure 4-29: SEM images of wear track from Ti 99.6 % dry tests. Resolution: A x100, B x2k, C x2k

4.5.1.2. PBS 7.4

The amount of wear debris is noticeably smaller in this solution, as seen in Figure 4-30, than the dry tests, and the wear mechanism is predominantly ductile deformation and abrasive plowing. Some fatigue wear is apparent, causing cracks

to form and large particles to come loose. The smooth surface is a good indication that the wear is predominantly of third-body mechanisms. The particles present are in addition very small, mostly in the range of 2-4 µm

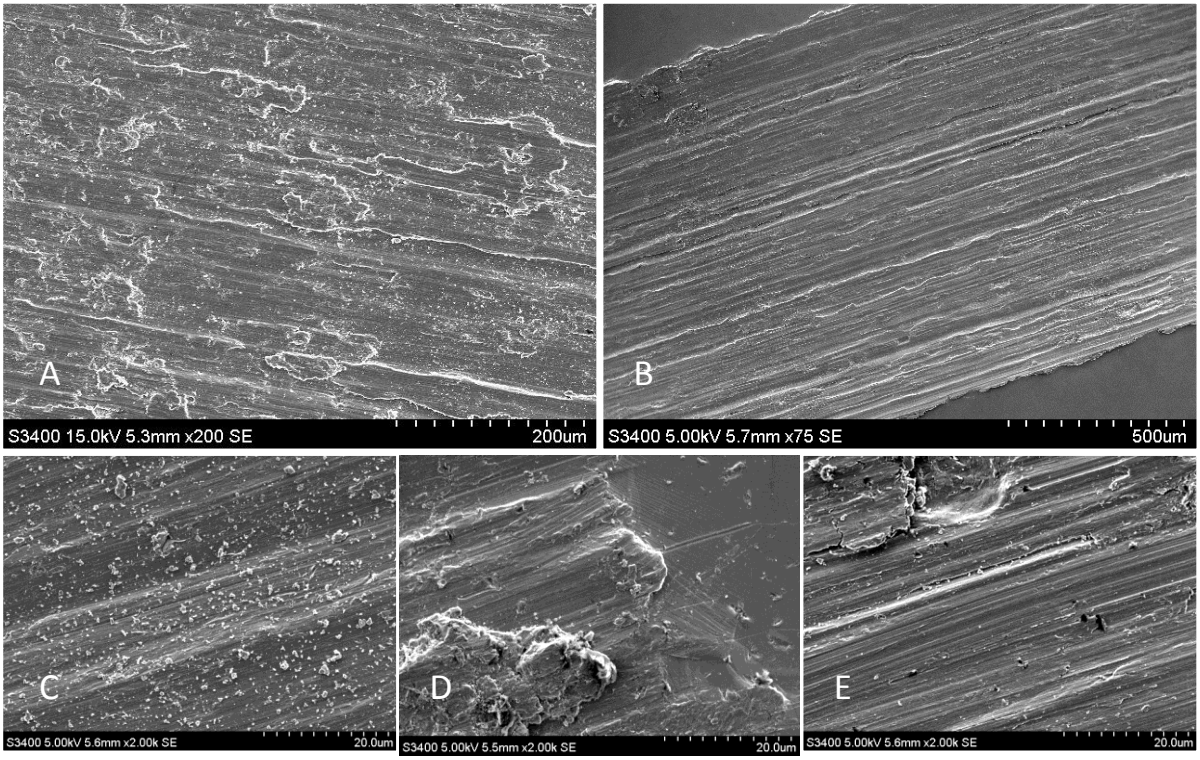

Figure 4-30: SEM images of wear track from Ti 99.6 % PBS 7.4 tests. Magnifications: A x200, B x75, C x2k, D x2k, E x2k

4.5.1.3. PBS 7.4 with protein

Figure 4-31 shows that the material suffers from mostly ductile deformation and fatigue wear. Some corrosion particles and scratching can also be observed in the wear track indicating third body wear mechanisms. The wear seems to have more of a fatigue component than in the test without protein, also more particles seem to be present in the wear track, despite the fact that these tests had a significantly smaller wear volume. These particles may not only be oxides, but proteins as well.

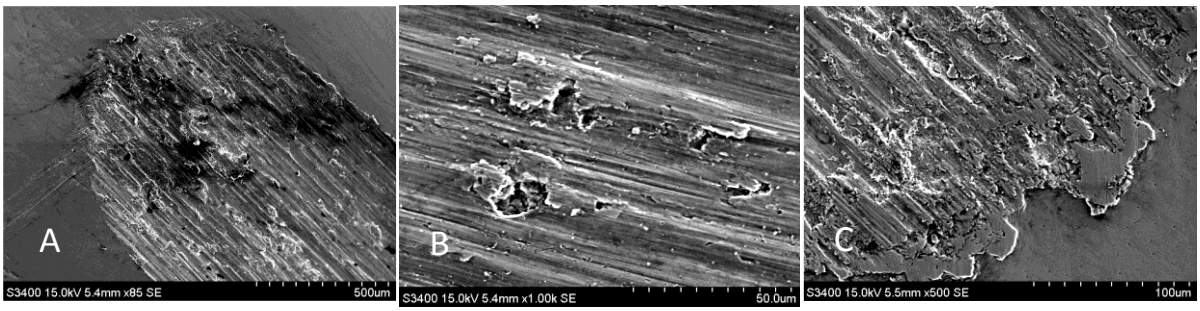

Figure 4-31: SEM images of wear track from Ti 99.6 % PBS 7.4 tests with protein. Magnifications: A x85, B x1k, C x500

4.5.1.4. PBS 5.2

The tests presented Figure 4-32 in show that there is evidence of fatigue wear, and oxide particles left in the wear track compared to the high pH tests. The particles also seem larger, which may account for the higher wear volume. The mechanism seems to be predominantly third body wear, as there is remnants of particles in the wear track.

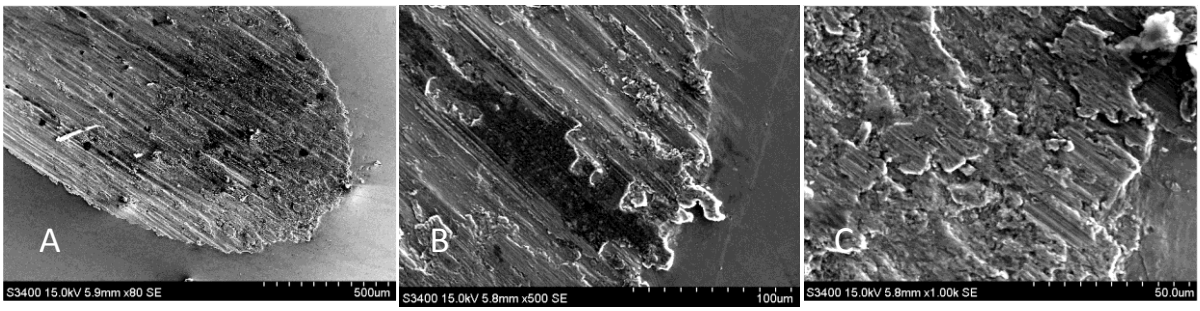

Figure 4-32: SEM images of wear track from Ti 99.6 % PBS 5.2 tests. Magnifications: A x80, B x500, C x1k

4.5.1.5. PBS 5.2 with protein

In Figure 4-33 more evidence of fatigue wear and ductile deformation is seen. In addition more particles still in the wear track (see especially figures in Appendix C) is observable, much like the test done at this pH without proteins, but here proteins will be a part of the particles observed. This shows that the wear mechanisms for this electrolyte are third body as well.

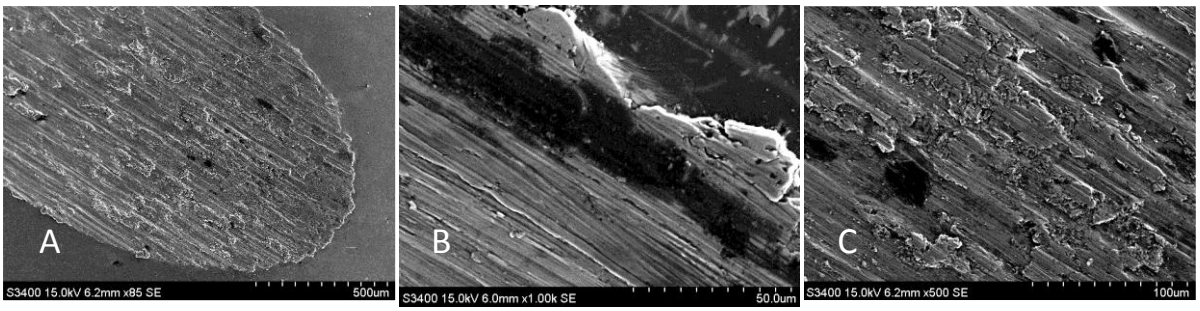

Figure 4-33: SEM images of wear track from Ti 99.6 % PBS 5.2 tests with protein. Magnifications: A x85, B x1k, C x500

4.5.2. CoCrMo

4.5.2.1. Dry Test

In Figure 4-34 very little debris are to be seen in the wear track. The wear mechanism is mostly abrasion and some ductile deformation and plowing, which are two-body wear mechanisms. This behavior is expected as it is classical hard on hard material wear. At the end of the track an accumulation of particles can be observed; this is caused by adhesive wear and is metal residue from cold welding. These particles are the cause of the plowing.

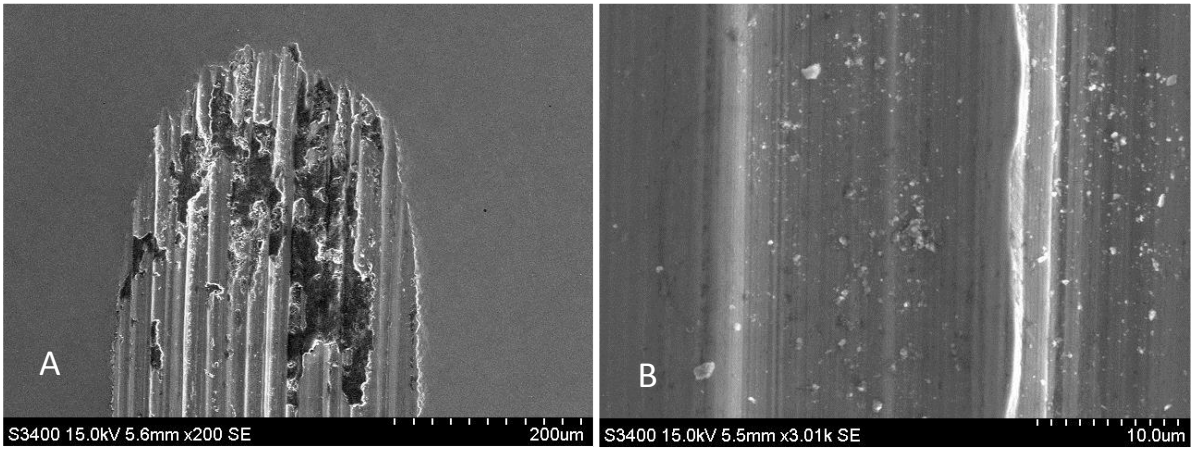

Figure 4-34: SEM images of wear track from CoCrMo dry tests. Magnifications: A x200, B x3k

4.5.2.2. PBS 7.4

The pictures in Figure 4-35 show that the wear is noticeable smaller than in the dry test; more oxide formation is observable, and the wear mechanism seems to be predominantly abrasion and plowing which means that two-body abrasive wear is the cause of the wear. That the wear is smaller than in the dry test may indicate that the oxide layer formed is functioning as a coating and shielding the metal from mechanical wear, and also that adhesive wear is eliminated.

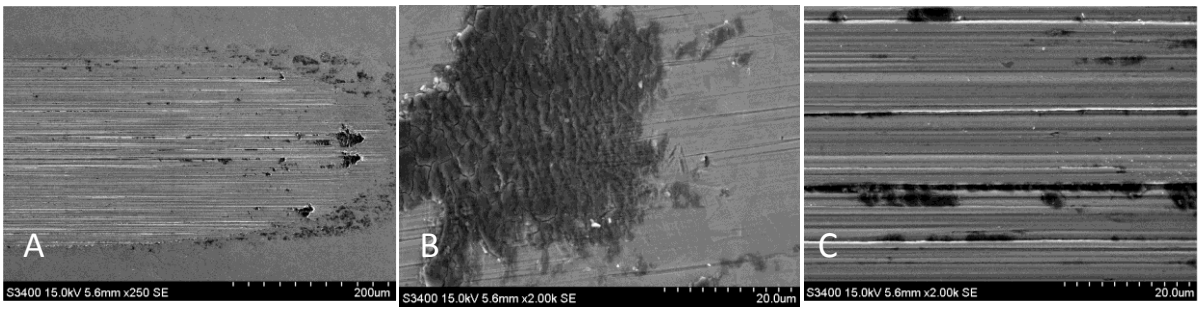

Figure 4-35: SEM images of wear track from CoCrMo PBS 7.4 tests. Magnifications: A x250, B x2k, C x2k

4.5.2.3. PBS 7.4 with protein

The wear volume was lower in this test presented in Figure 4-36 compared to the test without protein, this may indicate that the proteins adsorbing on the surface are acting as a lubricant due to the low normal force used. The corrosion debris seems to be smaller or non-existent, this is because it is pushed out of the wear track due to the two-body wear mechanism. The wear shows signs of plowing and ductile deformation here as well, again indicating two-body abrasive wear.

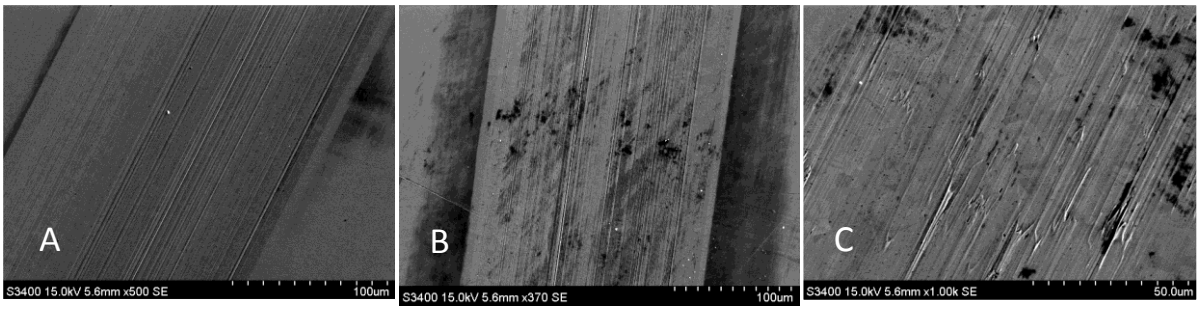

Figure 4-36: SEM images of wear track from CoCrMo PBS 7.4 tests with protein. Magnifications: A x500, B x370, C x1k

4.5.2.4. PBS 5.2

In accordance with the data from the tribocorrosion results and the wear volume measurements Figure 4-37 shows an increase in corrosion debris, larger particles and deeper scratching patterns. It is also possible to see the ductile deformation of the sides of the wear track, indicating more material displacement due to a deeper wear track. This increase in particles seems to suggest that the wear mechanisms are predominantly three-body mechanisms.

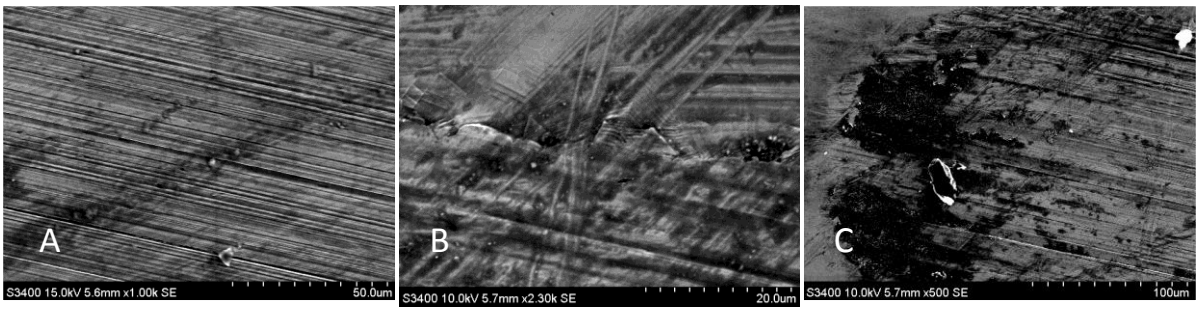

Figure 4-37: SEM images of wear track from CoCrMo PBS 5.2 tests. Magnifications: A x1k, B x2k, C x500

4.5.2.5. PBS 5.2 with protein

From the images in Figure 4-38 it is easy to see that the wear is very small. It is mostly caused by deformation of the material, and not as much by particles caught between the two moving bodies. Some corrosion is visible in the end of the wear scar, but even this is varying between the tests. Some abrasive wear is possible to detect, mostly plowing. The material seems again to be lubricated by the proteins, and that this is greatly decreasing the wear. The mechanisms observed here are mostly two-body abrasive wear. The "infinity" sign appearing in some of the images is thought to be caused by some form of error in the SEM, as it appears in many images, though only limited to the CoCrMo samples.

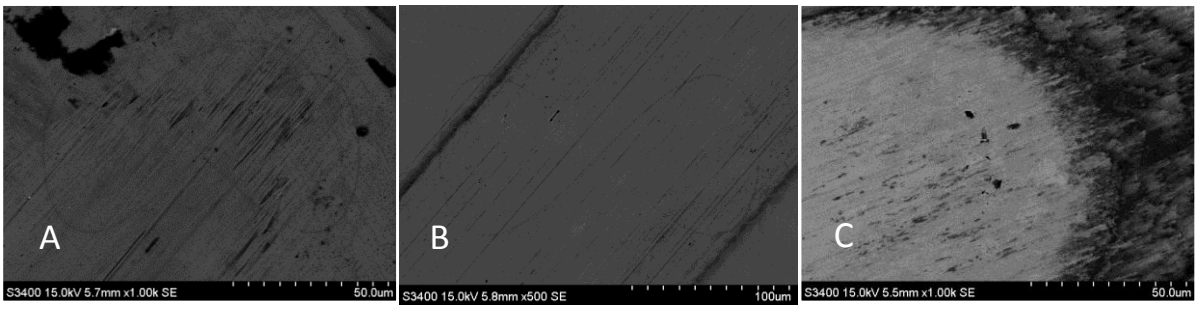

Figure 4-38: SEM images of wear track from CoCrMo PBS 5.2 tests with protein. Magnifications: A x1k, B x500, C x1k

4.5.3. BMG

4.5.3.1. Dry Test

For the BMG dry test Figure 4-39 shows a lot of adhesive wear and micro fatigues indicating that the material is harder than the CoCrMo and the Ti 99.6 %. Furthermore the material is showing a more plastic behavior than the higher alloyed BMG [52]. The amount of particles in the wear track indicates third-body wear mechanisms.

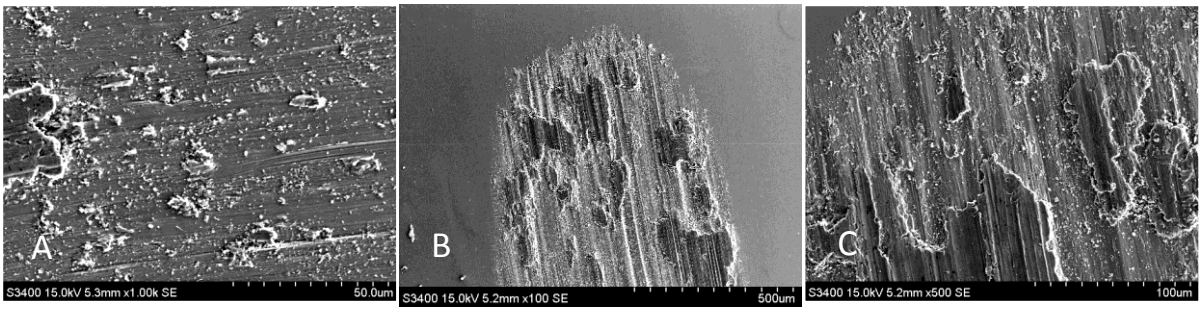

Figure 4-39: SEM images of wear track from BMG dry tests. Resolution: A x1k, B x100, C x500

4.5.3.2. PBS 7.4

From what can be seen in Figure 4-40 it is evident that there has been a lot of adhesive wear on some samples, but evidence of abrasive wear is also seen. Some particles are left in the wear track, and these are most likely surface particles that are much less plastic than the surrounding material. These particles are in the range of 30-50µm in size. In the top left picture there is some porous structure that might have been caused by pitting corrosion. This wear may be caused by microcrystalline inclusions, which were undetectable in the XRD. The mechanisms that there is evidence of here are predominantly third-body.

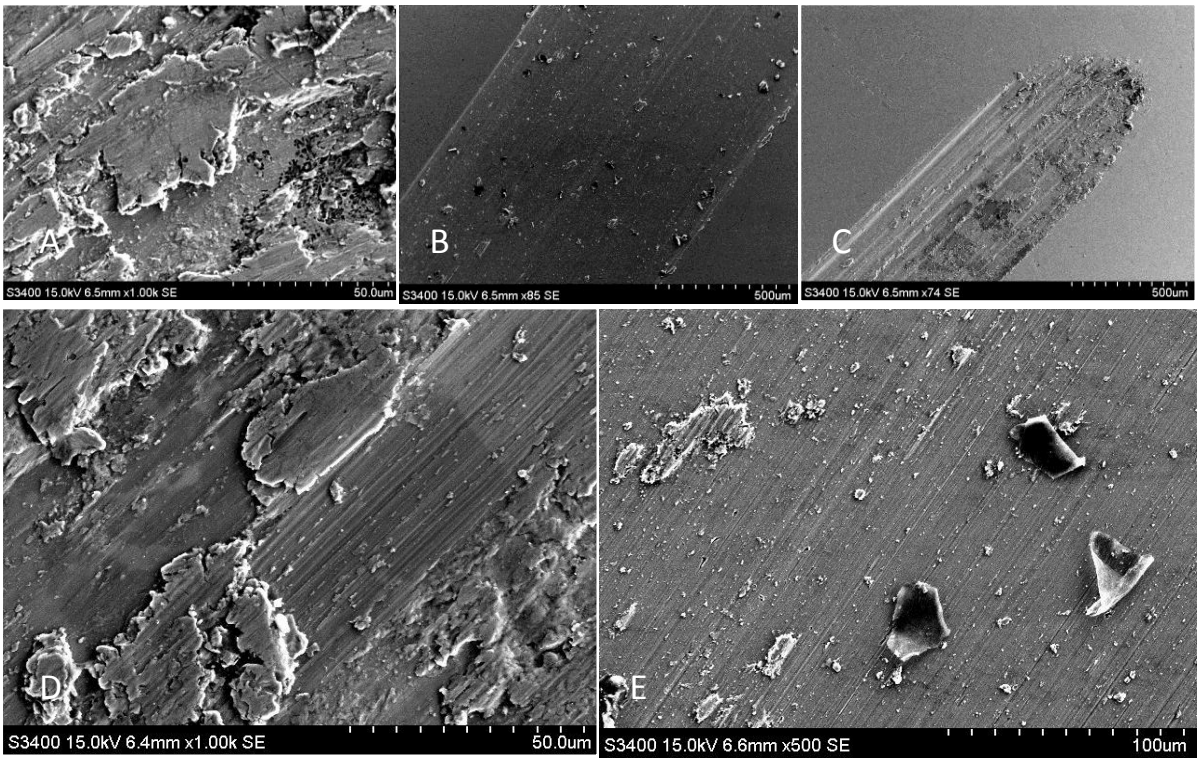

Figure 4-40: SEM images of wear track from BMG PBS 7.4 tests. Magnifications: A x1k, B x85, C x74, D x1k, E x500

4.5.3.3. PBS 7.4 with protein

Figure 4-41 shows a much cleaner wear track, with much less adhesive wear and particles. Plowing and abrasive wear are the most predominant mechanisms and some fatigue wear as well. This is most likely a mix of two-body and three-body regime, due to the smoothness of the surface, and the lack of wear particles in the track. In addition increased wear is often a sign of a two-body wear mechanism.

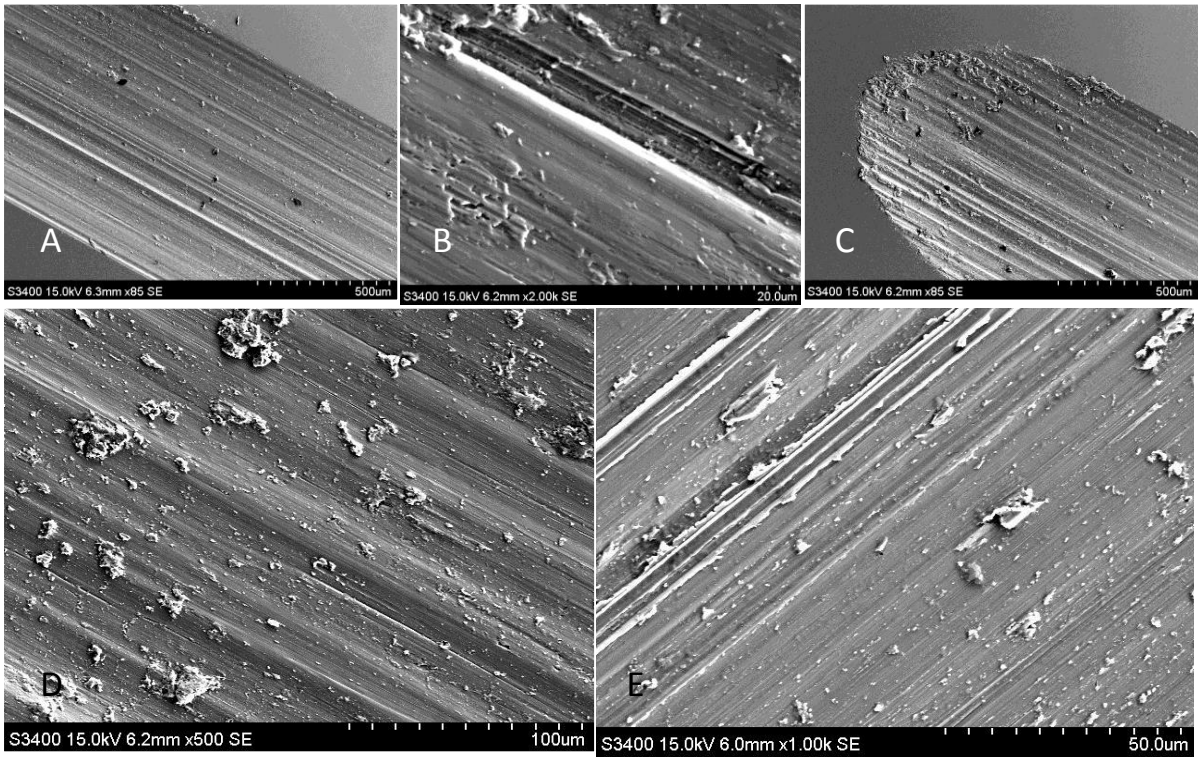

Figure 4-41: SEM images of wear track from BMG PBS 7.4 tests with protein. Magnifications: A x85, B x2k, C x85, D x500, E x1k

4.5.3.4. PBS 5.2

Figure 4-42 indicates that more corrosion has taken place during the tests, and that more oxide debris has been deposited in the wear track. In addition some adhesive wear, fatigue wear and abrasion can be observed. Some scratches may be caused by two body wear, but it seems to be predominantly third body mechanisms that have caused the wear.

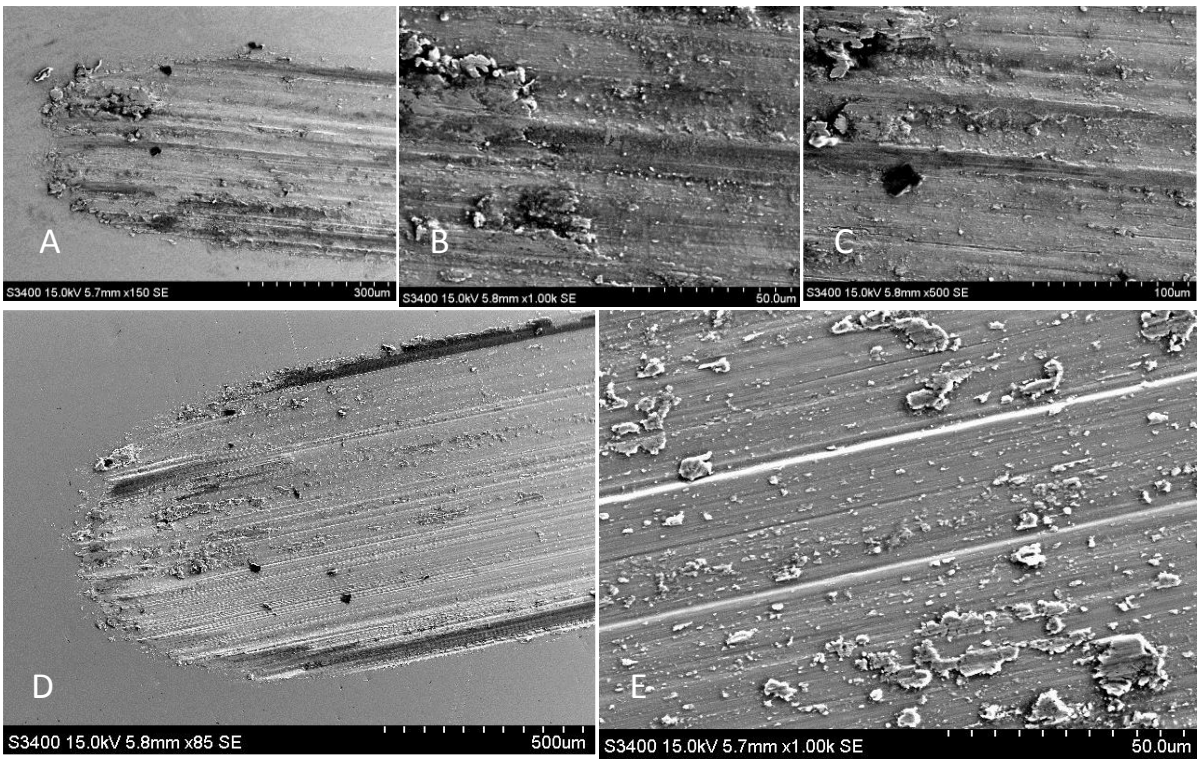

Figure 4-42: SEM images of wear track from BMG PBS 5.2 tests. Magnifications: A x150, B x1k, C x500, D x85, E x1k

4.5.3.5. BMG PBS 5.2 with protein

Figure 4-43 shows yet again the presumably beneficial effect of proteins. Very little deposition of particles and oxides are visible, and the surface is rather smooth. This indicates a third body wear mode, and in addition some fatigue wear is visible. But the lack of particles may also indicate some form of two-body wear, which is not positive in terms of durability.

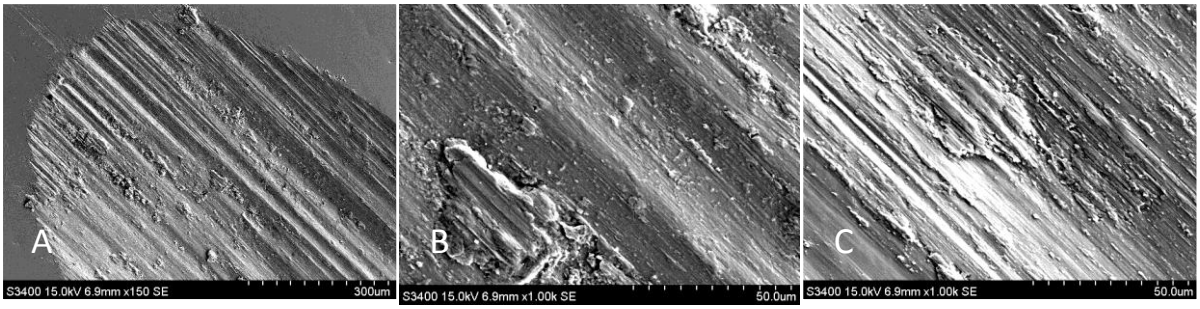

Figure 4-43: SEM images of wear track from BMG PBS 5.2 tests with protein. Magnifications: A x150, B x1k, C x1k

5. Conclusion

From the information gathered in the present work certain conclusions, based on a limited number of experiments, can be drawn. Firstly it should be mentioned that dealing with the human body as an environment creates many challenges, as no one person is alike. Therefore, a material clinically exposed might work perfectly for one person, and fail catastrophically when exposed in another. In other words, it is very difficult to find a general solution that would fit all patients in need of an implant. The materials that scientists are able to compare to are then of course taken from cases where the material has failed, because in the other case the patient will have its prosthesis for the rest of their lives. Secondly, as mentioned before, the evaluation of tribocorrosion properties for load-bearing materials exposed in artificial body solutions is a field which is relatively unexplored. The relationships between tribocorrosion and biomaterials has not been researched extensively, even the field of tribocorrosion in itself is relatively new. Due to this, the conclusions drawn here are based on general trends, and give an indication as to how the different materials may behave in the given situations.

The following conclusions are hereby drawn for each of the materials investigated:

- The CoCrMo alloy showed an increased performance in solutions with additions of protein, and was very stable in regards to its tribocorrosion properties, in both the low (5.2) and high (7.4) pH solutions.
- The wear volume of the CoCrMo alloy was, in general, very small (around 0.001 mm^3).
- The wear mechanisms for the CoCrMo alloy were predominantly two-body abrasive wear.
- When exposed in the low (5.2) pH solution Ti 99.6 % was more prone to tribocorrosive wear than in the high (7.4) pH environment.
- The wear mechanism for Ti 99.6 % was predominantly third body abrasion and plowing.
- The wear volume of Ti 99.6 % was, in general, around 0.165 mm^3.
- The BMG proved to suffer from more tribocorrosive wear in the high (7.4) pH solution than in the low (5.2) pH solution.

- The wear mechanisms observed for the BMG were predominantly three-body abrasive wear and plowing, but some two-body wear was also in effect.
- The wear volume of the BMG was, in general, around 0.05 mm^3.
- The BMG did not prove to have good corrosive properties under the conditions investigated; it was very unstable and gave low reproducibility of the results.

The following conclusions are hereby drawn in regards to the comparison between the materials:

- In all electrolytic solutions investigated, i.e. with and without the additions of proteins, as well as low (5.2) and high (7.4) pH, the CoCrMo alloy proved to be more tribocorrosion resistant than both the BMG and the Ti 99.6 %. Overall , Ti 99.6 % proved to suffer the most severe tribocorrosive wear and degradation
- Of the three materials investigated, the CoCrMo alloy was the only material proving to be suitable for use in the articulating surface of a load-bearing implant.

6. Further work

The tribocorrosion tests presented in the present work make use of a simple pin-on-plate tribology system. This is, however, far from the real life situation for materials in use in load-bearing implants, as it does not simulate the actual motion and changing load of a natural joint movement. Based on the results obtained, it is also impossible to evaluate changes in the material properties as a function of time. It should, in this regard, be noted that several different simulators exist, with their own strengths and limitations [80], and this may be something to build further research on.

The experimental tests carried out in the present work all had a duration of one hour, which is nowhere near the time aspect of real life prosthesis (which could be, on average, 10-15 years). Due to this, evidence for what might happen to the materials after continued wear over a prolonged period of time is therefore not available at this time. The BMG may, for instance, stabilize at a constant wear rate after the initial run-in. In other words, the wear is severe in the beginning, but might prove to hold longer than, for instance, the CoCrMo before it reaches a critical performance value, i.e. before the wear is too severe for the implant to function in a satisfying manner anymore. A good graphical representation of this can be seen in Figure 6-1.

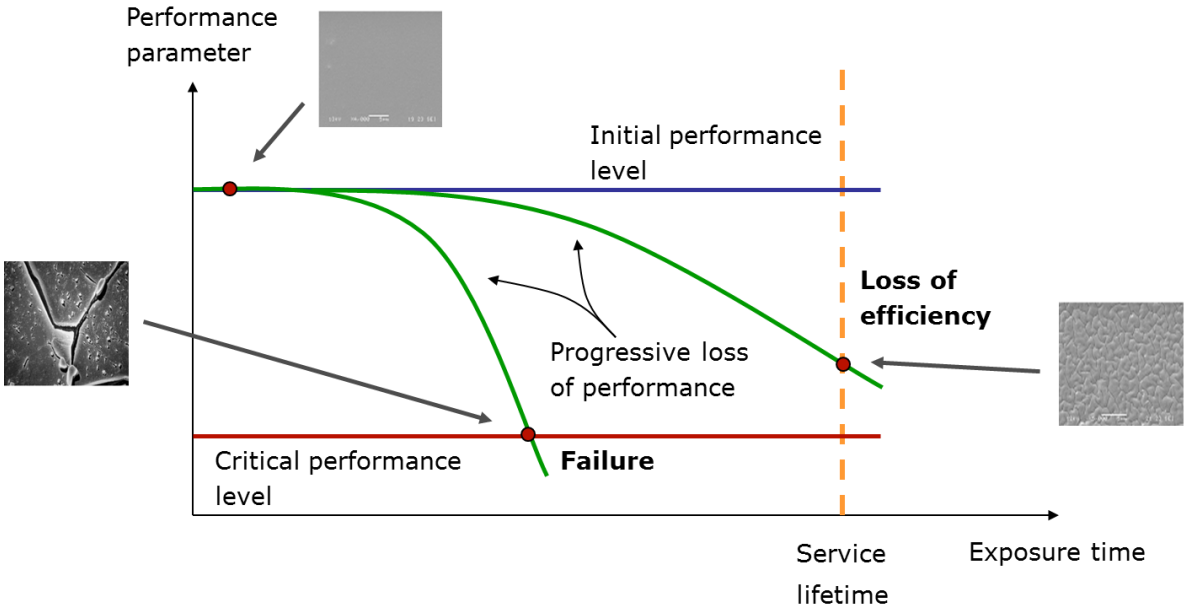

Figure 6-1: Material degradation over time [50]

It has already been mentioned; that the BMG alloy investigated in the present work contains cytotoxic alloying elements such as copper, nickel and aluminum. Research is therefore continuously being conducted in regards to produce zirconium based BMGs without the use of such elements with promising results [81] [82]. Further research into their biotribocorrosive properties is of key importance in order to establish whether or not they are generally viable as implant materials.

Due to the difficulty of producing large bulk quantities of the BMGs, an alternative is to shape the material into a resurfacing coat on top of another biomaterial. The idea is then that a few millimeter thick layer of a BMG alloy could act as a wear material, while the bulk material is made out of, for instance, stainless steel or titanium. This would greatly reduce the need for extremely low glass transition temperatures, as the material would have less volume to cool. It would also drastically reduce the production cost. Further research into this possibility is needed.

In view of the work conducted by the present author, further investigations of the biotribocorrosion properties in regards to the materials presently investigated is needed. Some of the aspects of immediate importance are listed below:

- Preliminary results indicated that proteins may have a beneficial contribution to the tribocorrosion system of the CoCrMo alloy and Ti 99.6 %, acting as a lubricant; further studies need to be conducted in order to see any clear trends. More experiments are also needed to establish whether or not the proteins only act lubricating due to the low normal force (2N) used.
- For the BMG alloy proteins seemed to increase the wear in both the low (5.2) and the high (7.4) pH regimes. To establish whether this is a trend or not, further investigations are needed. As the BMG alloy also seemed less prone to WAC (Wear Accelerated Corrosion) in the low (5.2) pH solution, further experiments are needed to confirm even this. In addition it is necessary to see if these trends are composition dependent
- A counter body of the same material, or materials commonly used as counter body in joint implants, i.e. UHMWPE or CoCrMo alloy, should be tested to better simulate real life conditions

- Different surface treatments/modifications of the materials, including nitriding and DLC (Diamond Like Carbon) should also be tested, to see the effect on the material properties.
- The influence of the formation of nano-crystals on the surface of the BMG alloys should also be assessed, to try to improve the overall tribocorrosion properties.
- There should be established a standard grinding/polishing method for BMGs to assure optimal surface quality/finish.
- Cu, Ni and Al free BMGs need to be produced and evaluated to find completely non-toxic alternatives.
- The electrolyte from the different tribocorrosion experiments should be analyzed with the use of ICP-MS (Inductively Coupled Mass Spectrometry) to establish the different materials chemical stability in regards to metal ion release.

In other word, in regards to establishing whether or not (i) BMGs in some form is a viable biomaterial, (ii) if it is better than the crystalline counterpart, and (iii) if it is able to compete with the CoCrMo alloy used in load-bearing implants today, further experiments need to be performed. The hope for the future is that BMG alloys can take the place as the most used, most stable, and least toxic biomaterial to date, improving the quality of life for the patients in need of these implants.

Bibliography

[1] L. Engesæter, O. Furnes og L. I. Havelin, «Annual Report Norwegian National Joint Registry,» Helse Bergen HF, Bergen, 2011.

[2] G. Garellick, J. Kärrholm, C. Rogmark and P. Herberts, “Annual Report Swedish Hip Arthroplasty Registry,” Swedish Hip Arthroplasty Registry, Göteborg, 2010.

[3] “Life expectancy increase and low infant mortality,” 2011. [Online]. Available: http://www.ssb.no/english/subjects/02/02/10/dode_en/ . [Accessed 29 June 2012].

[4] K. Elsharkawy, C. A. Higuera, A. K. Klika and W. K. Barsoum, "Evolution of bearing surfaces in total hip arthroplasty: a review," *Current Orthopaedic Practice,* vol. 21, no. 2, pp. 198-208, March/April 2010.

[5] R. Singh and N. B. Dahotre, "Corrosion degradation and prevention by surface modification of biometallic materials," *J Mater Sci: Mater Med,* pp. 725-751, 2007.

[6] G. Thorwarth, C. Falub, U. Müller, B. Weisse, C. Voisard, M. Tobler and R. Hauert, "Tribological behavior of DLC-coated articulating joint implants," *Acta Biomaterialia,* no. 6, pp. 2335-2341, 2010.

[7] M. S. H. Nazari, Wear characteristics of materials for artificial hip joints, Göteborg: Department of Materials and Manufacturing Technology, Chalmers University of Technology, 2005.

[8] M. T. Mathew, P. S. Pai, R. Pourzal, A. Fischer and M. A. Wimmer, "Significance of Tribocorrosion in Biomedical Applications:," *Advances in Tribology,* pp. 1-12, 2009.

[9] D. F. Williams and R. L. Williams, "Degradative Effects of the Biolocical Environment on Metals and Ceramics," in *Biomaterials Science - An introduction to materials in medicine*, 2. ed., B. D. Ratner, A. S. Hoffman, F. J. Schoen and J. E. Lemons, Eds., San Diego, Elsevier Academic Press, 2004, pp. 430-438.

[10] J. M. Anderson, A. Rodriguez and D. T. Chang, “Foreign Body Reactions to Biomaterials,” *Semin Immunol,* no. 20, pp. 86-100, April 2008.

[11] Y. Yan, A. Neville and D. Dowson, "Biotribocorrosion of CoCrMo orthopaedic implant materials - Assessing the formation and effect of the biofilm," *Tribology International,* no. 40, pp. 1492-1499, 6 April 2007.

[12] Y. Sawae, A. Yamamoto and T. Murakami, "Influence of protein and lipid concentration of the test lubricant on the wear of ultra high molecular weight polyethylene," *Tribology International,* no. 41, pp. 648-656, 2008.

[13] M. Nezafati, "Study over Corrosion properties and ion release of Zr55Cu30Ni5Al10 Bulk Metallic Glass for hip joint implants," Swerea KIMAB, Stockholm, 2010.

[14] S. E. Majd, "Zr55Cu30Ni5Al10 Bulk Metallic Glass - Characterization of Tribo-corrosion Properties under Simulated in Vivo Conditions," Royal Institute of Technology, Stockholm, 2011.

[15] N. J. Hallab, J. J. Jacobs and J. L. Katz, "Orthopedic applications," in *Biomaterials Science - An Introduction to Materials in Medicine*, 2. ed., B. D. Ratner, A. S. Hoffman, F. J. Schoen and J. E. Lemons, Eds., San Diego, California: ELSEVIER, 2004, pp. 526-555.

[16] A. Faller, M. Schünke, G. Schünke and E. Taub, in *The human body : an introduction to structure and function*, Stuttgart, Thieme, 2004, pp. 174-175.

[17] "Wikipedia - Kugelgelenk," Wikimedia, [Online]. Available: http://upload.wikimedia.org/wikipedia/commons/0/00/Kugelgelenk.jpg. [Accessed 21 June 2013].

[18] "Wikipedia - Joint," Wikimedia, [Online]. Available: http://upload.wikimedia.org/wikipedia/commons/1/19/Joint.png. [Accessed 21 June 2013].

[19] D. Stock, "Total Hip Replacement," Nucleus Medical Art, 2012. [Online]. Available: http://doctorstock.photoshelter.com/image/I0000hazwGcDnRQ4. [Accessed 20 May 2013].

[20] C. Delaunay, "The Charnley Total Hip Replacement - The Gold Standard of Primary Hip Replacement 36 Years on," 1998. [Online]. Available: http://www.maitrise-orthop.com/corpusmaitri/orthopaedic/mo83_delaunay/delaunay_us.shtml. [Accessed 20 June 2012].

[21] S. Desai, B. Bidanda and P. Bártolo, "Metallic and Ceramic Biomaterials: Current and Future Developments," in *Bio-Materials and prototyping Applications in Medicine*, B. Bidanda and P. B. rtolo, Eds., Springer, 2008, pp. 1-14.

[22] Pilliar R., "Metallic Biomaterials," in *Biomedical Materials*, Springer Science, 2009, pp. 41-81.

[23] L. Nilsen, «Nye hofteproteser gir flere reoperasjoner,» Juli 2002. [Internett]. Available:

http://www.dagensmedisin.no/nyheter/nye-hofteproteser-gir-flere-reoperasjoner/. [Funnet 19 Juli 2012].

[24] M. M. e. a. Kevin J. Bozic, "The Epidemiology of Revision Total Hip Arthroplasty in the United States," *The Journal of Bone & Joint Surgery,* vol. 91A, pp. 128-133, January 2009.

[25] T. M. Wright and S. B. Goodman, "What are the local and biologic reactions to wear debris," in *Implant Wear in Total Joint Replacement: Clinical and Biologic*, T. M. Wright and S. B. Goodman, Eds., American Academy of Orthopaedic Surgeons, 2001, pp. 61-70.

[26] C. Migliaresi and H. Alexander, "Composites," in *Biomaterials Science - An Introduction to Materials in Medicine*, 2. ed., P. Buddy D. Ratner, S. Allan S. Hoffman, M. P. Frederick J. Schoen and P. Jack E. Lemons, Eds., San Diego, California: ELSEVIER Academic Press, 2004, p. 194.

[27] Rothman Institute Orthopaedics, "Total Hip Replacement," [Online]. Available: http://www.rothmaninstitute.com/specialties/treatments/total-hip-replacement. [Accessed 18 July 2012].

[28] D. Kluess, H. Martin, W. Mittelmeier, K.-P. Schmitz and R. Bader, "Influence of femoral head size on impingement, dislocation," *Medical Engineering & Physics,* no. 29, pp. 465-471, 2007.

[29] J. M. Steckelberg and D. R. Osmon, "Prosthetic Joint Infections," in *Infections Associated with Indwelling Medical Devices*, 3. ed., F. A. Waldvogel and A. L. Bisno, Eds., Washington, Columbia: ASM Press, 2000, pp. 173-175.

[30] S. P. Gorman and D. S. Jones, “Antimicrobial Biomaterials for Medical Devices,” ELSEVIER, 2002.

[31] A. Tabeshian, “Production, Characterization and Electrochemical Properties of Advanced Bulk Metallic Glasses for Hip Implant Applications,” NTNU, Trondheim, 2011.

[32] C. Wallis, "Joint Replacements Expected to Soar," 6 March 2008. [Online]. Available: http://www.time.com/time/health/article/0,8599,1720041,00.html#ixzz1yW3vIccC. [Accessed 21 June 2012].

[33] B. Shi and H. Liang, "Tribological applications of biomaterials: an overview," *SCIENCE IN CHINA,* no. 44, pp. 297-306, August 2001.

[34] A. Borruto, "A new material for hip prosthesis without considerable debris release," *Medical Engineering & Physics,* no. 32, pp. 908-913, 24 June 2010.

[35] T. M. Wright and S. B. Goodman, "What are the systemic consequences of wear debris clinically?," in *Implant Wear in Total Joint Replacement: Clinical and Biologic*, T. M. Wright and S. B. Goodman, Eds., American Academy of Orthopaedic Surgeons, 2001, pp. 31-42.

[36] J. C. Rubio, M. C. Garcia-Alonso, C. Alonso, M. A. Alobera, C. Clemente, L. Munuera and M. L. Escudero, "Determination of metallic traces in kidneys, livers, lungs and spleens of rats with metallic implants after a long implantation time," *Journal of Materials Science: Materials in Medicine,* pp. 1-12, 3 July 2007.

[37] M. B. Mayor, K. Merritt and S. A. Brown, "Metal Allergy and the Surgical Patient," *Scientific Papers,* no. 139, pp. 477-479, April 1980.

[38] J. Schroers, G. Kumar, T. M. Hodges, S. Chan and T. R. Kyriakides, "Bulk Metallic Glasses for Biomedical," *JOM (Journal of the Minerals, Metals and Materials Society),* vol. 61, no. 9, pp. 21-29, September 2009.

[39] T. Aihara, E. Akiyama, K. Aoki, M. S. El-Eskandarany, H. Habazaki, K. Hashimoto, A. Kawashima, M. Naka, Y. Ogino, K. Sumiyama, K. Suzuki and T. Yamasaki, "Methods for Production of Amorphous and Nanocrystalline Materials and Their Unique Properties," in *Amorphous and Nanocrystalline Materials*, A. Inoue and K. Hashimoto, Eds., Sendai, Miyagi: Springer, 2001, pp. 87-132.

[40] "Vacuum Arc Remelting (VAR)," ALD Vacuum Technologies, [Online]. Available: http://web.ald-vt.de/cms/?id=62. [Accessed 17 March 2013].

[41] C. Suryanarayana and A. Inoue, Bulk Metallic Glasses, Boca Raton, Florida: CRC Press, 2011.

[42] "High Pressure Die Casting," [Online]. Available: http://ars.els-cdn.com/content/image/1-s2.0-S0921509307007174-gr1.jpg. [Accessed 23 June 2013].

[43] X. H. Lin and W. L. Johnson, "Formation of Ti-Zr-Cu-Ni bulk metallic glasses," *Journal of Applied Physics,* vol. 78, no. 11, pp. 6514-6519, 1 December 1995.

[44] C. S. C.Y. Tam, "Abrasive wear of Cu60Zr30Ti10 bulk metallic glass," *Materials Science and Engineering A,* no. 384, pp. 138-142, 2004.

[45] A. Bakai, A. Shpak, N. Wanderka, S. Kotrechko, T. Mazilova and I. Mikhailovskij,

"Inherent strength of zirconium-based bulk metallic glass," *Journal of Non-Crystalline Solids,* pp. 1-5, 2010.

[46] M. D. Demetriou, M. E. Launey, G. Garrett, J. P. Schramm, D. C. Hofmann, W. L. Johnson and a. R. O. Ritchie, "A damage-tolerant glass," *Nature Materials,* pp. 1-6, 9 January 2011.

[47] "Metallic Implant Materials," in *Biomaterials - an introduction*, 3. ed., New York, New York: Springer, 2007, pp. 99-137.

[48] K. Friedrich, Friction and wear of polymer composites, Amsterdam: Elsevier Science Publishers, 1986.

[49] D. F. Moore, Principles and applications of tribology, Oxford: Pergamon Press, 1975.

[50] P. R. E. Aune, *Tribology of artificial joints,* Trondheim, 2013.

[51] G. W. Stachowiak and A. W. Batchelor, Engineering Tribology, Elsevier, 2005.

[52] C. T. Rodríguez, "Bulk Metallic Glasses (BMG) for biomedical applications – a tribocorrosion investigation of Zr55Cu30Ni5Al10 in simulated body fluid," NTNU, Trondheim, 2011.

[53] A. Unsworth, "Tribology of human and artificial joints 1991," *Journal of Engineering in Medicine,* no. 205, pp. 163-172, 1991.

[54] C. R. Bragdon, D. O'Connor, J. D. Lowenstein, M. Jastry and W. D. Syniuta, "The importance of multidirectional motion on the wear of polyethylene," *Journal of Engineering in Medicine 1996,* no. 210, pp. 157-165, 1996.

[55] Y. Yan, A. Neville, D. Dowson and S. Williams, "Tribocorrosion in implants—assessing high carbon and low carbon Co–Cr–Mo alloys by in situ electrochemical measurements," *Tribology International,* no. 39, pp. 1509-1517, 2006.

[56] D. Landolt, S. Mischler and M. Stemp, "Electrochemical methods in tribocorrosion: a critical appraisal," *Electrochimica Acta,* no. 46, pp. 3913-3929, 2001.

[57] T. M. Wright and S. B. Goodman, Eds., "What are the wear mechanisms and what control them?," in *Implant Wear in Total Joint Replacement: Clinical and Biologic Issues, Material and Design Considerations*, American Academy of Orthopaedic Surgeons, 2001, pp. 176-185.

[58] S. Mischler, "Triboelectrochemical techniques and interpretation methods in tribocorrosion: A comparative evaluation," *Tribology International,* no. 41, pp. 573-

583, 2008.

[59] University of California, Berkeley, “Buffer tables,” [Online]. Available: http://microscopy.berkeley.edu/Resources/instruction/buffers.html. [Accessed 25 Nov 2012].

[60] D. F. Williams, "Definitions in Biomaterials," *Proceedings of a Concensus Conference of the European Society of Biomaterials,* vol. 4, 3-5 March 1987.

[61] J. A. Horton and D. E. Parsell, "Biomedical Potential of a Zirconium-Based BulkMetallic Glass," *Materials Research Society Symposium Proceedings,* no. 754, pp. 179-184, 2003.

[62] L. Liu, C. Qiu, C. Huang, Y. Yu, H. Huang and S. Zhang, "Biocompatibility of Ni-free Zr-based bulk metallic glasses," *Intermetallics,* no. 17, pp. 235-240, 2009.

[63] L. Liu, K. C. Chan, C. L. Qiu and Q. Chen, "Formation and Biocompatibility of Ni-Free Zr60Nb5Cu20Fe5Al10 Bulk Metallic Glass," *Materials Transactions,* vol. 48, no. 7, pp. 1879-1882, 2007.

[64] L. Liu, C. Qiu, M. Sun, Q. Chen, K. Chan and G. K. Pang, "Improvements in the plasticity and biocompatibility of Zr–Cu–Ni–Al bulk metallic glass by the microalloying of Nb," *Materials Science and Engineering A,* pp. 193-197, 2007.

[65] A. Gebert, K. Buchholz, A. Leonhard, K. M. J. Eckert and L. Schultz, "Investigations on the electrochemical behaviour of Zr-based bulk metallic glasses," *Materials Science and Engineering A,* no. 267, pp. 294-300, 1999.

[66] V. Raju, U. Kühn, U. Wolff, F. Schneider, J. Eckert, R. Reiche and A. Gebert, “Corrosion behaviour of Zr-based bulk glass-forming alloys containing Nb or Ti,” *Materials Letters,* no. 57, pp. 173-177, November 2002.

[67] M. Skjellerudsveen, “Zr55Cu30Ni5Al10 Bulk Metallic Glass – Preparation of amorphous metal and the possibility of its application asarticulating surface material in an artificial hip joint,” NTNU, Trondheim, 2010.

[68] Y. Yan, A. Neville and D. Dowson, "Biotribocorrosion—an appraisal of the time dependence of wear and corrosion interactions: I. The role of corrosion," *JOURNAL OF PHYSICS D: APPLIED PHYSICS,* no. 39, pp. 3200-3205, 21 July 2006.

[69] S. Buzzi, K. Jin, P. J. Uggowitzer, S. Tosatti, I. Gerber and J. F. Löffler, "Cytotoxicity of Zr-based bulk metallic glasses," *Intermetallics,* no. 14, pp. 729-734, 2006.

[70] J. B. Brunski, "Chemical Compositions of Metals Used for Implants," in *Biomaterials Science - An Introduction to Materials in Medicine*, 2nd ed., B. D. Ratner, A. S. Hoffman, F. J. Schoen and J. E. Lemons, Eds., San Diego, California: Elsevier Academic Press, 2004, pp. 823-824.

[71] G. Bellefontaine, “The Corrosion of CoCrMo Alloys for Biomedical Applications,” University of Birmingham, Birmingham, 2010.

[72] S. S. d. Rocha, G. L. Adabo, G. E. P. Henriques and M. A. d. A. Nóbilo, "Vickers Hardness of Cast Commercially Pure Titanium and Ti-6Al-4V Alloy Submitted to Heat Treatments," *Braz Dent J,* no. 17, pp. 126-129, 2006.

[73] B. Taylor and E. Weidmann, "Metallographic preparation of titanium," Struers, March 2008. [Online]. Available: http://www.struers.com/resources/elements/12/104827/Application_Note_Titanium_English.pdf. [Accessed 14 Nov 2012].

[74] S. Ge, K. Kojio, A. Takahara and T. Kajiyama, "Bovine serum albumin adsorption onto immobilized organotrichlorosilane surface: influence of the phase separation on protein adsorption patterns," *J Biomater Sci Polym,* pp. 131-150.

[75] M. Kosmulski, Chemical properties of material surfaces, New York: Marcel Dekker, 2001.

[76] A. Raman, R. Quiñones, L. Barriger, R. Eastman, A. Parsi and E. S. Gawalt, "Understanding Organic Film Behavior on Alloy and Metal Oxides," *Langmuir,* pp. 1747-1754, 2 February 2010.

[77] E. Weeks, "How does a confocal microscope work?," Emory University, [Online]. Available: http://www.physics.emory.edu/~weeks/confocal/. [Accessed 24 May 2013].

[78] G. Rice, "Fluorescent Microscopy," Carleton College, 16 March 2013. [Online]. Available: http://serc.carleton.edu/microbelife/research_methods/microscopy/fluromic.html. [Accessed 24 May 2013].

[79] C. V. Vidal, "Study of the degradation mechanisms of the CoCrMo alloy in physiological media by electrochemical techniques and surface analysis," Universistat Politècnica De València, Valencia, 2012.

[80] S. Affatato, W. Leardini and Z. M., "Hip Joint Simulators: State of the Art," *Ceramics in*

Orthopaedics, pp. 171-180, 2006.

[81] Z. Liu, K. C. Chan and L. L., "Development of Ni- and Cu-Free Zr-Based Bulk Metallic Glasses for Biomedical Applications," *Materials Transactions,* vol. 52, no. 1, pp. 61-67, 2011.

[82] N. Hua, R. Li, J. Wang and T. Zhang, "Biocompatible Zr-Al-Fe bulk metallic glasses with large plasticity," *Physics, Mechanics & Astronomy,* vol. 55, no. 9, pp. 1664-1669, 2012.

[83] M. Pourbaix, Atlas of electrochemical equilibria in aqueous solutions, 2nd English ed. ed., Houston, Texas: National Association of Corrosion Engineers, 1974.

Appendix A: Pourbaix Diagrams

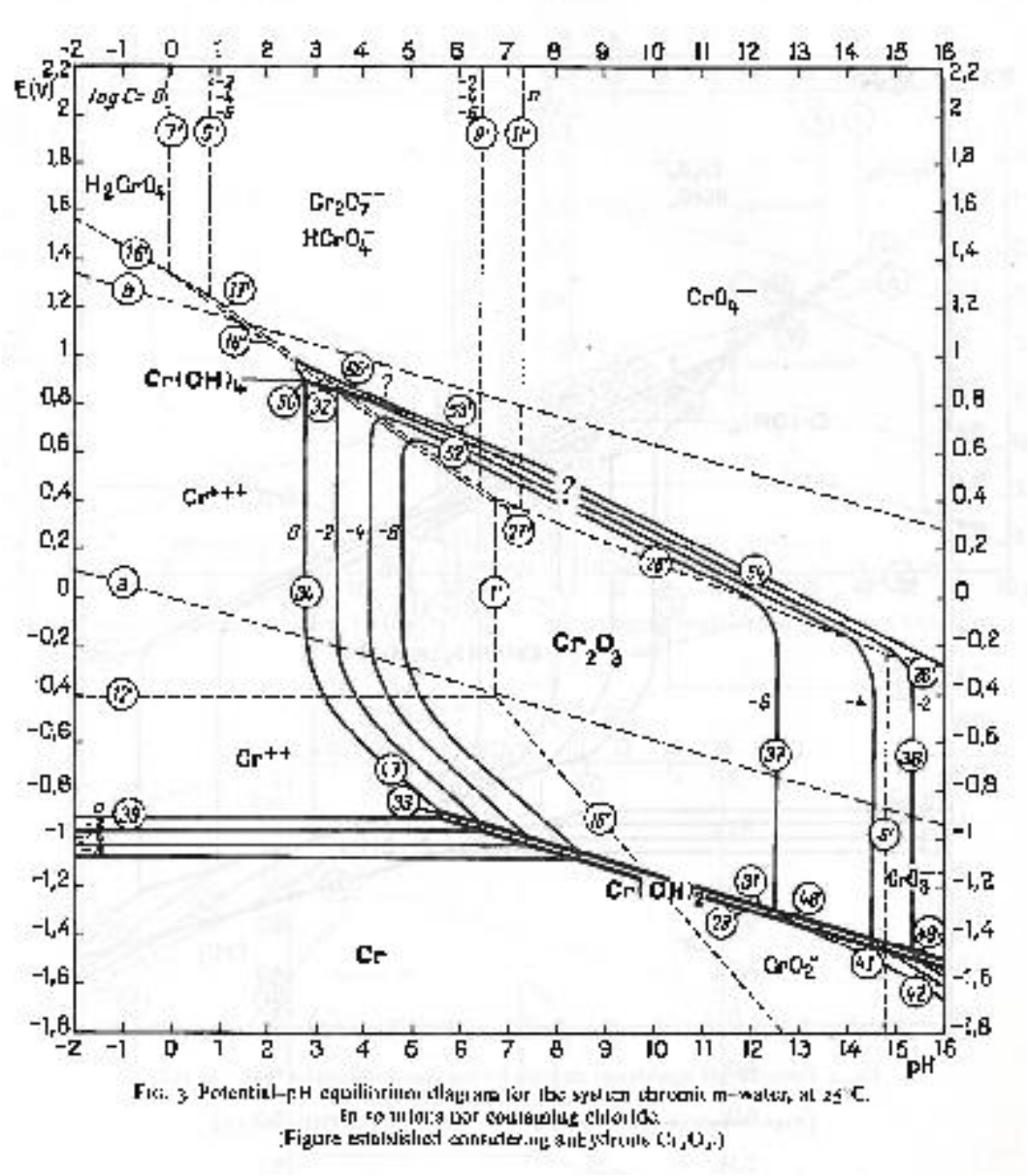

Fig. 3. Potential–pH equilibrium diagram for the system chromium–water, at 25 °C.
[illegible] for containing chloride.
[illegible] established considering anhydrous Cr_2O_3.

Figure 0-1: Pourbaix Diagram for Chromium, [83]

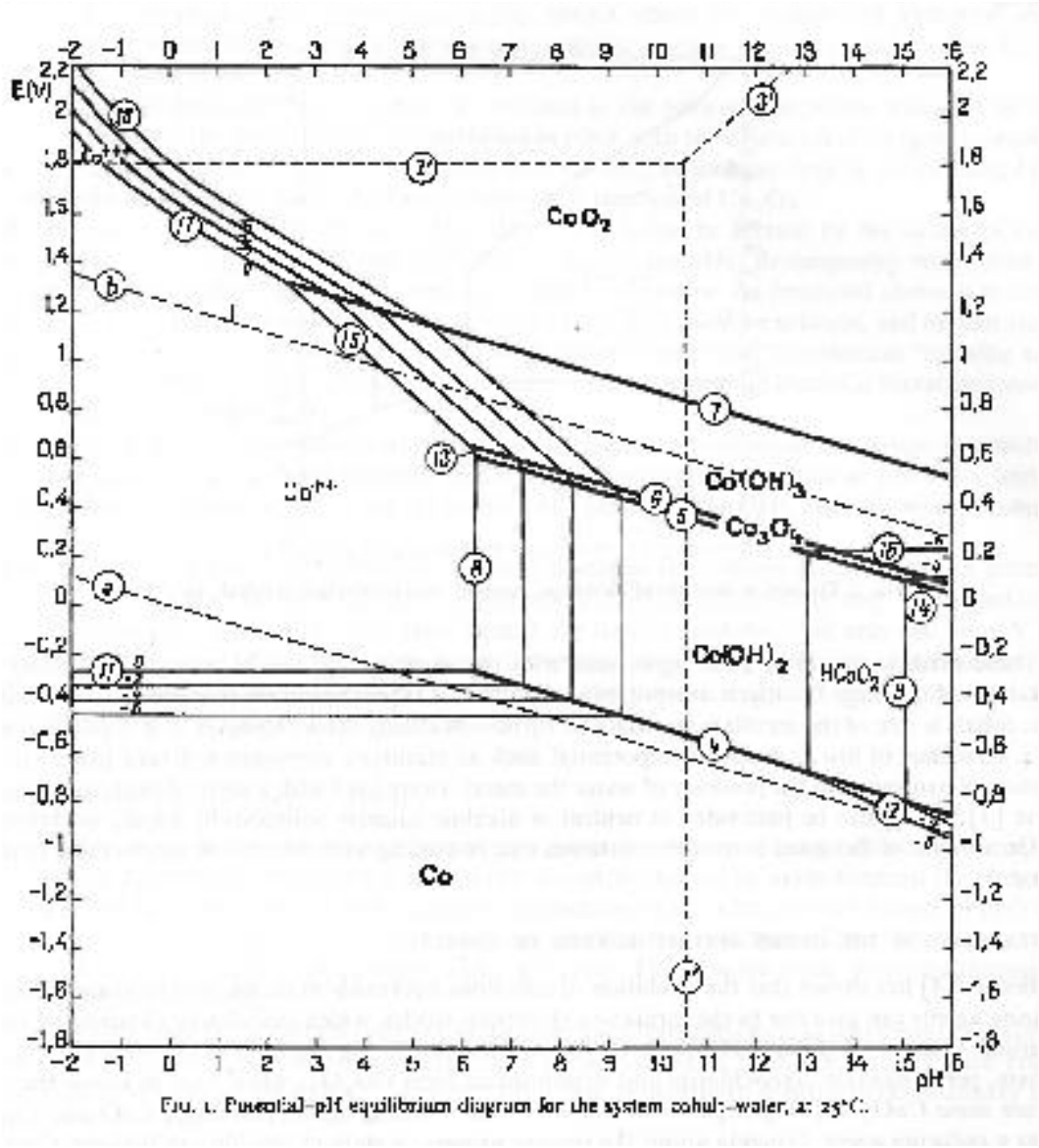

Figure 0-2 Pourbaix Diagram for Cobalt, [83]

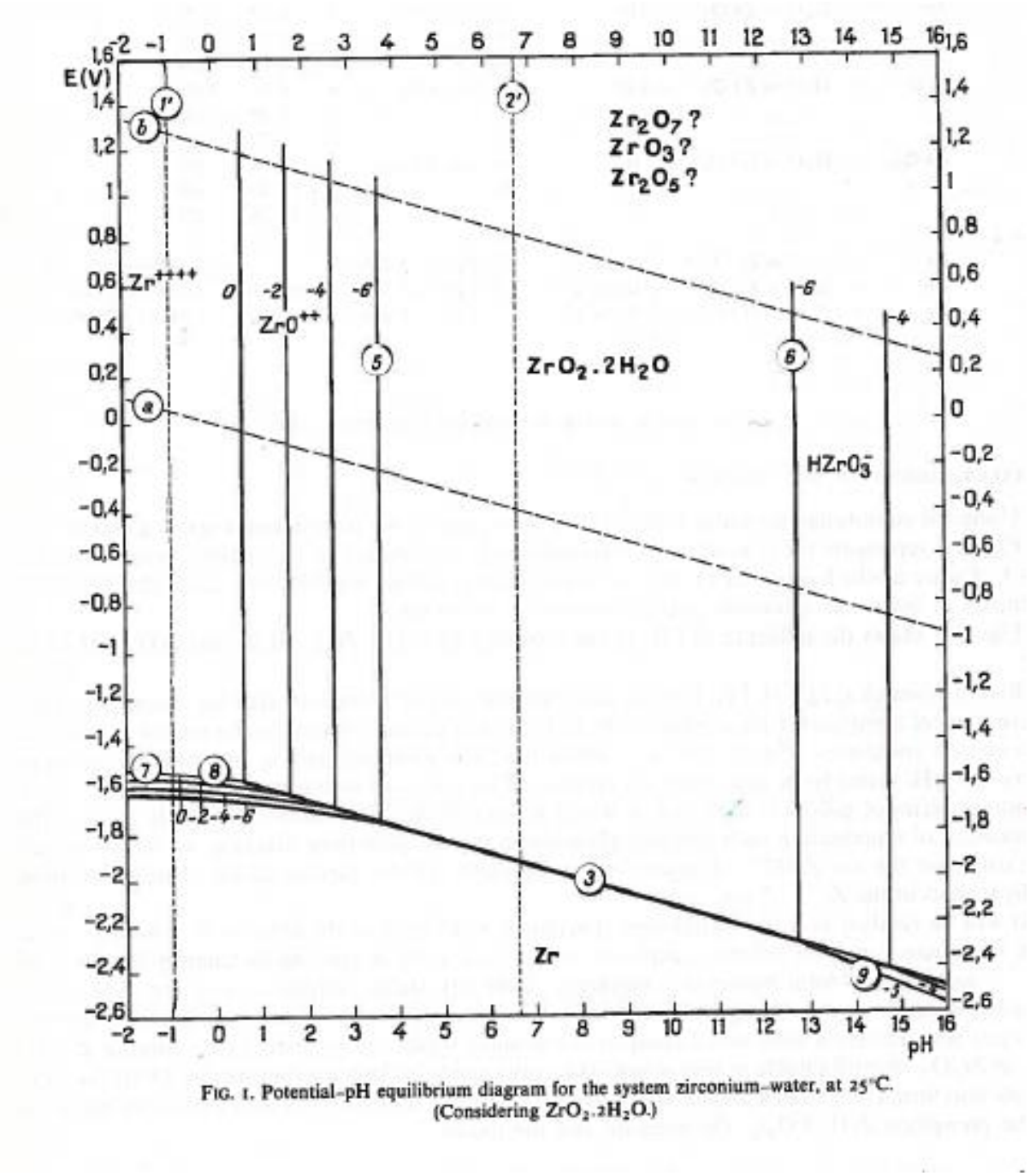

FIG. 1. Potential–pH equilibrium diagram for the system zirconium–water, at 25°C. (Considering $ZrO_2.2H_2O$.)

Figure 0-3: Pourbaix Diagram for Zirconium, [83]

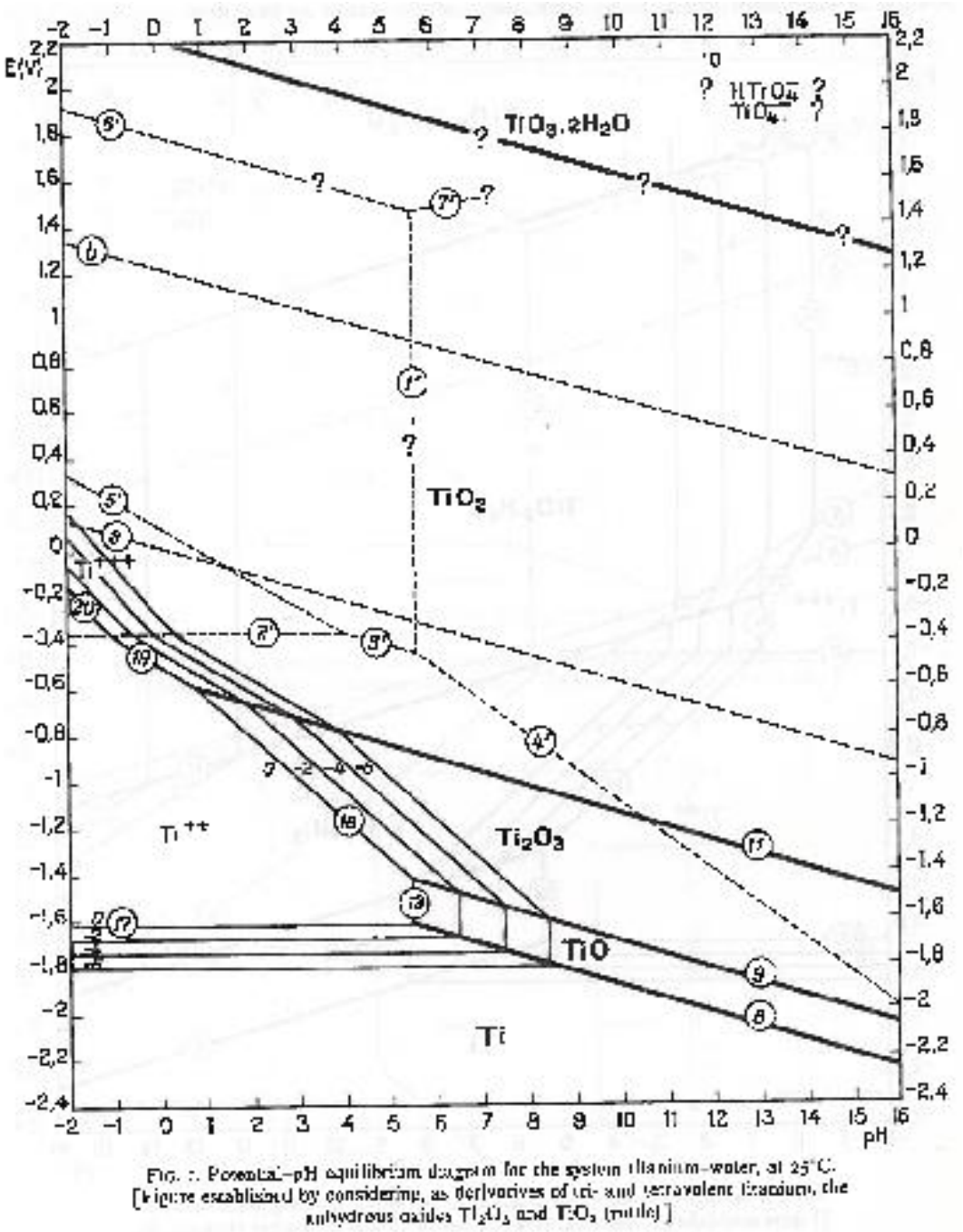

Figure 0-4: Pourbaix Diagram for Titanium, [83]

Appendix B: Photographs of material surfaces after wear, and their respective alumina balls

a. Ti 99.6%

i. Dry tests

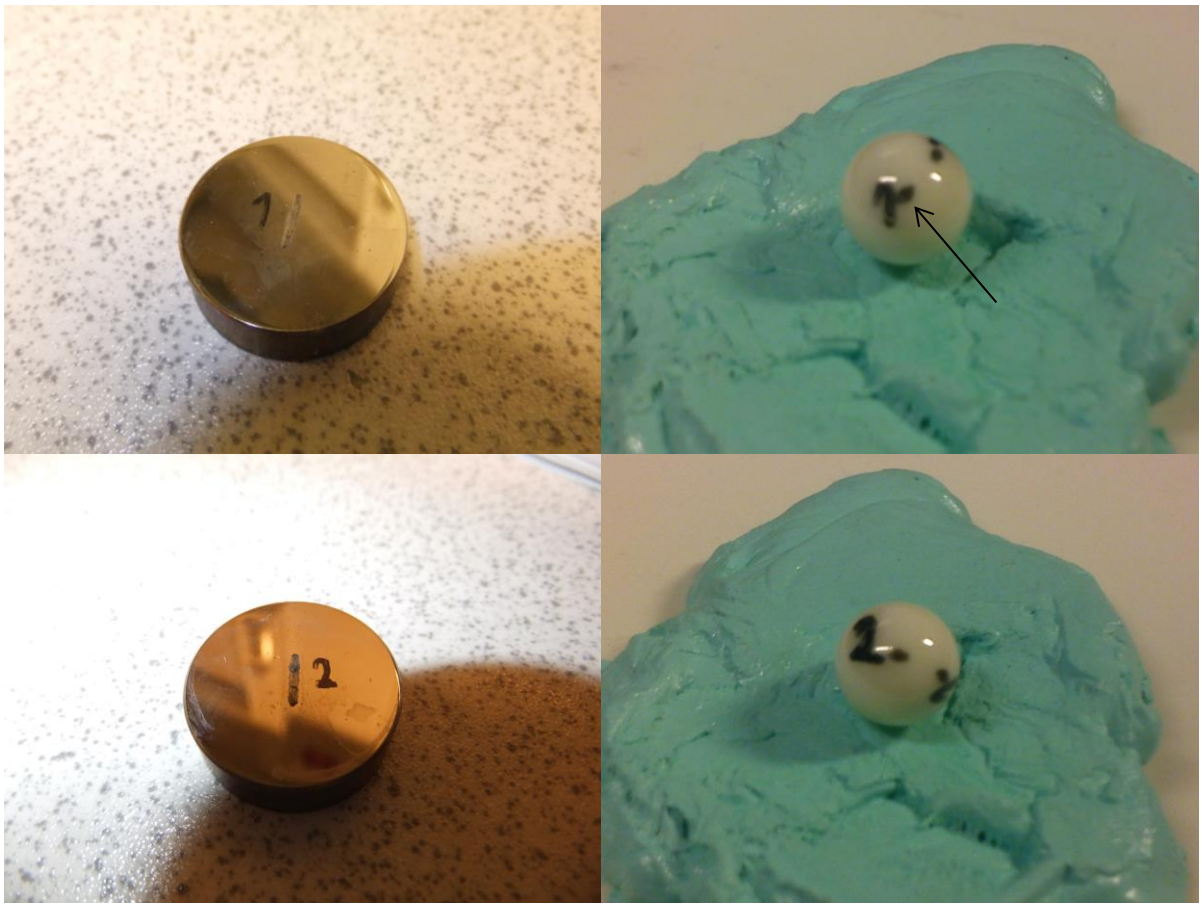

ii. PBS 7.4

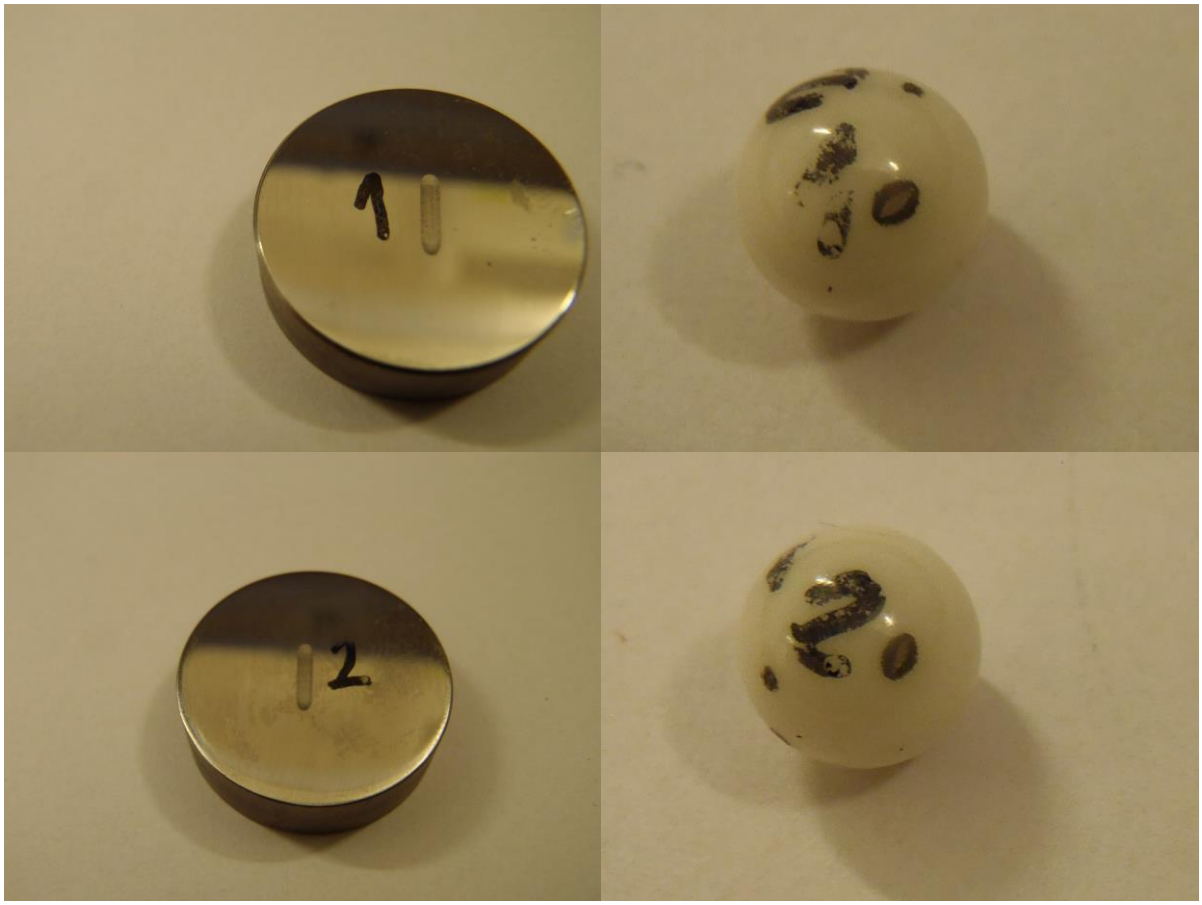

iii. PBS 7.4 with protein

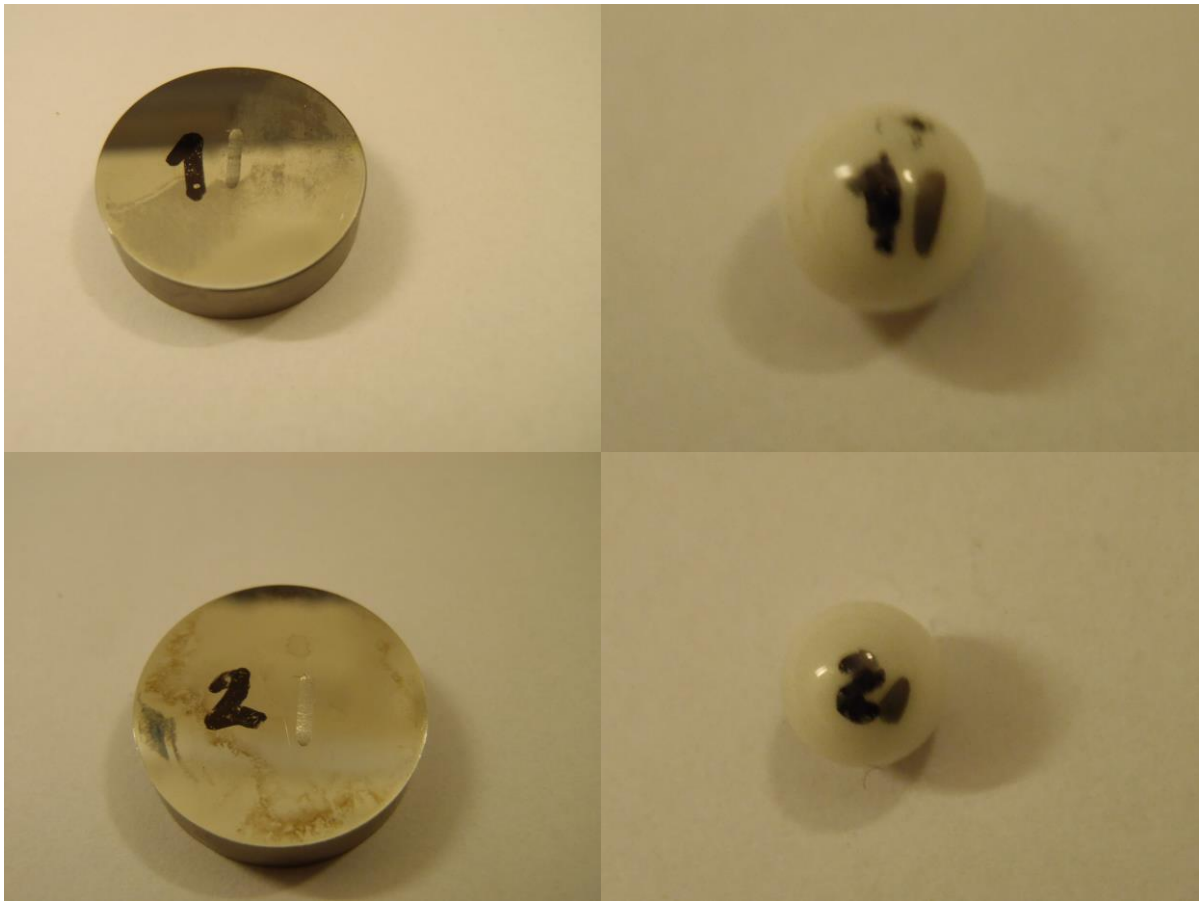

iv. PBS 5.2

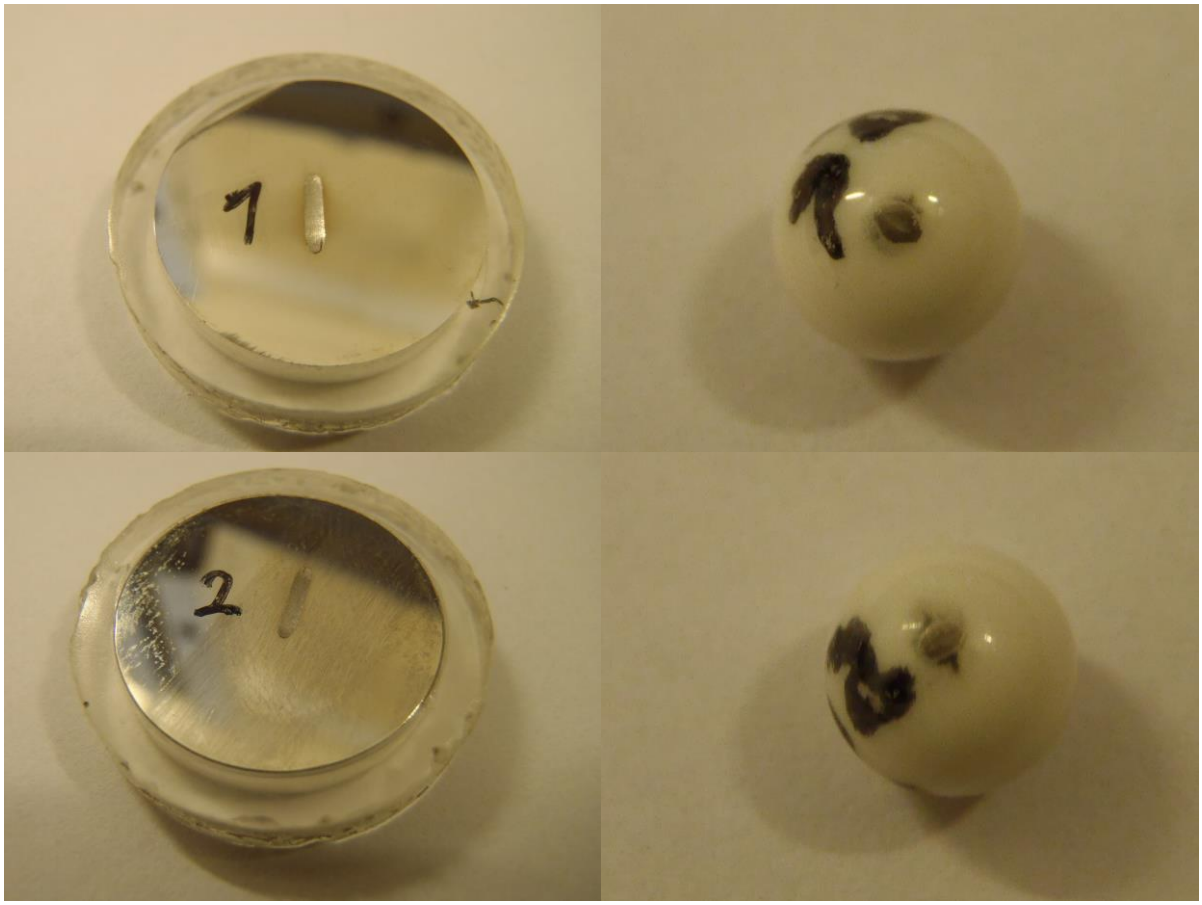

v. PBS 5.2 with protein

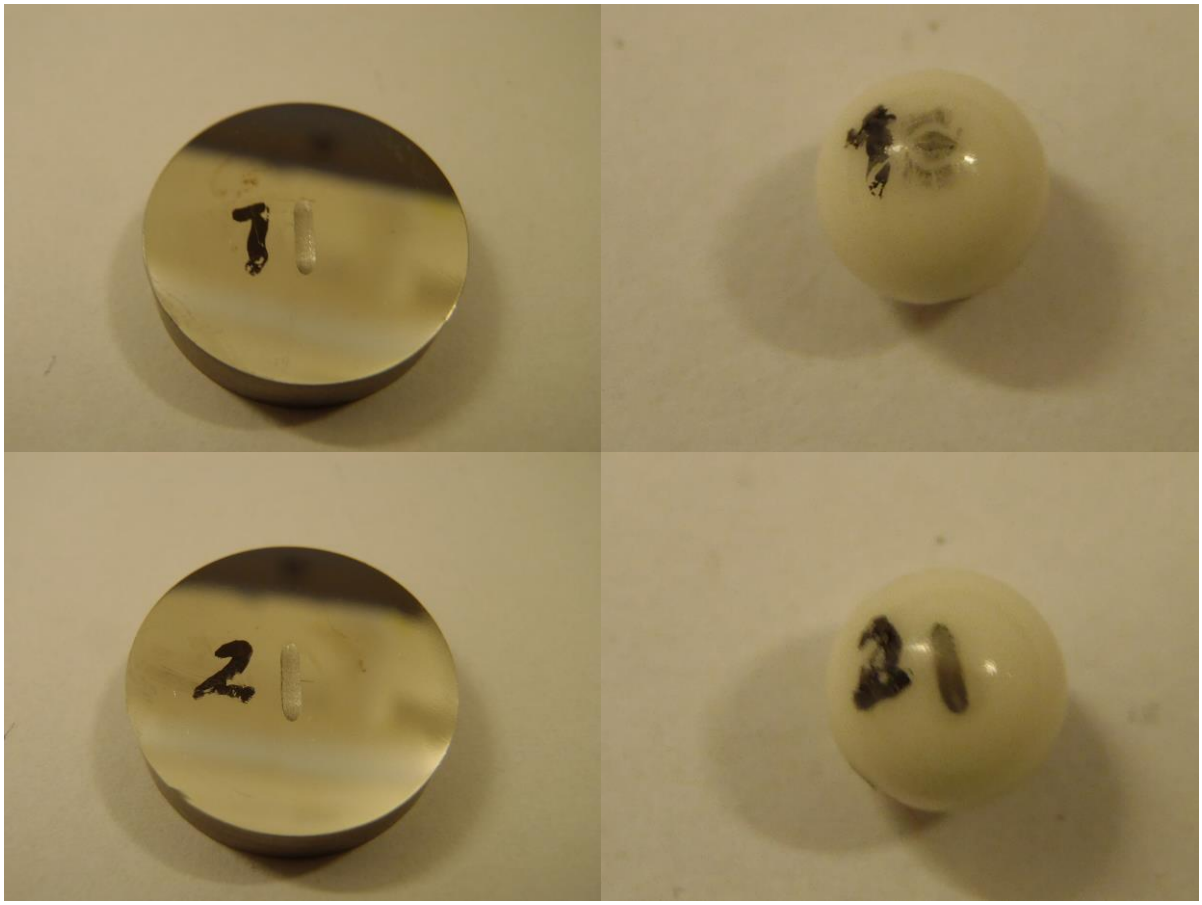

b. CoCrMo

i. Dry tests

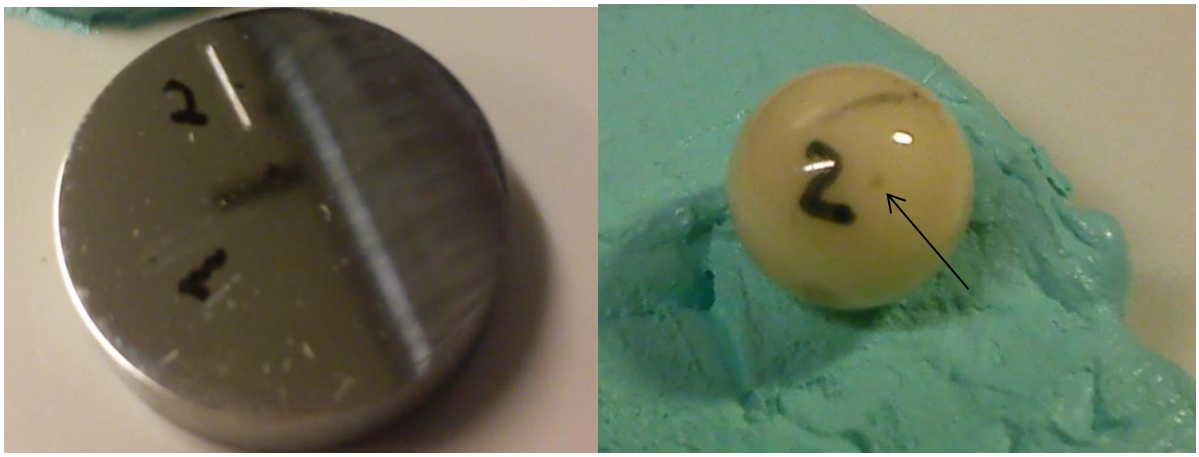

ii. PBS 7.4

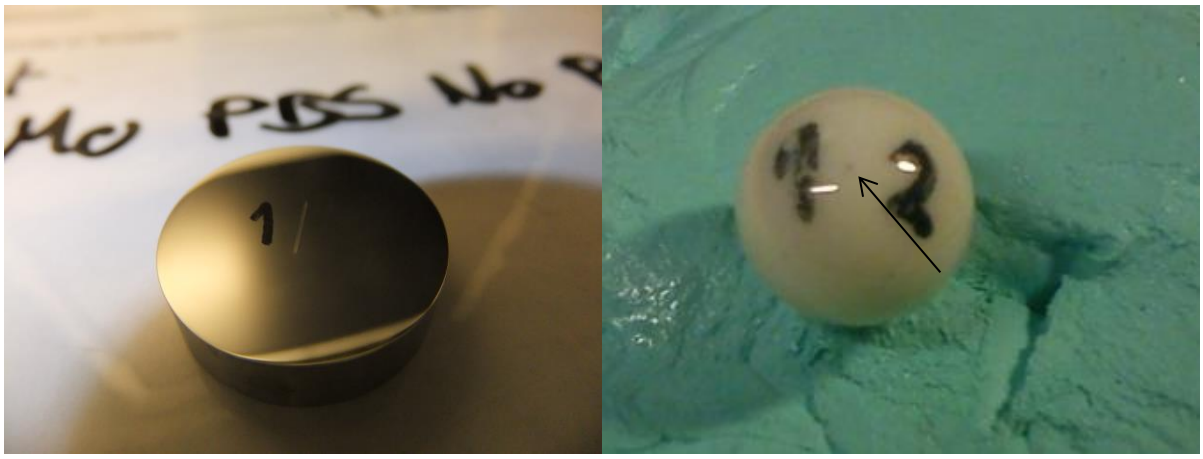

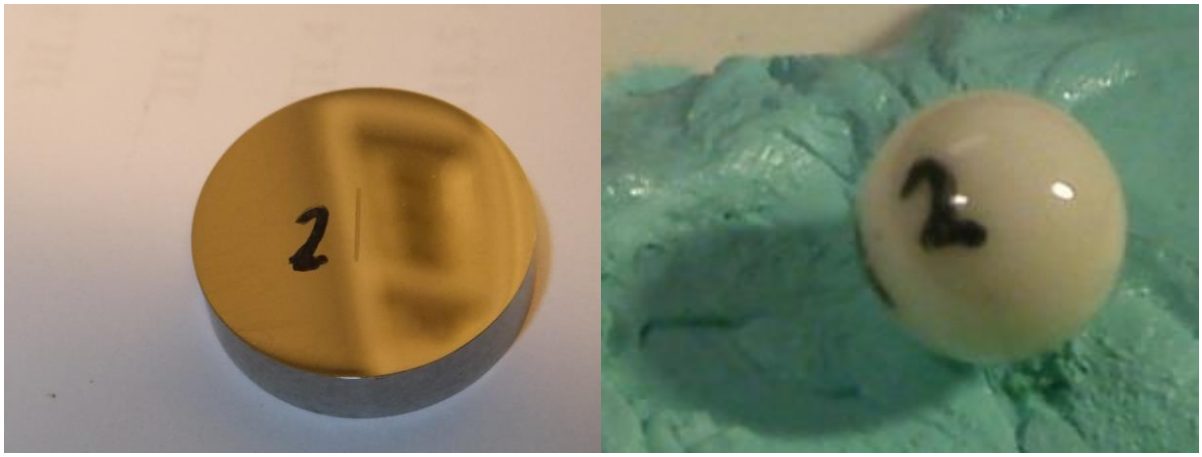

iii. PBS 7.4 with protein

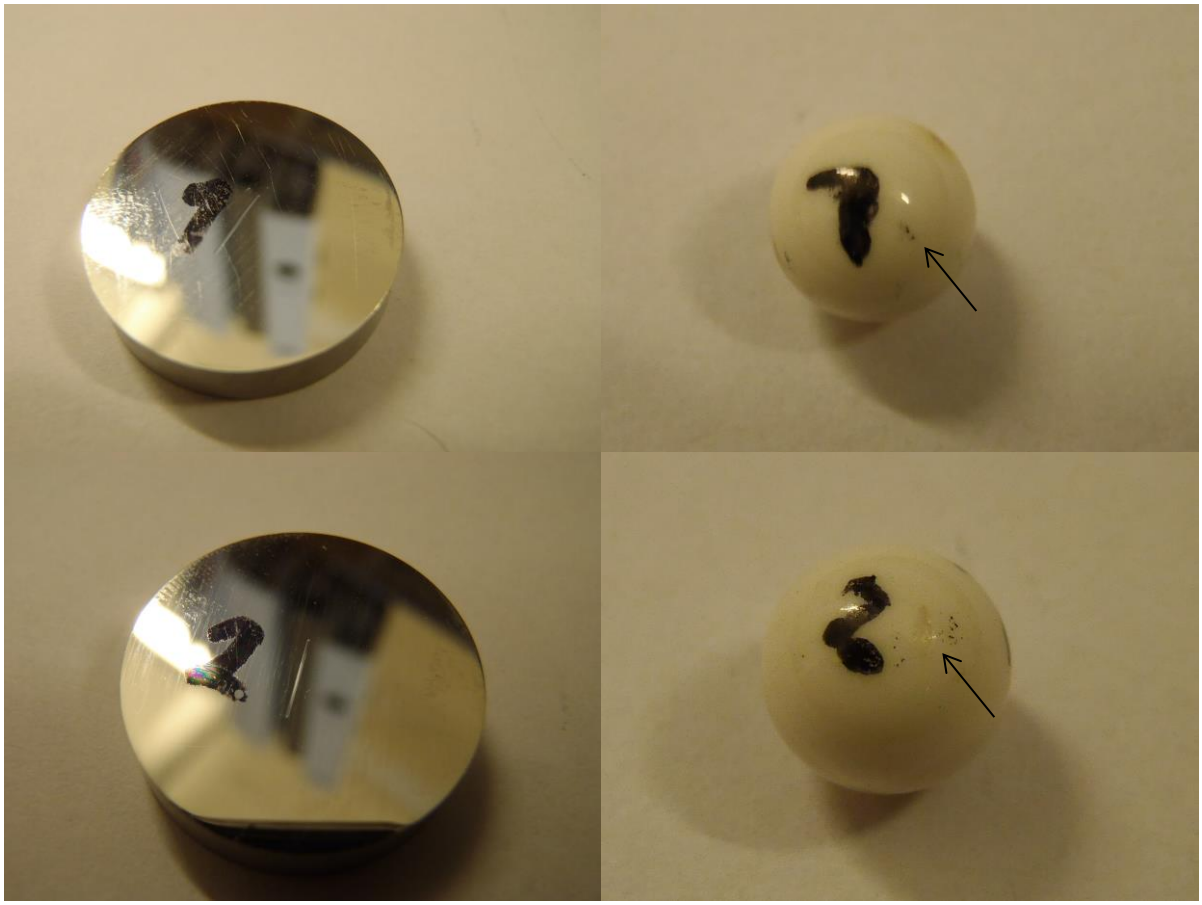

iv. CoCrMo PBS 5.2

v. CoCrMo PBS 5.2 with protein

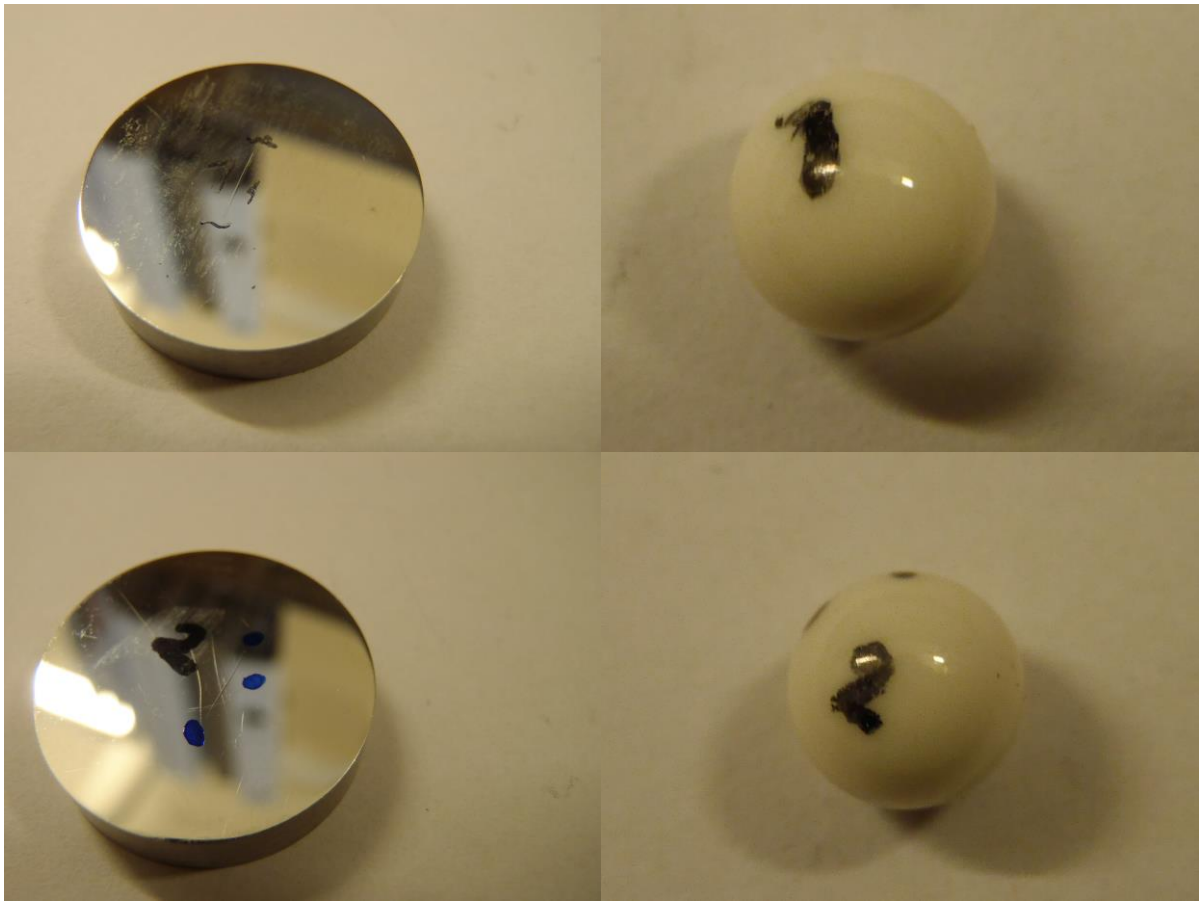

c. BMG

i. Dry tests

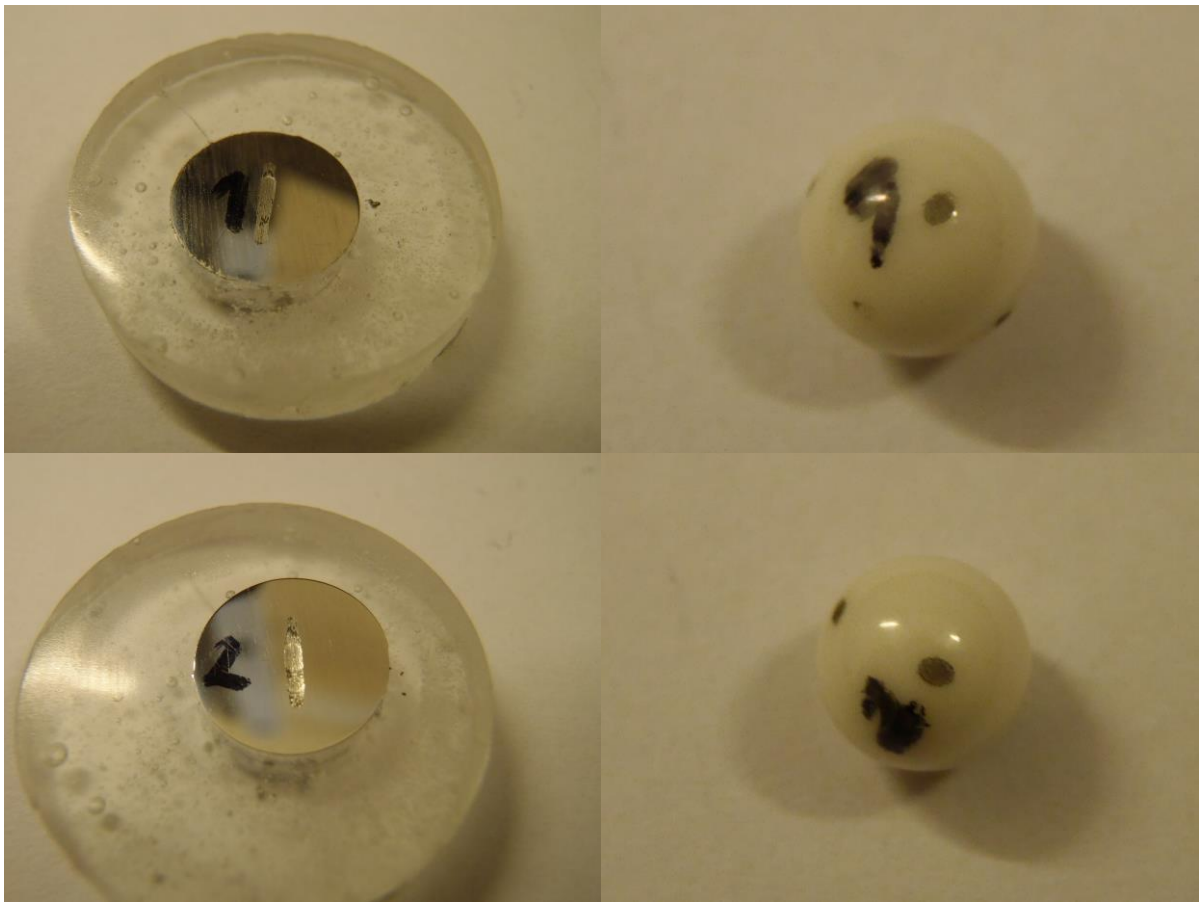

ii. PBS 7.4

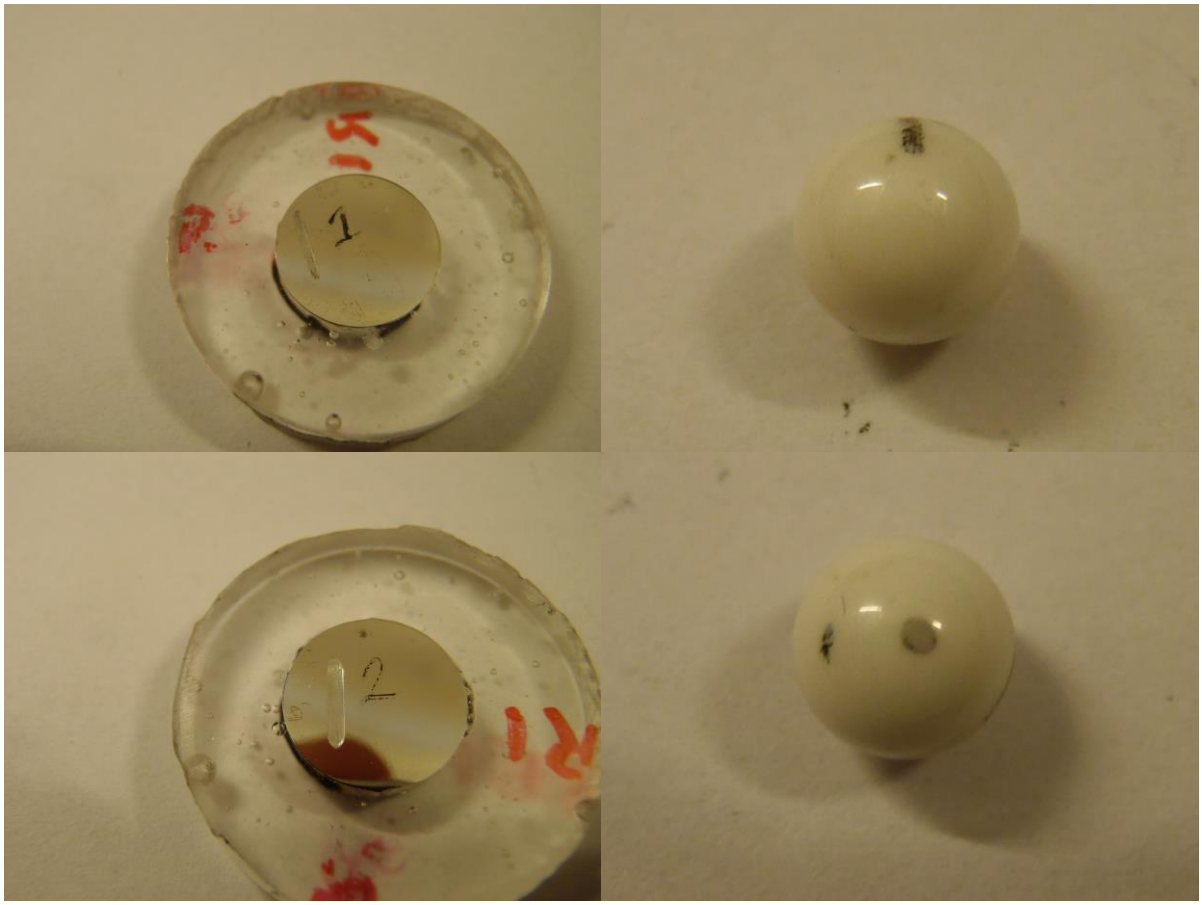

iii. PBS 7.4 with protein

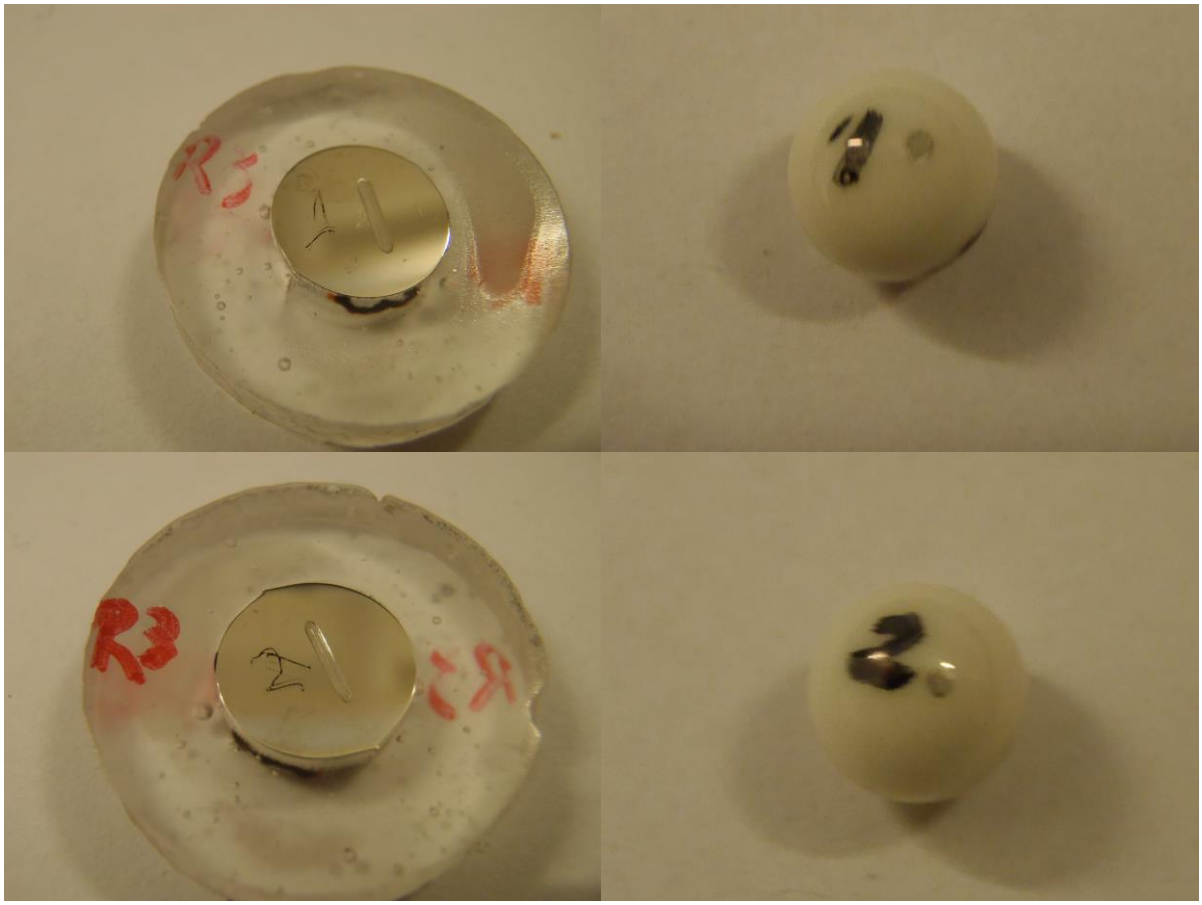

iv. PBS 5.2

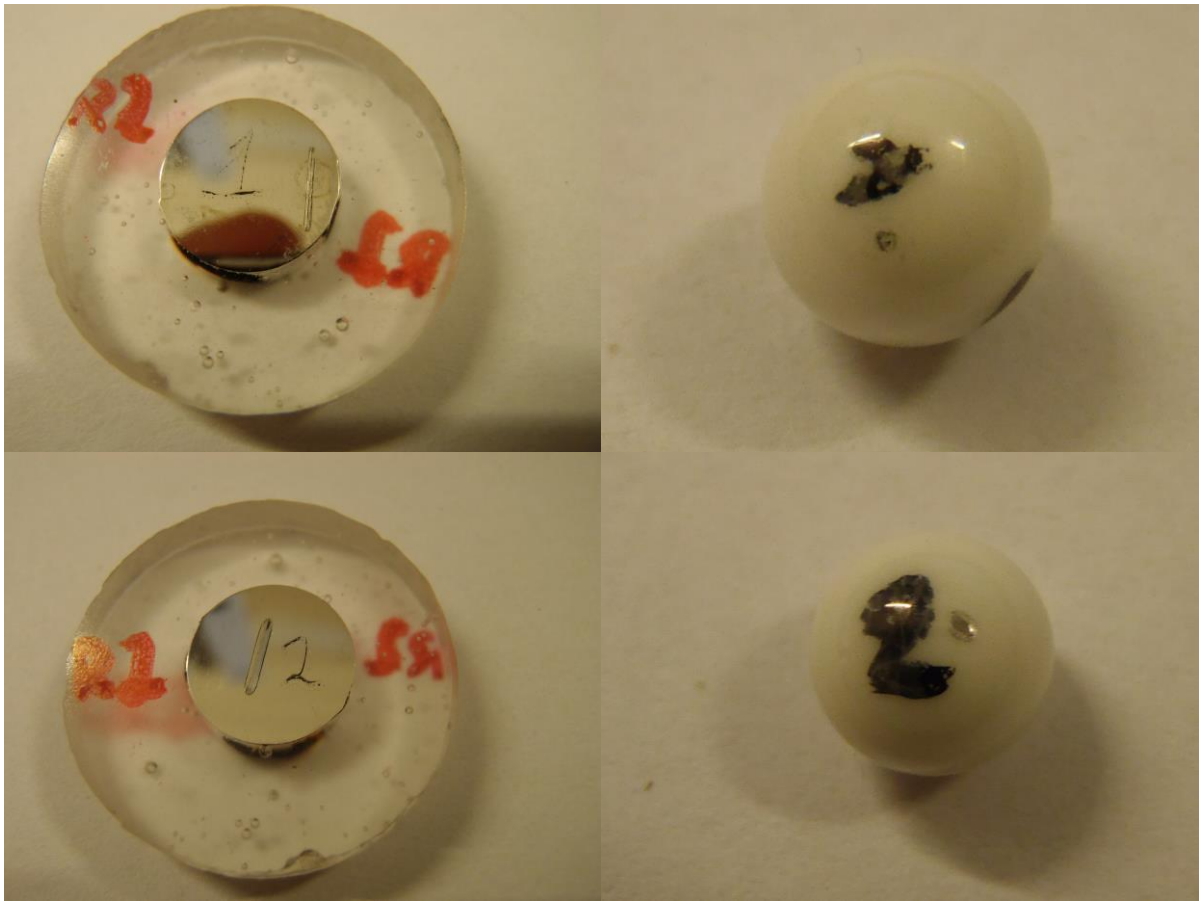

v. PBS 5.2 with protein

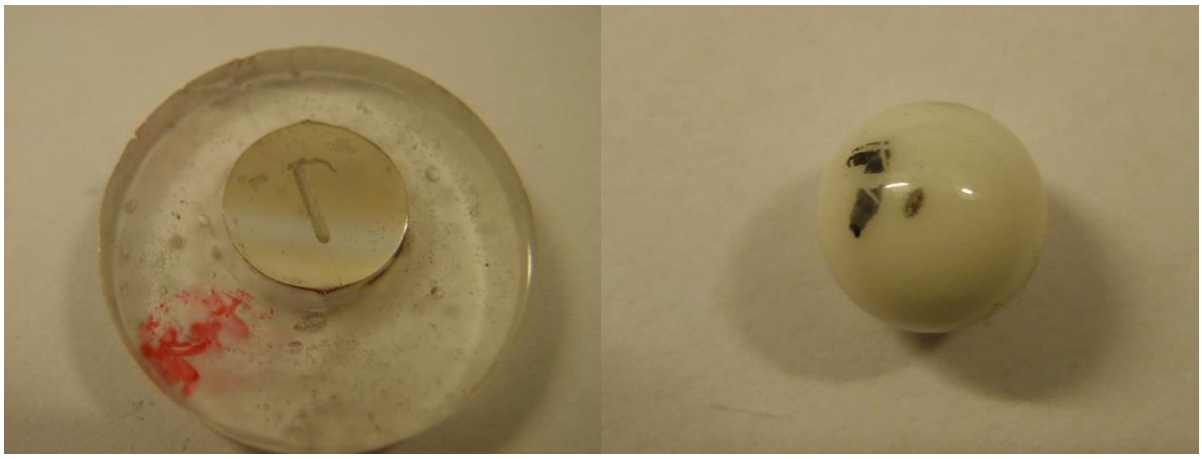

Appendix C: Further results

1. Tribocorrosion tests

a. Ti 99.6 %

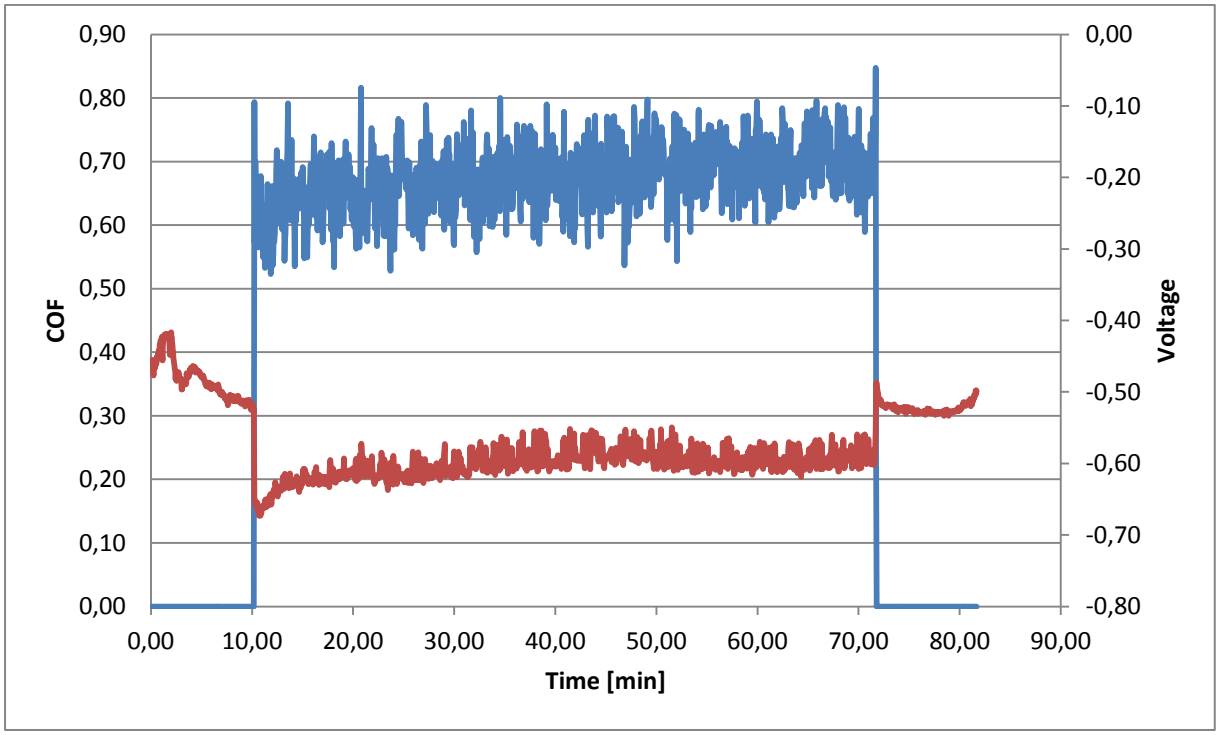

Figure 0-1: Tribocorrosion diagram for Ti 99.6 % in PBS 7.4

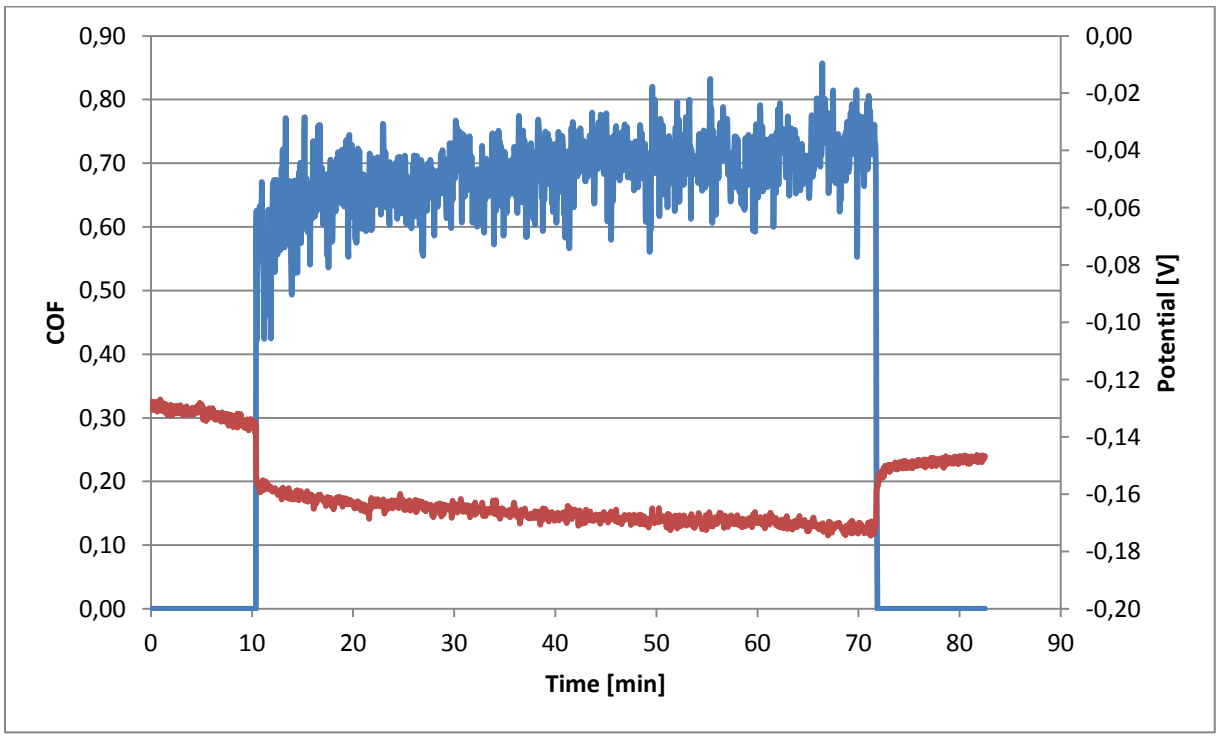

Figure 0-2: Tribocorrosion diagram for Ti 99.6 % in PBS 7.4 with protein

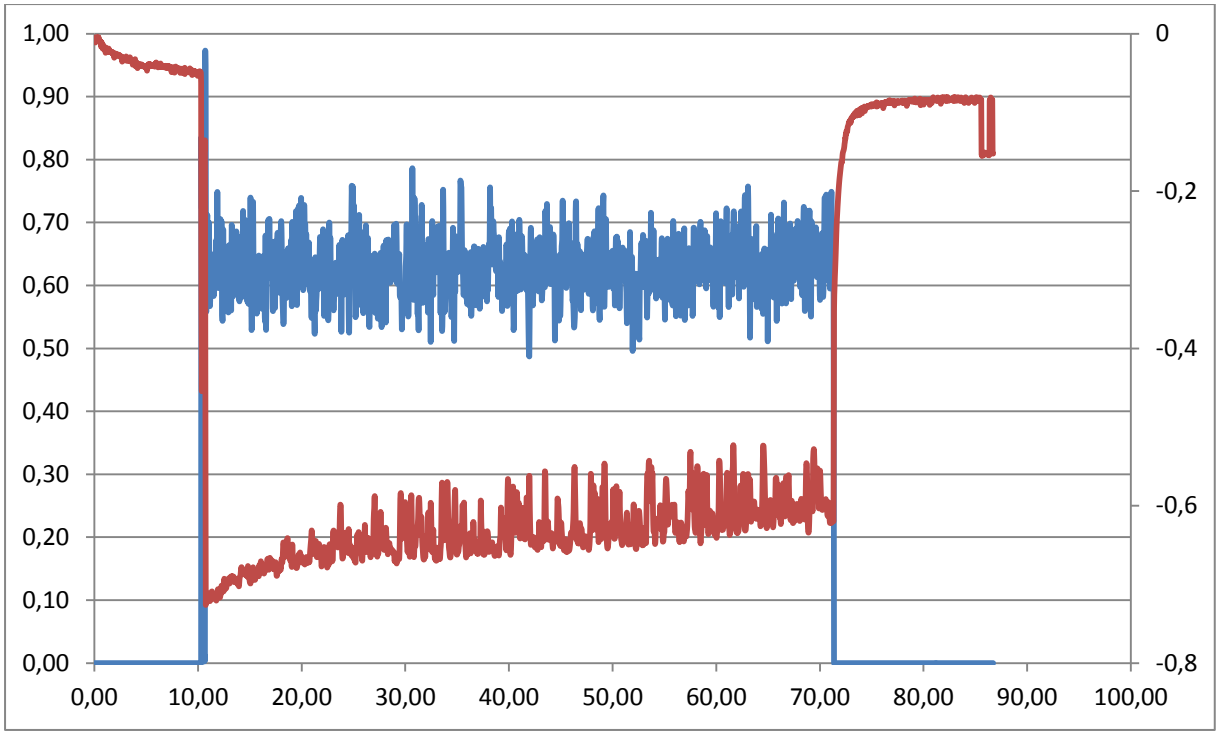

Figure 0-3: Tribocorrosion diagram for Ti 99.6 % in PBS 5.2

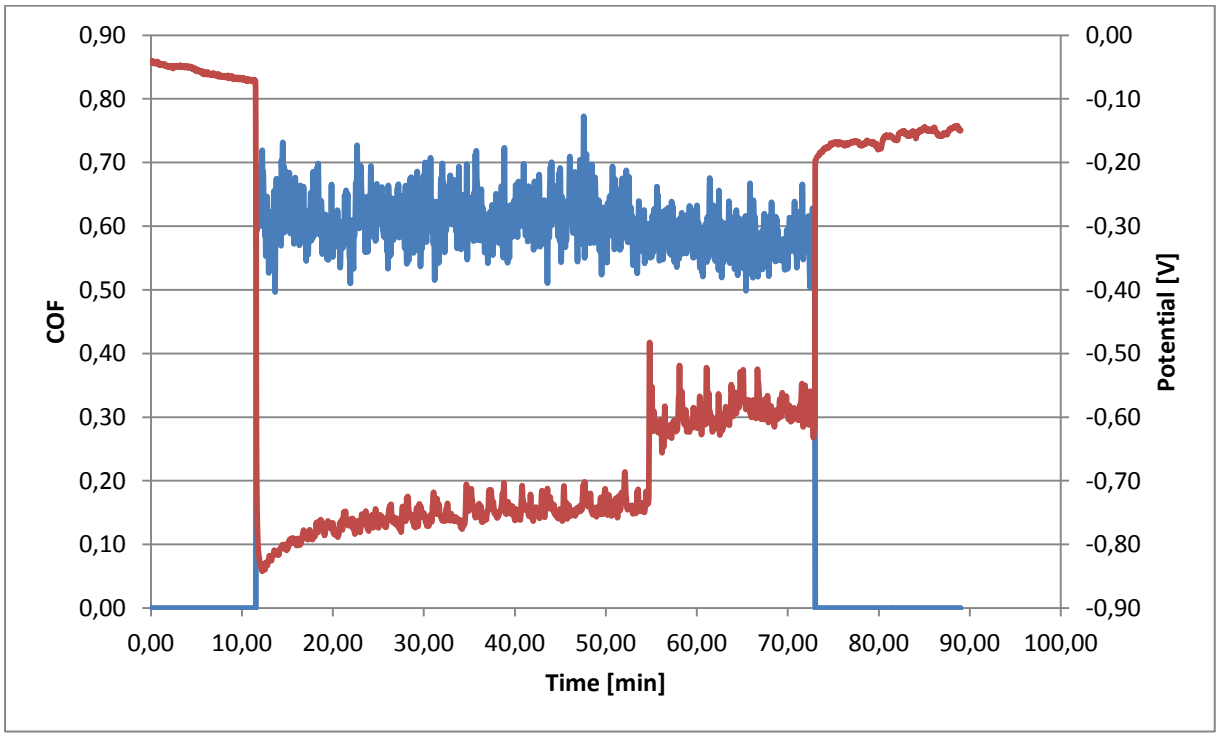

Figure 0-4: Tribocorrosion diagram for Ti 99.6 % in PBS 5.2 with protein

b. CoCrMo

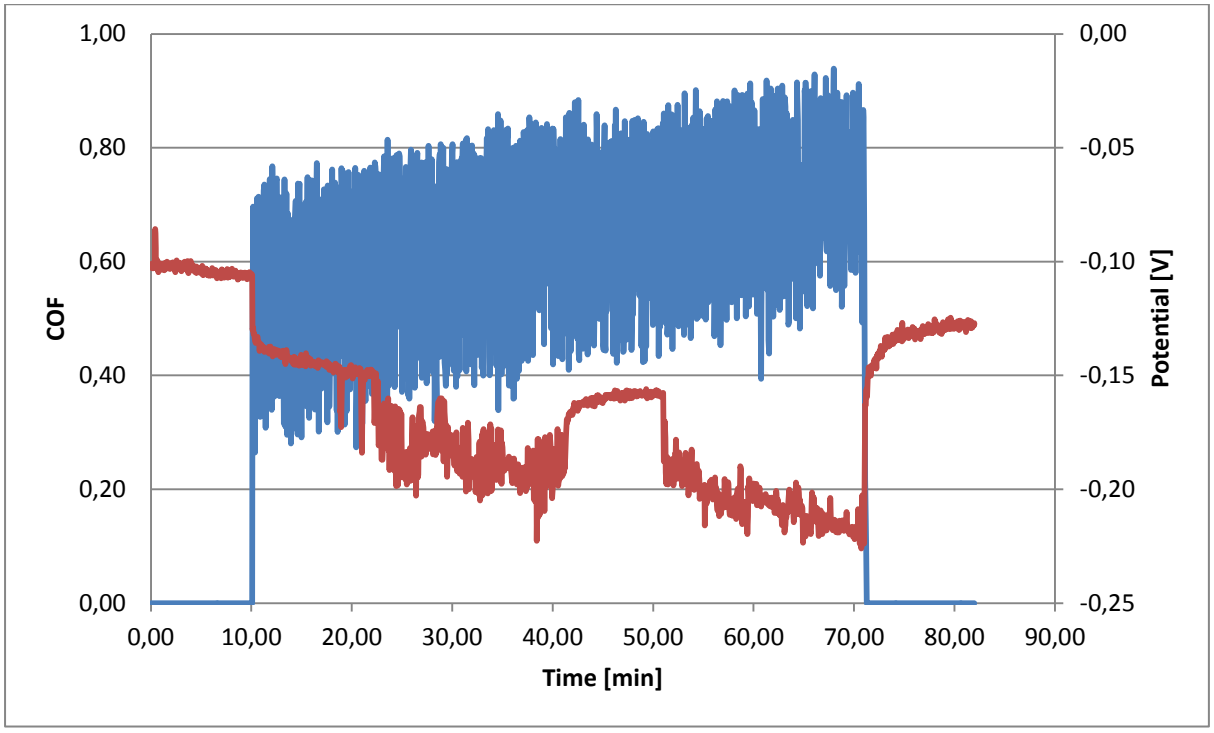

Figure 0-5: Tribocorrosion diagram for CoCrMo in PBS 7.4

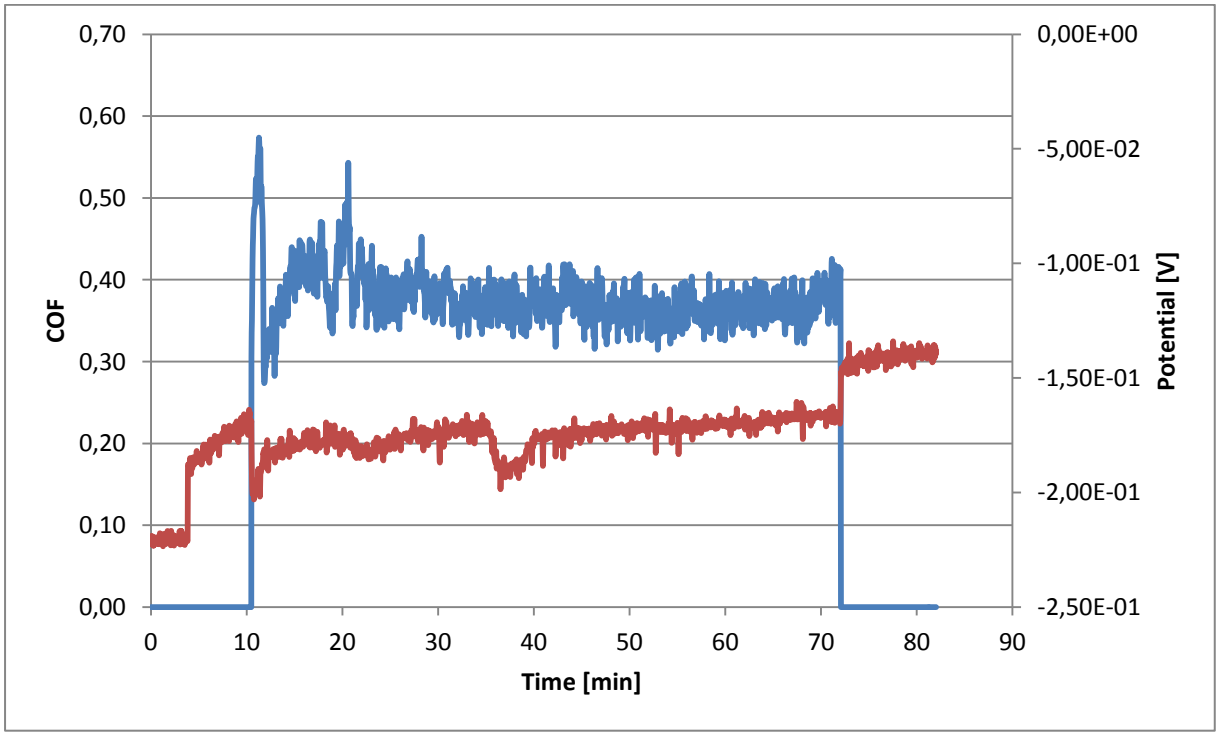

Figure 0-6: Tribocorrosion diagram for CoCrMo in PBS 7.4 with protein

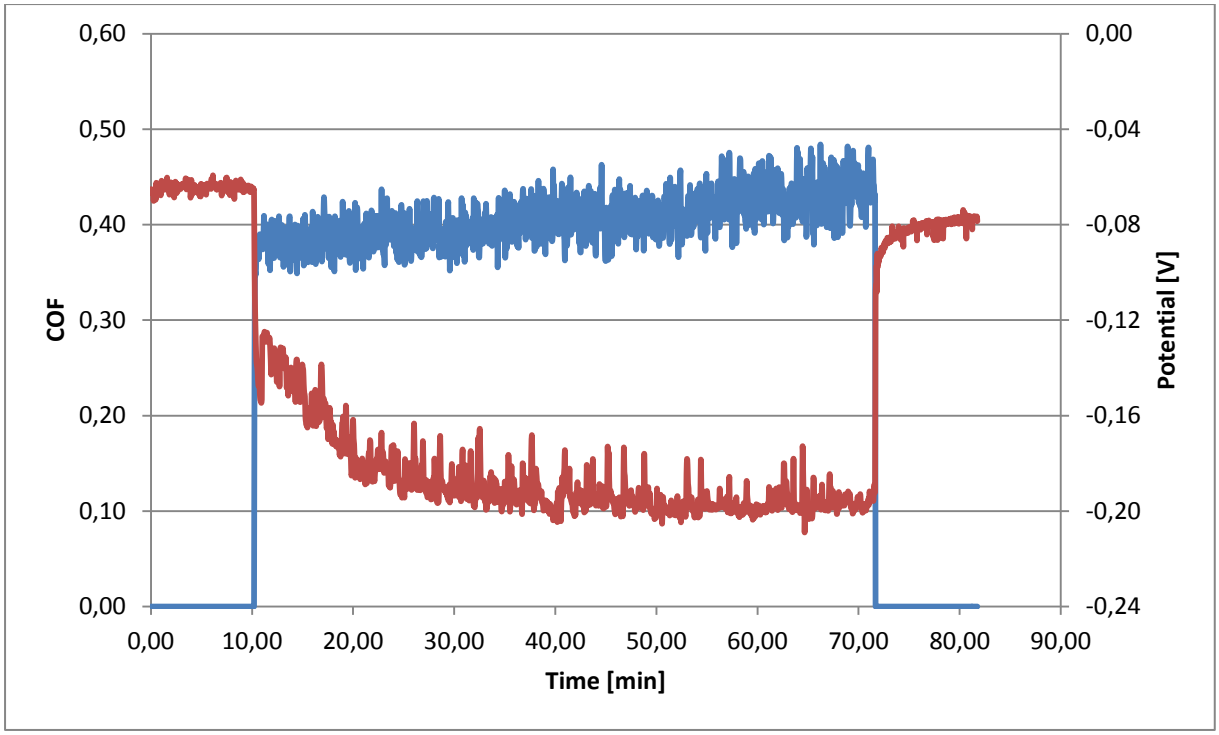

Figure 0-7: Tribocorrosion diagram for CoCrMo in PBS 5.2

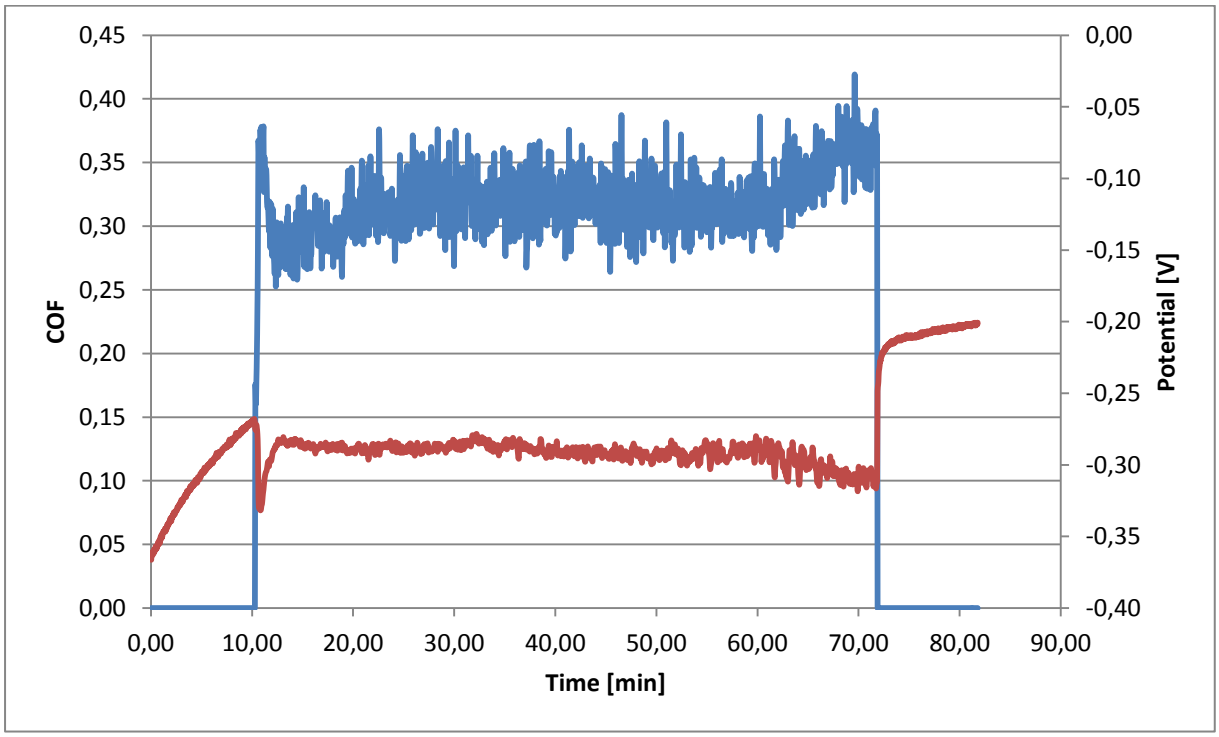

Figure 0-8: Tribocorrosion diagram for CoCrMo in PBS 5.2 with protein

a. BMG

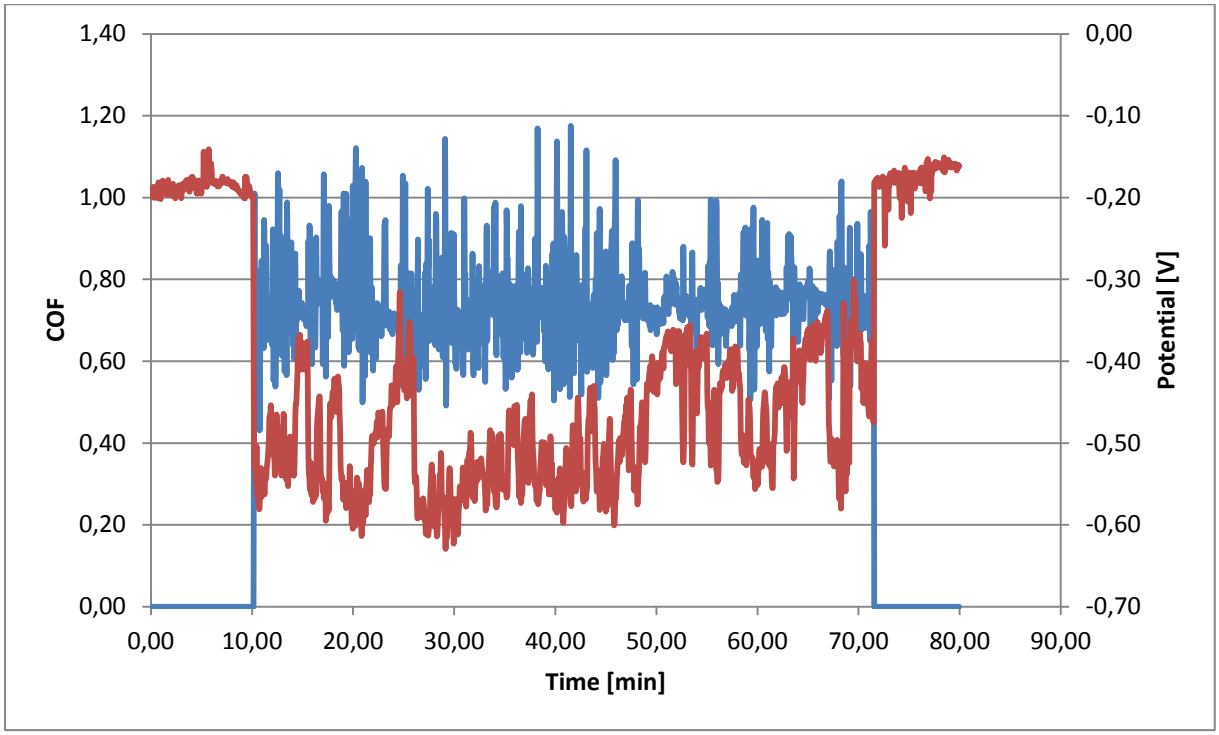

Figure 0-9: Tribocorrosion diagram for BMG in PBS 7.4

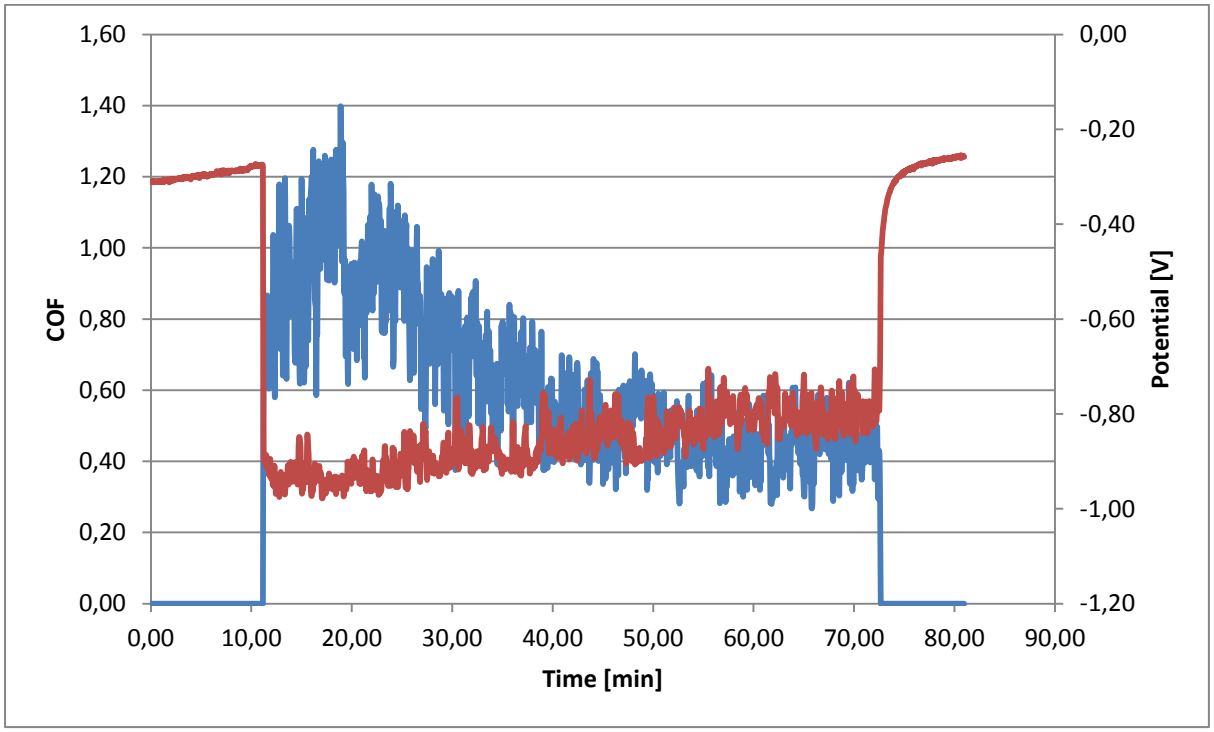

Figure 0-10: Tribocorrosion diagram for BMG in PBS 7.4 with protein

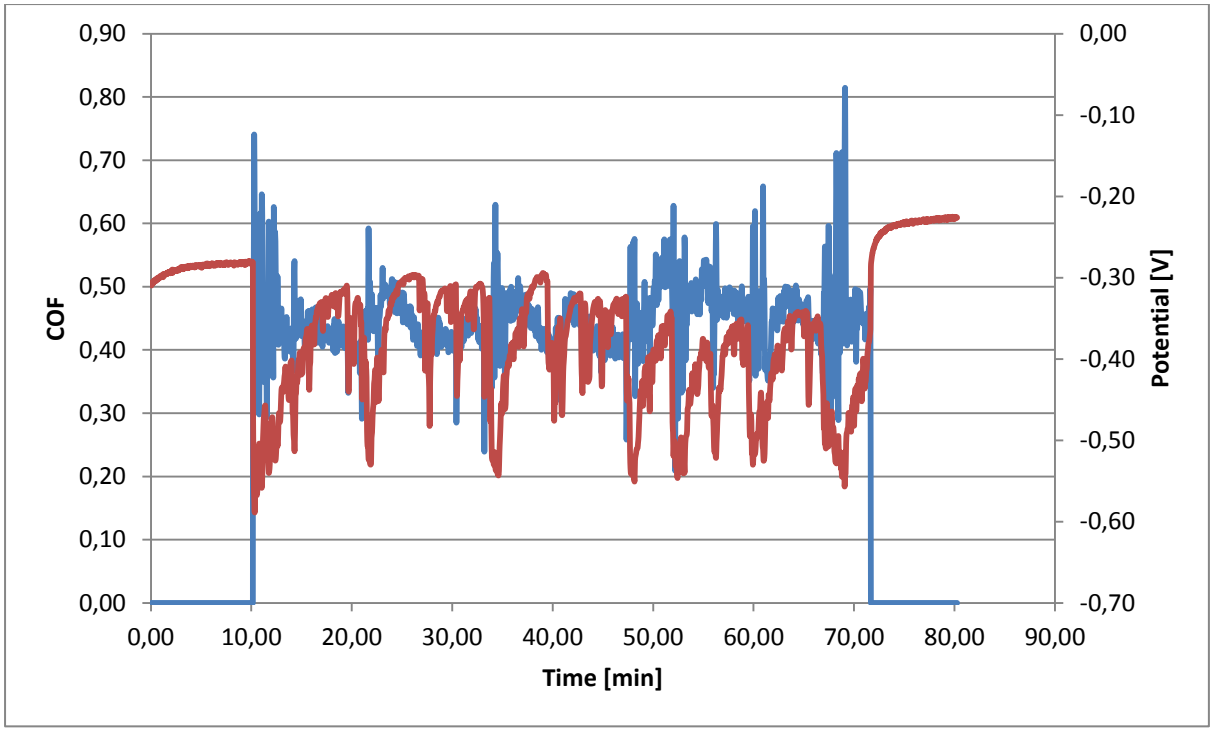

Figure 0-11: Tribocorrosion diagram for BMG in PBS 5.2

2. Confocal Microscopy Images

a. Ti 99.6 %

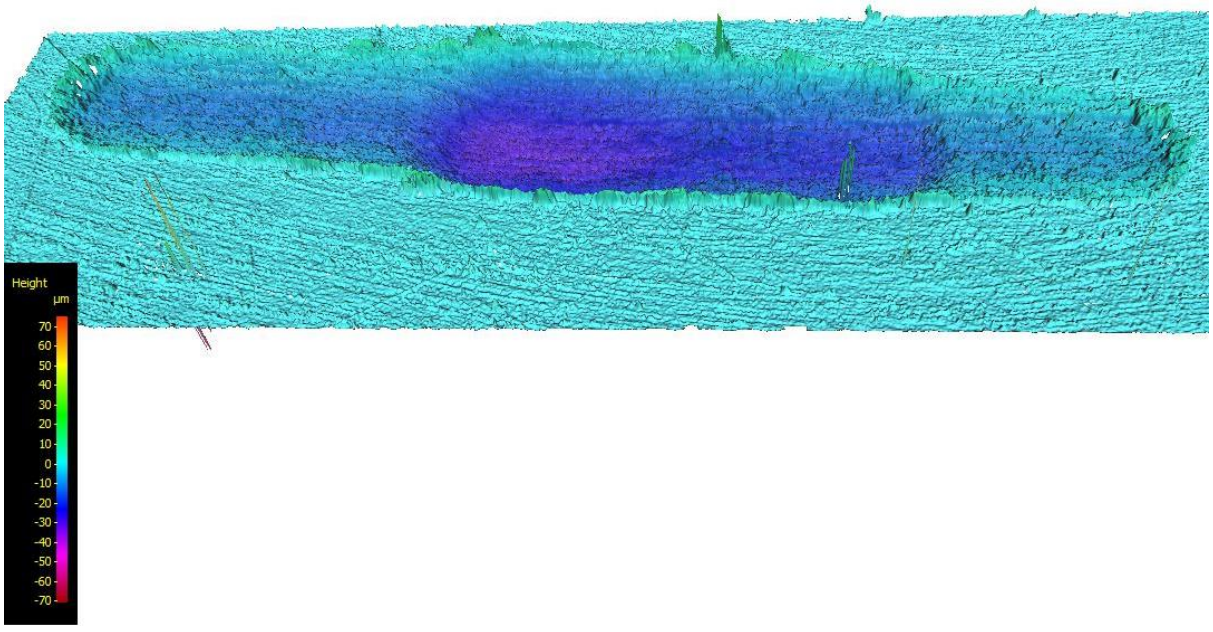

Figure 0-12: Confocal 3d image of Ti 99.6 % dry test 1

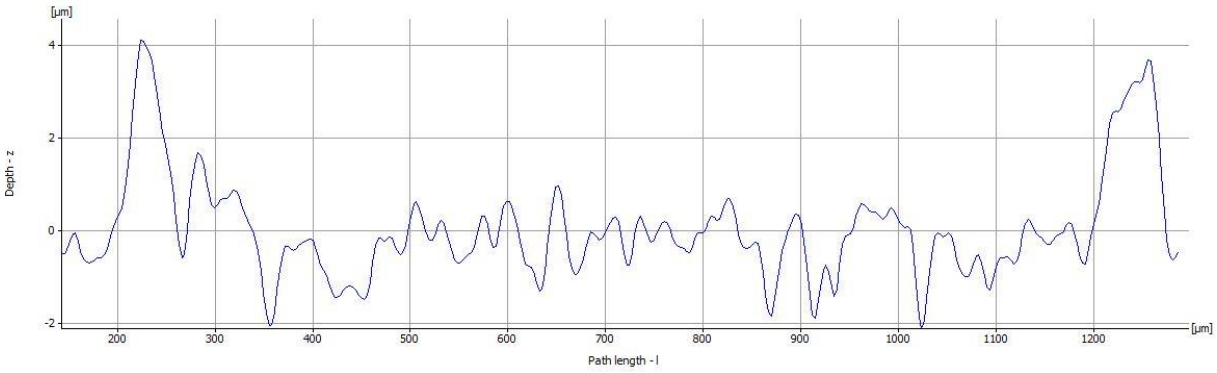

Figure 0-13: Confocal cross section roughness profile of Ti 99.6 % dry test 1

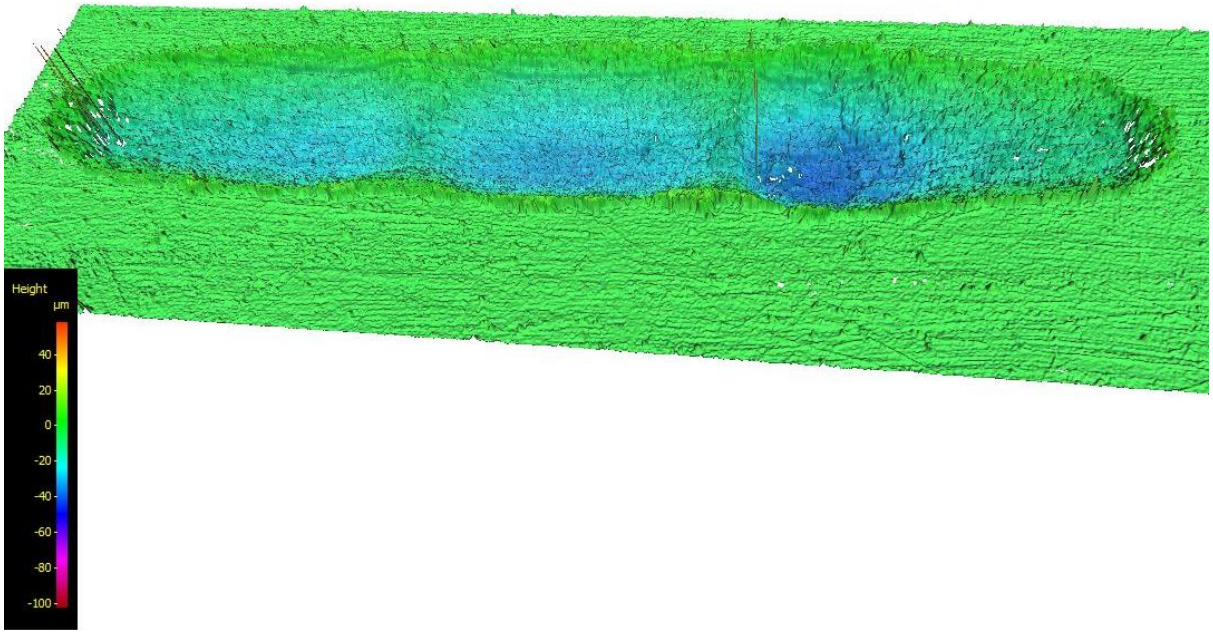

Figure 0-14: Confocal 3d image of Ti 99.6 % dry test 2

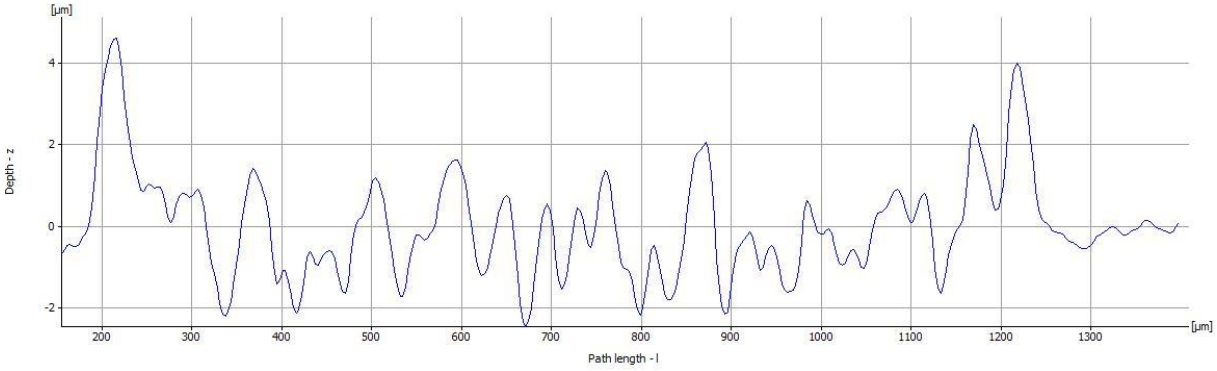

Figure 0-15: Confocal cross section roughness profile of Ti 99.6 % dry test 2

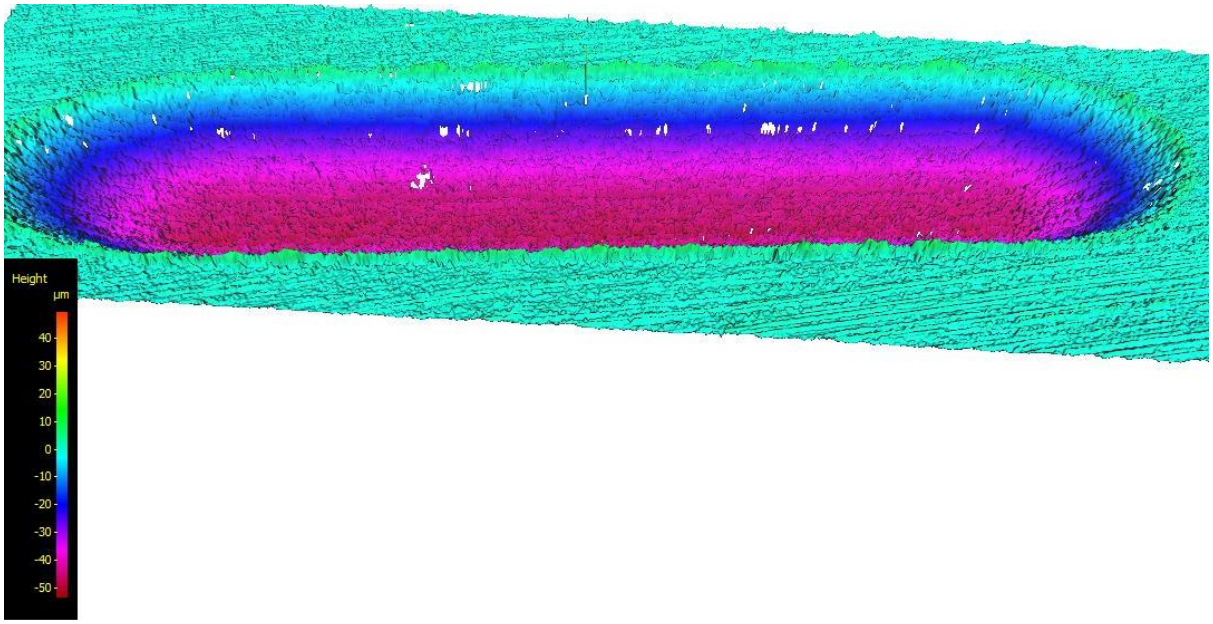

Figure 0-16: Confocal 3d image of Ti 99.6 % PBS 7.4 test 1

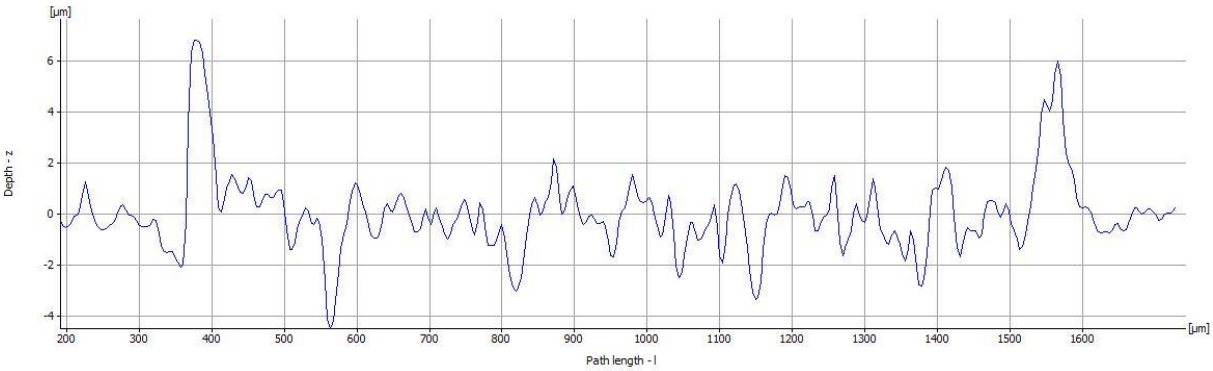

Figure 0-17: Confocal cross section roughness profile of Ti 99.6 % PBS 7.4 test 1

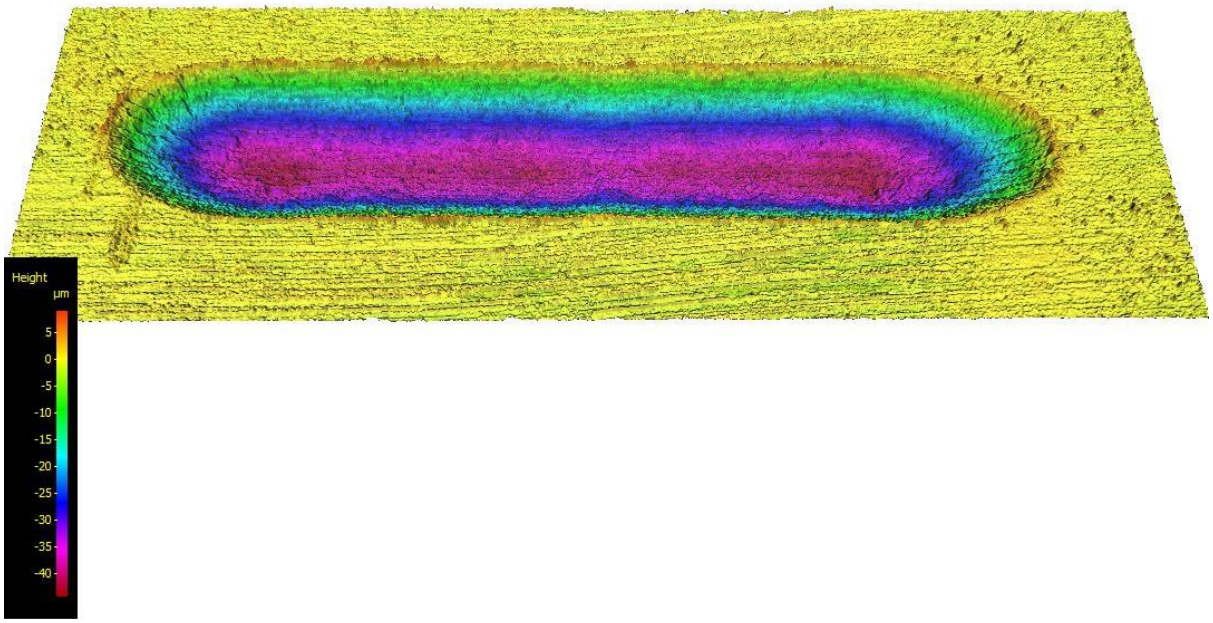

Figure 0-18: Confocal 3d image of Ti 99.6 % PBS 7.4 with protein test 1

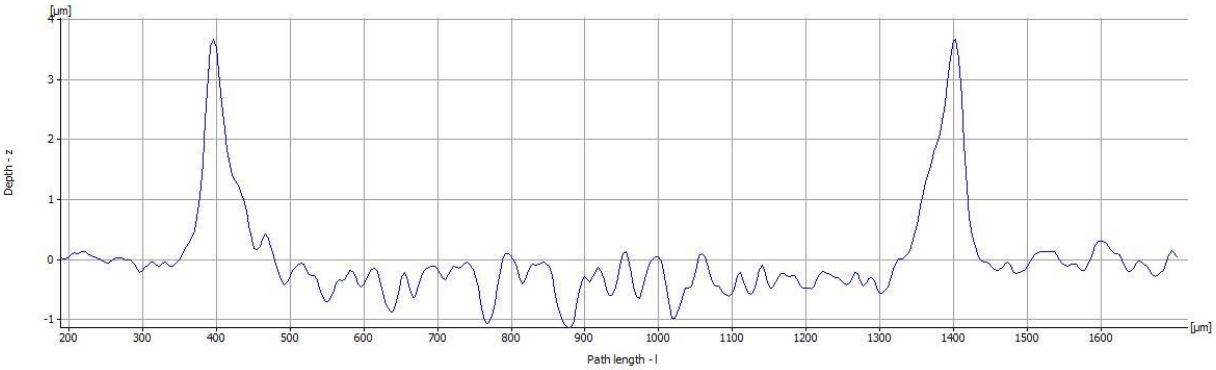

Figure 0-19: Confocal cross section roughness profile of Ti 99.6 % PBS 7.4 with protein test 1

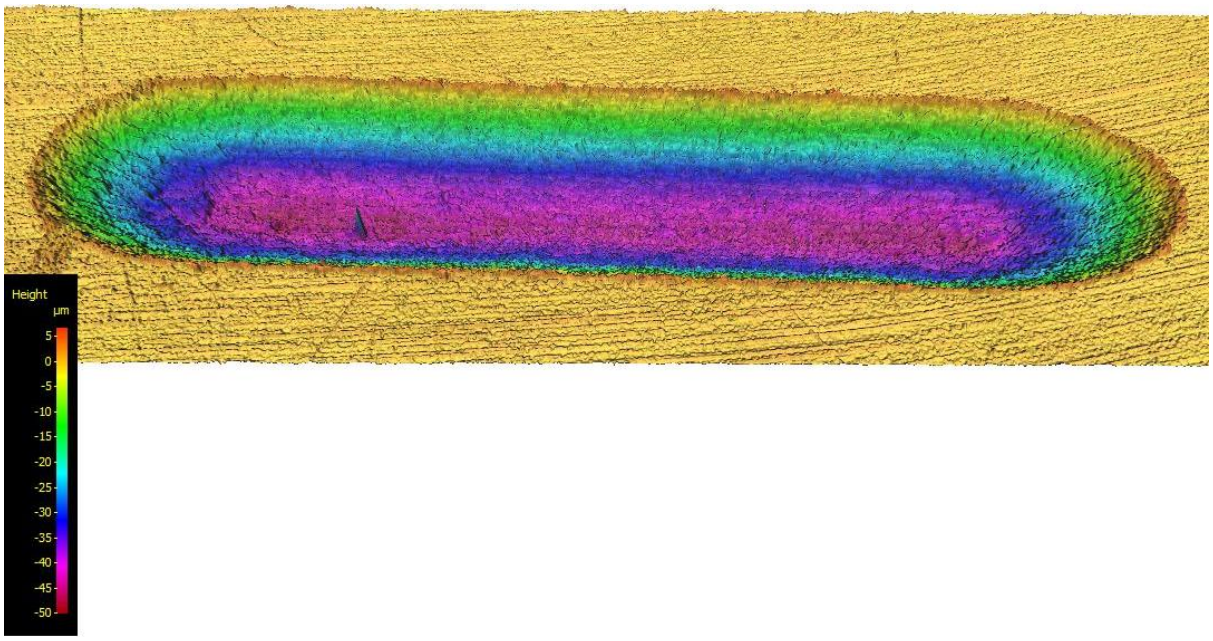

Figure 0-20: Confocal 3d image of Ti 99.6 % PBS 7.4 with protein test 2

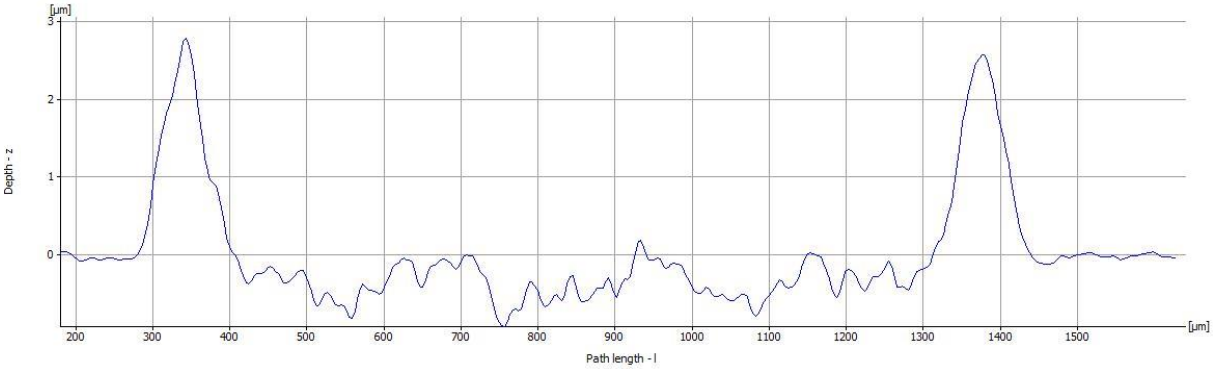

Figure 0-21: Confocal cross section roughness profile of Ti 99.6 % PBS 7.4 with protein test 2

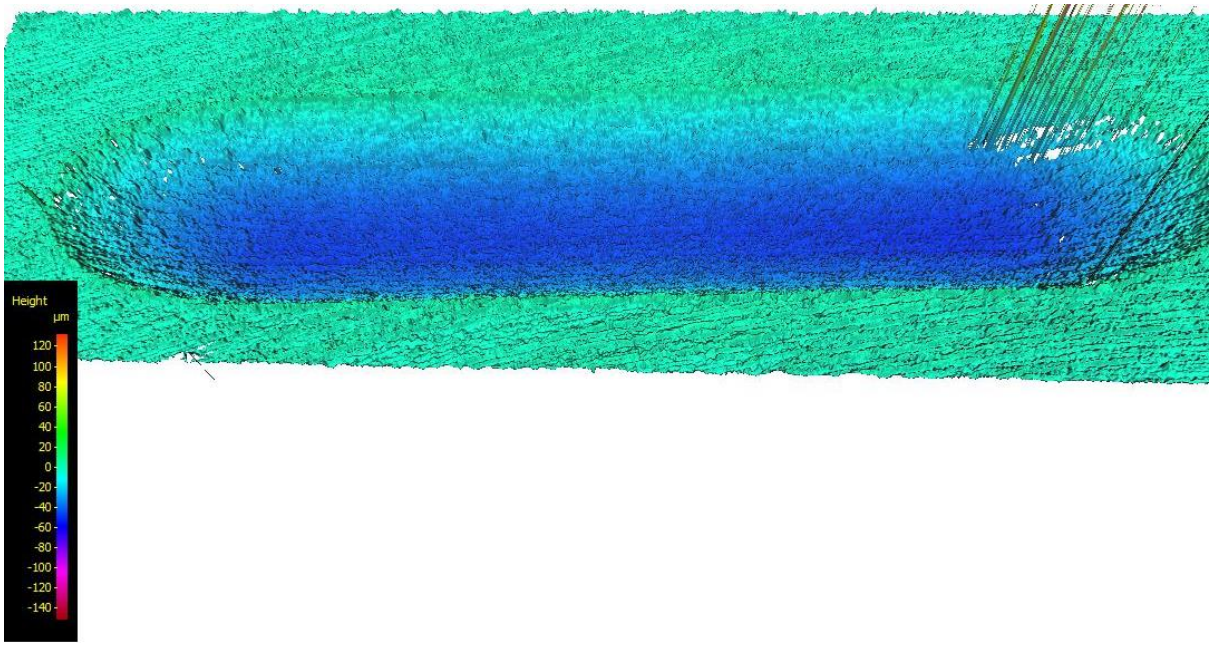

Figure 0-22: Confocal 3d image of Ti 99.6 % PBS 5.2 test 1

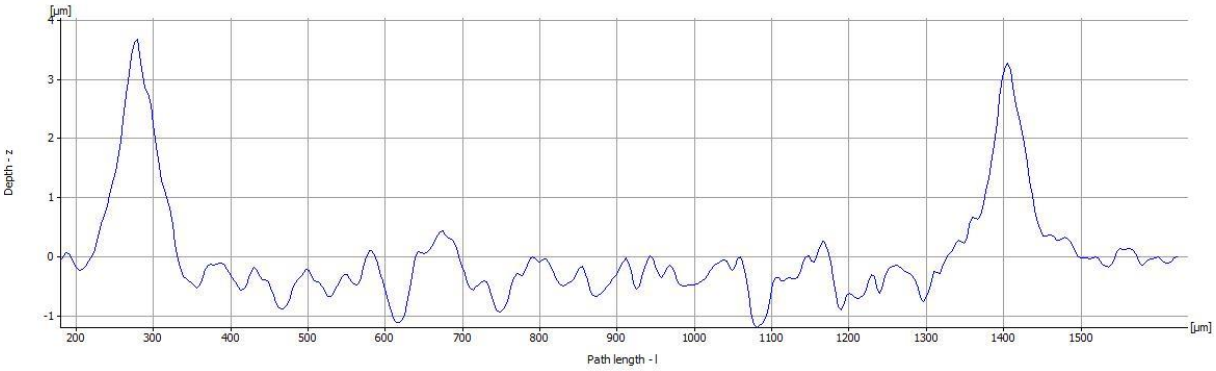

Figure 0-23: Confocal cross section roughness profile of Ti 99.6 % PBS 5.2 test 1

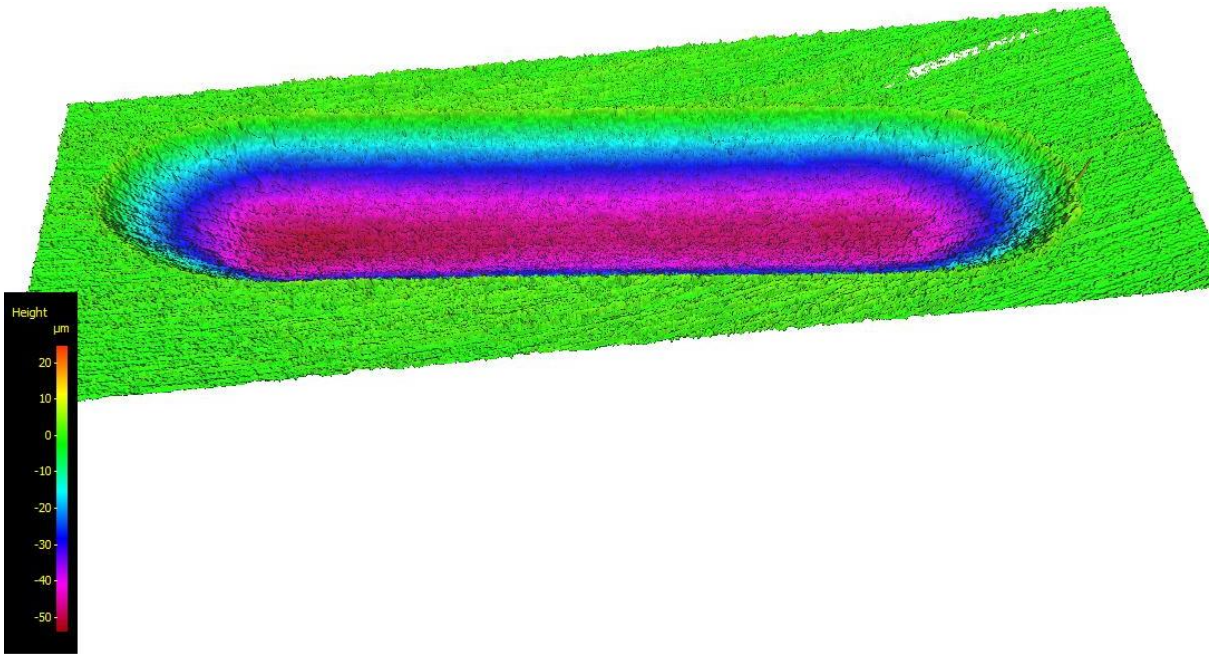

Figure 0-24: Confocal 3d image of Ti 99.6 % PBS 5.2 test 2

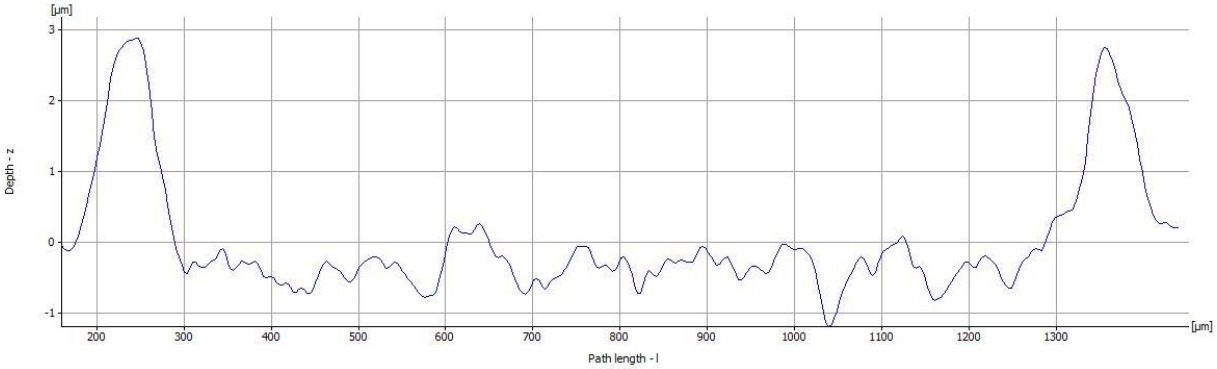

Figure 0-25: Confocal cross section roughness profile of Ti 99.6 % PBS 5.2 test 2

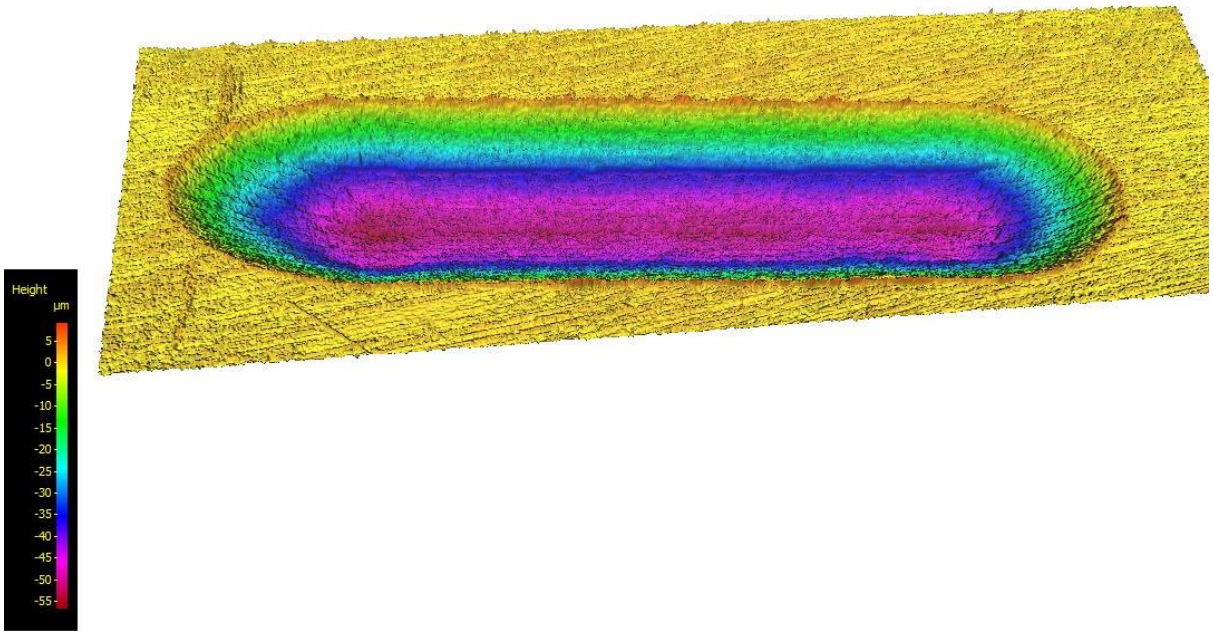

Figure 0-26: Confocal 3d image of Ti 99.6 % PBS 5.2 with protein test 1

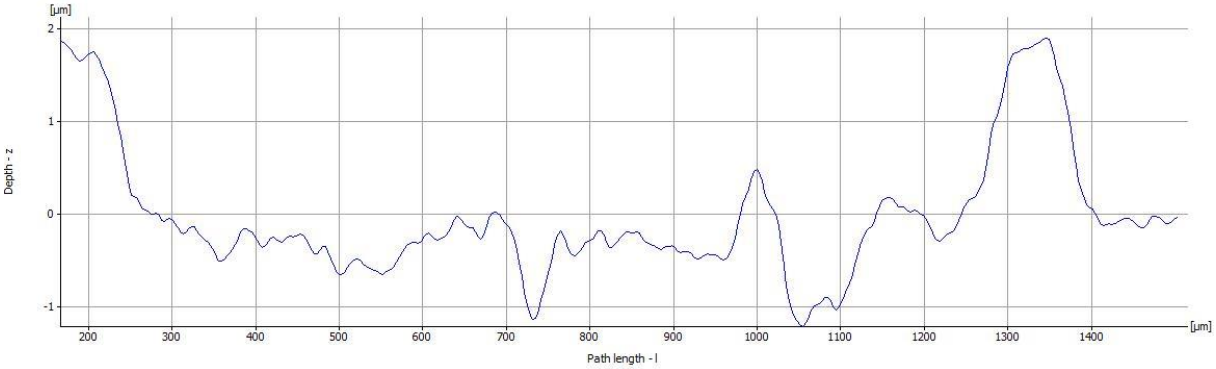

Figure 0-27: Confocal cross section roughness profile of Ti 99.6 % PBS 5.2 with protein test 1

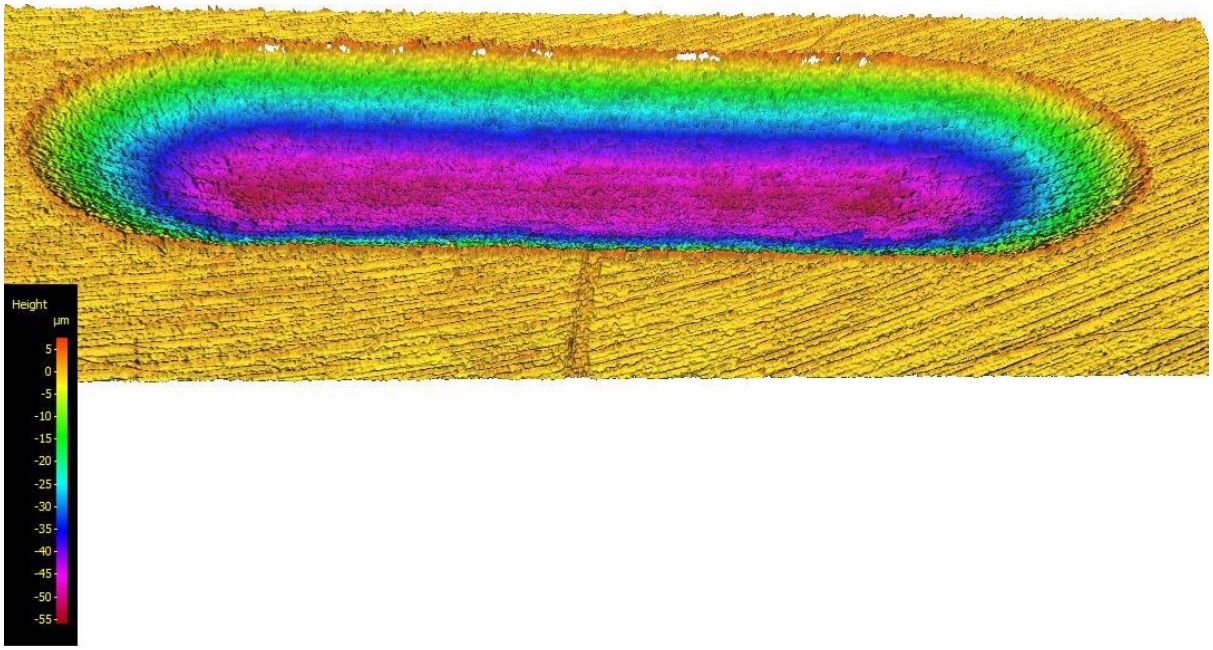

Figure 0-28: Confocal 3d image of Ti 99.6 % PBS 5.2 with protein test 2

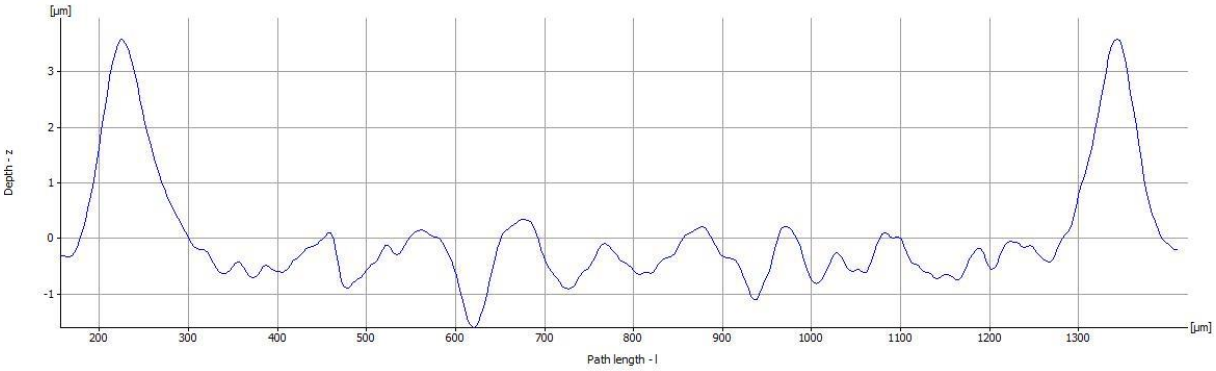

Figure 0-29: Confocal cross section roughness profile of Ti 99.6 % PBS 5.2 with protein test 2

b. CoCrMo

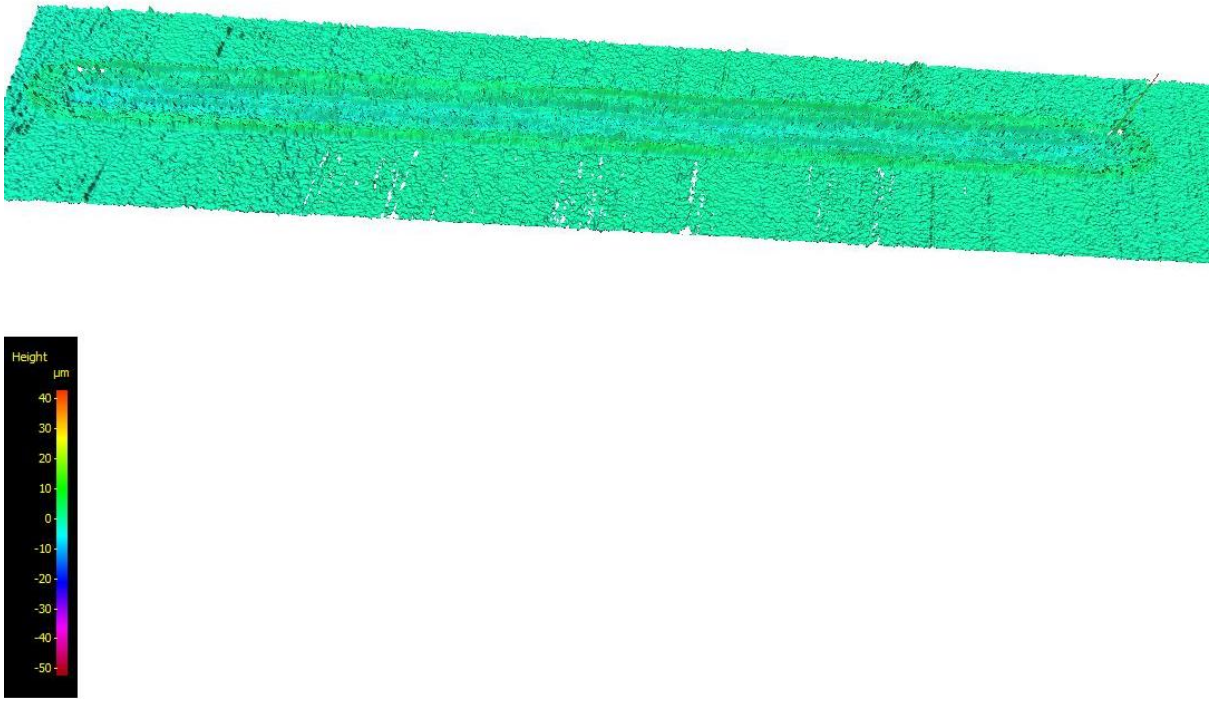

Figure 0-30: Confocal 3d image of CoCrMo dry test 1

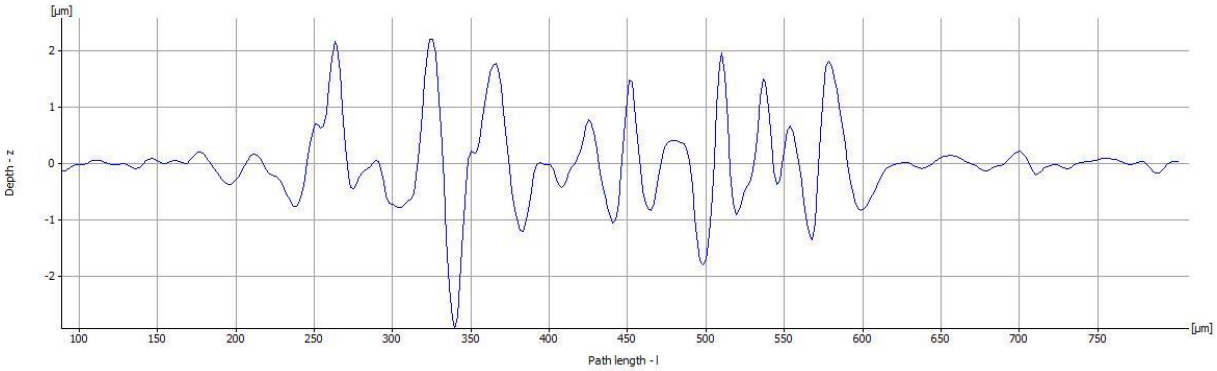

Figure 0-31: Confocal cross section roughness profile of CoCrMo dry test 1

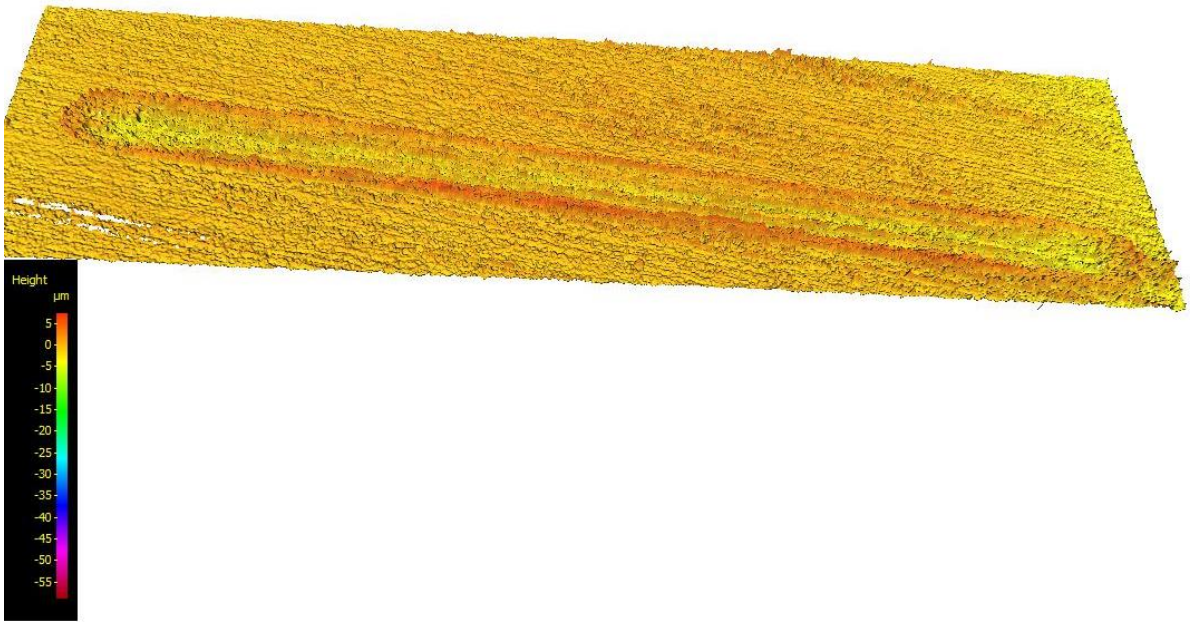

Figure 0-32: Confocal 3d image of CoCrMo dry test 2

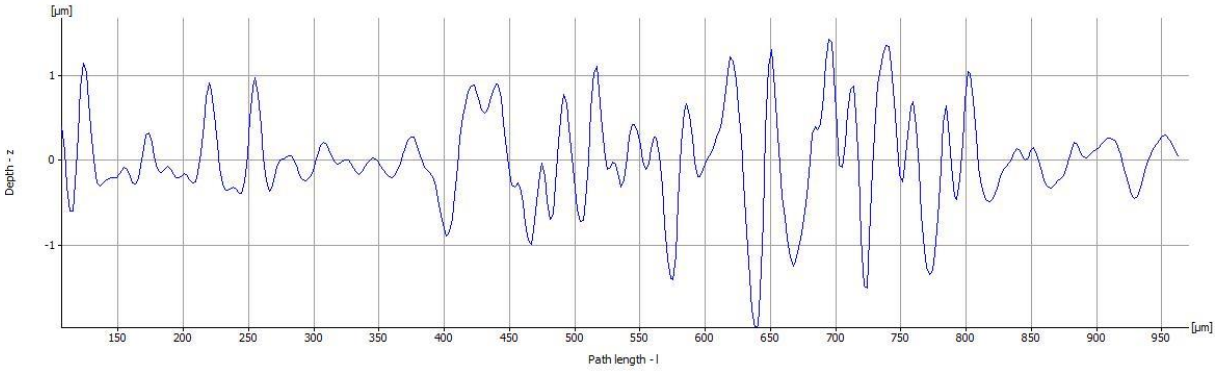

Figure 0-33: Confocal cross section roughness profile of CoCrMo dry test 2

Figure 0-34: Confocal 3d image of CoCrMo PBS 7.4 test 1

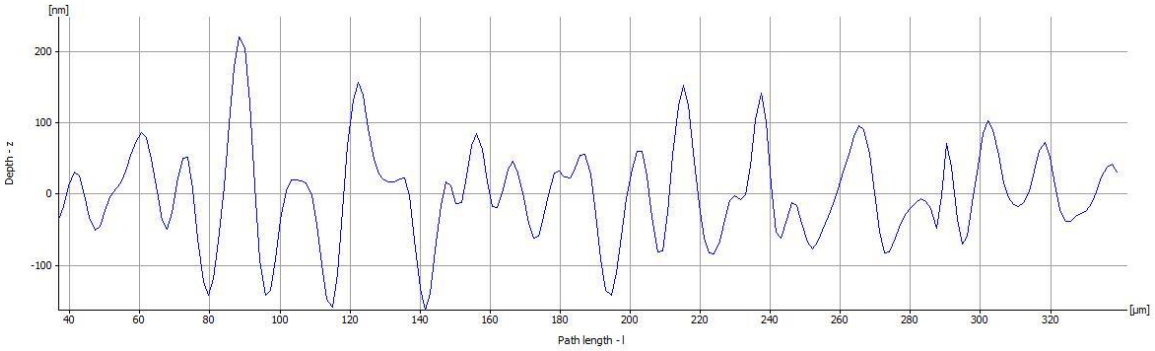

Figure 0-35: Confocal cross section roughness profile of CoCrMo PBS 7.4 test 1

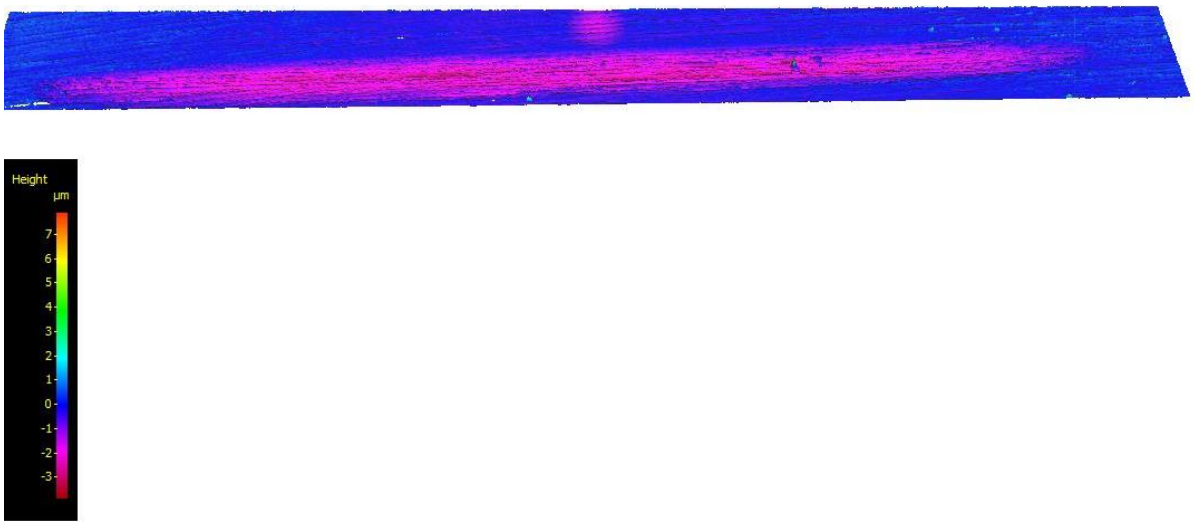

Figure 0-36:Confocal 3d image of CoCrMo PBS 7.4 test 2

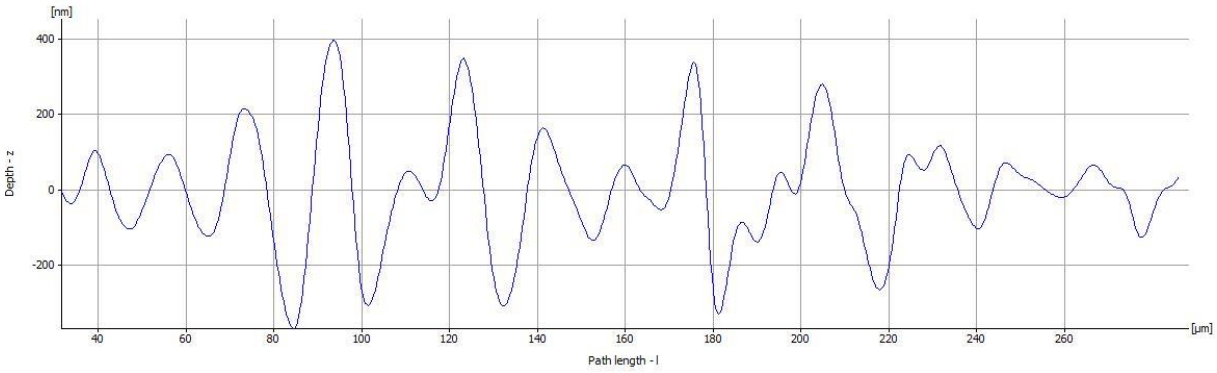

Figure 0-37: Confocal cross section roughness profile of CoCrMo PBS 7.4 test 2

Figure 0-38: Confocal 3d image of CoCrMo PBS 7.4 with protein test 2

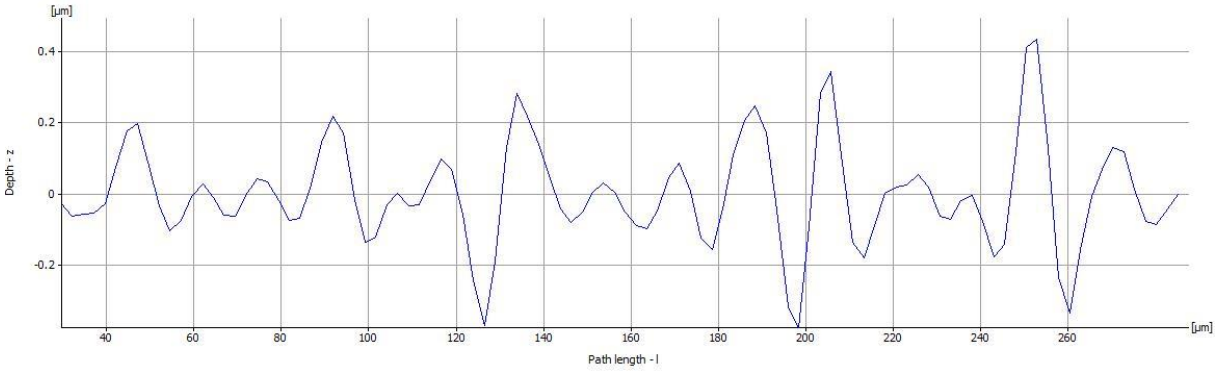

Figure 0-39: Confocal cross section roughness profile of CoCrMo PBS 7.4 with protein test 2

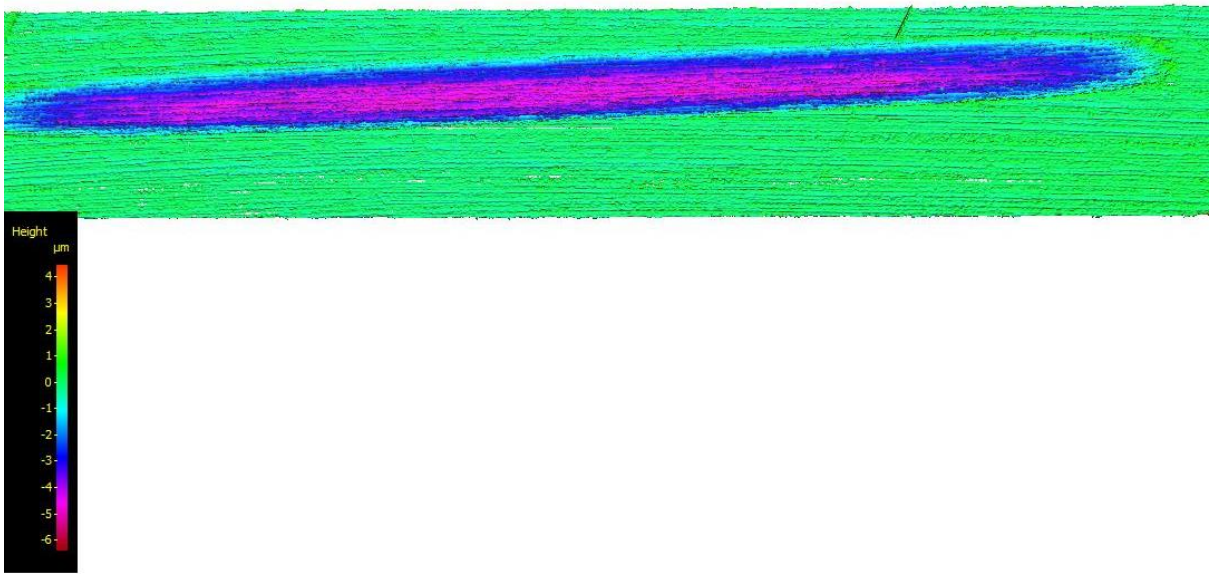

Figure 0-40: Confocal 3d image of CoCrMo PBS 5.2 test 1

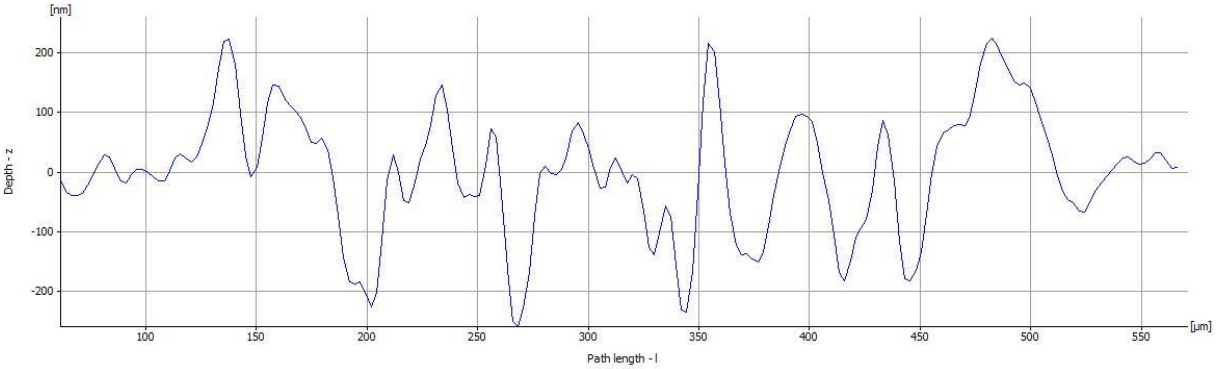

Figure 0-41: Confocal cross section roughness profile of CoCrMo PBS 5.2 test 1

a. BMG

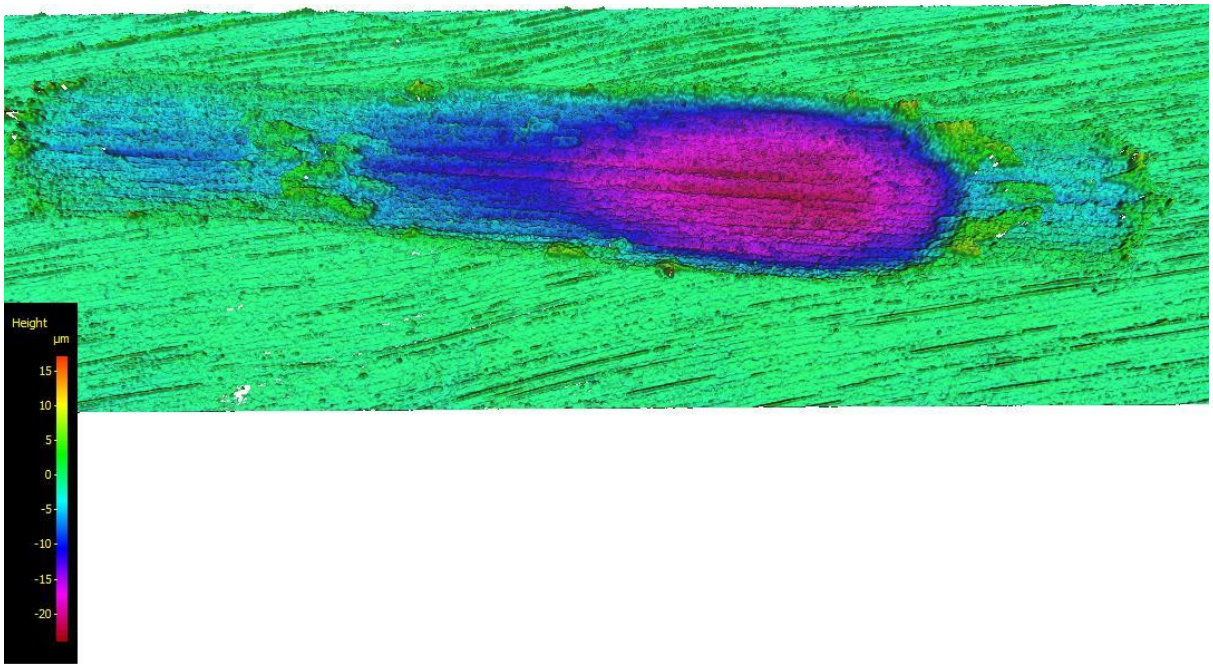

Figure 0-42: Confocal 3d image of BMG dry test 1

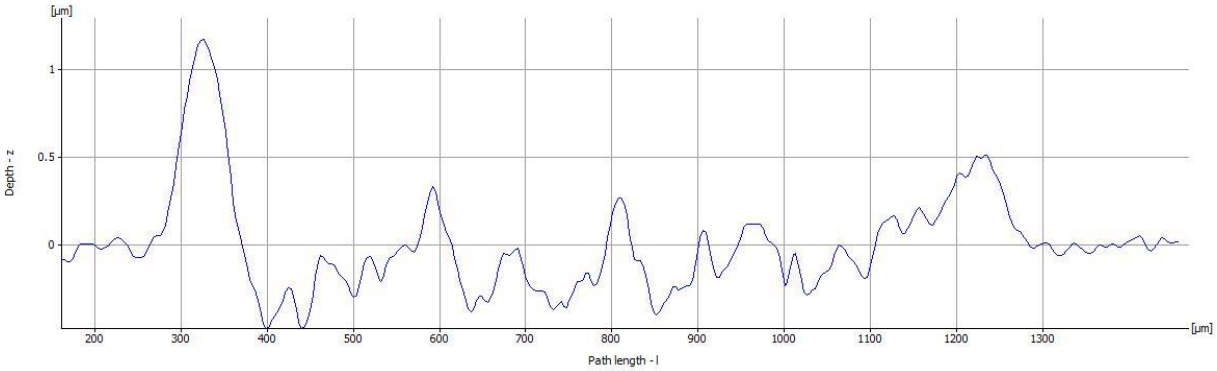

Figure 0-43: Confocal cross section roughness profile of BMG dry test 1

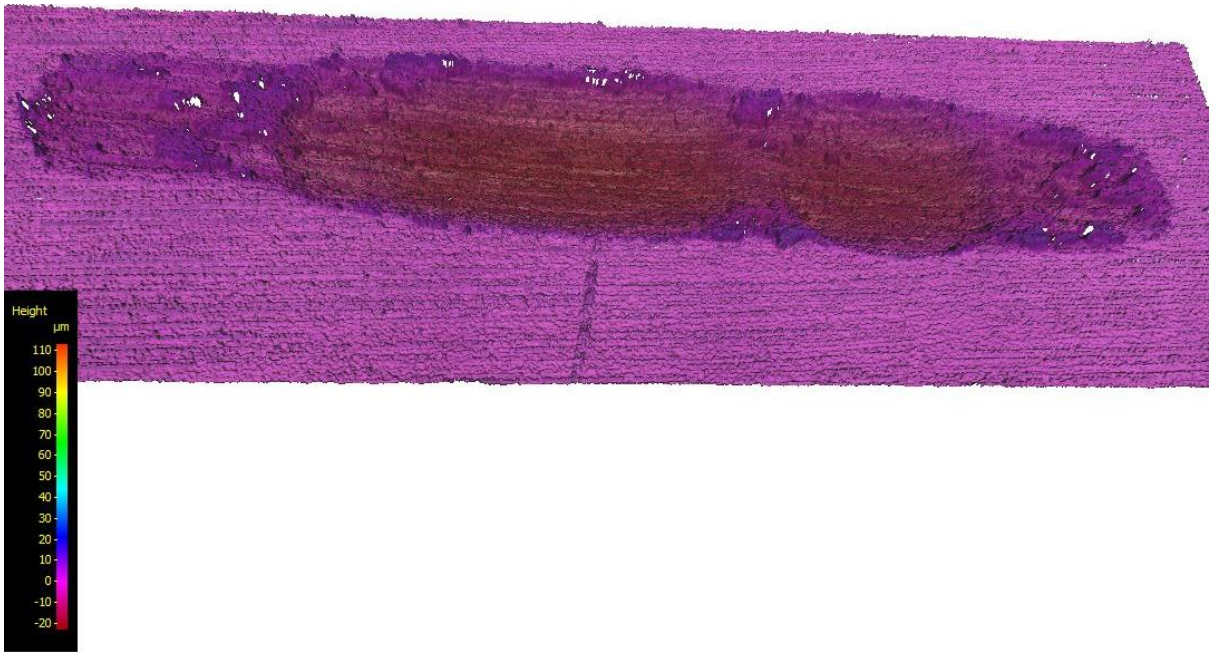

Figure 0-44: Confocal 3d image of BMG dry test 2

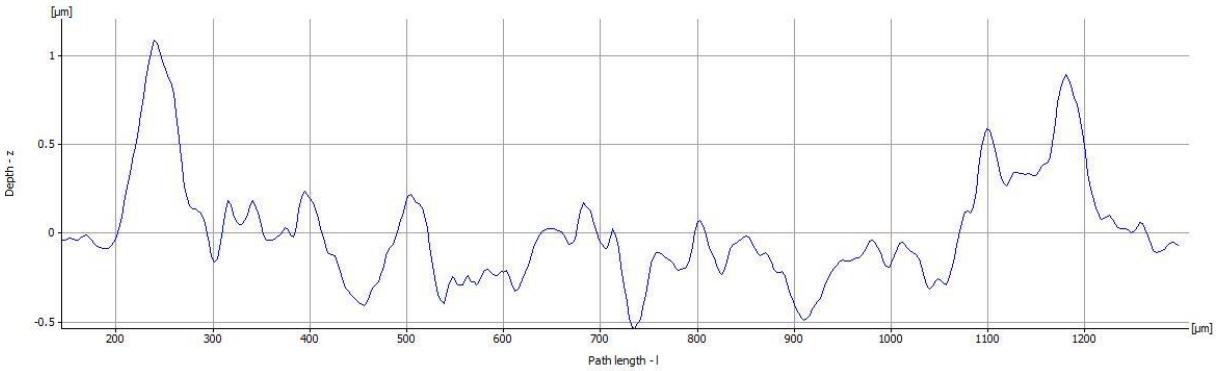

Figure 0-45: Confocal cross section roughness profile of BMG dry test 2

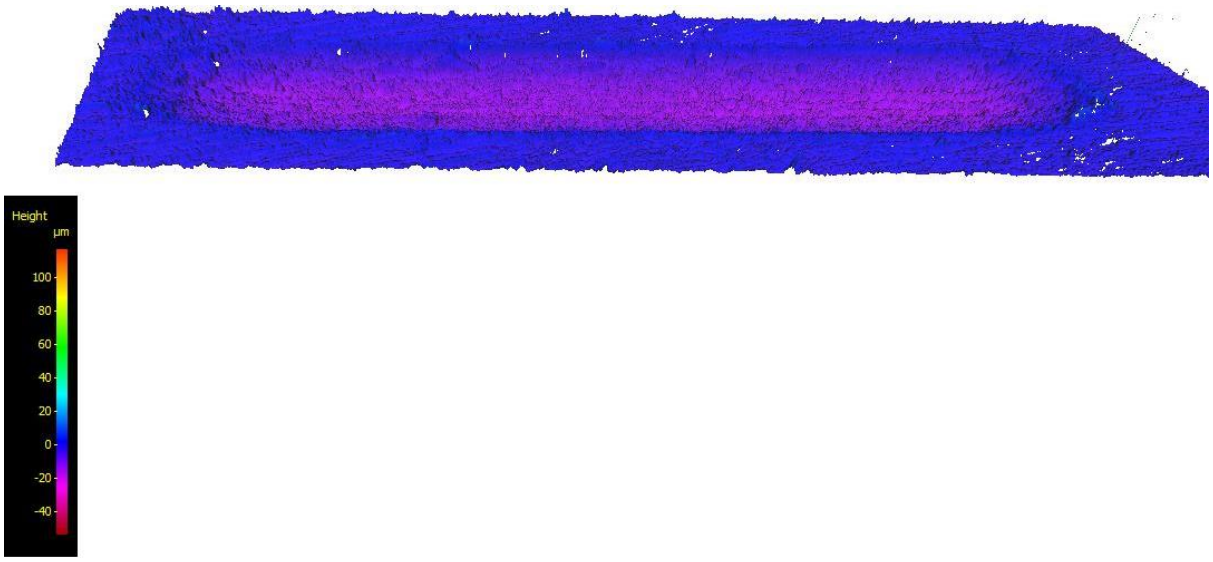

Figure 0-46: Confocal 3d image of BMG PBS 7.4 test 1

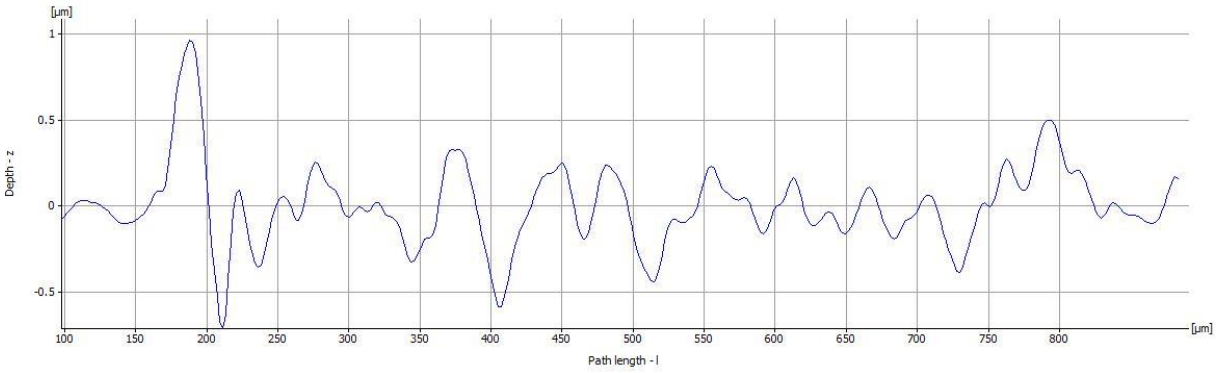

Figure 0-47: Confocal cross section roughness profile of BMG PBS 7.4 test 1

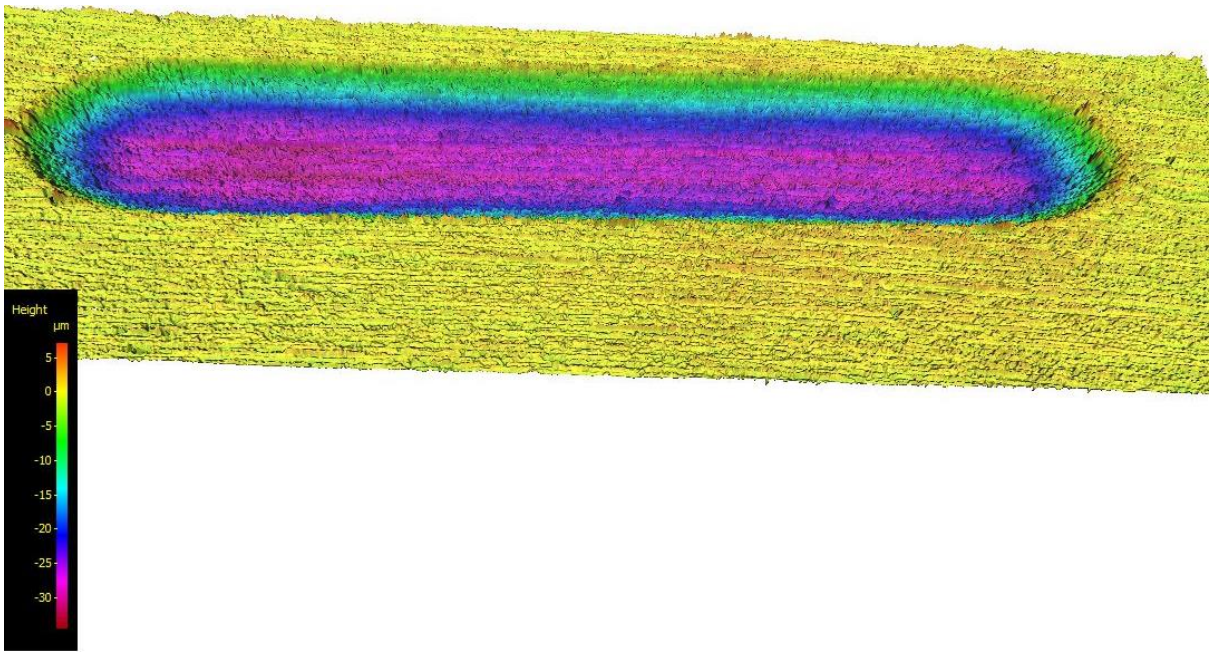

Figure 0-48: Confocal 3d image of BMG PBS 7.4 protein test 1

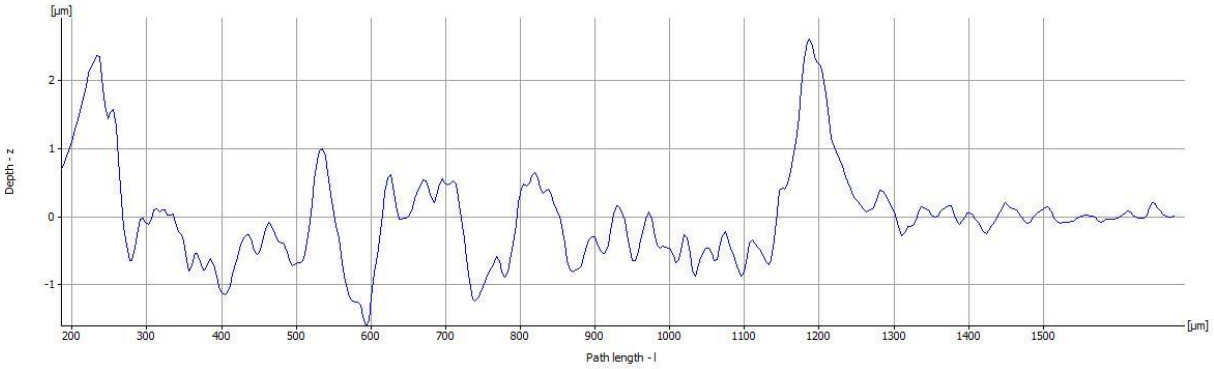

Figure 0-49: Confocal cross section roughness profile of BMG PBS 7.4 protein test 1

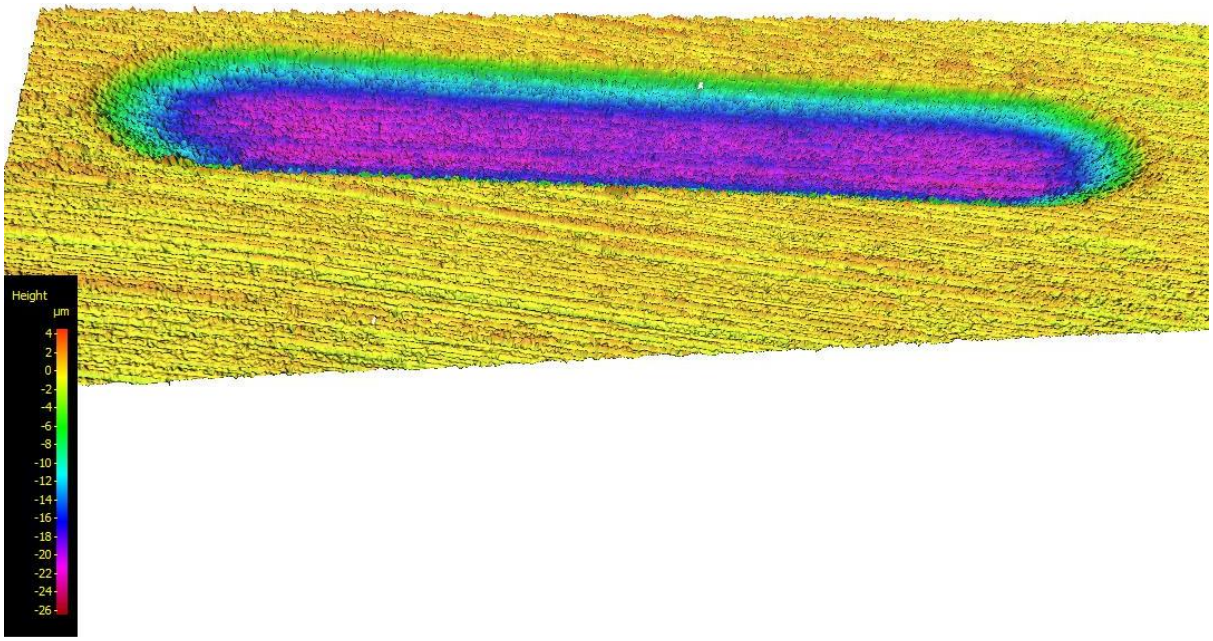

Figure 0-50: Confocal 3d image of BMG PBS 7.4 protein test 2

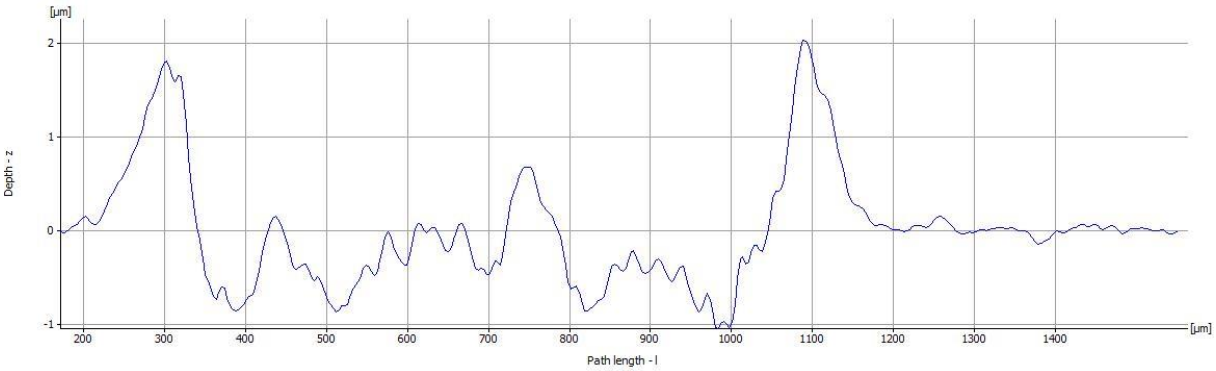

Figure 0-51: Confocal cross section roughness profile of BMG PBS 7.4 protein test 2

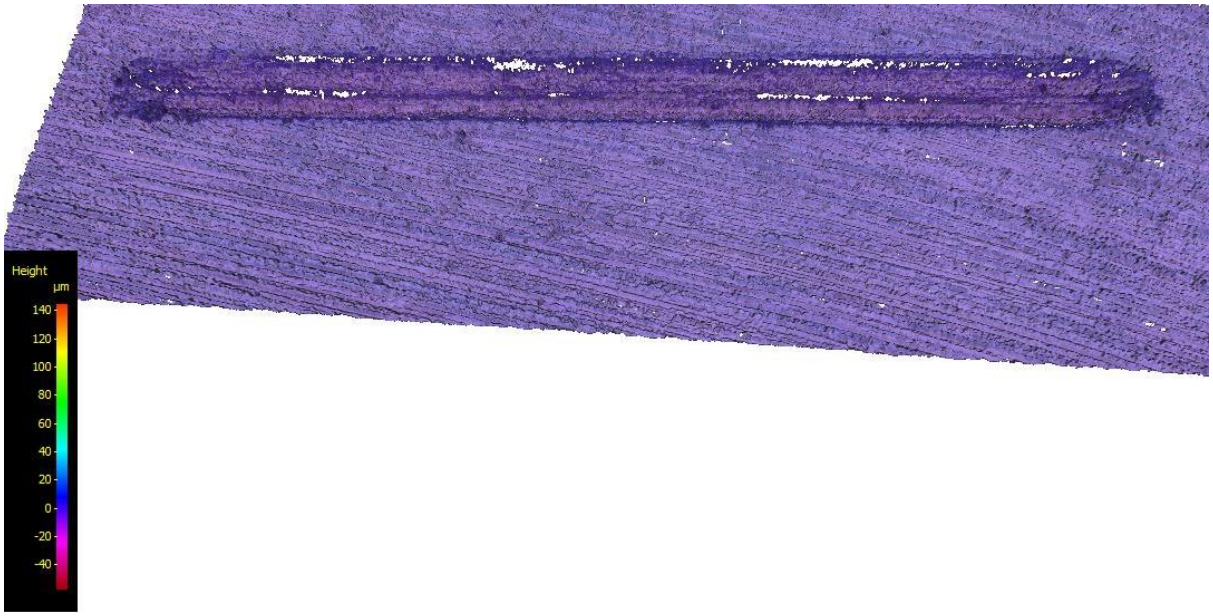

Figure 0-52: Confocal 3d image of BMG PBS 5.2 test 1

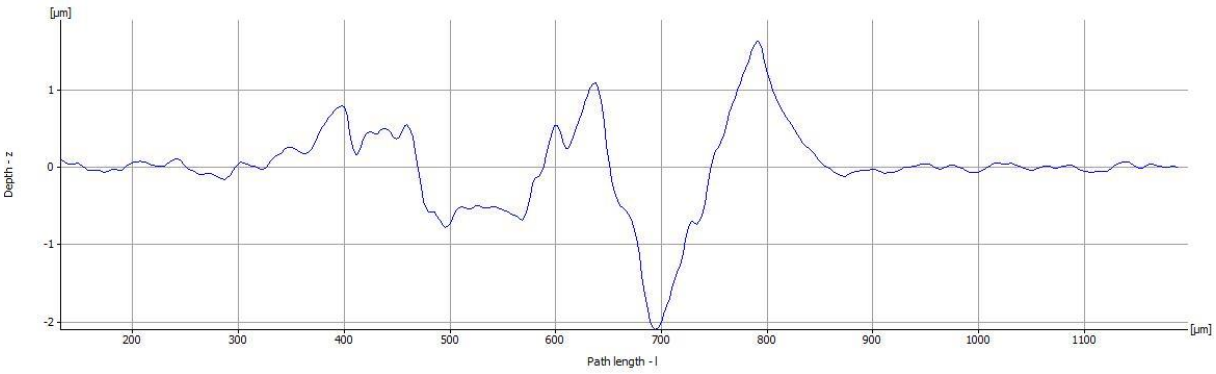

Figure 0-53: Confocal cross section roughness profile of BMG PBS 5.2 test 1

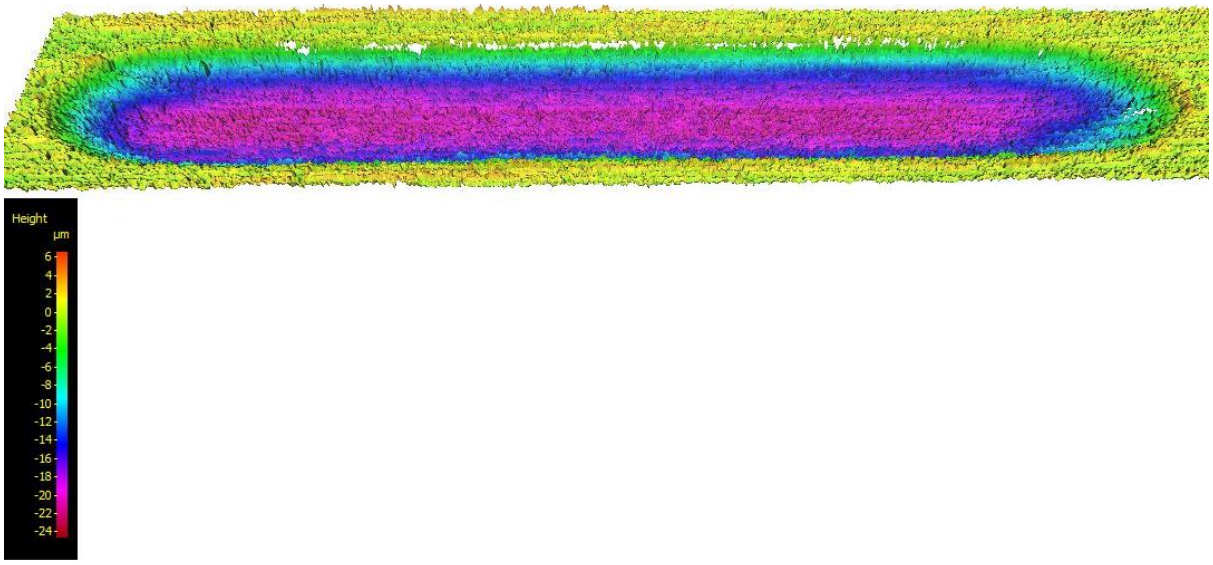

Figure 0-54: Confocal 3d image of BMG PBS 5.2 test 2

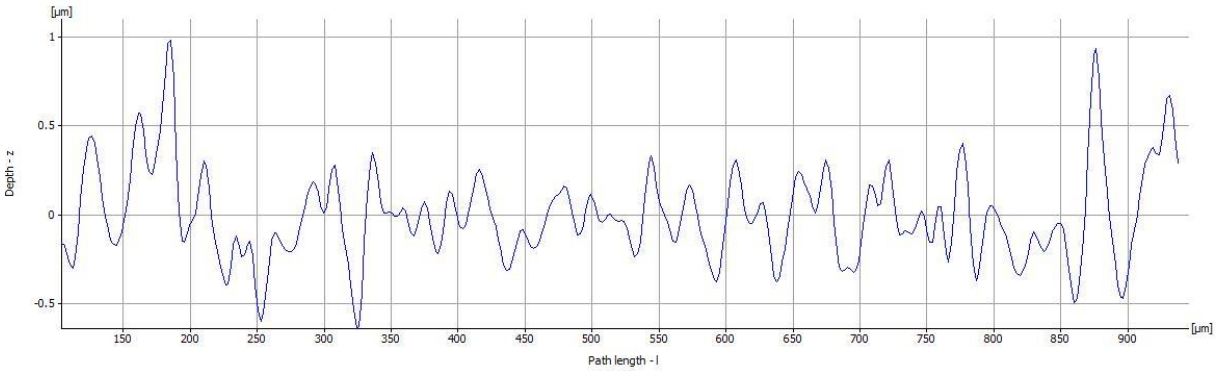

Figure 0-55: Confocal cross section roughness profile of BMG PBS 5.2 test 2

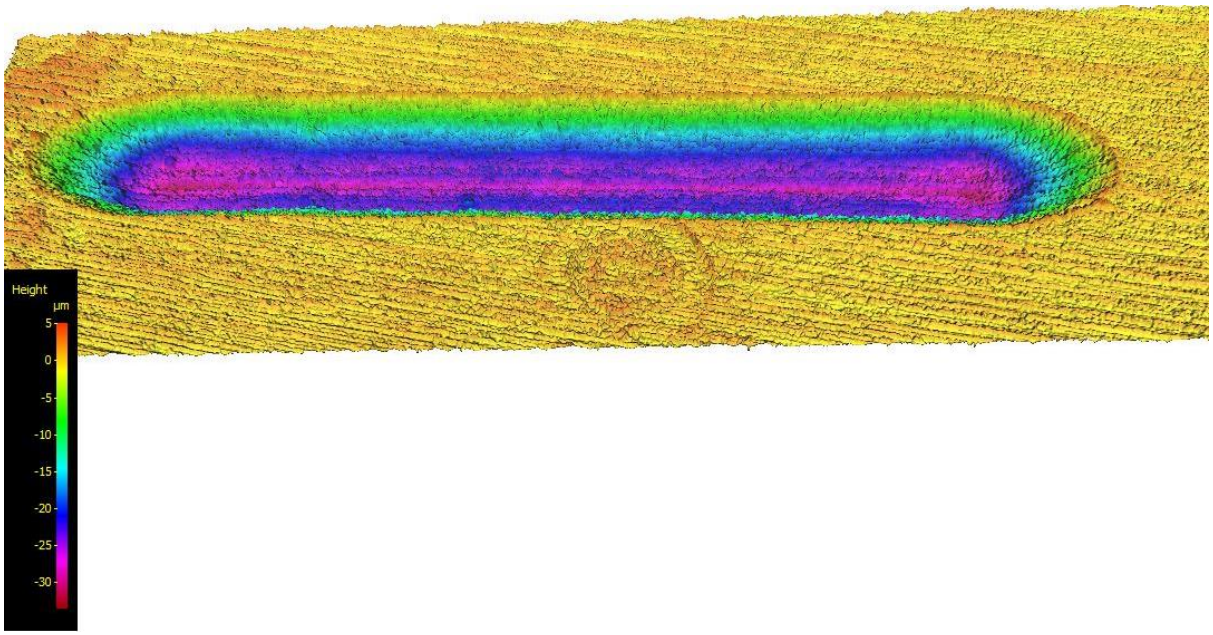

Figure 0-56: Confocal 3d image of BMG PBS 5.2 protein test 1

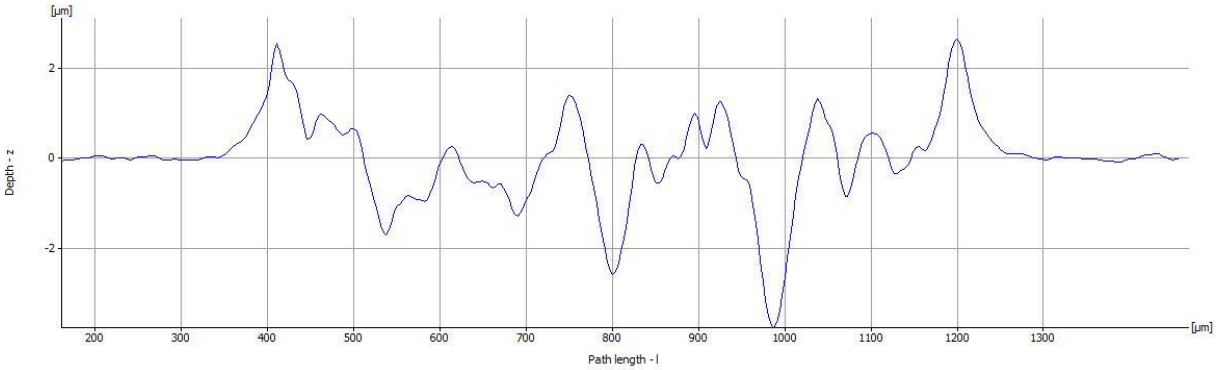

Figure 0-57: Confocal cross section roughness profile of BMG PBS 5.2 protein test 1

2. Wear volume test results

		Material		
Condition	Sample #	BMG	CoCrMo	Ti 99.6 %
Dry	1	0.0299	0.0015	0.0518
	2	0.0401	0.0012	0.0697
PBS 7.4	1	0.0251	0.0008	0.1755
	2	0.0932	0.0013	0.1521
PBS 7.4 with	1	0.0948	0.0014	0.1181
protein	2	0.0576	0.0003	0.1356
PBS 5.2	1	0.0069	0.0041	0.1694
	2	0.0526	-*	0.168
PBS 5.2 with	1	0.0661	-**	0.1685
protein	2	-***	-**	0.1643

***wear track unusable due to slipping of the pin-holder**

****no image obtainable due to low contrast caused by extremely small wear track**

*****no test performed due to time constrain**

3. SEM Images

a. Ti 99.6 %

i. Dry tests

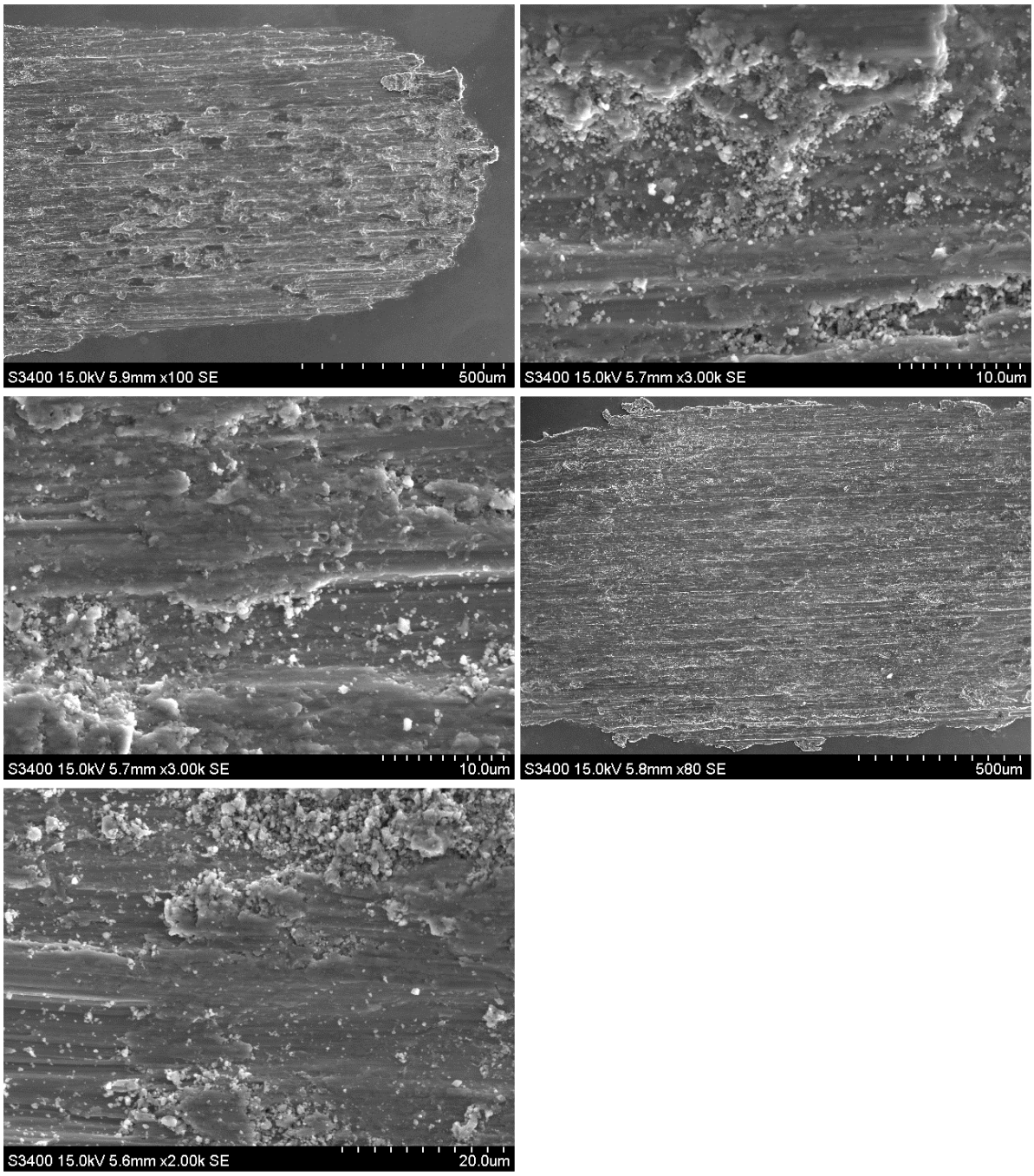

Figure 0-58: SEM images of Ti 99.6 % dry test 1

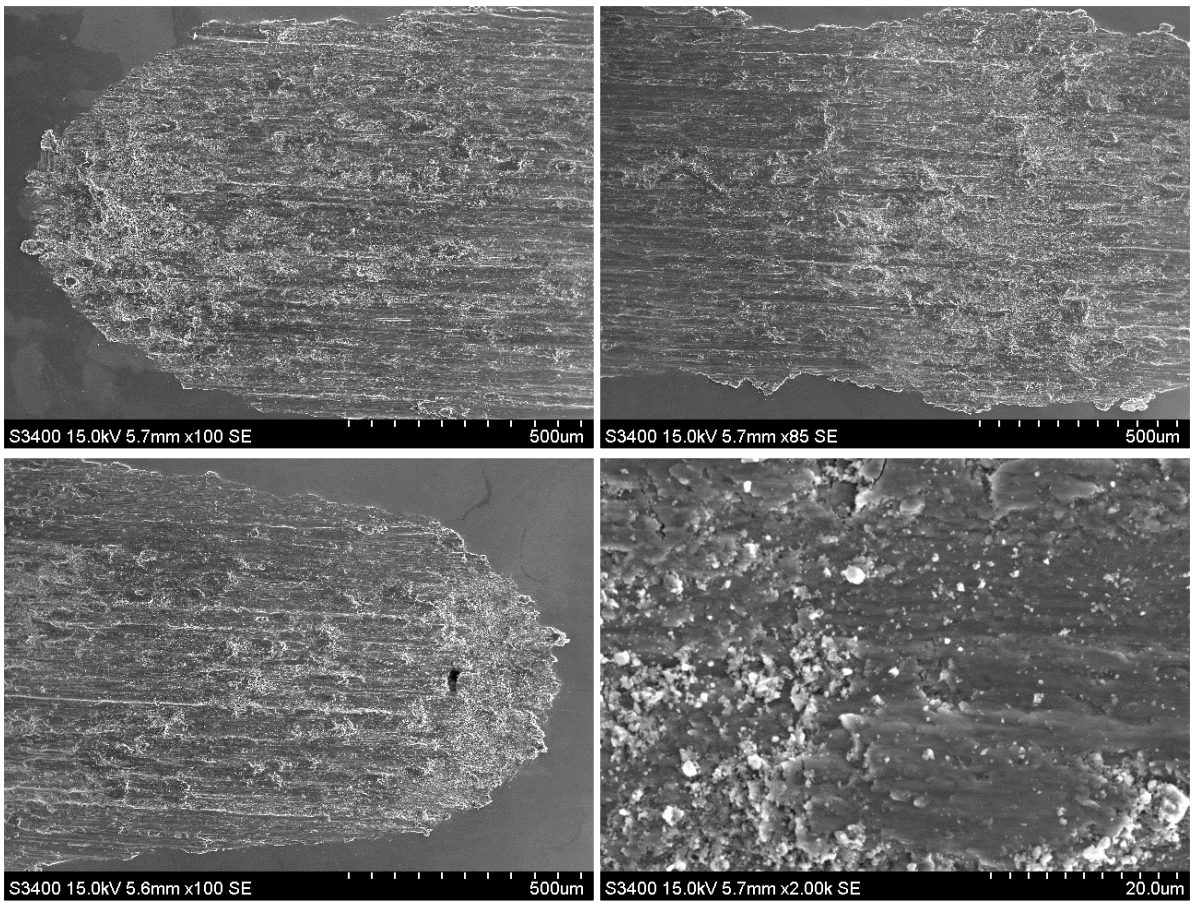

Figure 0-59: SEM images of Ti 99.6 % dry test 2

ii. PBS 7.4 tests

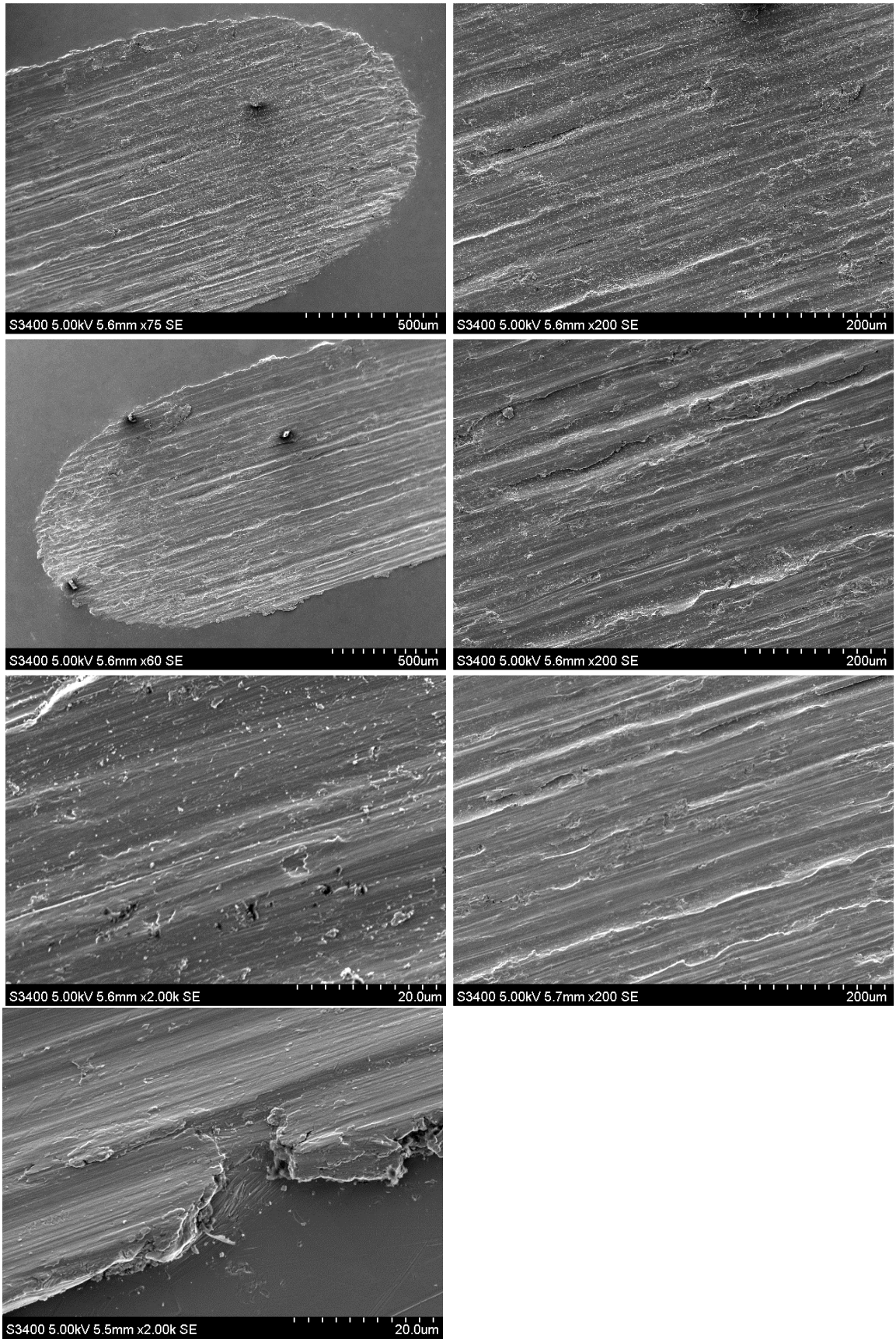

Figure 0-60: SEM images of Ti 99.6 % PBS 7.4 test 1

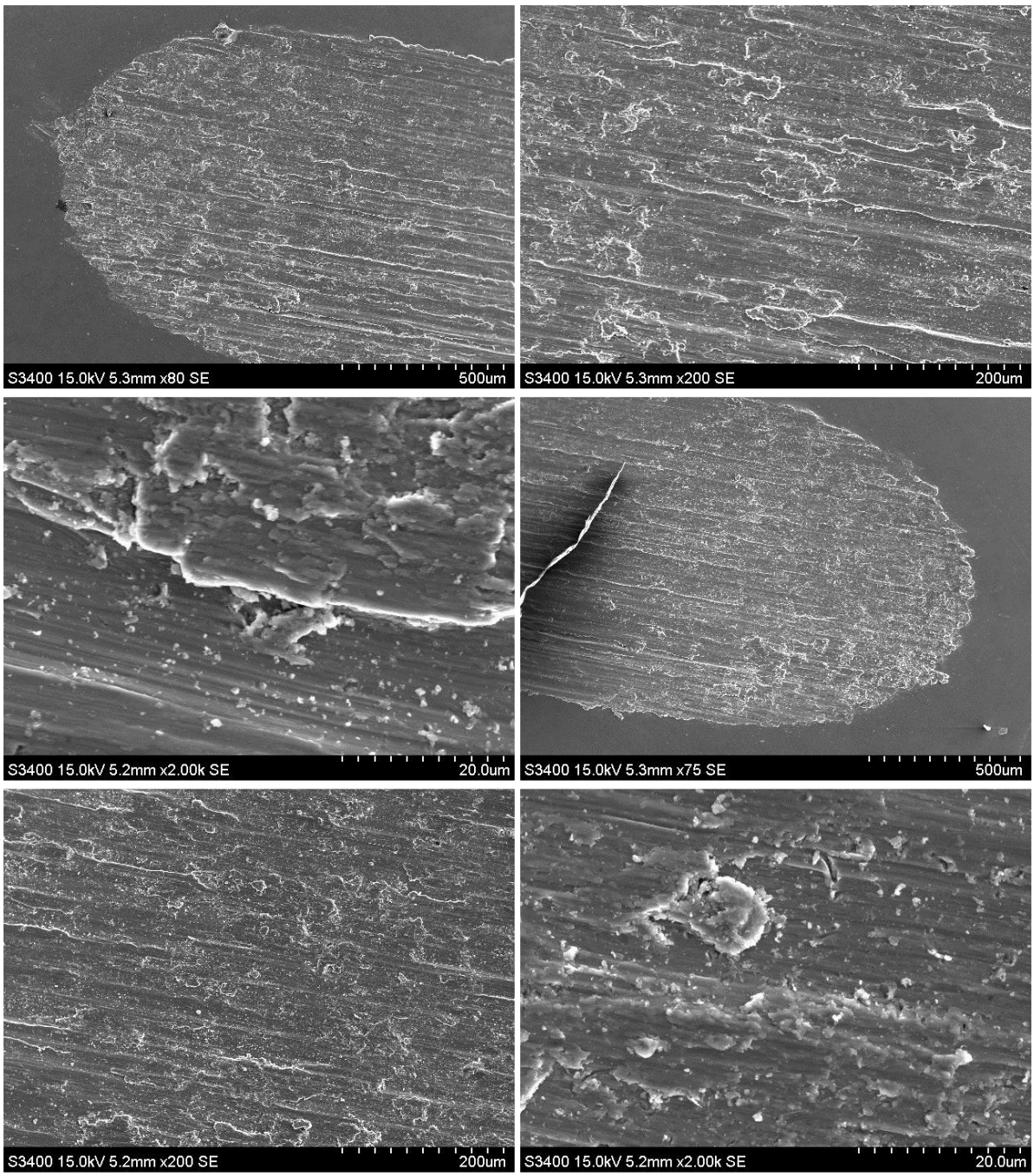

Figure 0-61: SEM images of Ti 99.6 % PBS 7.4 test 2

iii. PBS 7.4 with protein tests

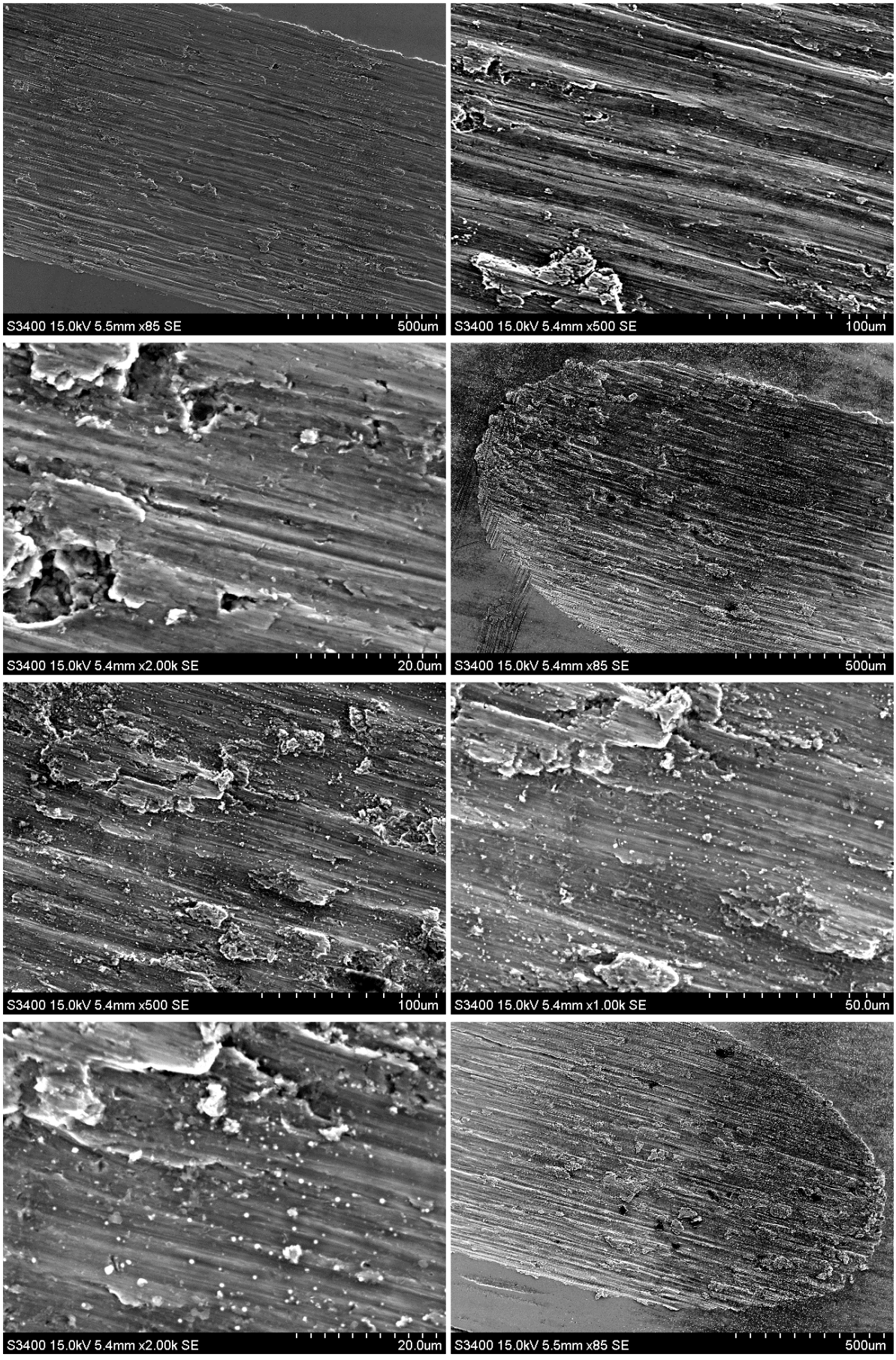

Continued from the previous page

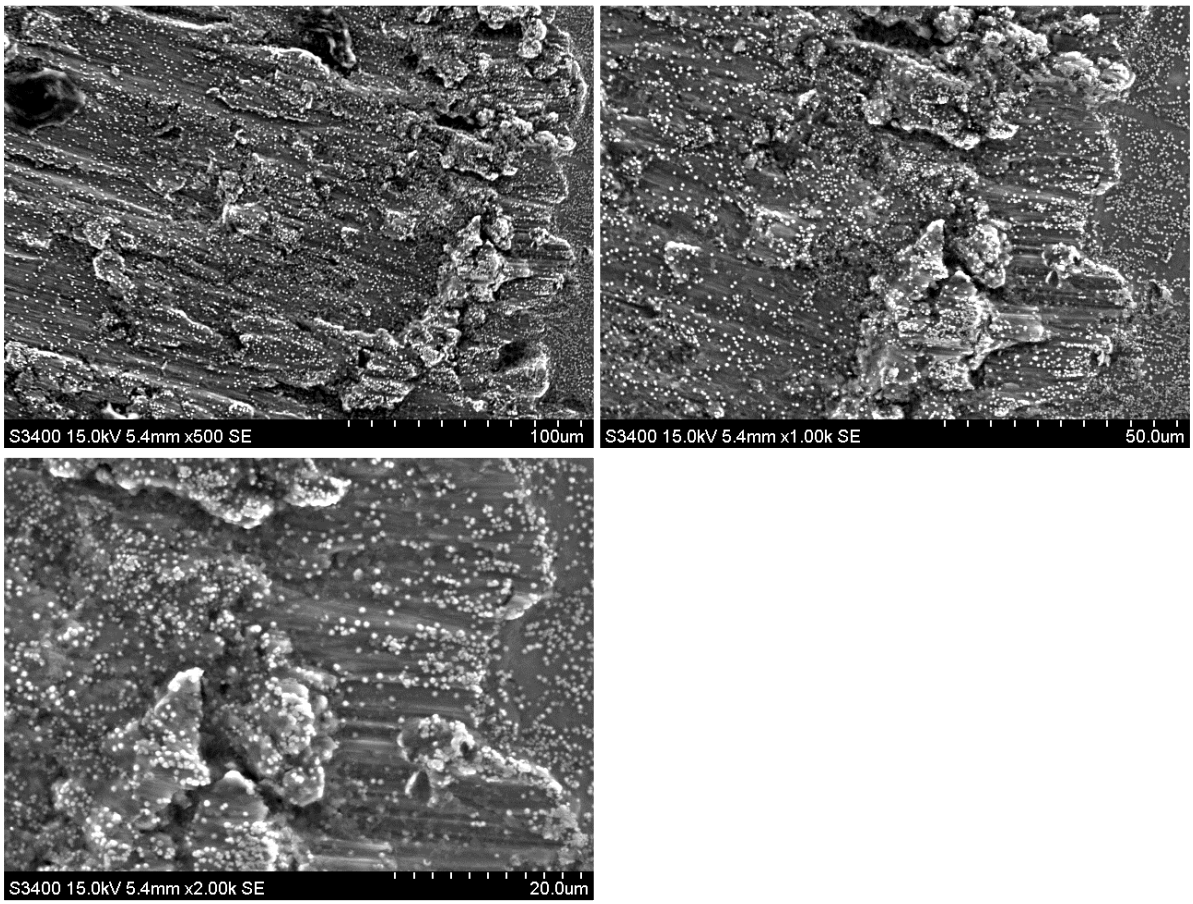

Figure 0-62: SEM images of Ti 99.6 % PBS 7.4 with protein test 1

The following 12 images are of test 2

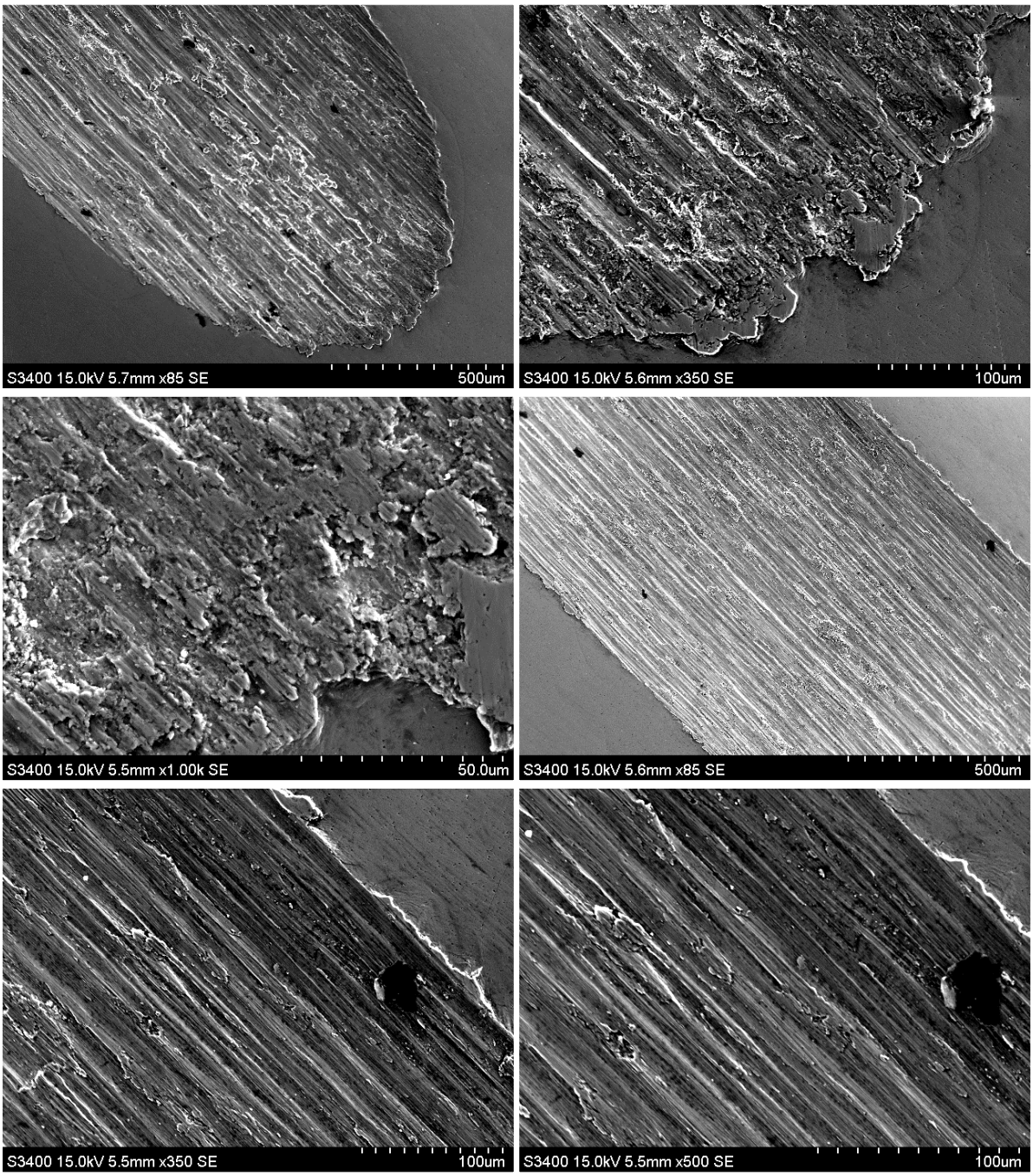

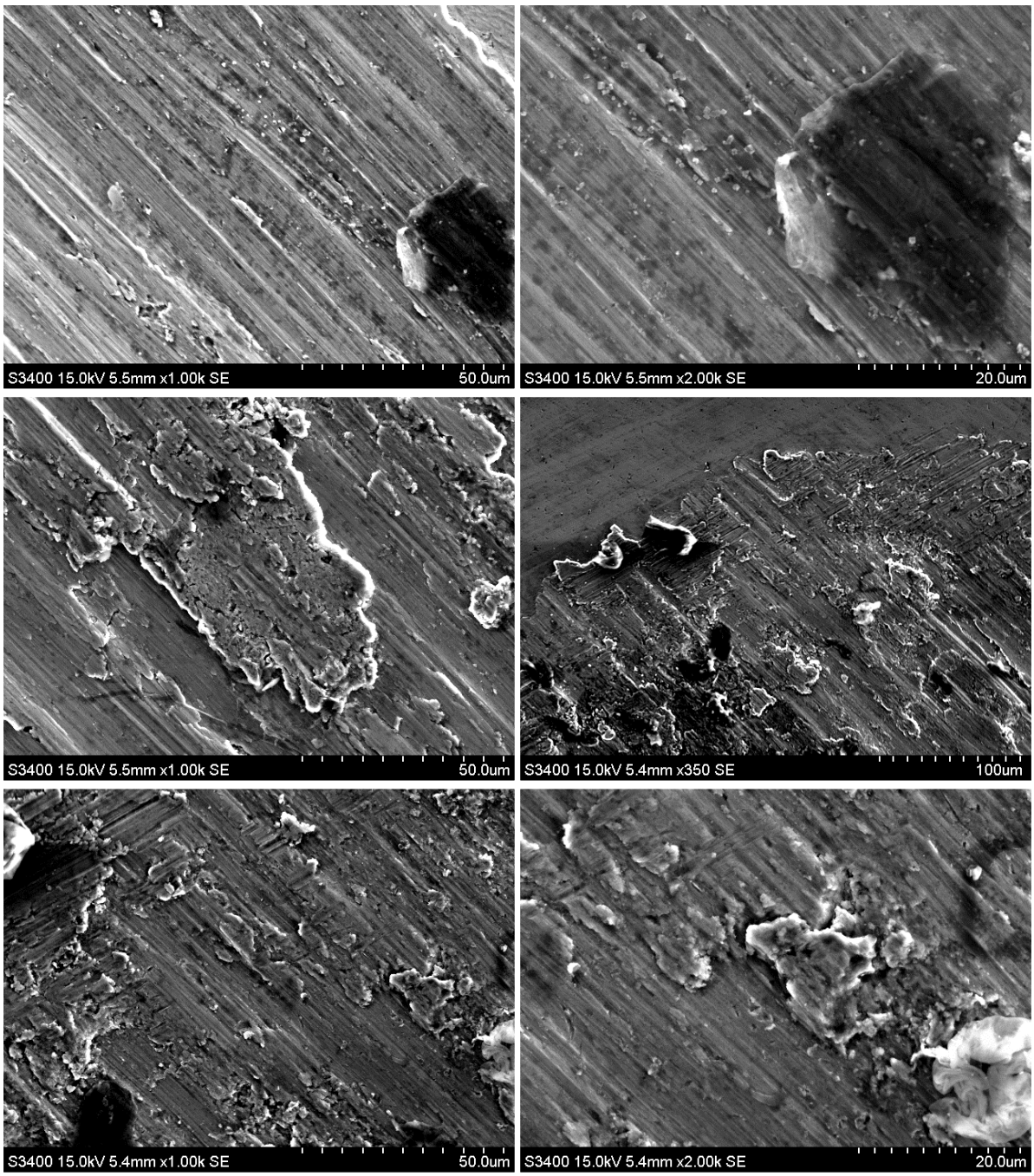

Figure 0-63: SEM images of Ti 99.6 % PBS 7.4 with protein test 2

iv. PBS 5.2 tests

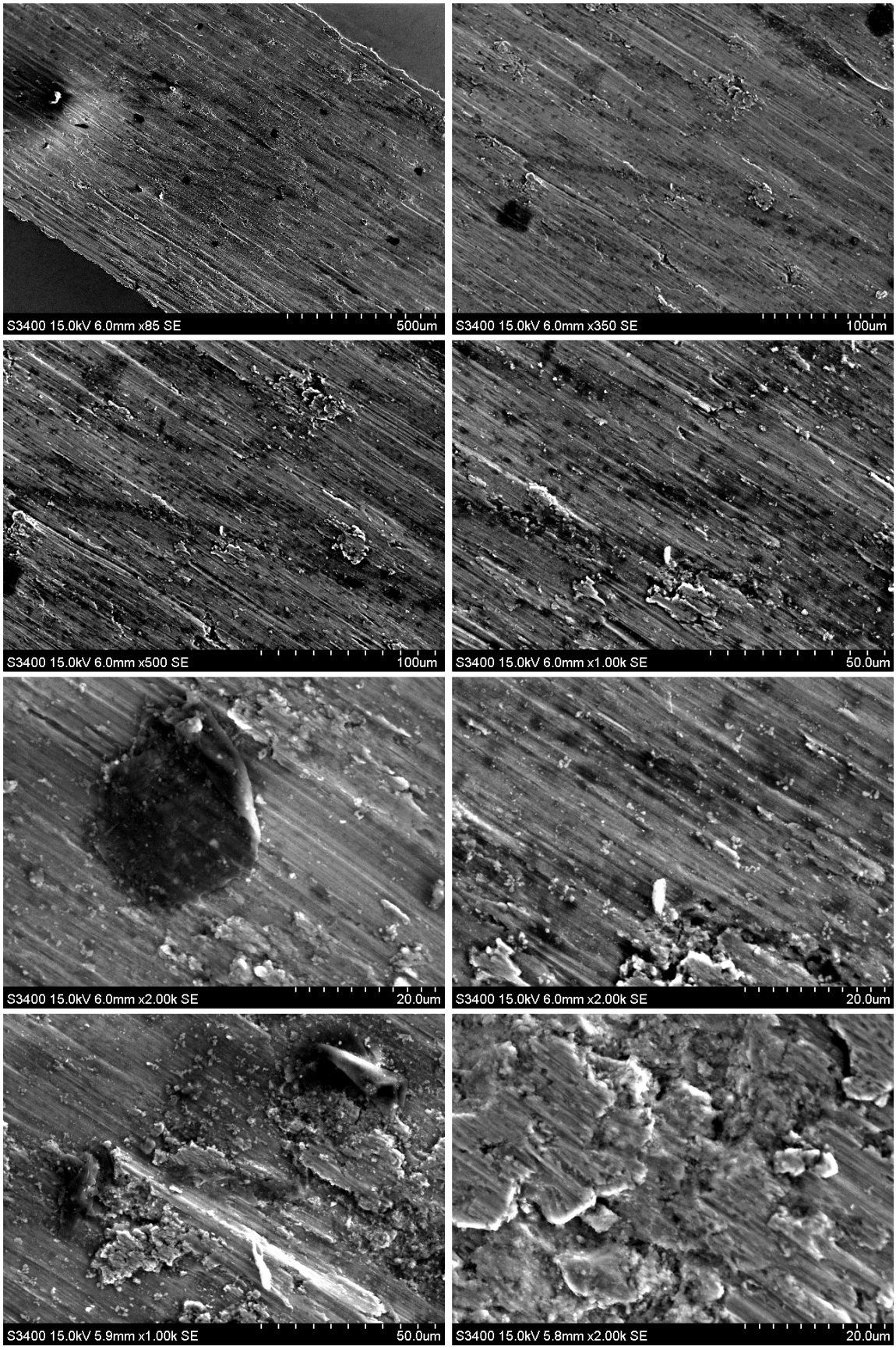

Figure 0-64: SEM images of Ti 99.6 % PBS 5.2 test 1

The following 16 images are of test 2

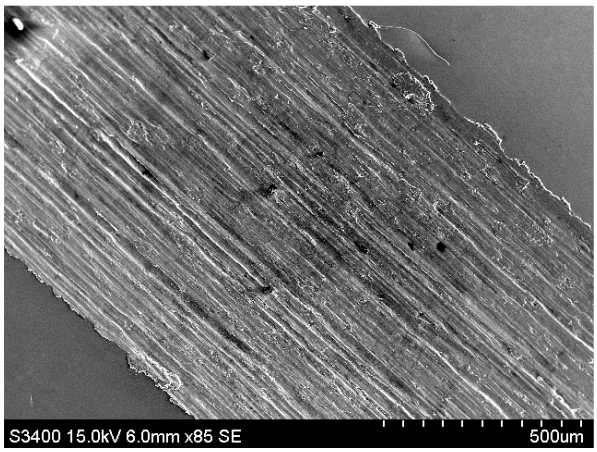

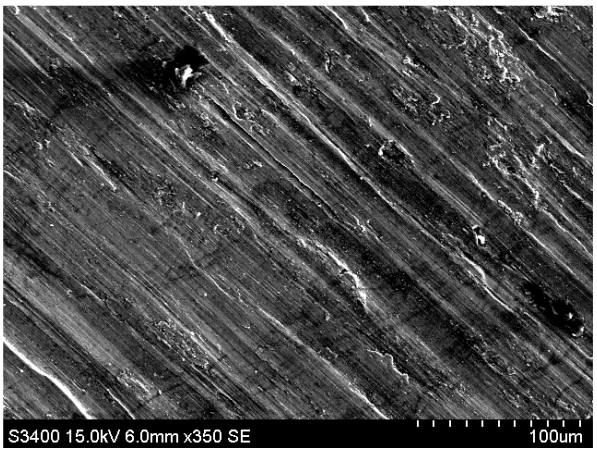

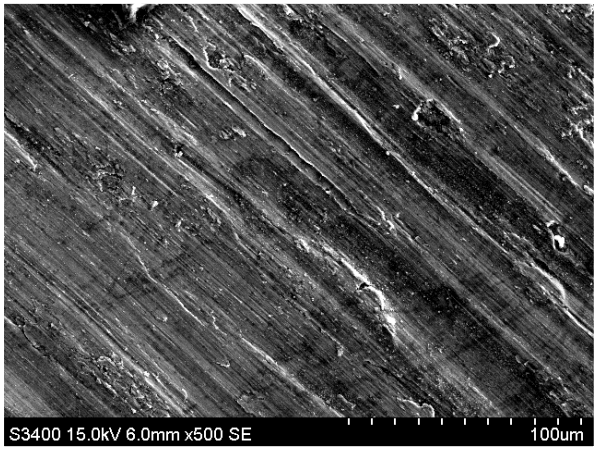

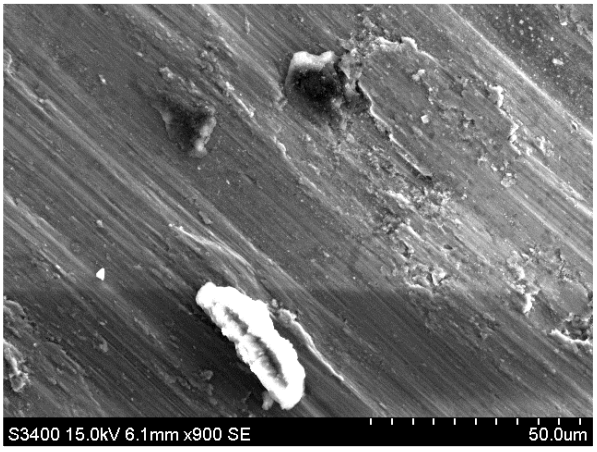

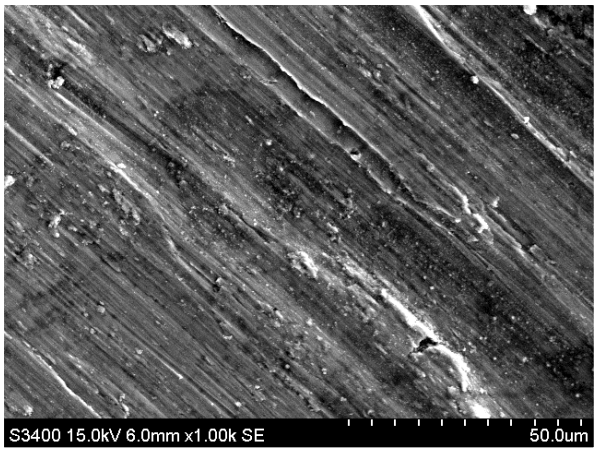

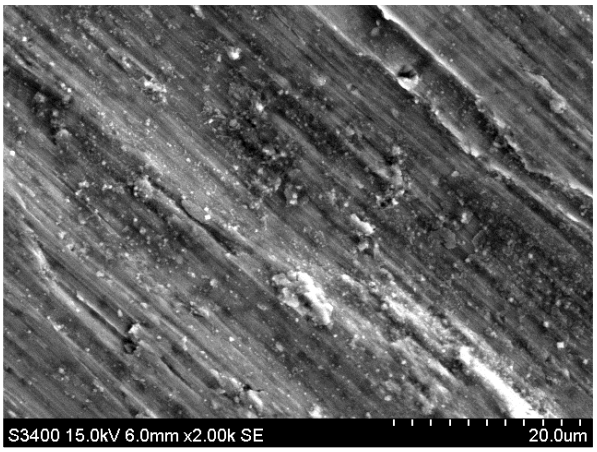

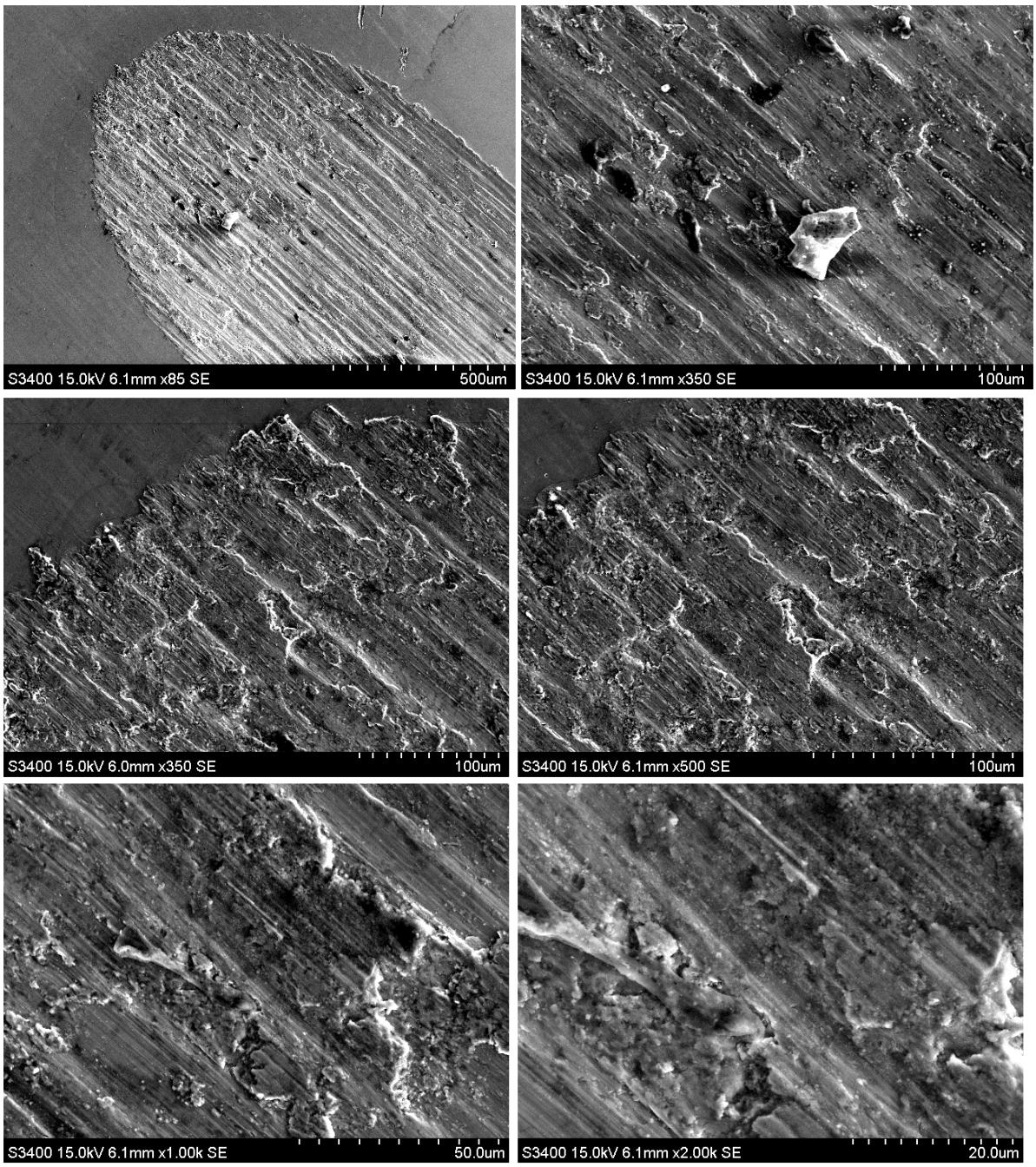
S3400 15.0kV 6.1mm x85 SE
500um
S3400 15.0kV 6.1mm x350 SE
100um
S3400 15.0kV 6.0mm x350 SE
100um
S3400 15.0kV 6.1mm x500 SE
100um
S3400 15.0kV 6.1mm x1.00k SE
50.0um
S3400 15.0kV 6.1mm x2.00k SE
20.0um

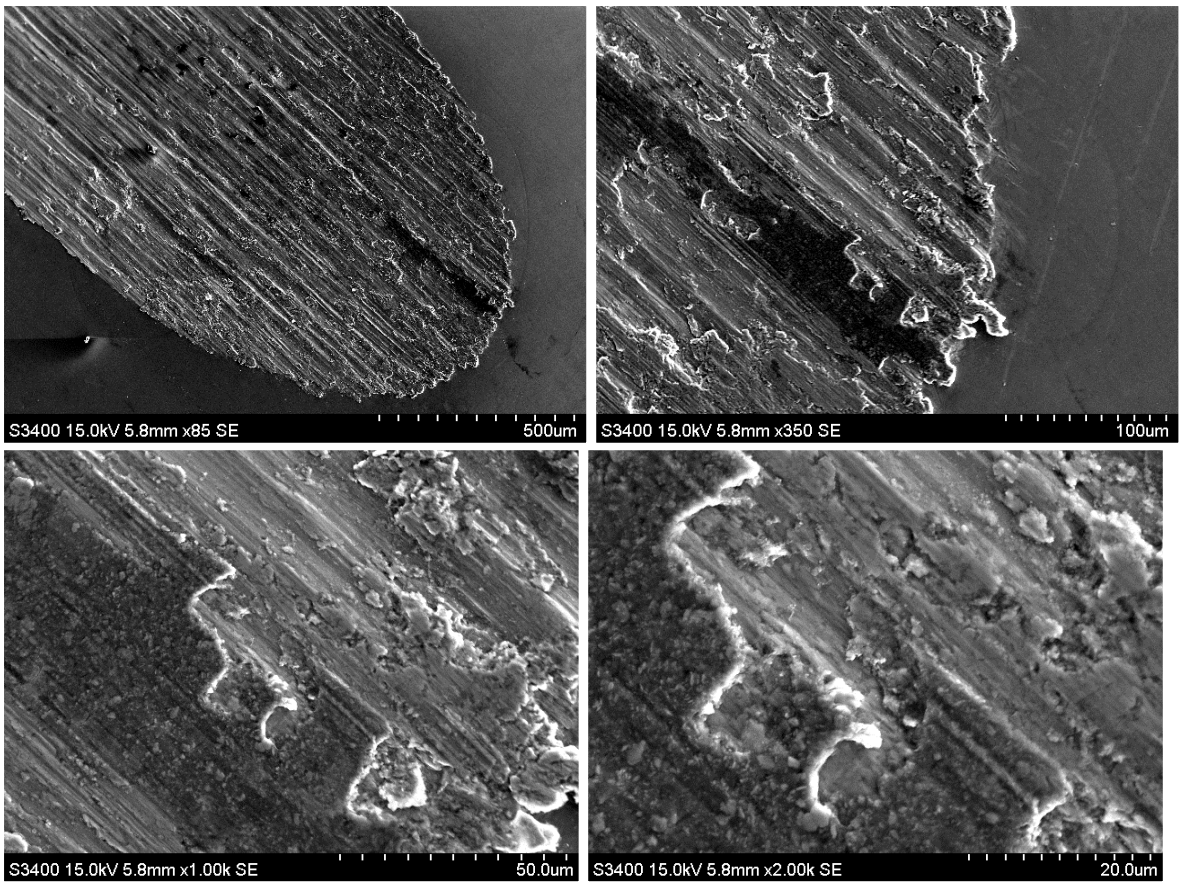

Figure 0-65: SEM images of Ti 99.6 % PBS 5.2 test 2

v. PBS 5.2 with protein tests

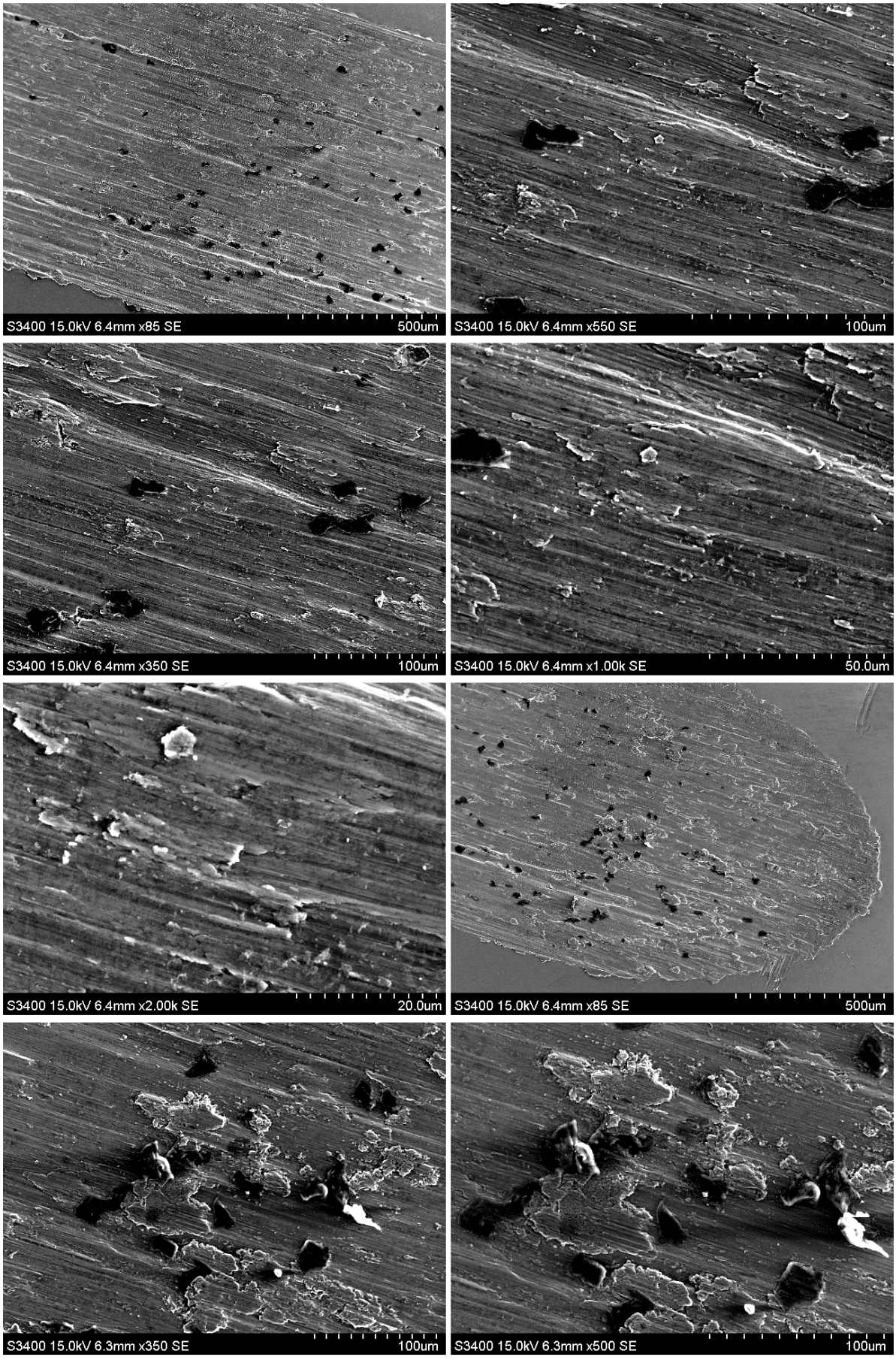

Continued from previous page

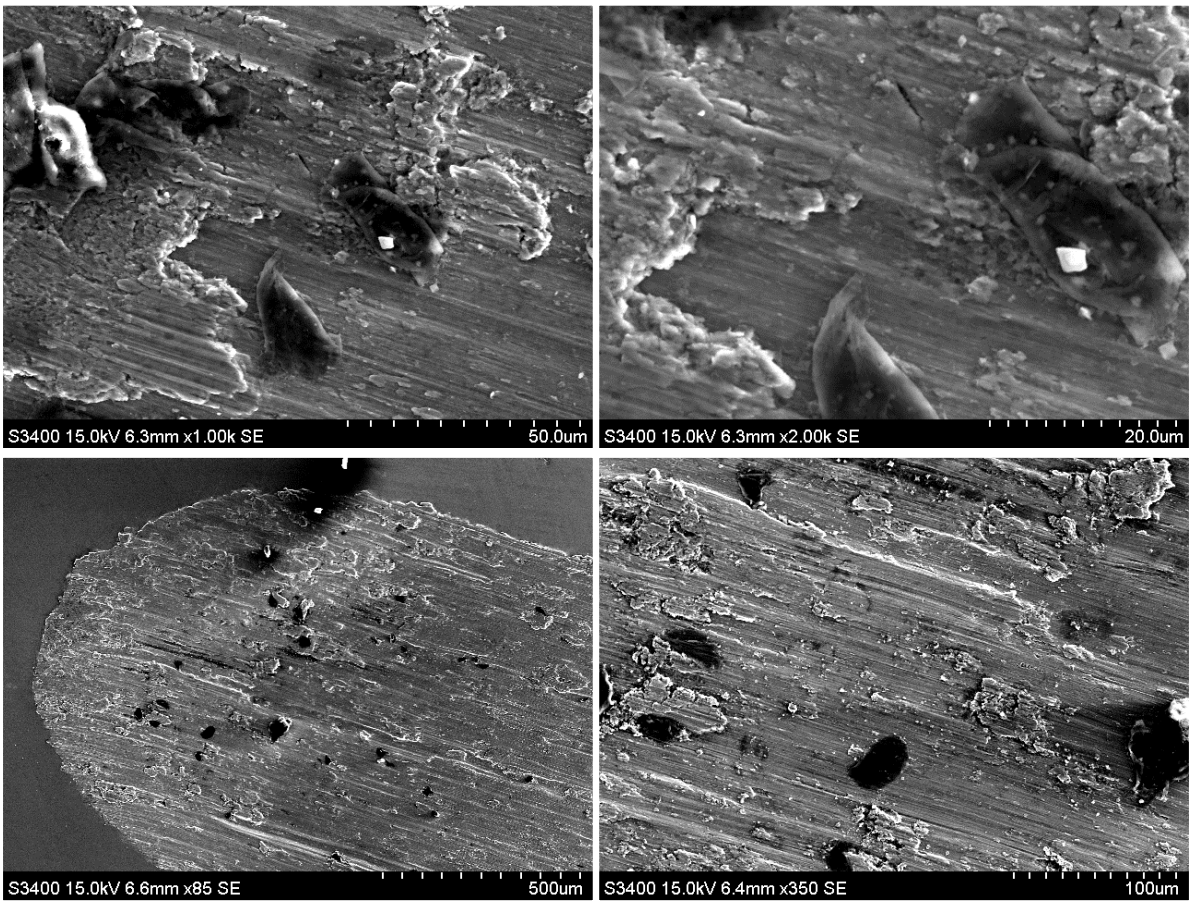

Continued on the next page

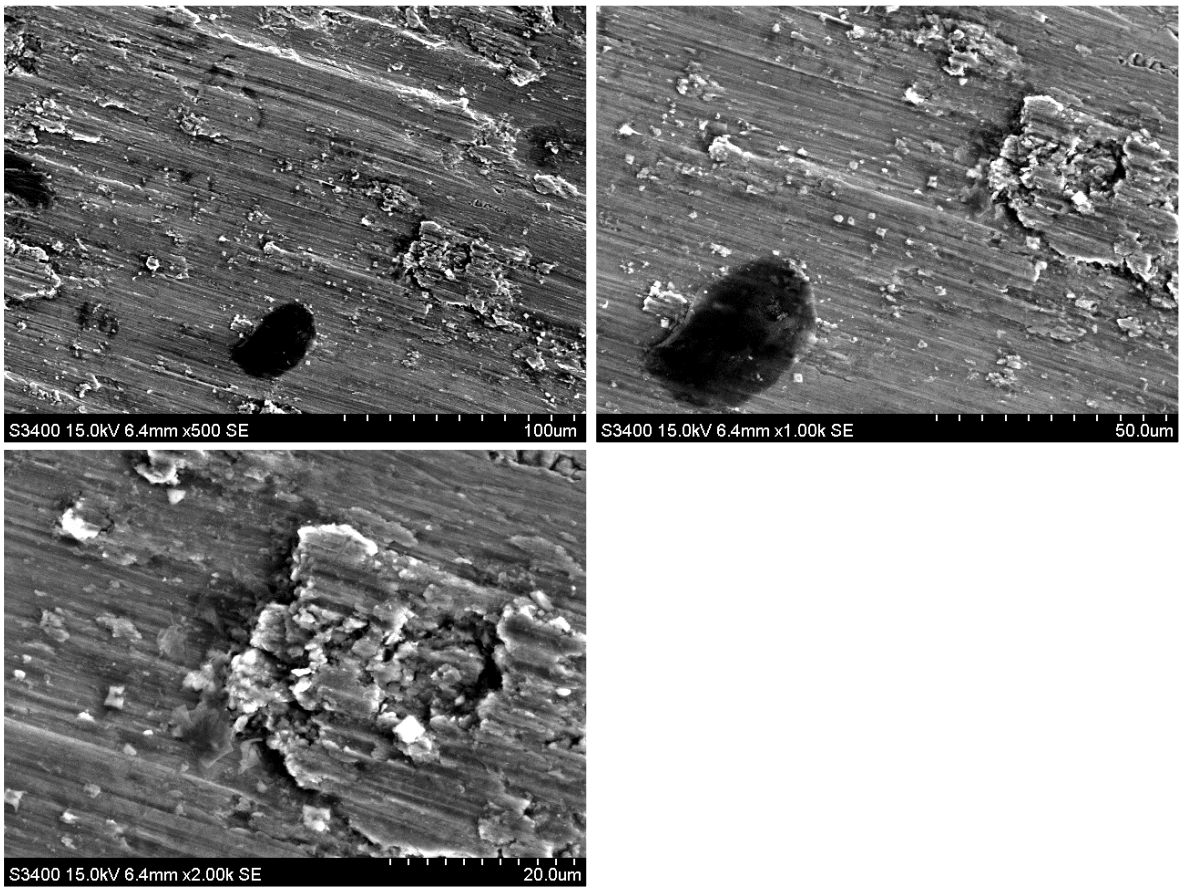

Figure 0-66: SEM images of Ti 99.6 % PBS 5.2 with proteins test 1

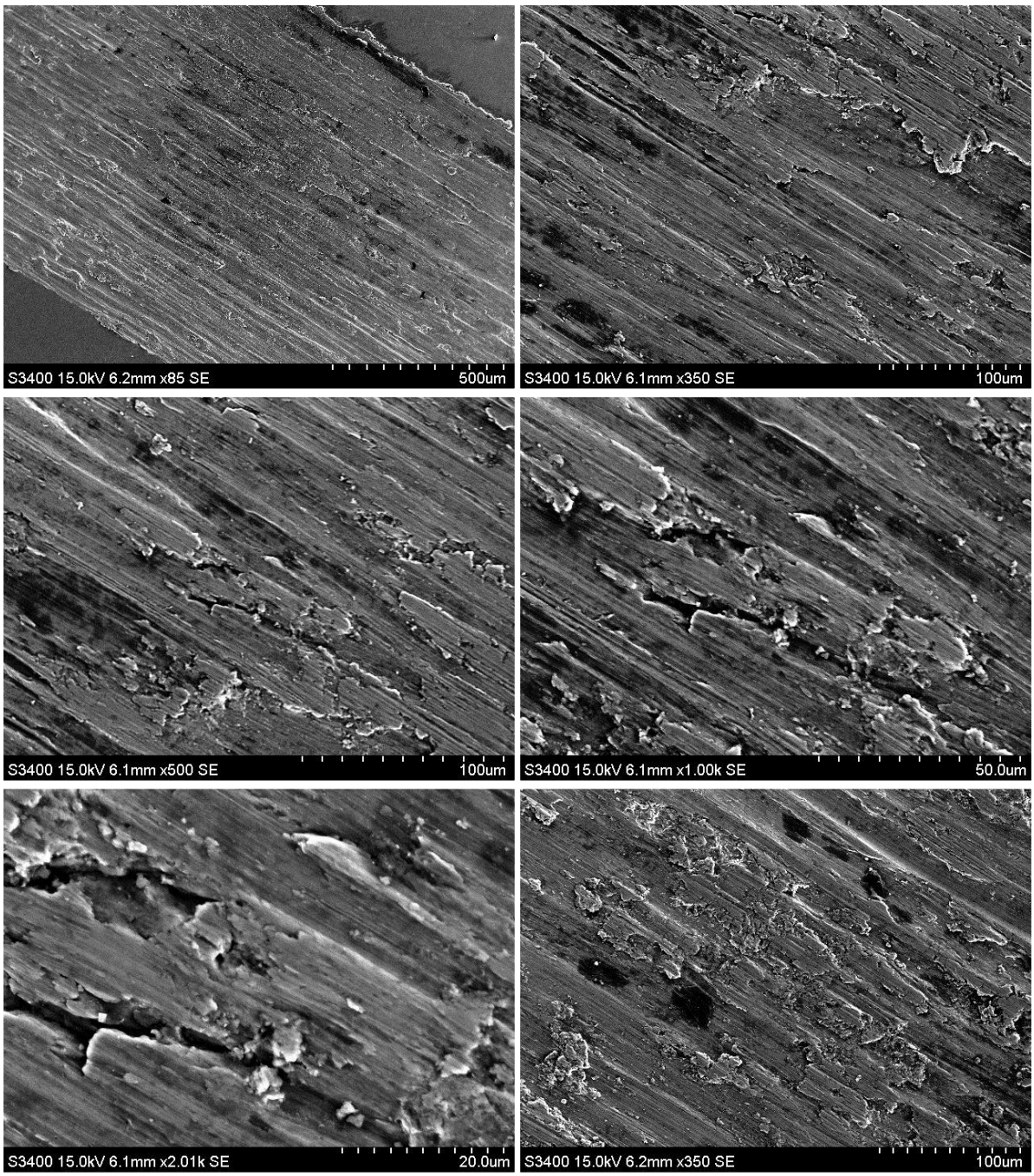

Continued on the next page.

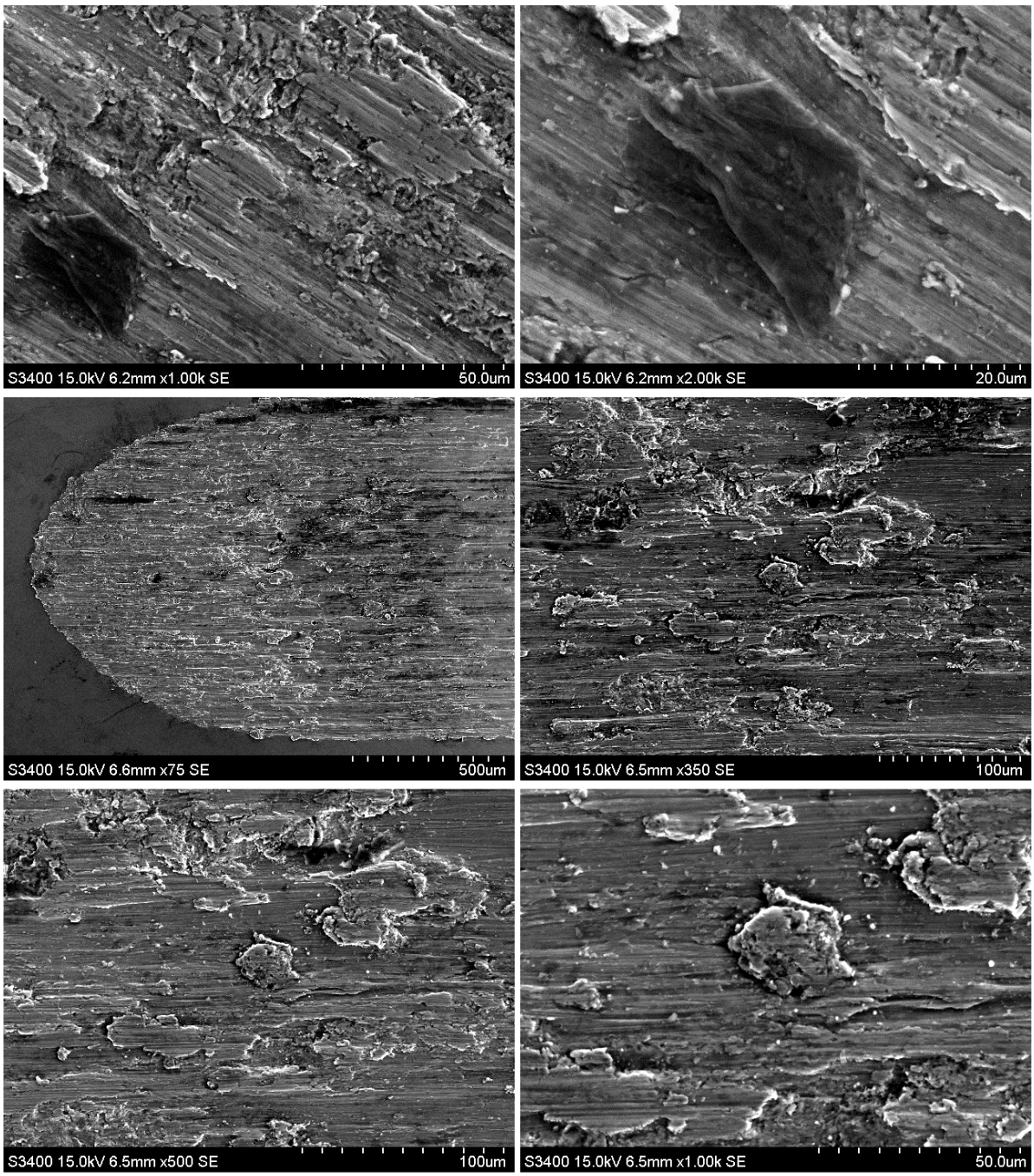

Continued on the next page.

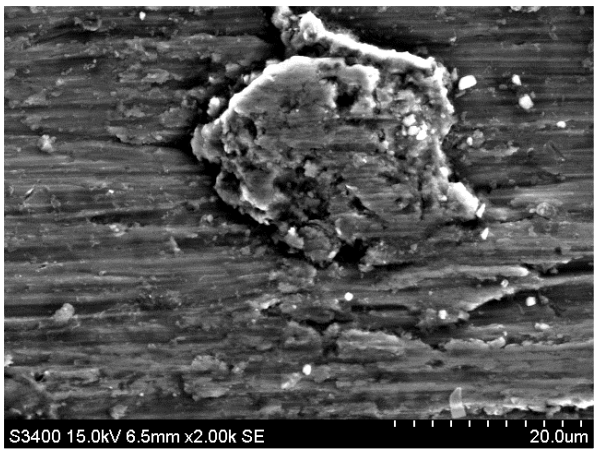

Figure 0-67: SEM images of Ti 99.6 % PBS 5.2 with proteins test 2

b. CoCrMo

i. Dry tests

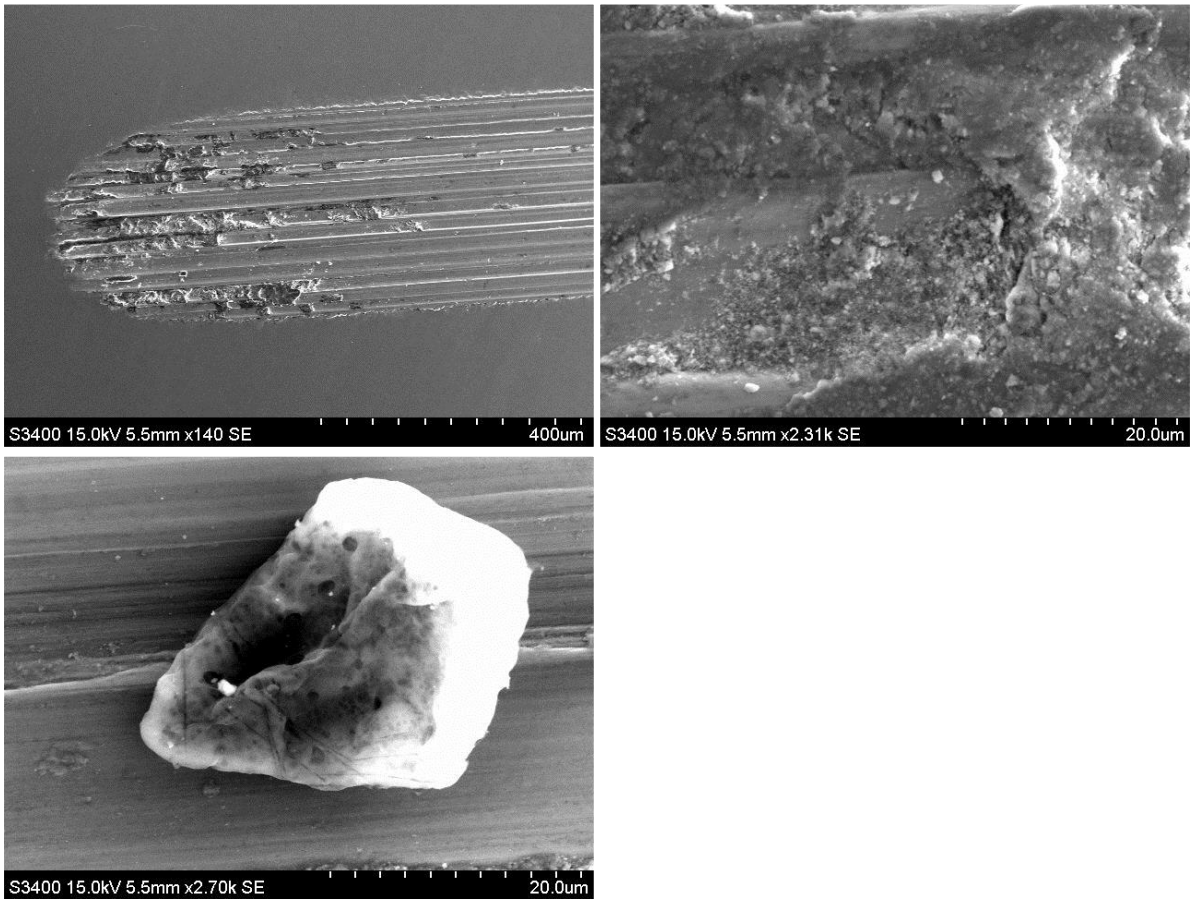

Figure 0-68: SEM images of CoCrMo dry test 1

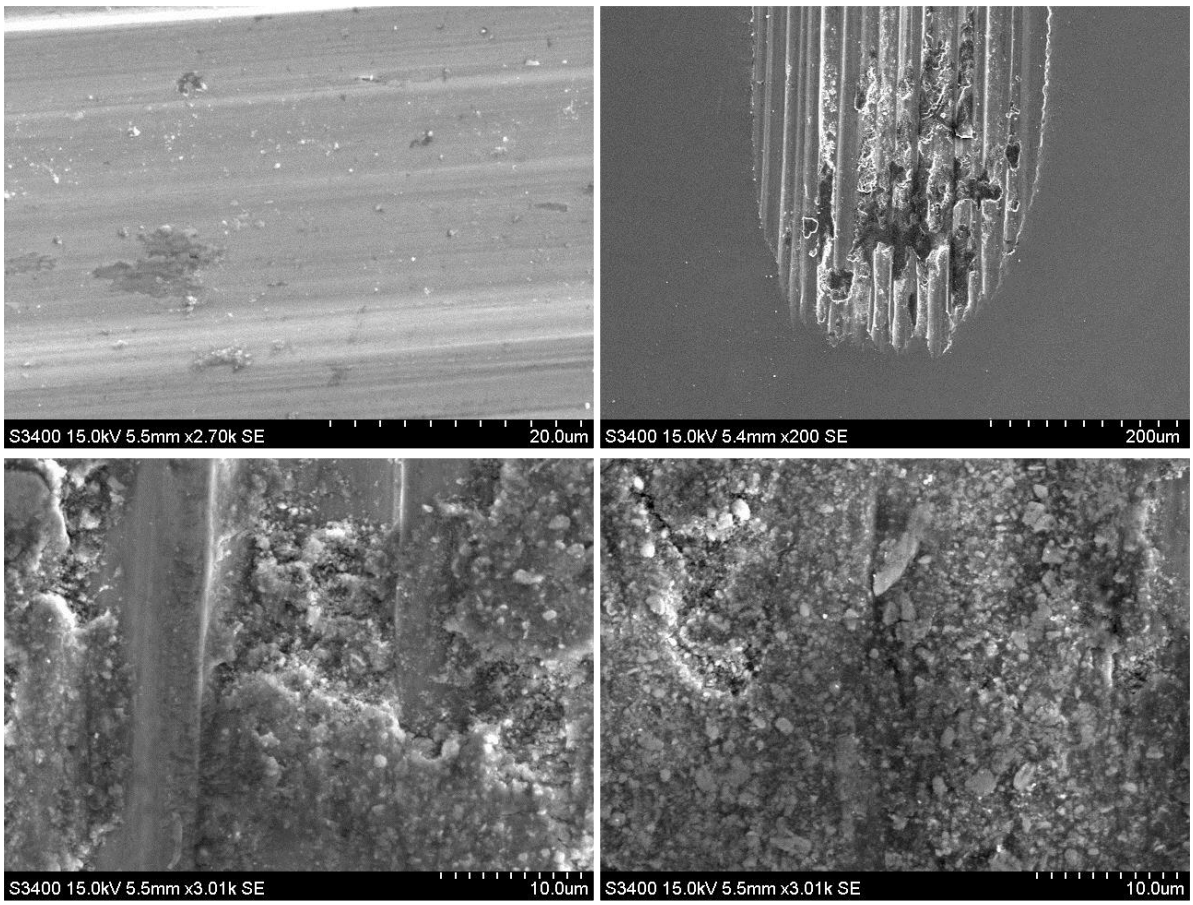

Figure 0-69: SEM images of CoCrMo dry test 2

ii. PBS 7.4 tests

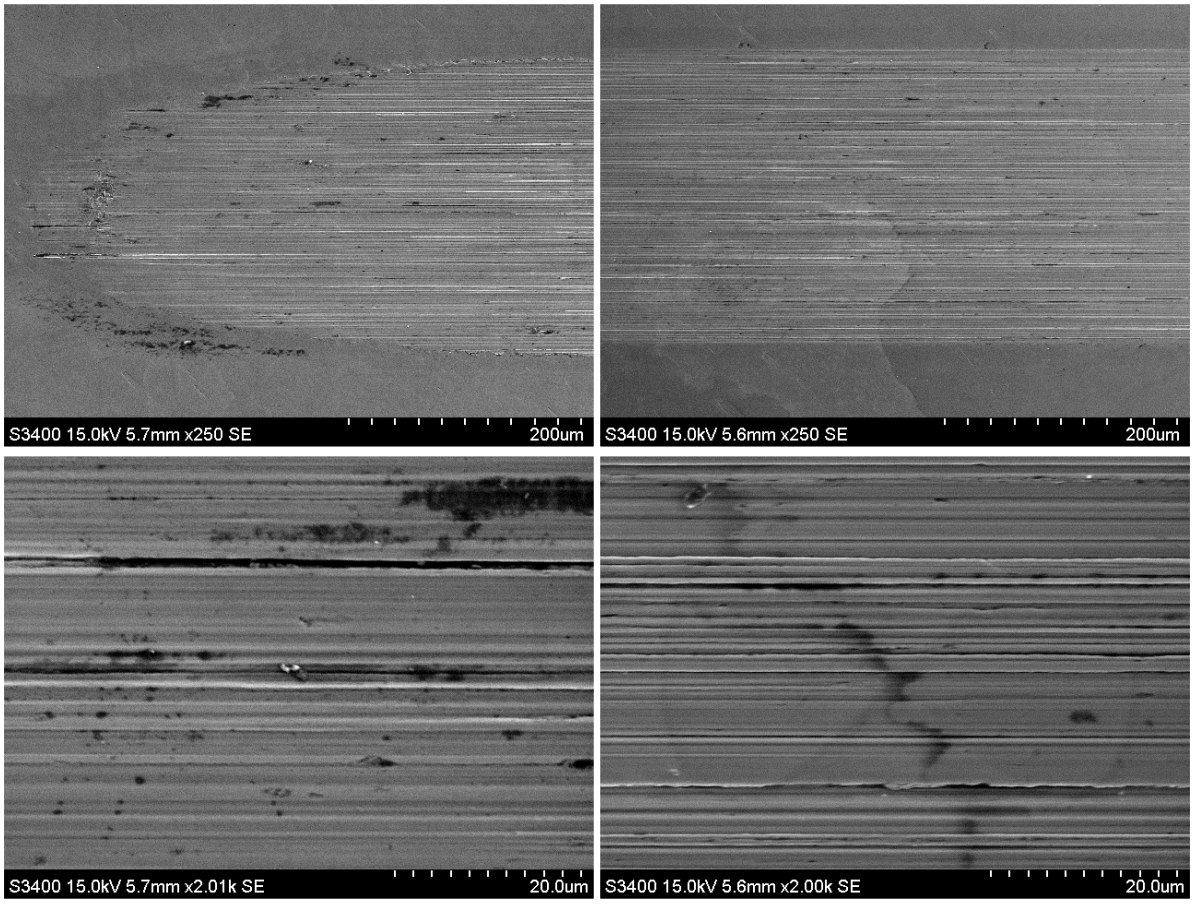

Figure 0-70: SEM images of CoCrMo PBS 7.4 test 1

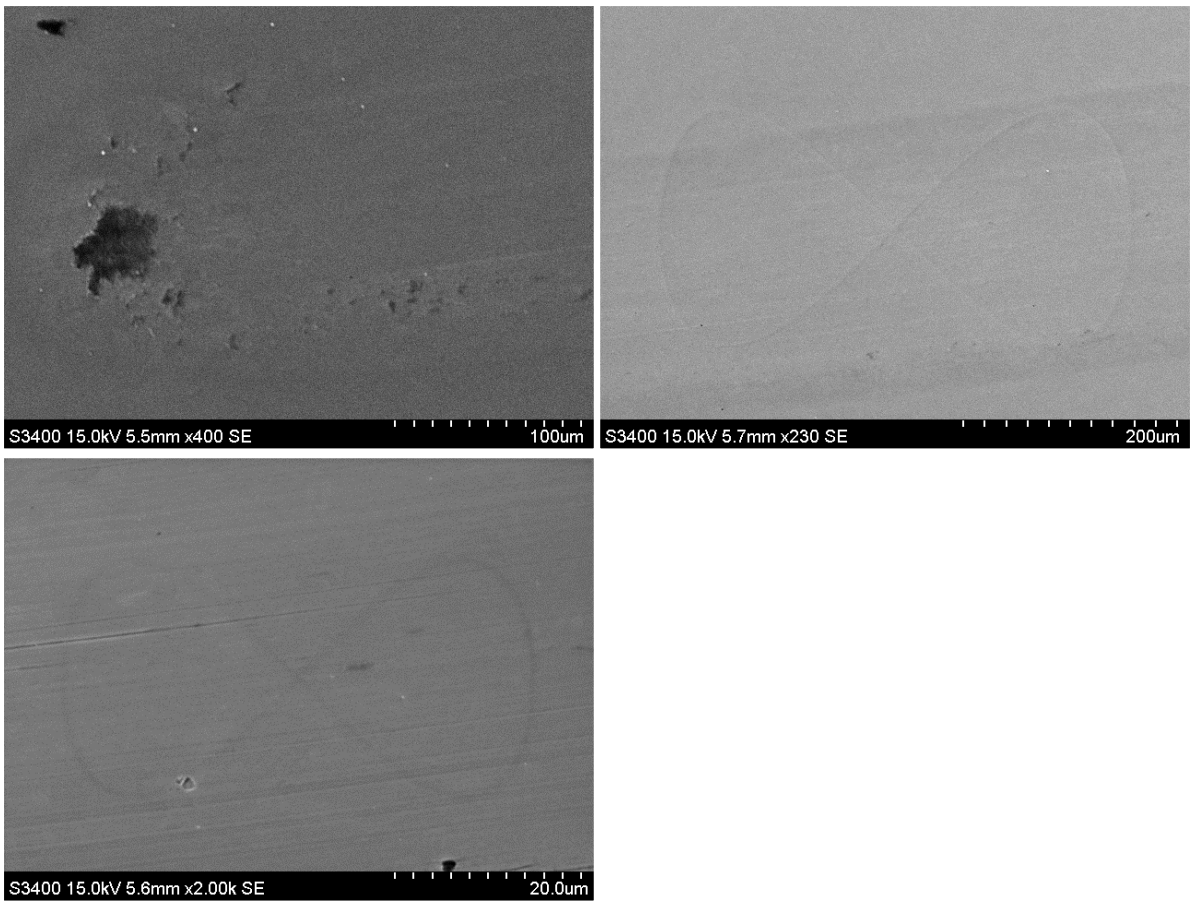

Figure 0-71: SEM images of CoCrMo PBS 7.4 test 2

iii. PBS 7.4 with protein tests

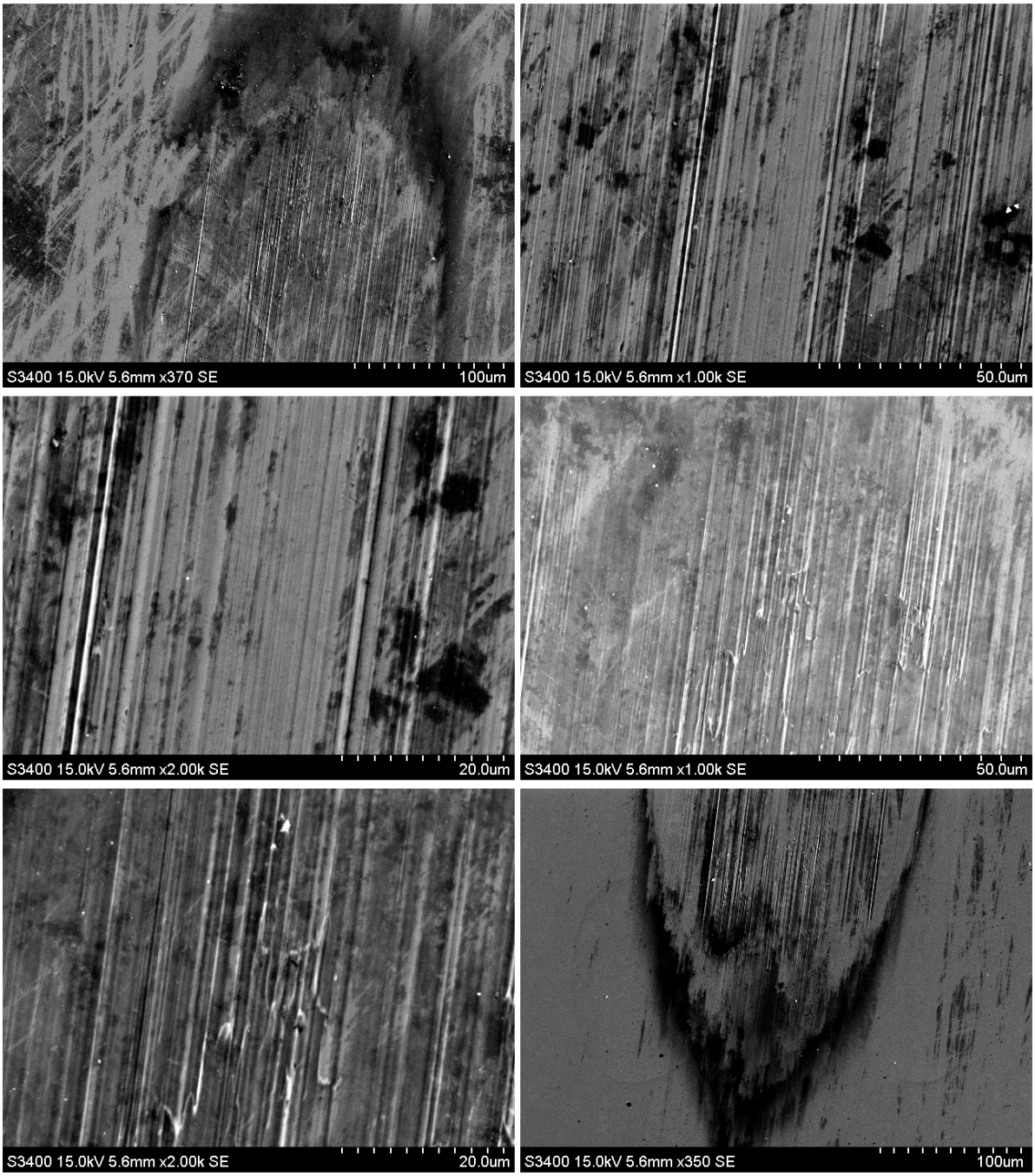

Continued on the next page

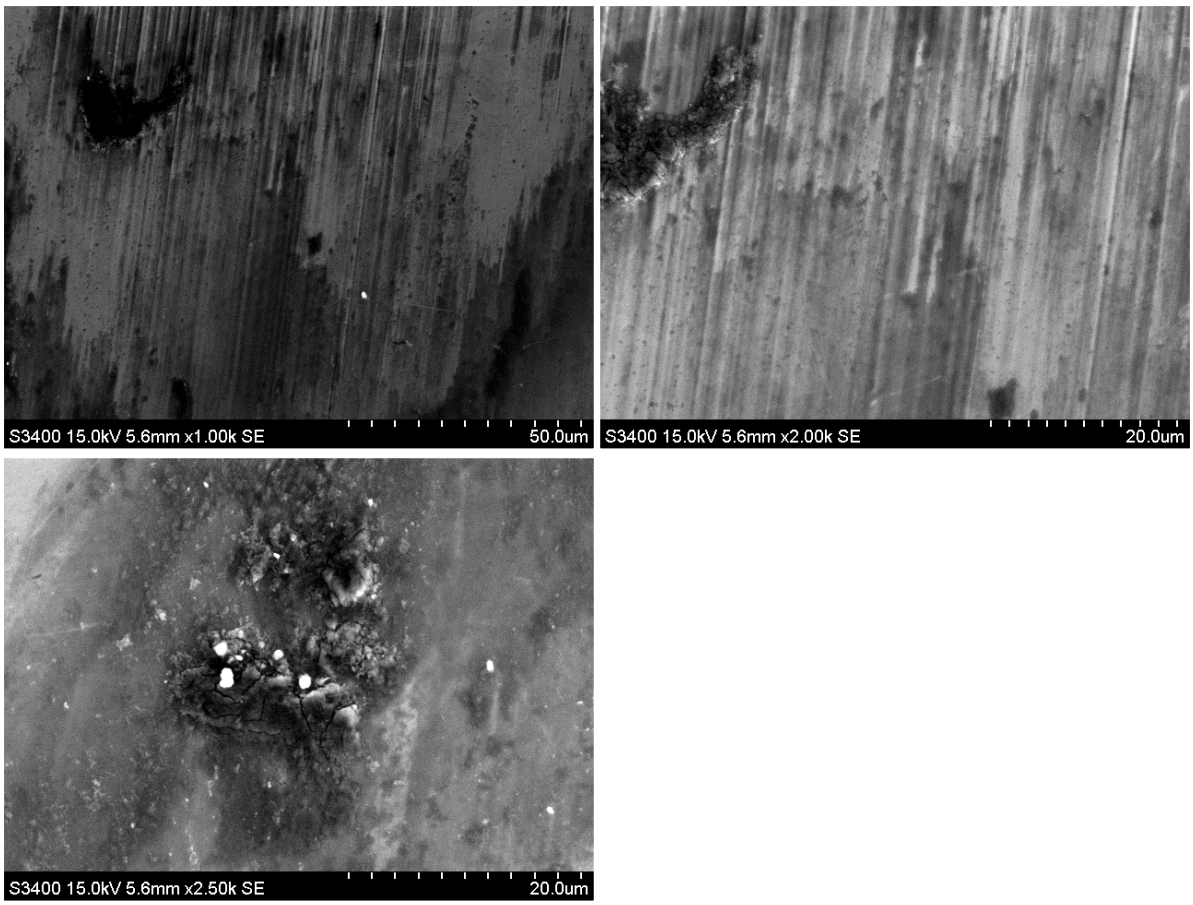

Figure 0-72: SEM images of CoCrMo PBS 7.4 with protein test 1

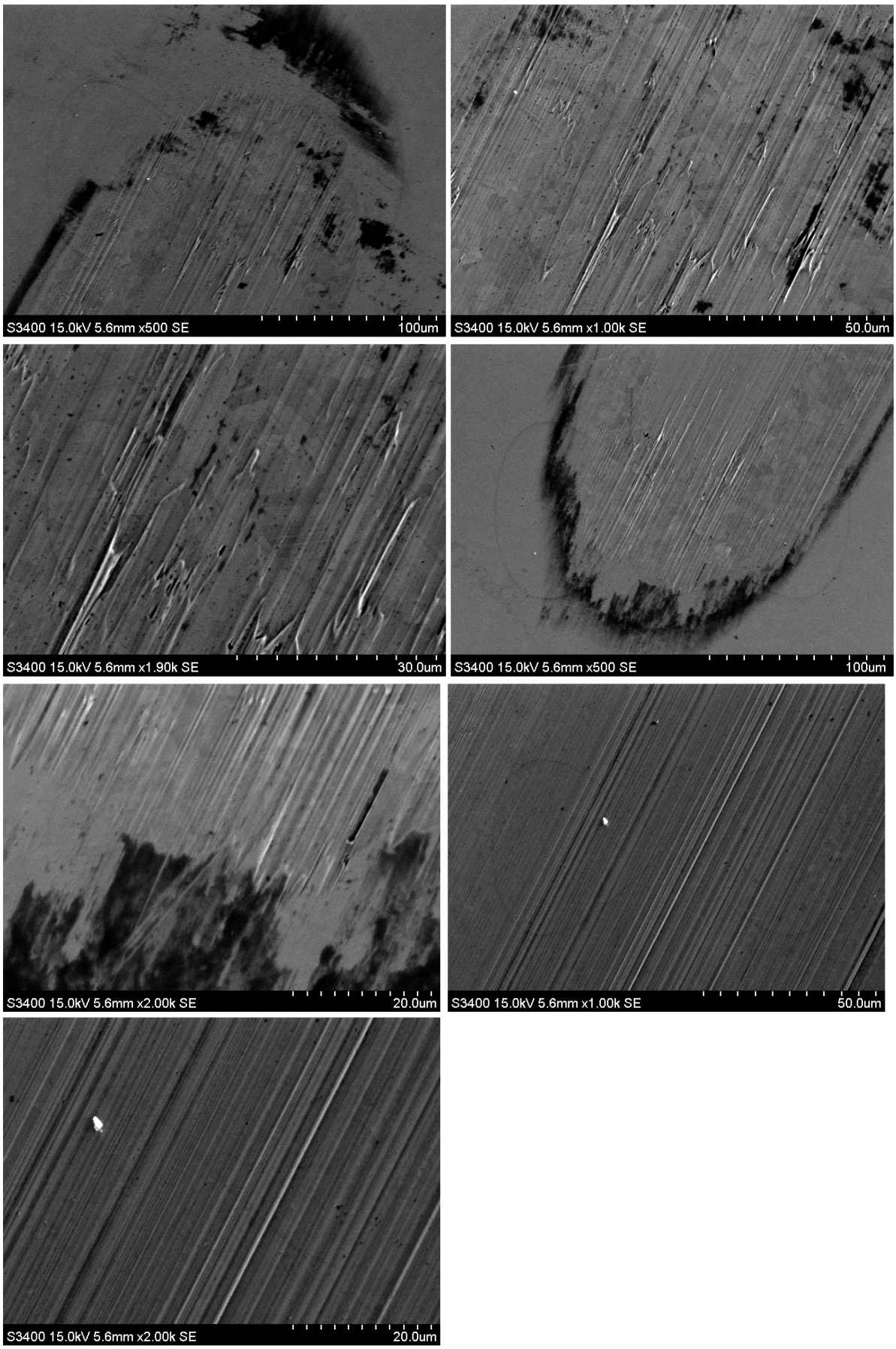

Figure 0-73: SEM images of CoCrMo PBS 7.4 with protein test 2

iv. PBS 5.2 tests

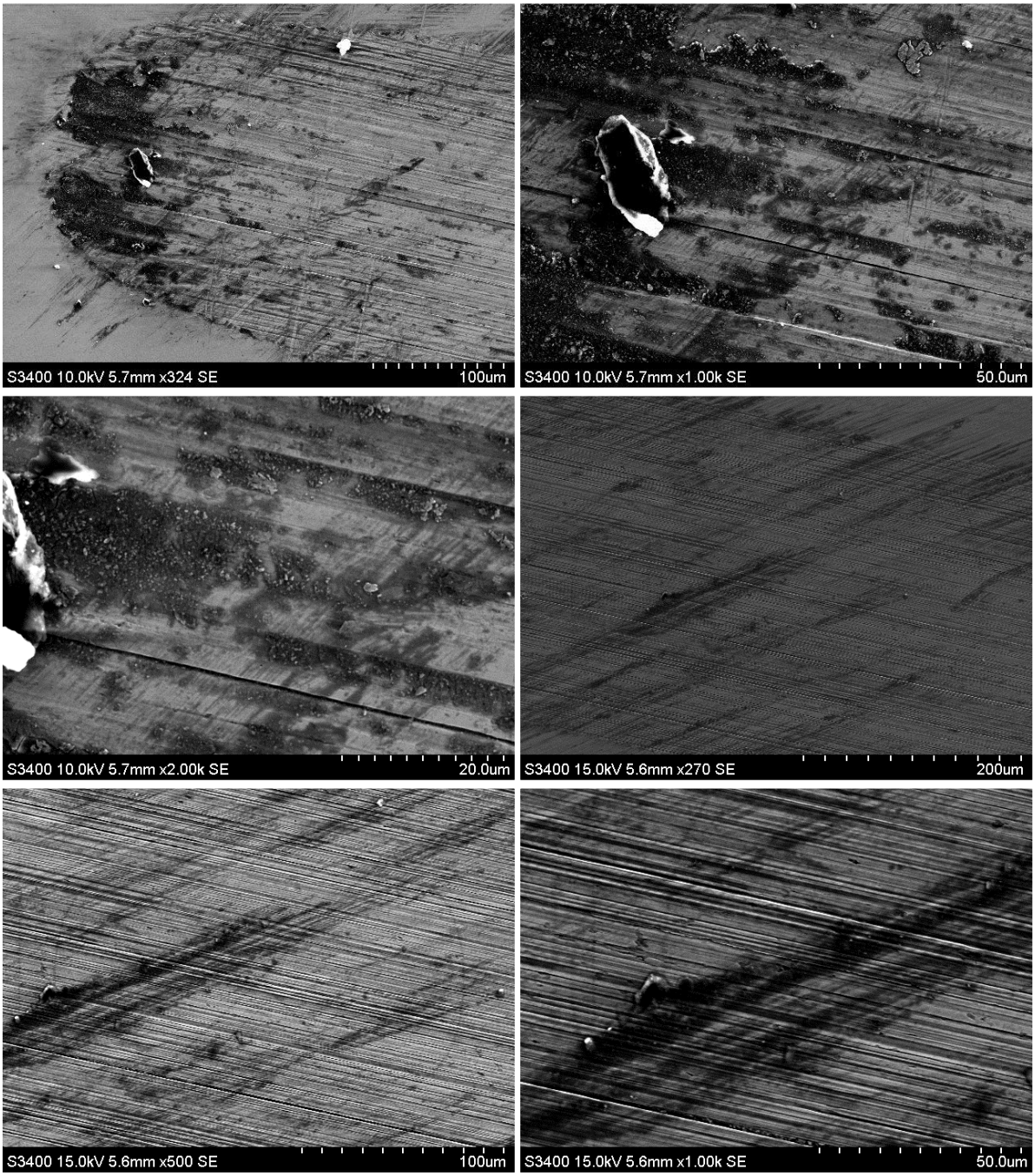

Continued on the next page

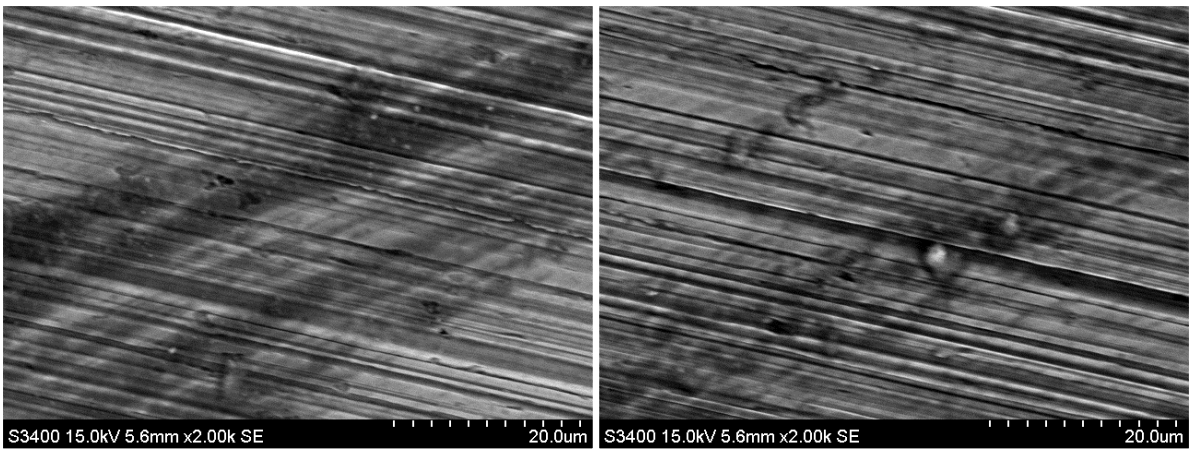

Figure 0-74: SEM images of CoCrMo PBS 5.2 test 1

v. PBS 5.2 with protein tests

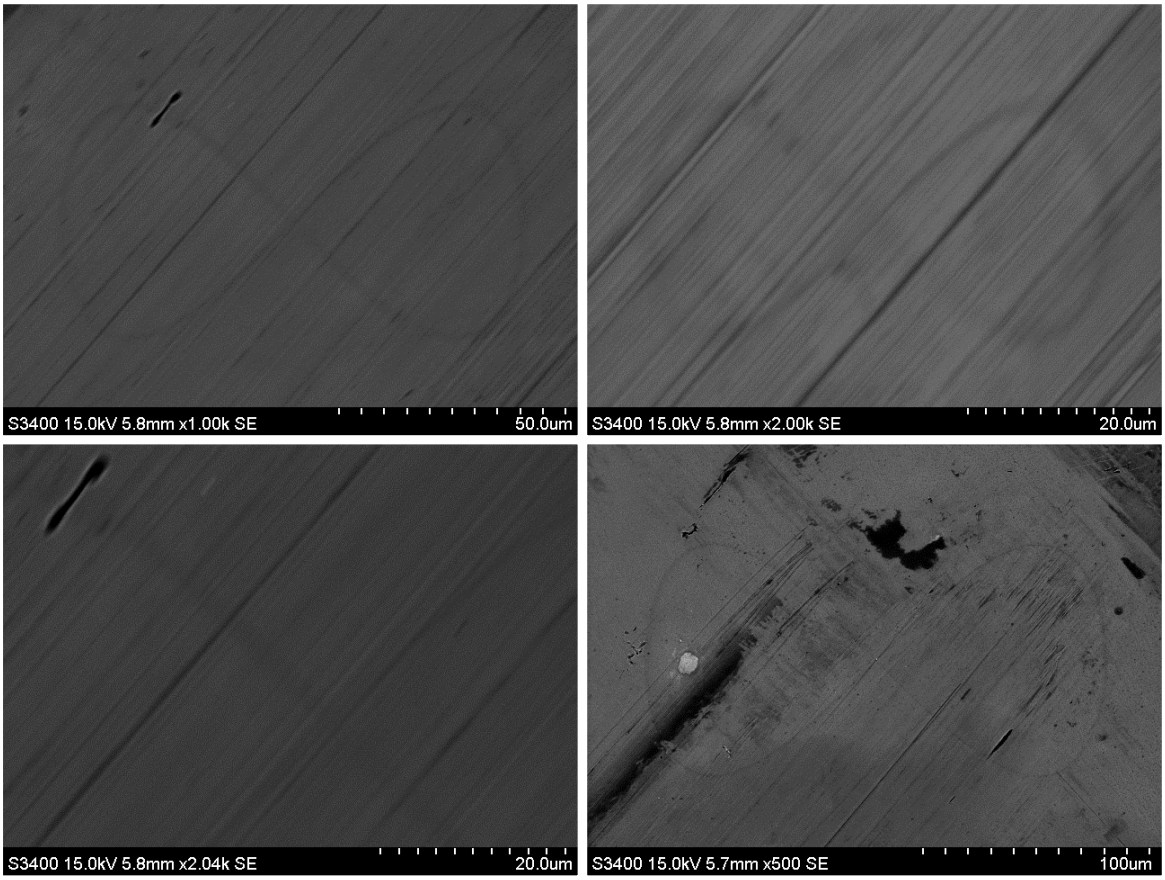

Continued on the next page

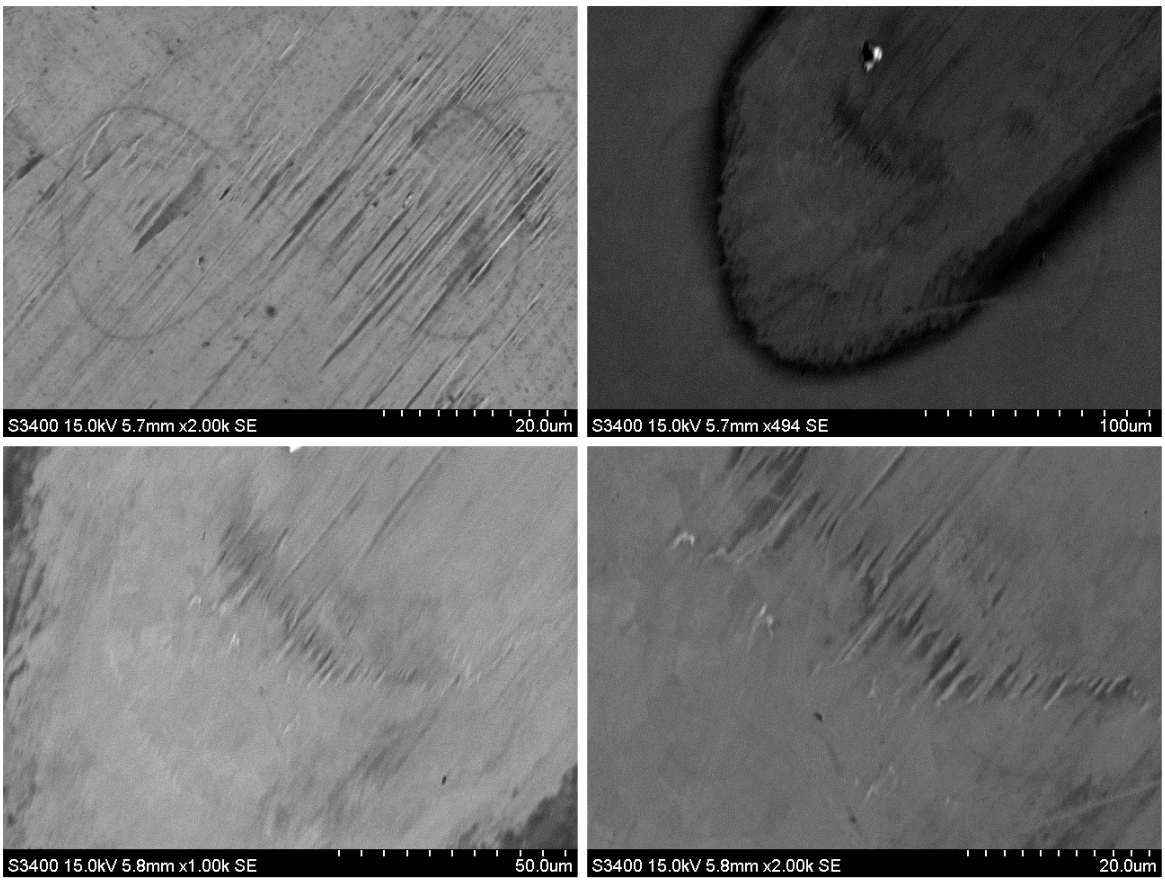

Figure 0-75: SEM images of CoCrMo PBS 5.2 with proteins test 1

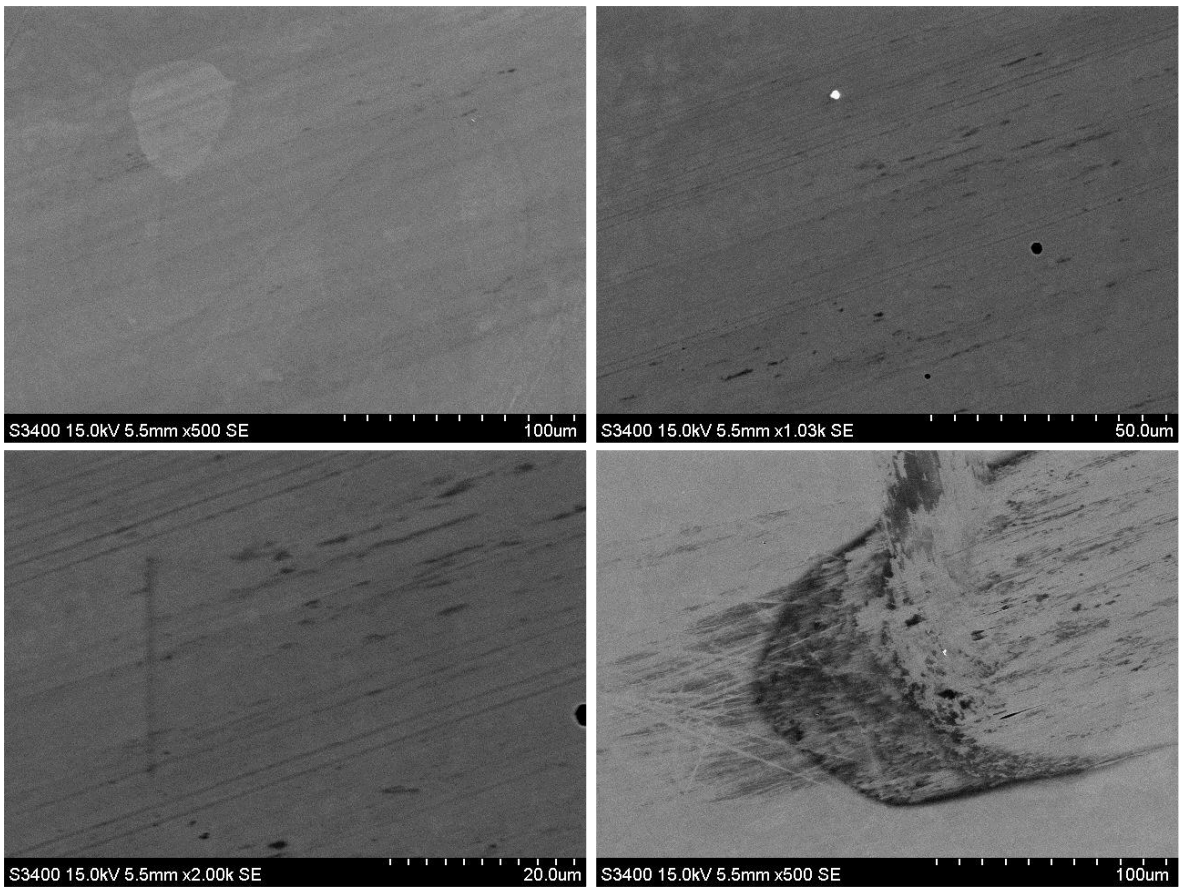

Continued on the next page

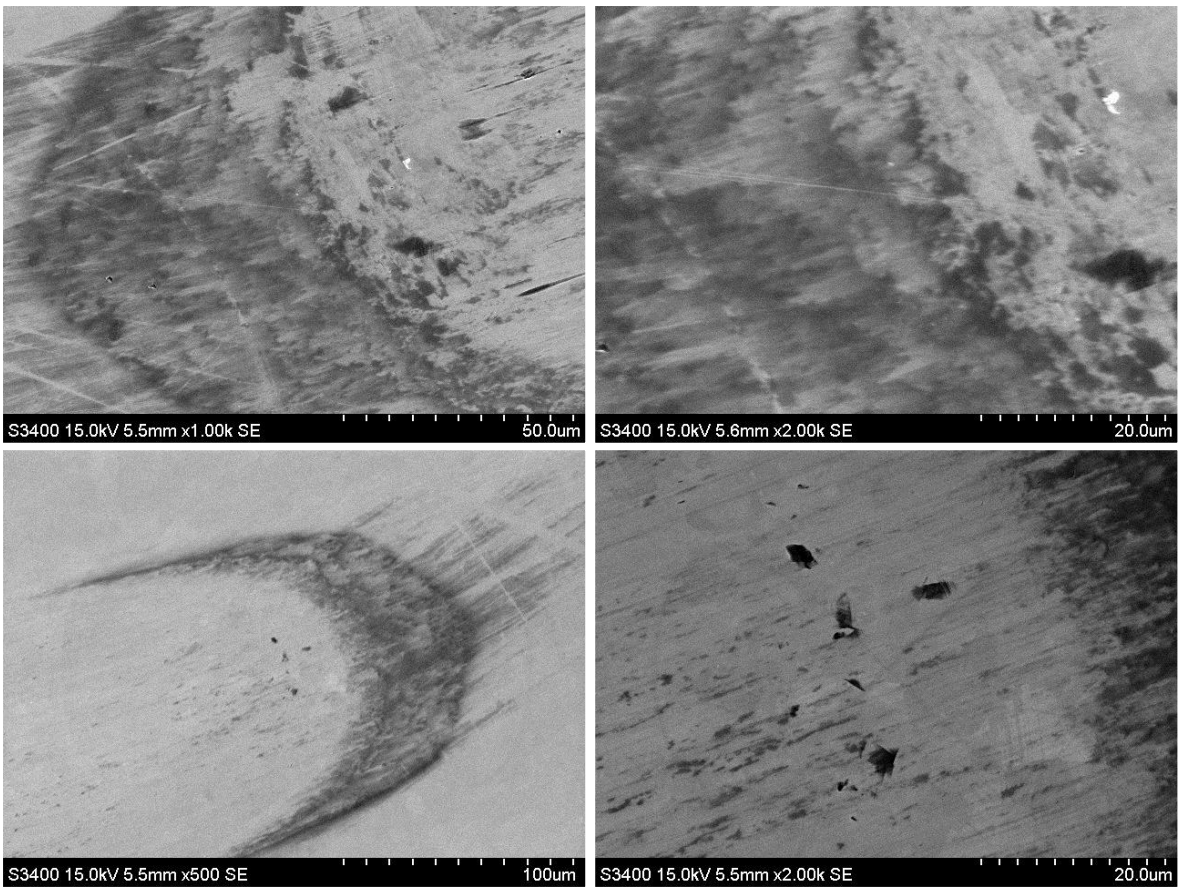

Figure 0-76: SEM images of CoCrMo PBS 5.2 with proteins test 2

c. BMG

i. Dry tests

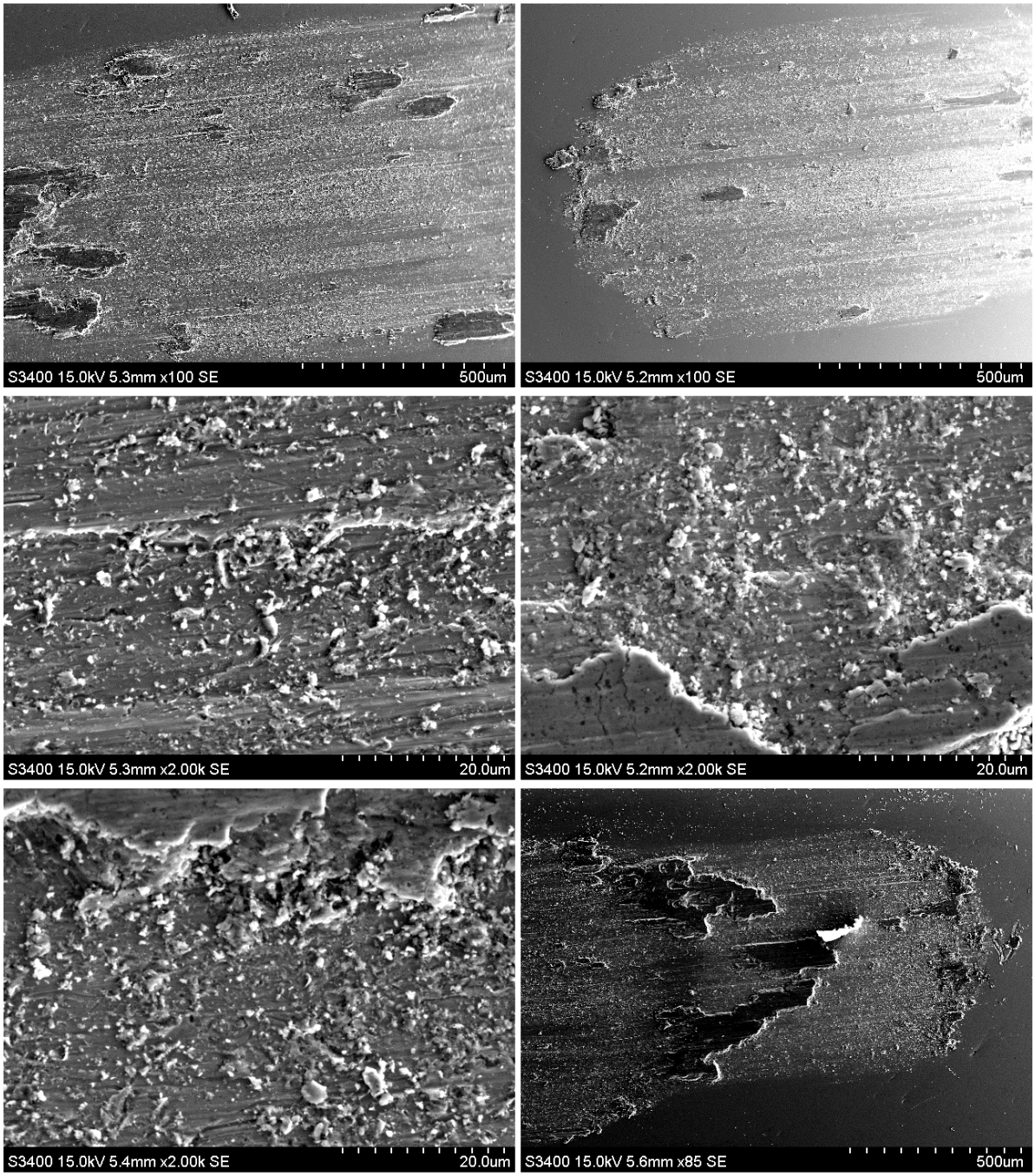

Figure 0-77: SEM images of BMG dry test 1

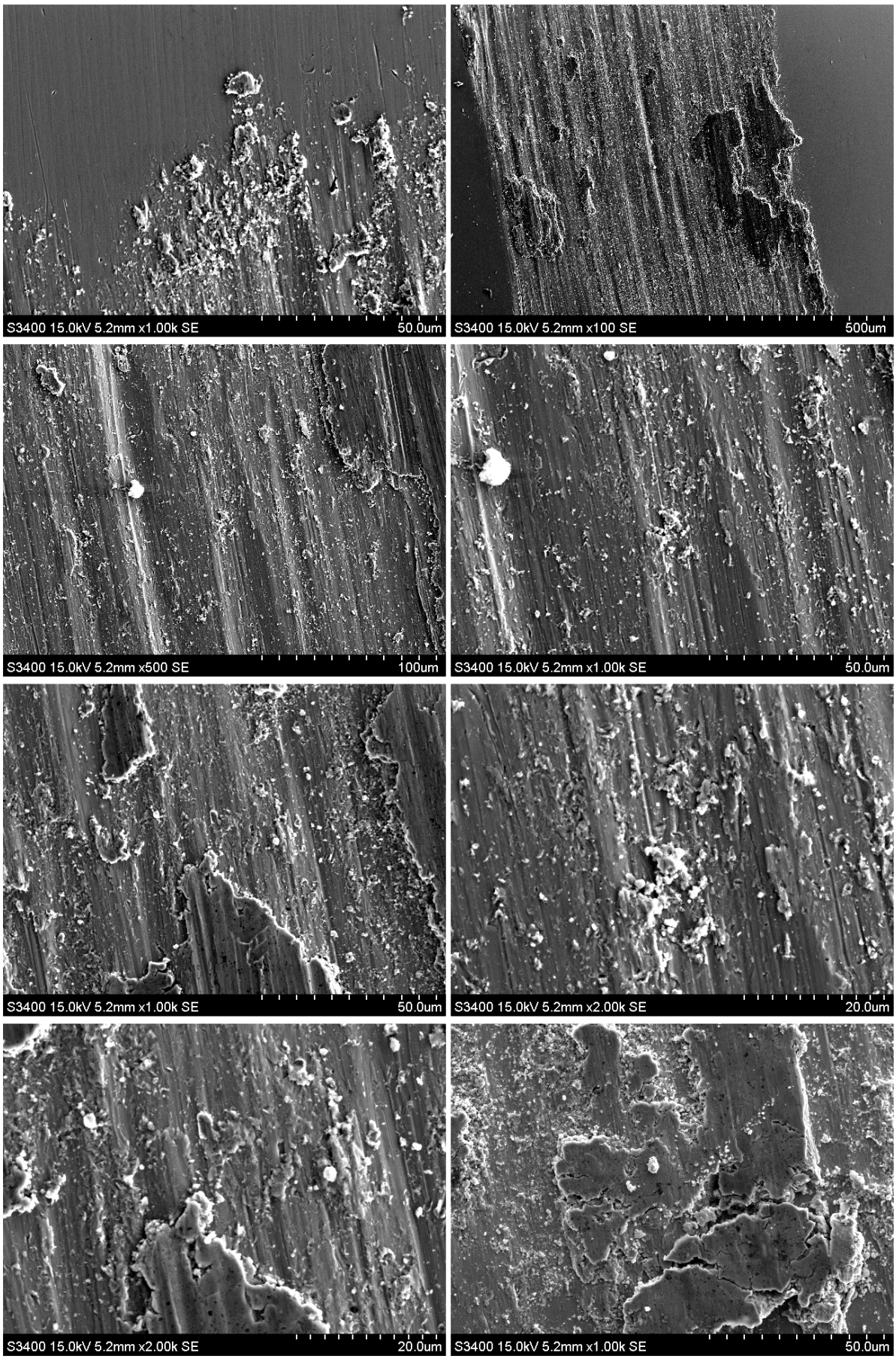
S3400 15.0kV 5.2mm x1.00k SE
50.0um
S3400 15.0kV 5.2mm x100 SE
500um
S3400 15.0kV 5.2mm x500 SE
100um
S3400 15.0kV 5.2mm x1.00k SE
50.0um
S3400 15.0kV 5.2mm x1.00k SE
50.0um
S3400 15.0kV 5.2mm x2.00k SE
20.0um
S3400 15.0kV 5.2mm x2.00k SE
20.0um
S3400 15.0kV 5.2mm x1.00k SE
50.0um

Continued from the previous page

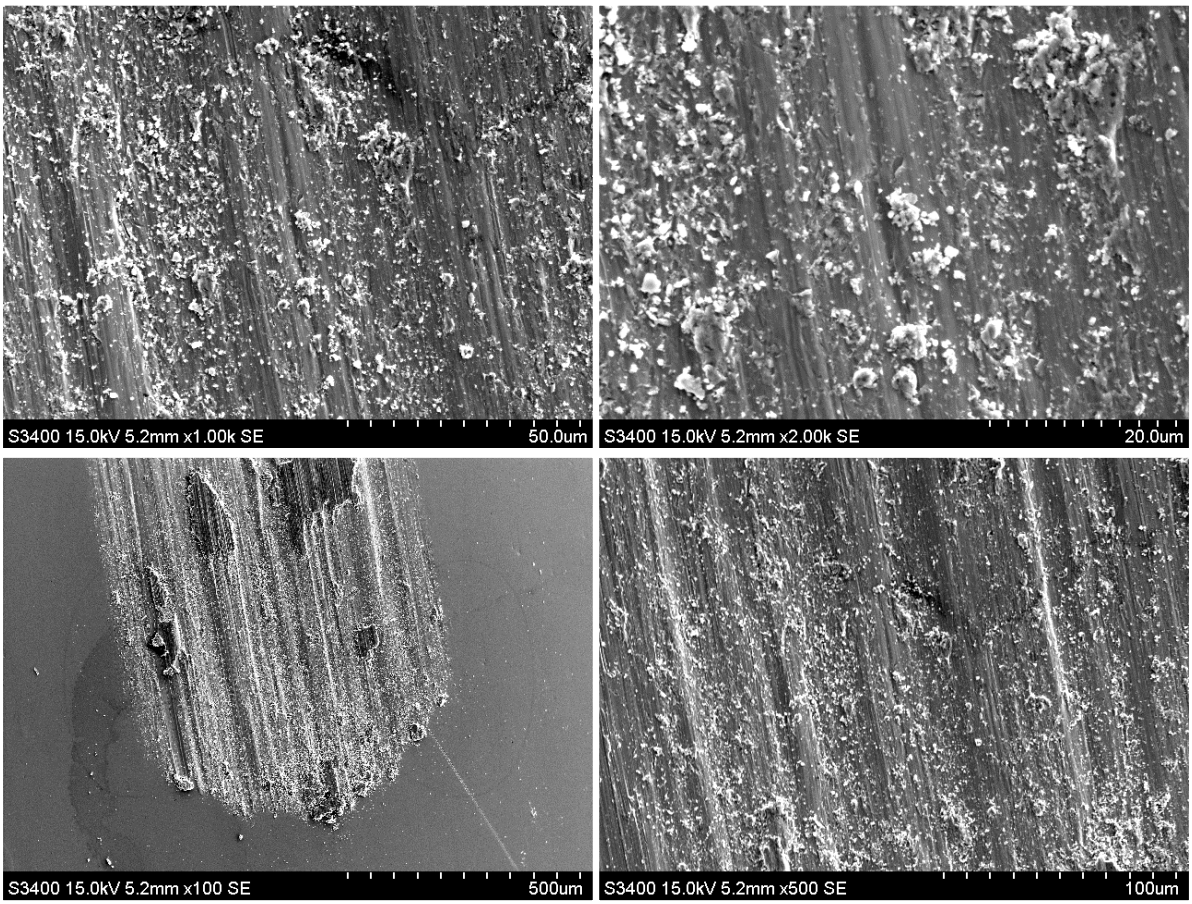

Figure 0-78: SEM images of BMG dry test 2

ii. PBS 7.4 tests

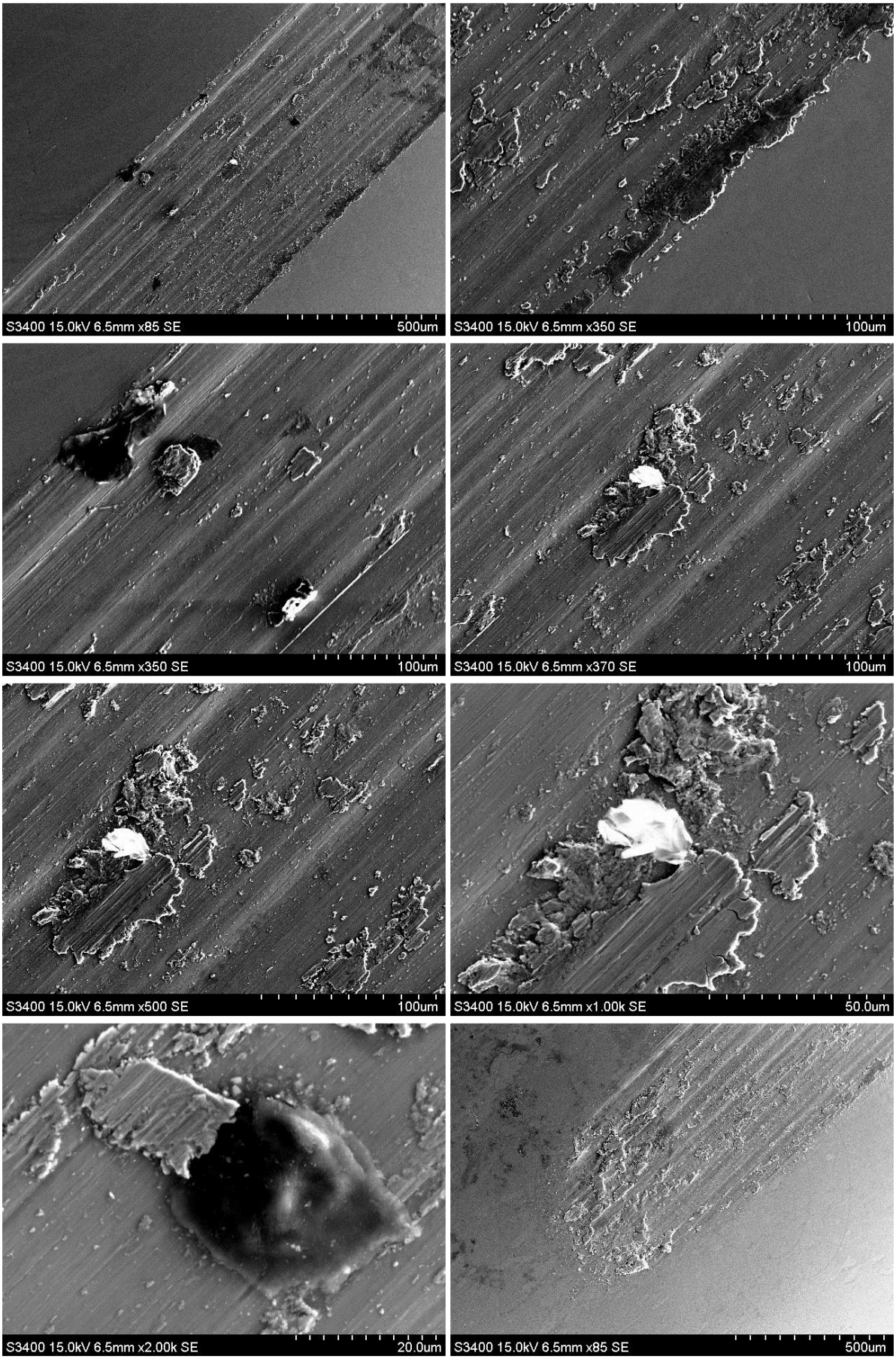

Continued from the previous page

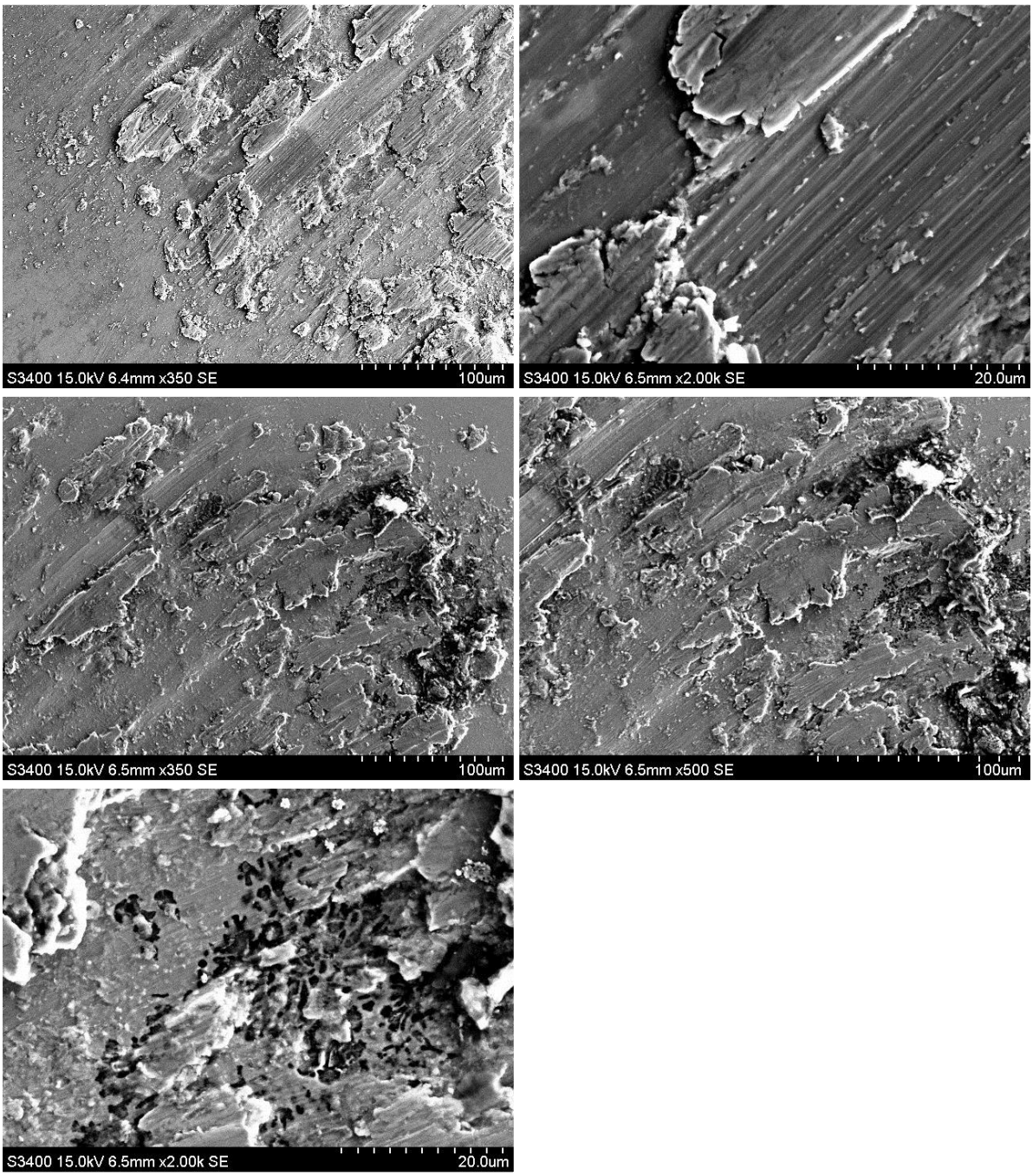

Figure 0-79: SEM images of BMG PBS 7.4 test 1

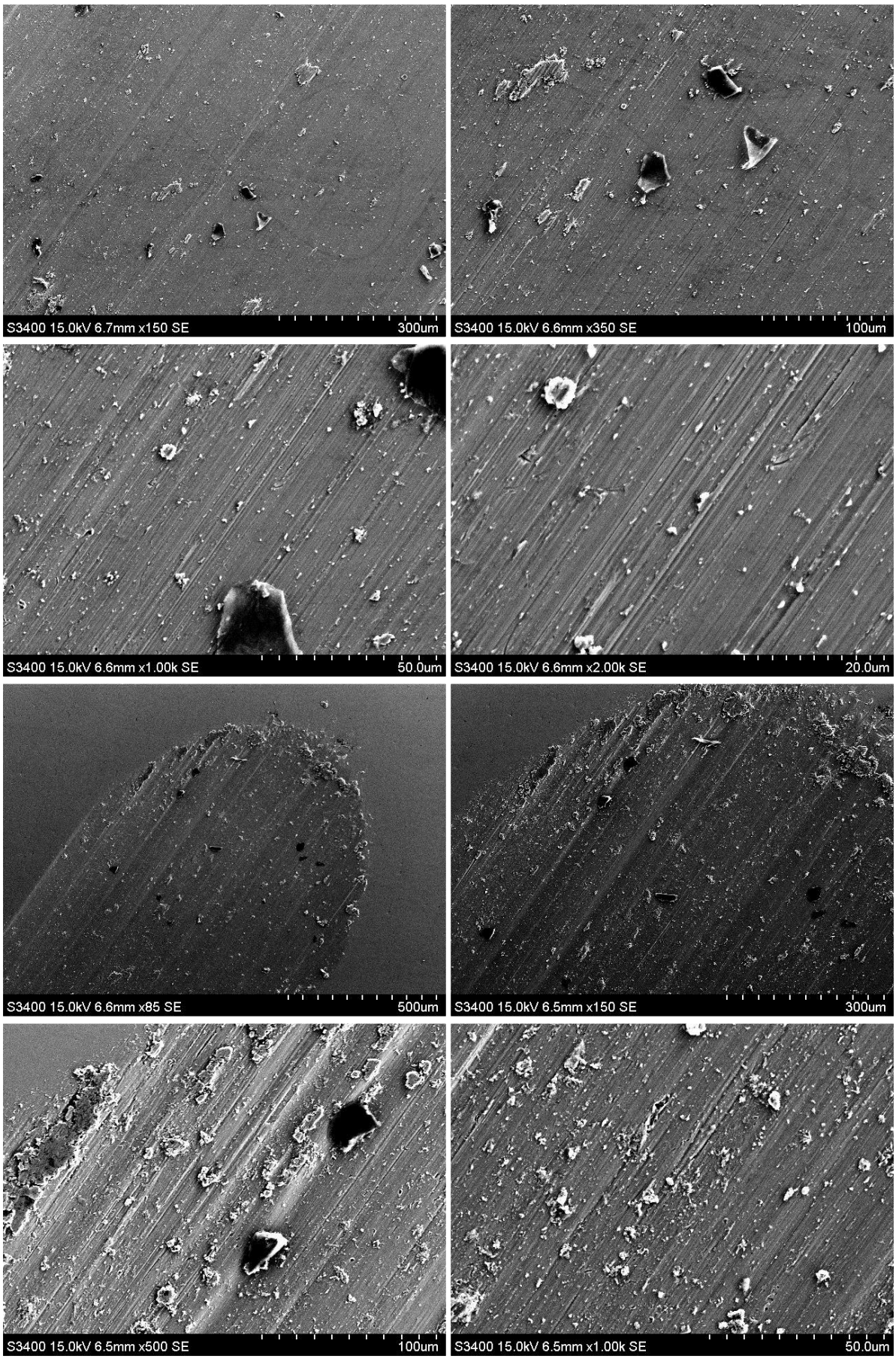

Continued on the next page

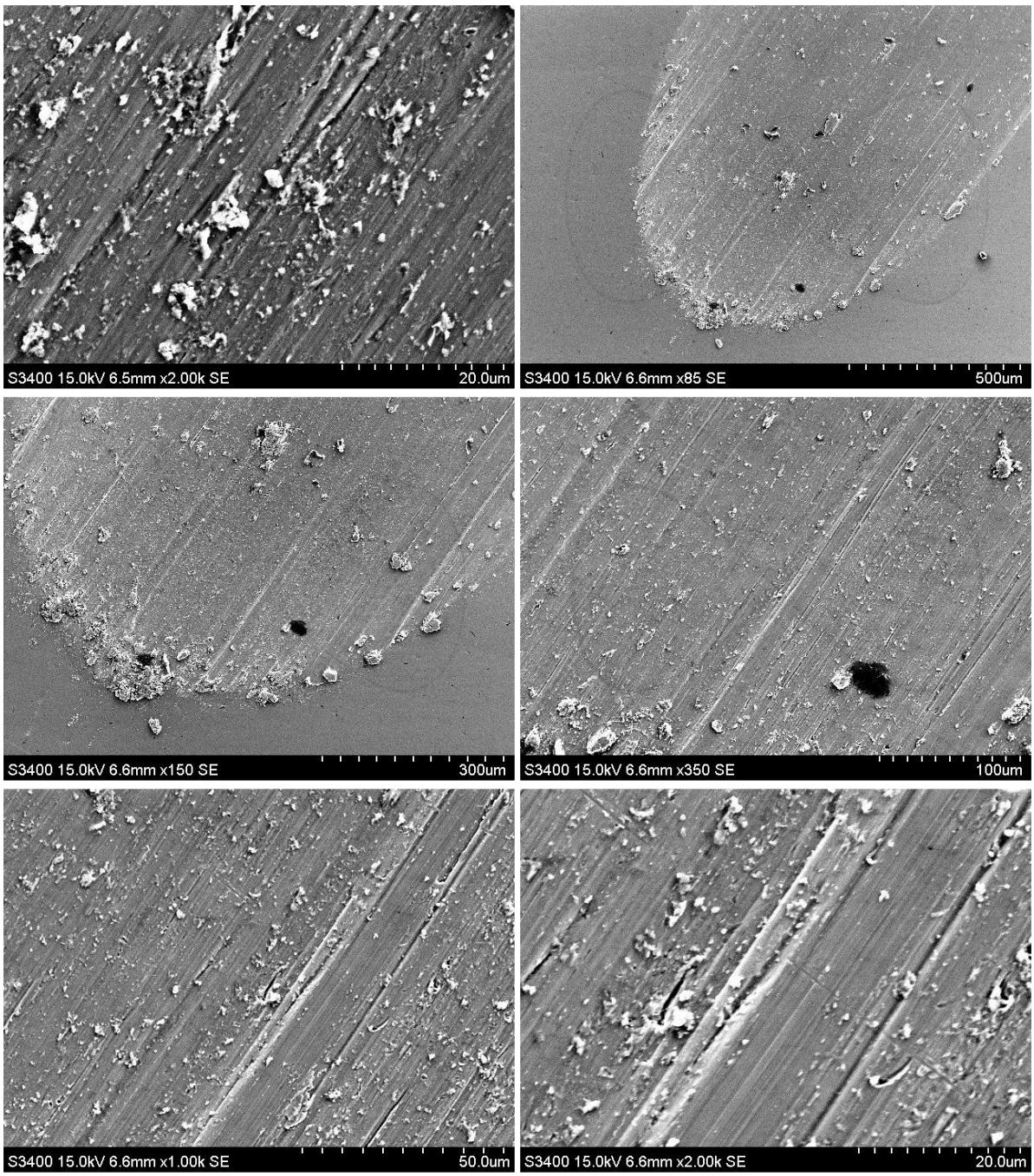

Figure 0-80: SEM images of BMG PBS 7.4 test 1

iii. PBS 7.4 with protein tests

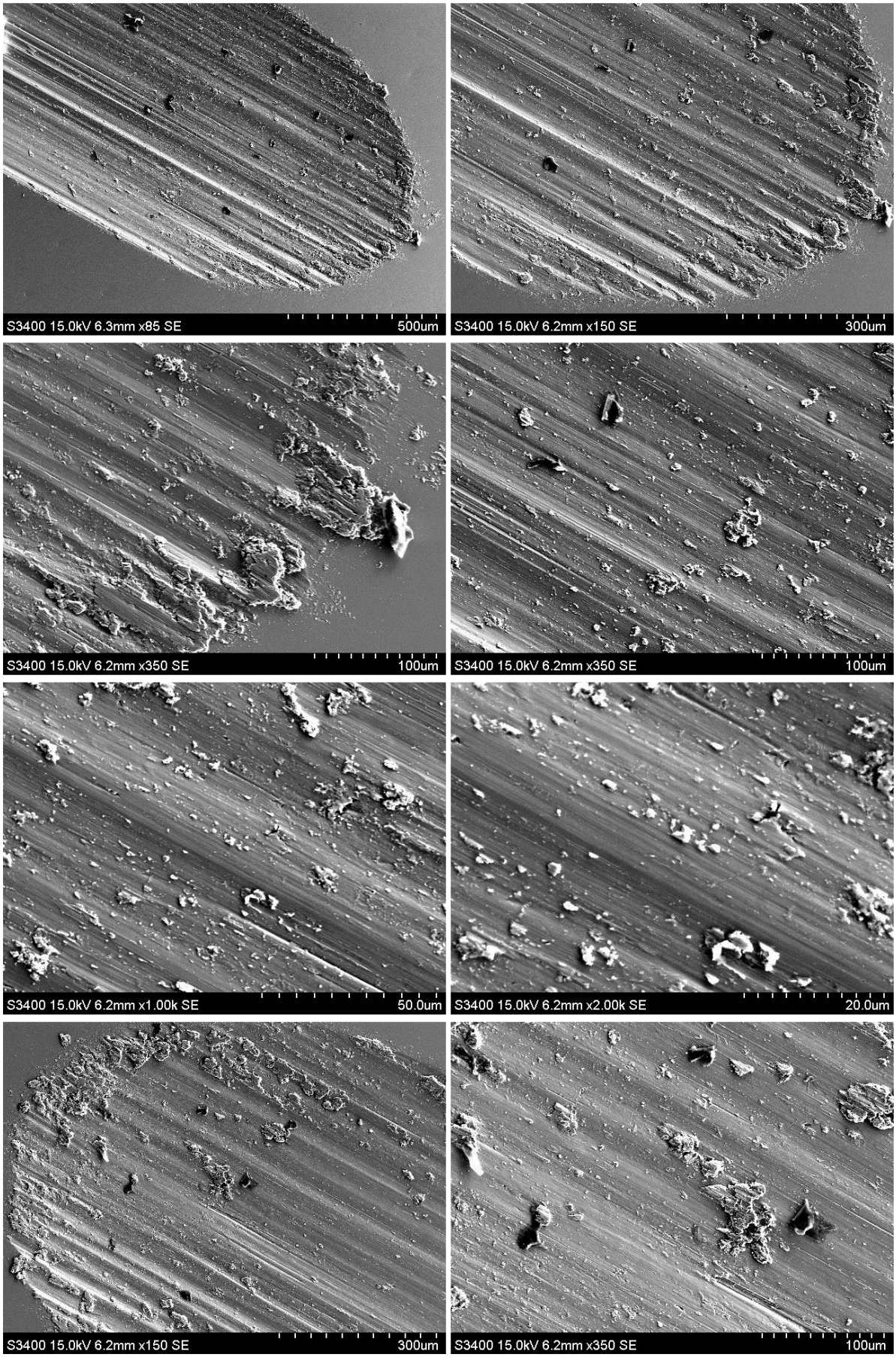

Continued from the previous page

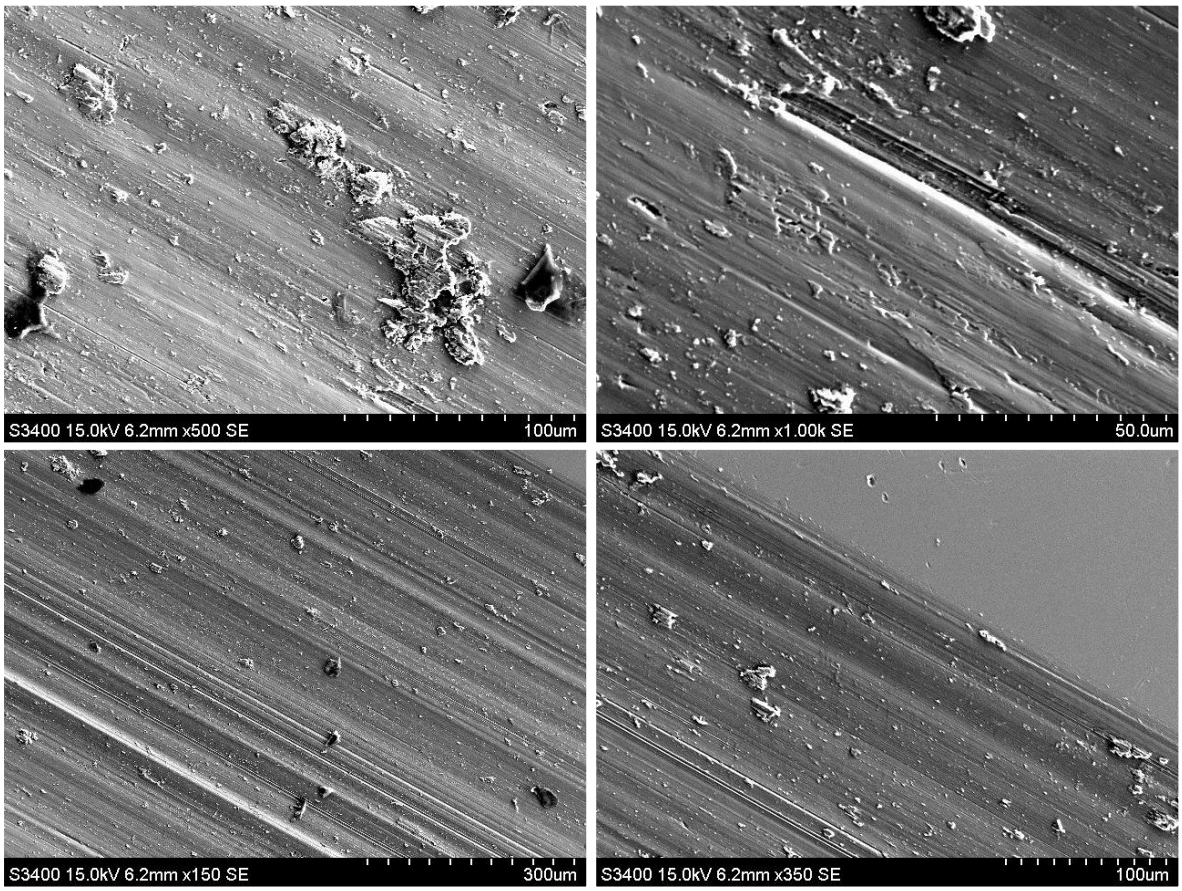

Continued on the next page

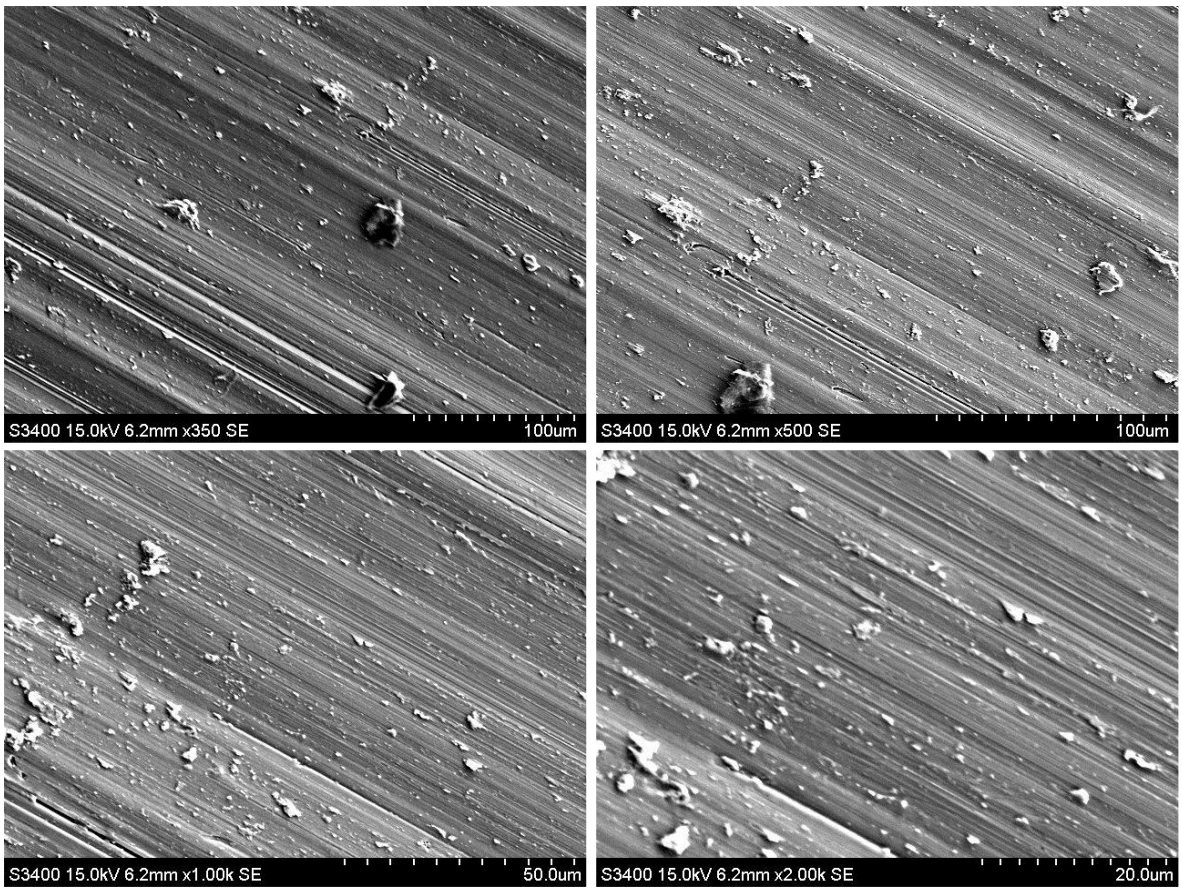

Figure 0-81: SEM images of BMG PBS 7.4 with protein test 1

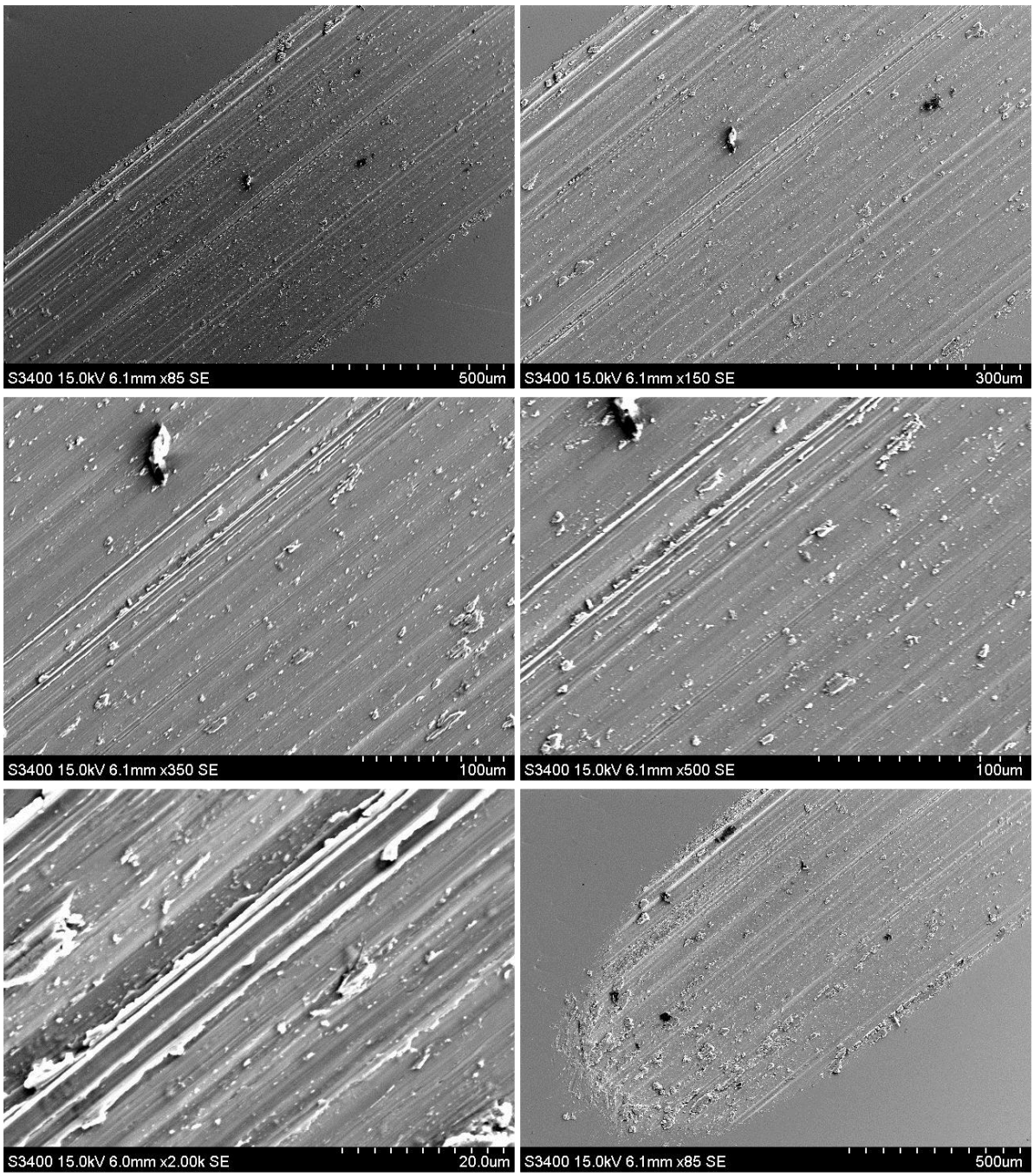

Continued on the next page

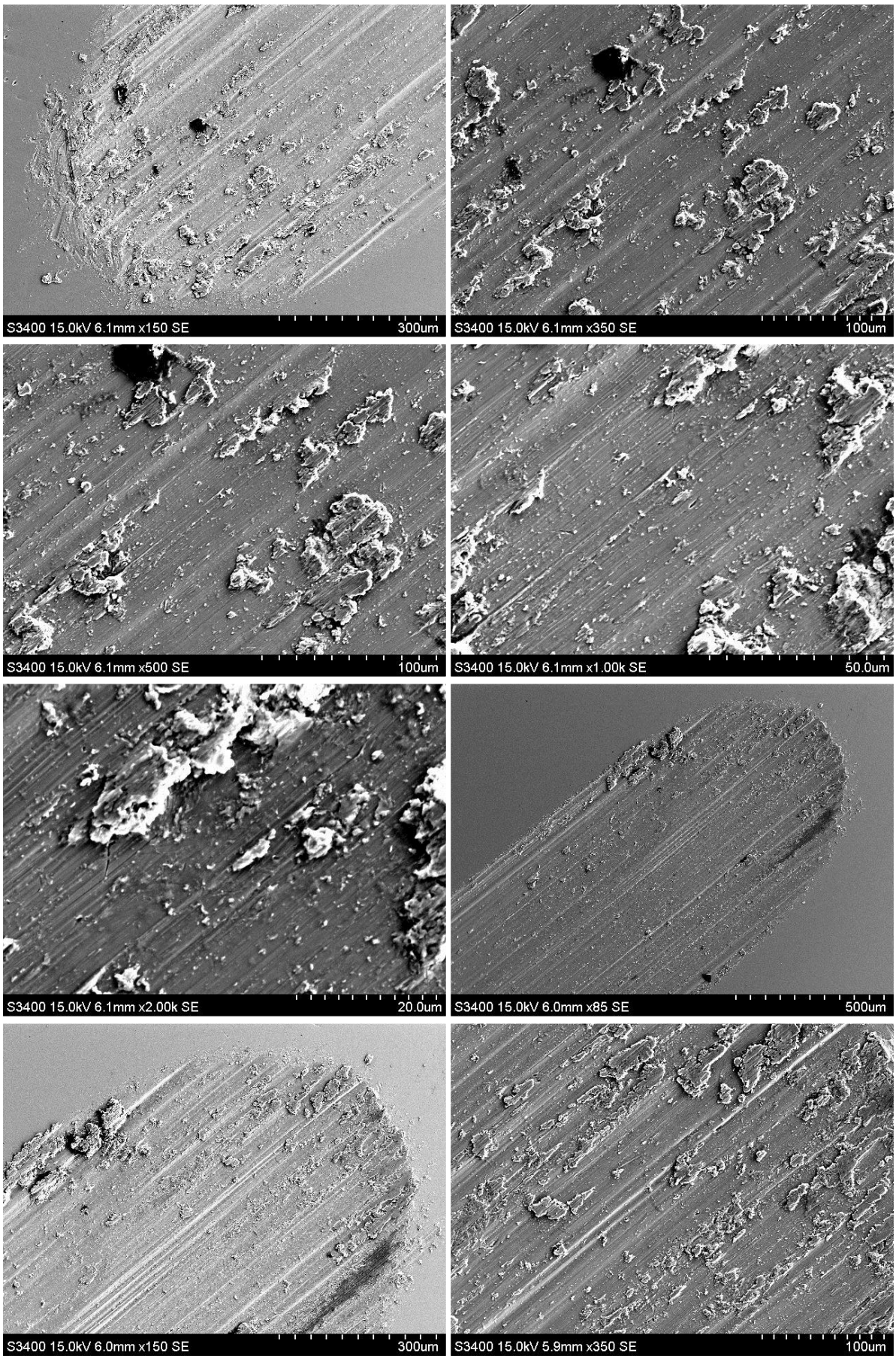

Continued on the next page

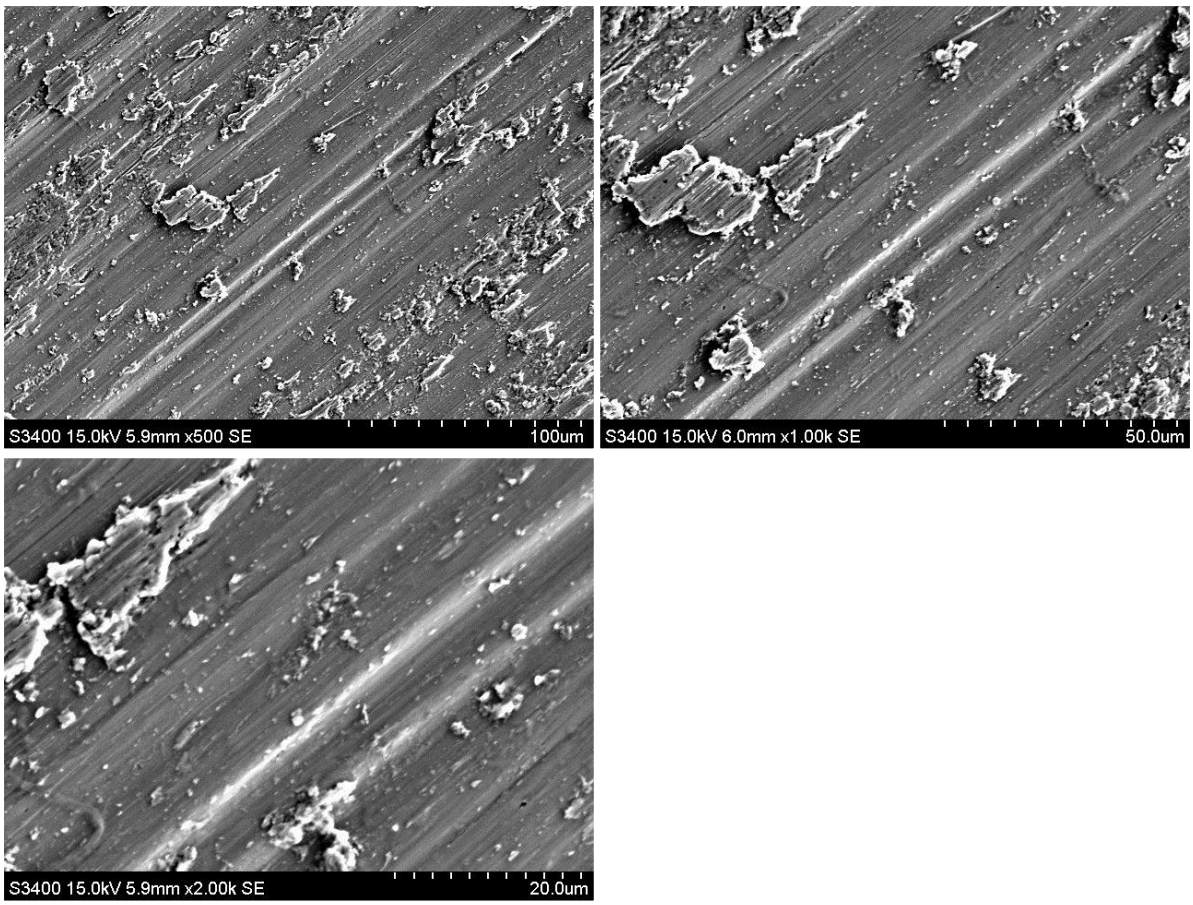

Figure 0-82: SEM images of BMG PBS 7.4 with protein test 2

iv. PBS 5.2 tests

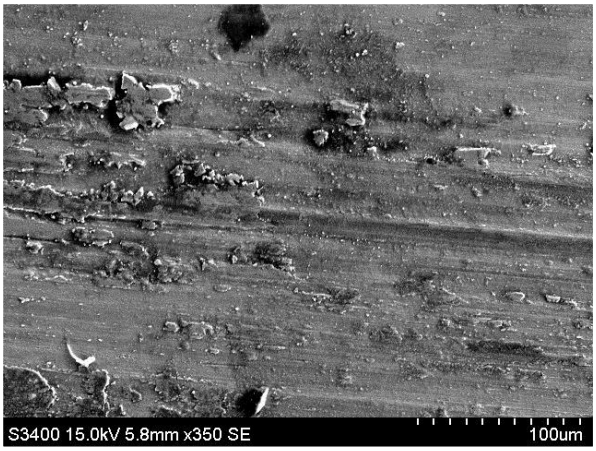

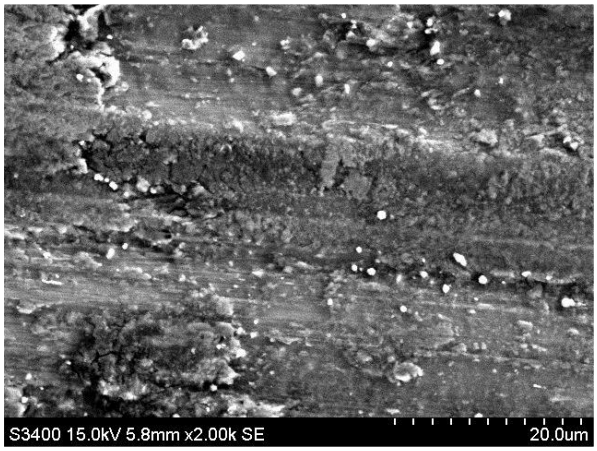

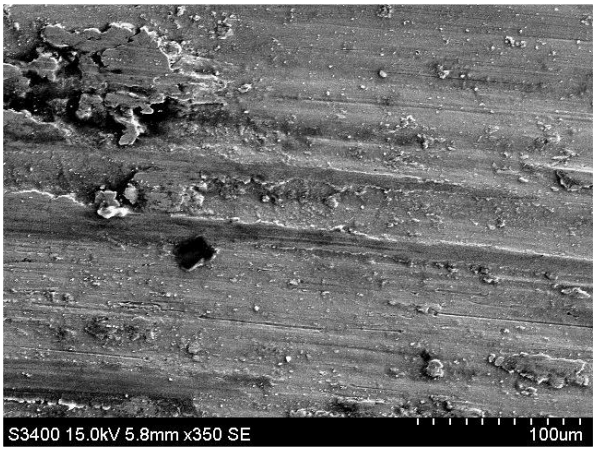

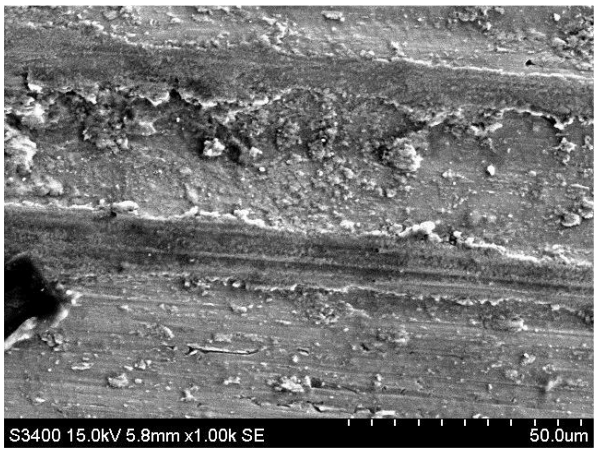

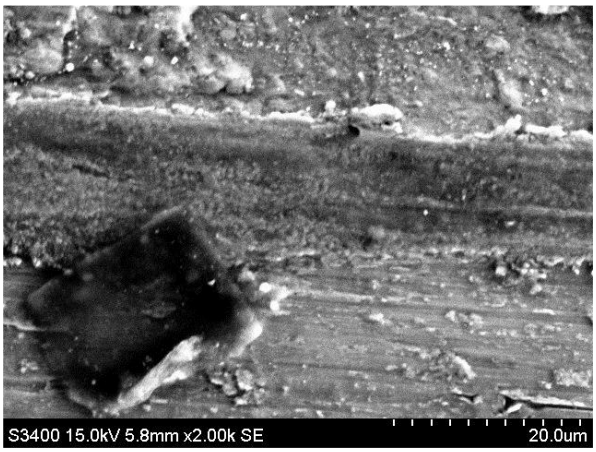

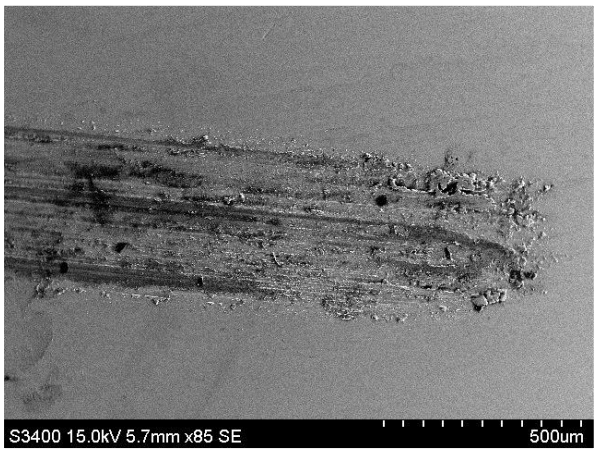

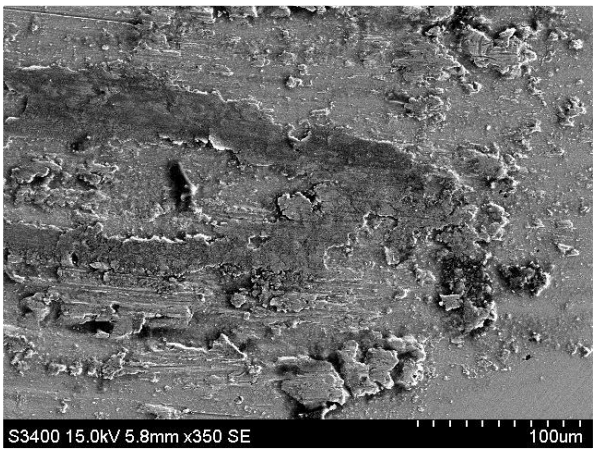

Continued from the previous page

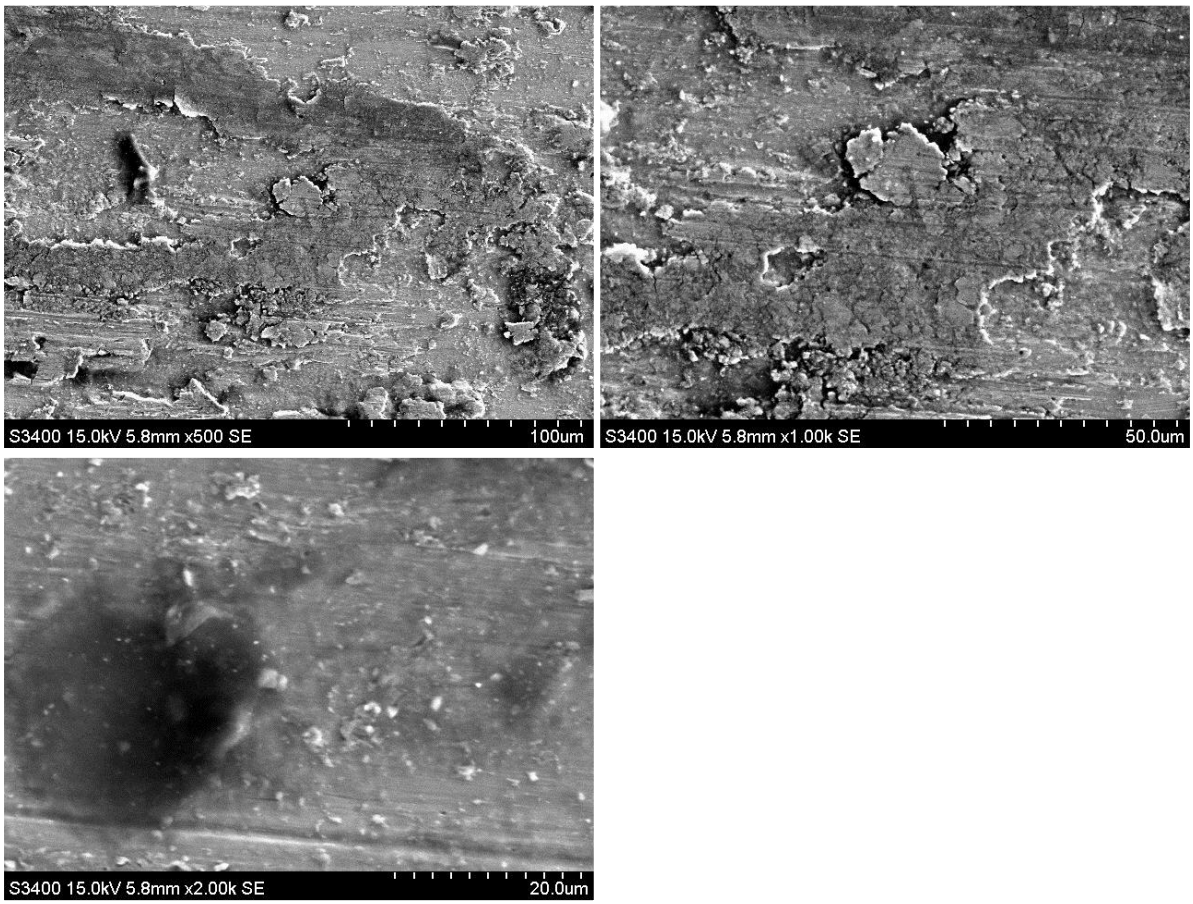

Figure 0-83: SEM images of BMG PBS 5.2 test 1

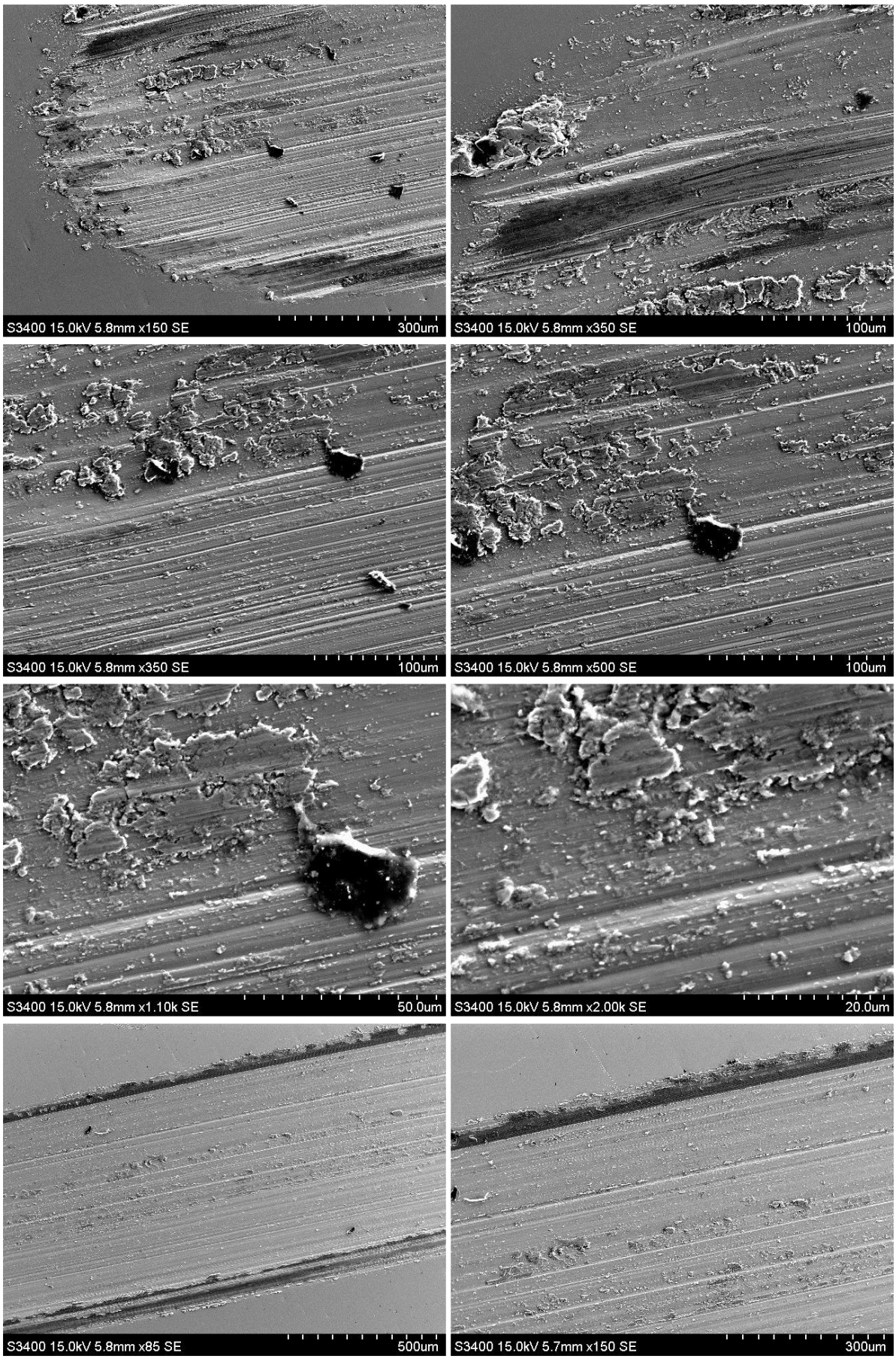

Continued on the next page

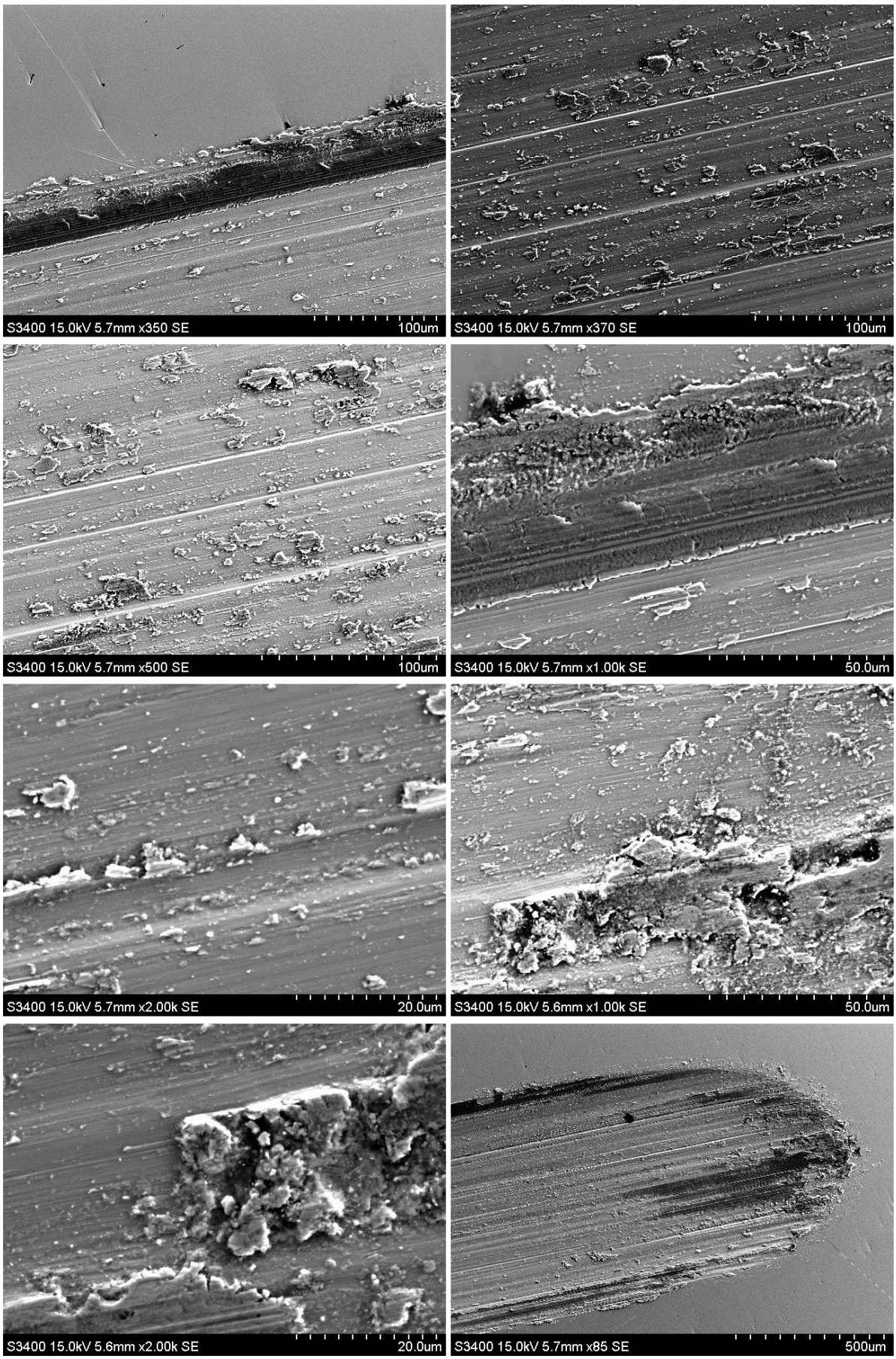

Continued on the next page

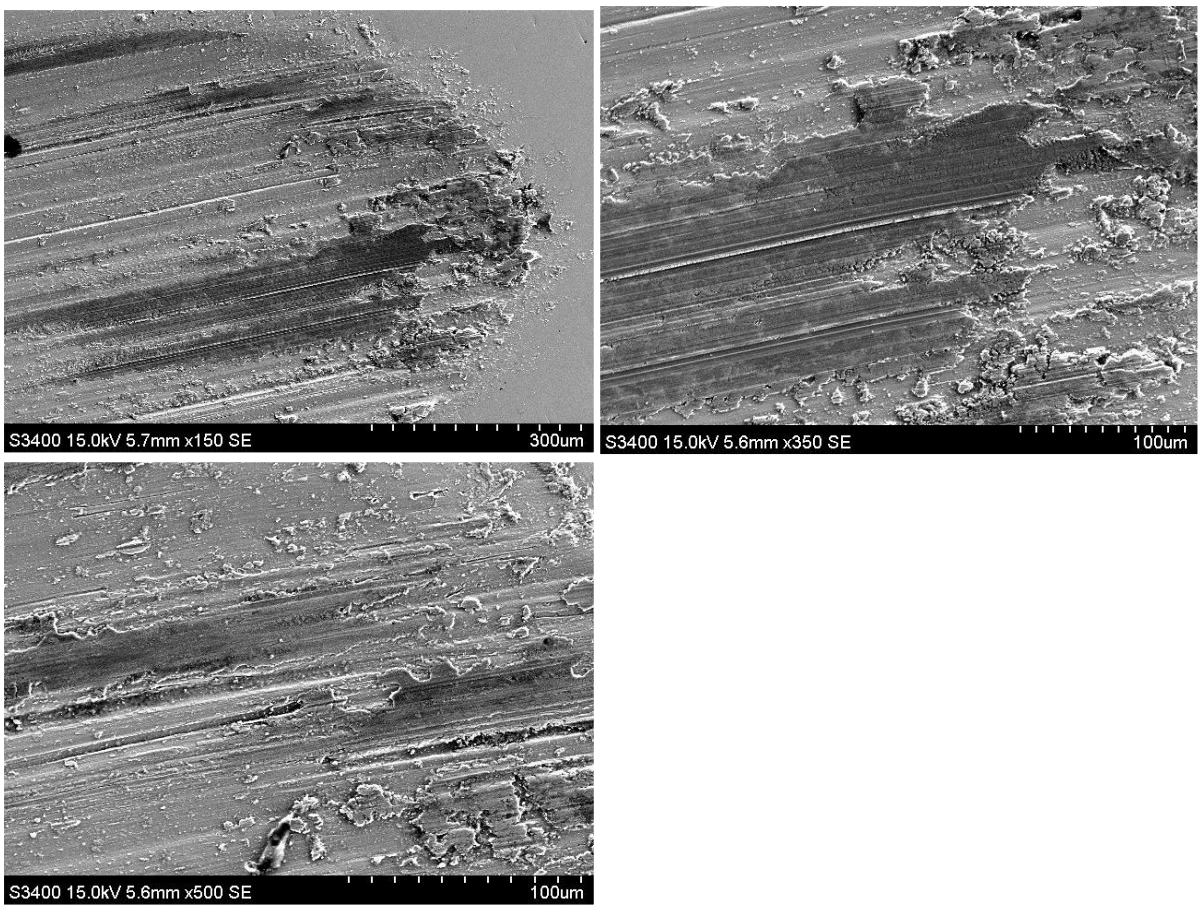

Figure 0-84: SEM images of BMG PBS 5.2 test 2

v. PBS 5.2 with protein tests

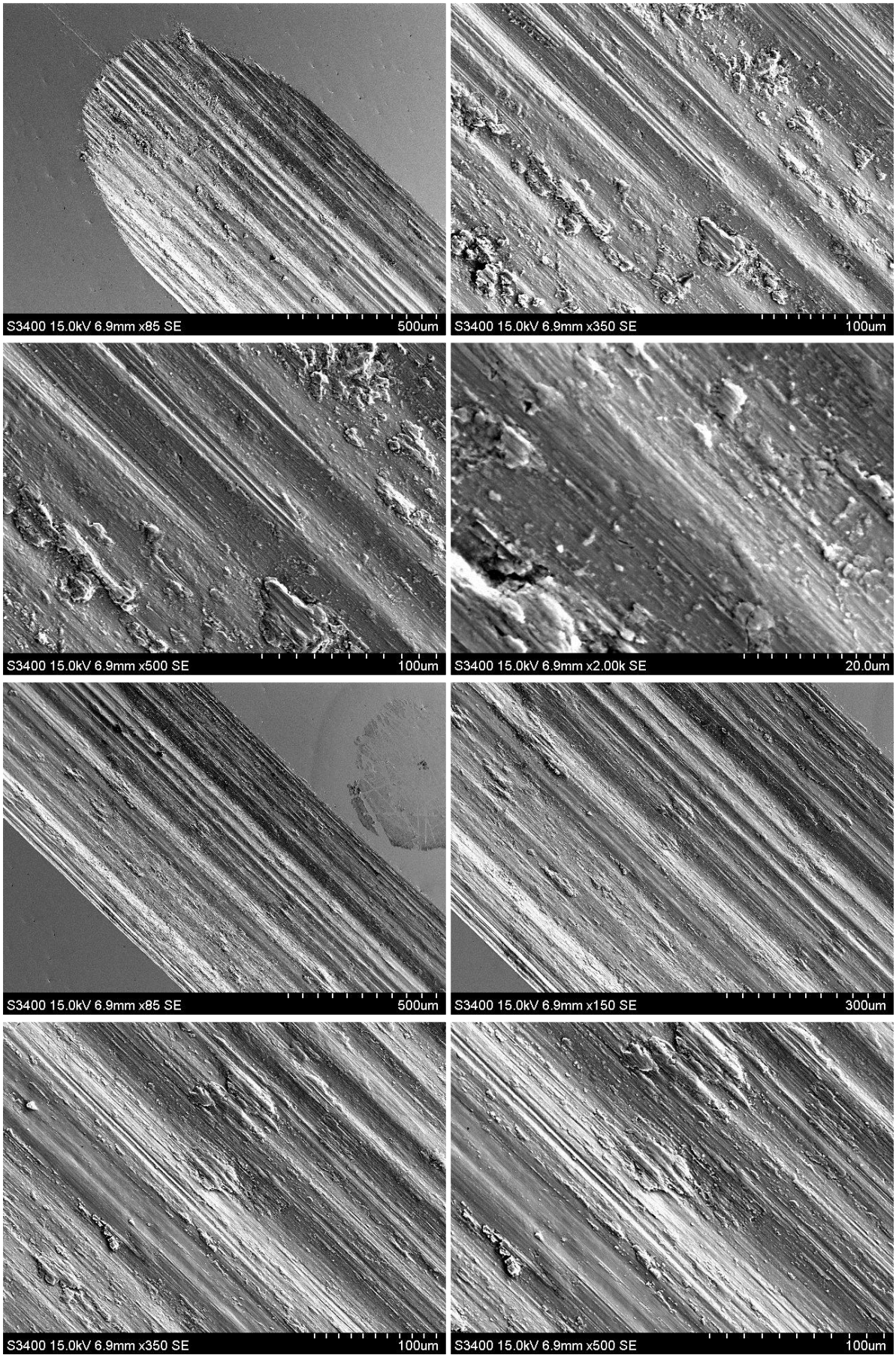

Continued from the previous page

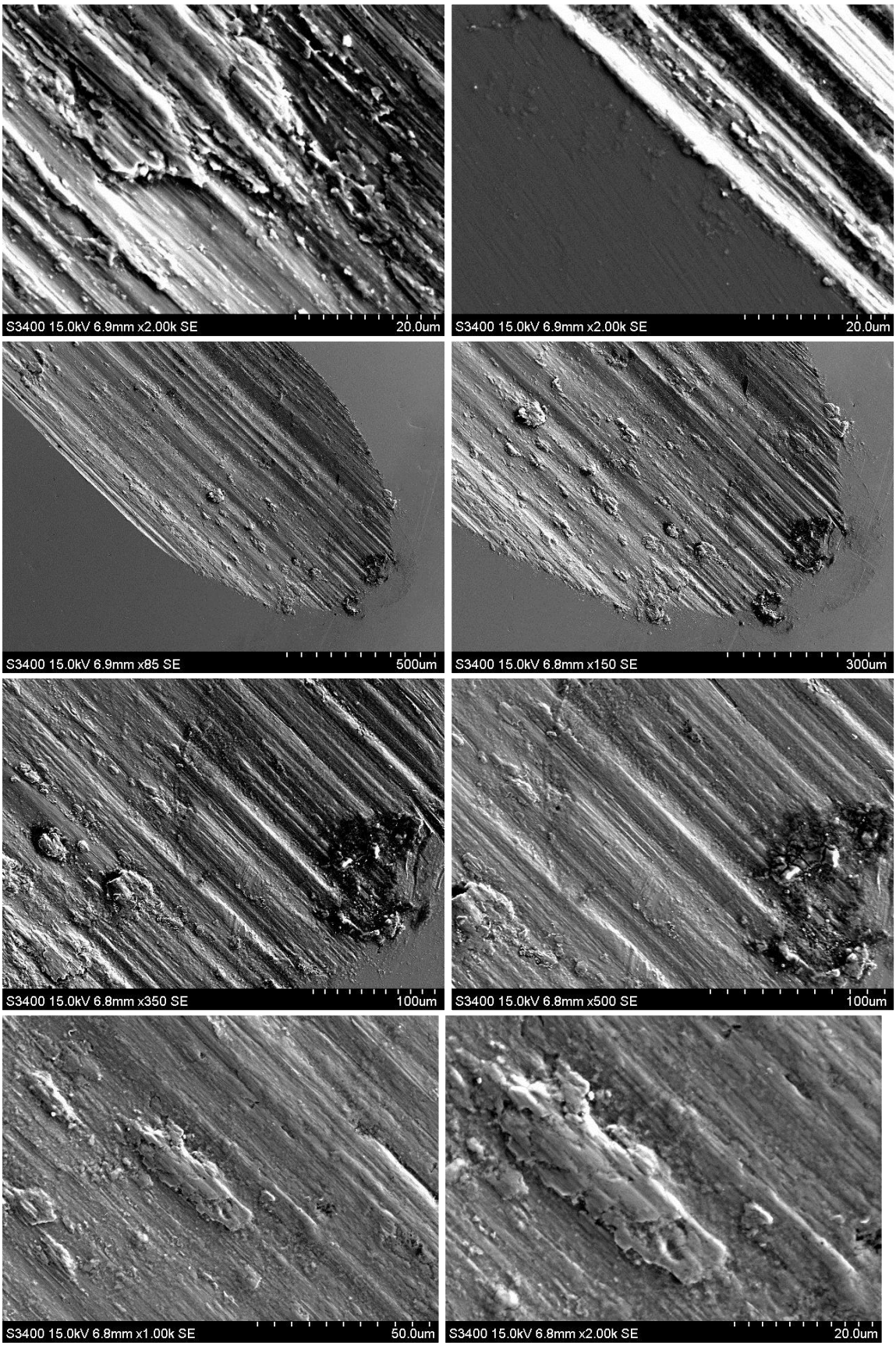

Figure 0-85: SEM images of BMG PBS 5.2 with protein